Assessment of the habitability of Mars' surface through the inventory of organic matter with the SAM (MSL mission) and MOMA (Exomars mission) space experiments

Ophélie Mcintosh

THÈSE DE DOCTORAT

NNT : 2023UPASP090

Assessment of the habitability of Mars' surface through the inventory of organic matter with the SAM (MSL mission) and MOMA (Exomars mission) space experiments

Evaluation de l'habitabilité de la surface de Mars en inventoriant la matière organique avec les expériences spatiales SAM (mission MSL) et MOMA (mission Exomars)

Thèse de doctorat de l'université Paris-Saclay et de l'université de Florence

École doctorale n° 127 Astronomie et Astrophysique d'Ile-de-France (AAIF)
Spécialité de doctorat : Astronomie et Astrophysique
Graduate School : Physique. Référent : Université de Versailles Saint-Quentin-en-Yvelines

Thèse préparée dans les unités de recherche **LATMOS** (Université Paris-Saclay, UVSQ, CNRS) et **Osservatorio Astrofisico di Arcetri** (Université de Florence, INAF), sous la direction de **Cyril SZOPA**, Professeur, la co-direction de **Guido RISALITI**, Professeur, et le co-encadrement de **John BRUCATO**, senior research scientist, et de **Caroline FREISSINET,** chargée de recherche CNRS.

Thèse soutenue à Guyancourt, le 27 septembre 2023, par

Ophélie MCINTOSH

Composition du Jury

Membres du jury avec voix délibérative

Franck MONTMESSIN Professeur des universités, LATMOS	Président
Cornélia MEINERT Directrice de recherche, HDR, Université Côte d'Azur	Rapporteur & Examinatrice
Alessandra ROTUNDI Professeure, Università degli Studi di Napoli "Parthenope"	Rapporteur & Examinatrice
Paola MANINI Professeure, University of Naples Federico II	Examinatrice

université PARIS-SACLAY

ÉCOLE DOCTORALE
Astronomie
et Astrophysique
d'Île-de-France (AAIF)

Titre : Evaluation de l'habitabilité de la surface de Mars en inventoriant la matière organique avec les expériences spatiales SAM (mission MSL) et MOMA (mission Exomars).

Mots clés : Mars, molécules organiques, analyses *in situ*, sels, GC-MS, radiations UV

Résumé : Ma thèse de doctorat porte sur la détection de molécules organiques sur Mars. Je présente l'influence des sels sur la préservation et la détectabilité de ces molécules. En effet, des sels de chlorure ont été observés à plusieurs endroits sur Mars, mais les conséquences de leur présence dans des échantillons contenant de la matière organique restent à explorer. J'ai mené des expériences en laboratoire pour reproduire les conditions dans lesquelles les échantillons martiens sont traités *in situ* par les suites instrumentales à bord de plusieurs sondes martiennes. J'ai travaillé sur un ensemble spécifique d'instruments présents dans la charge utile des sondes martiennes Viking, Curiosity et Rosalind Franklin afin d'analyser la composition moléculaire des échantillons de la surface de Mars : la chromatographie en phase gazeuse couplée à la spectrométrie de masse (GC-MS). J'ai d'abord testé l'influence des sels de chlorure et d'une matrice de phyllosilicate sur la préservation des composés organiques soumis aux rayonnements UV. Les résultats de cette étude ont montré que les sels de chlorure avaient le potentiel pour préserver les molécules organiques de la dégradation photocatalytique et pouvaient donc représenter d'excellents candidats pour l'analyse moléculaire des échantillons martiens.

Ces résultats ont conduit à explorer l'influence des sels de chlorure sur plusieurs composés organiques d'intérêt pour l'astrobiologie au cours d'expériences de pyrolyse-GC-MS. J'ai montré que lors de l'analyse, la présence de ces sels pouvait gêner la détection des composés organiques mais aussi former des précurseurs de composés chlorés, comme cela a déjà été détecté sur Mars. Enfin, l'interaction entre les phases inorganiques et organiques dans l'environnement martien et lors des analyses *in situ* m'a amené à explorer la détectabilité d'un autre type de composés : les sels organiques aromatiques. Les sels organiques sont des molécules réfractaires, difficiles à détecter. J'ai utilisé les techniques de pyrolyse et de dérivatisation GC-MS utilisées par les instruments de vol pour comprendre le comportement et la signature de ces composés. Malgré leur nature non volatile, j'ai découvert qu'ils pouvaient être indirectement identifiés en combinant ces différentes techniques. Dans l'ensemble, cette thèse de doctorat vise à faciliter l'interprétation des données *in situ* obtenues par les instruments embarqués à bord des anciennes, actuelles et futures missions martiennes, ainsi qu'à guider la recherche d'échantillons susceptibles de contenir des biosignatures.

université PARIS-SACLAY

ÉCOLE DOCTORALE
Astronomie
et Astrophysique
d'Île-de-France (AAIF)

Title : Assessment of the habitability of Mars' surface through the inventory of organic matter with the SAM (MSL mission) and MOMA (Exomars mission) space experiments

Keywords : Mars, organic molecules, *in situ* analysis, salts, GC-MS, UV radiations

Abstract : My Ph.D. thesis focuses on the detection of organic molecules on Mars. I will present the influence of salts on the preservation and detectability of organic molecules at the Mars surface. Chloride salts have been observed at several locations on Mars, but the consequences of their presence in samples containing organic matter are yet to be explored. I conducted laboratory experiments to reproduce conditions in which Martian samples are processed *in situ* by the instrument suites onboard several Martian probes. I worked on a specific set of instruments present in the analytical chemistry payload of the Viking, Curiosity, and Rosalind Franklin surface probes to analyze *in situ* the molecular composition of Mars surface samples: Gas Chromatography-Mass Spectrometry (GC-MS). I first tested the influence of chloride salts and a phyllosilicate matrix on preserving organic compounds subjected to UV radiation reaching the Martian surface. The results of this study showed that chloride salts had the potential to preserve organic molecules from photocatalytic degradation and could represent, therefore, excellent candidates for sample analysis. These results led to exploring the influence of chloride salts on several organic compounds of interest for astrobiology during pyrolysis-GC-MS experiments. I showed that during molecular analysis, the presence of these salts could hinder the detection of organic compounds but could also form precursors of chlorinated molecules, as already detected on Mars. Finally, the interaction between inorganic and organic phases in the Martian environment and during *in situ* analyses led me to explore the detectability of another type of compound: aromatic organic salts. Organic salts are refractory molecules, challenging to detect. I used pyrolysis and derivatization GC-MS techniques as used in the flight instruments to understand the behavior and signature of these compounds. Despite their non-volatile nature, I found that they could be indirectly identified by combining these different techniques. Overall, this Ph.D. thesis aims to help interpreting *in situ* data as performed by the instruments onboard former, current, and future Martian missions, as well as guide the search for samples that could contain preserved biosignatures.

TABLE OF CONTENTS

LIST OF ABBREVIATIONS

BSW	bi-silylated water
CB	Cumberland
COSAC	Cometary Sampling and Composition experiment
CRISM	Compact Reconnaissance Imaging Spectrometer for Mars
DFT	Density Functional Theory
DKP	diketopiperazines
DMF	N,N-Dimethylformamide
DMFDMA	N,N-Dimethylformamide dimethyl acetal
DRIFT	Diffuse Reflectance InfraRed Fourier Transform Spectroscopy
EGA	Evolved Gas Analysis
ESA	European Space Agency
ETU	Engineering Test Unit
FTIR	Fourier Transform Infrared spectroscopy
GC-MS	Gas Chromatography-Mass Spectrometry
GCR	Galactic Cosmic Rays
GEX	Gas Exchange experiment
QMS	Quadrupole Mass Spectrometer
GVPT2	Generalized second-order Vibrational Perturbation Theory approach
HC	Hydrocarbon Trap
HCl	Hydrogen chloride
IR	InfraRed
IT	Injection Trap

LAM	Large Amplitude-Motion
LATMOS	Laboratoire Atmosphères,Observations Spatiales
MA	Mary Anning
Ma-MISS	Mars Multispectral Imager for Subsurface Studies
MOMA	Mars Organic Molecule Analyser
MRO	Mars Reconnaissance Orbiter
MSL	Mars Science Laboratory
MTBSTFA	N-Methyl-N-(tert-butyldimethylsilyl)trifluoroacetamide
MW	Mass Weight
NASA	National Aeronautics and Space Administration
NIR	Near Infrared
NIST	National Institute of Standards and Technology
OD	Opportunistic Derivatization
OG	Ogunquit Beach
PAH	Polycyclic Aromatic Hydrocarbon
SAM	Sample Analysis at Mars
SCS	Sample Catching System
SEP	Solar Energetic Particles
SHERLOC	Scanning Habitable Environments with Raman and Luminescence for Organics and Chemicals
SIM	Selected-Ion Monitoring
SPaH	Sample Processing and Handling system
TIC	Total Ion Current
TLS	Tunable Laser Spectrometer
TMAH	Tetramethylammonium hydroxide

ToF-SIMS	Time-of-Flight Secondary Ion Mass Spectrometer
UV	UltraViolet
VL-1&2	Viking Landers 1 and 2
XRPD	X-ray Powder Diffraction

CHAPTER 1: INTRODUCTION

1. HABITABILITY OF THE SOLAR SYSTEM

Understanding what makes a planetary body habitable, the criteria involved, and the potential habitable worlds within our solar system is crucial in our quest to uncover the existence of life beyond Earth. The discovery of exoplanets and the identification of potentially habitable environments have sparked a renewed interest in our own celestial neighbourhood. By examining the habitability potential of various solar system bodies, we can gain valuable insights into the conditions necessary for life and the likelihood of its existence elsewhere. When considering planetary bodies like moons or planets as habitable, several criteria are typically taken into account. While these factors can vary depending on the specific context and the type of life being considered, here are some general criteria:

a. *Solvent*: Liquid water is considered a fundamental requirement for life as it is essential for biochemical reactions to occur (Cockell et al., 2016). Currently, it stands as the sole compound recognized for its utilization as the principal biochemical solvent within living organisms, although there have been suggestions concerning the potential use of alternative solvents such as liquid ammonia, organic solvents like methane and ethane, formamide, and sulfuric acid (Benner et al., 2004; Schulze-Makuch & Irwin, 2006). Habitability assessments look for evidence of liquid water on or below the surface, such as lakes, rivers, oceans, or subsurface reservoirs.
b. *Suitable Temperature Range*: The temperature range should be conducive to the existence of liquid water. It is possible for liquid water to persist at temperatures below the freezing point threshold thus, suitable for colder planetary environments. Indeed, eutectic solutions containing salts such as oxychlorines, have freezing points as low as ~-65 °C (Chevrier et al.,

2009), which is considerably beneath the current lower limit for metabolic activity. However, due to the constraints on the viability of life, only a portion of the range of liquid water is considered habitable. Microbial metabolic activity can endure temperatures as low as ~-25 °C (Junge et al., 2004; Mykytczuk et al., 2013), but there is currently no compelling evidence of reproductive capability below ~-15 °C (Breezee et al., 2004; Wells & Deming, 2006).

c. *Energy Sources*: Life requires a source of energy to sustain its metabolic processes. Habitability assessments consider the availability of energy sources, which can include sunlight, chemical energy derived from redox processes, or geothermal energy (Cockell et al., 2016).

d. *Availability of Essential Elements and Nutrients*: Habitable environments require an adequate supply of essential elements and nutrients. Among the elements of the periodic table, six are considered ubiquitous in the molecules of known life: carbon (C), hydrogen (H), nitrogen (N), oxygen (O), phosphorus (P), and sulfur (S). These elements are building blocks for organic compounds and vital for the functioning of biological processes (Remick & Helmann, 2023). The assessment of potential habitability on planetary bodies can be based on the relationship between C,H,N,O,P,S elements, as well as the availability of energy. In 2010, Stoker et al. discussed the application of this approach to evaluate the habitability of the Phoenix landing site on Mars.

These criteria have been described by Cockell et al. (2016) as "instantaneous habitability" factors meaning that at a specific moment and in a specific location, these set of prerequisites must be fulfilled for known organisms to be actively functional. But other criteria such as mass, atmospheric conditions, plate tectonic, magnetic field and other astronomical aspects described as "continuous planetary habitability" factors must be fulfilled to allow the necessary conditions for a planetary body that possess instantaneous habitability to persists over long periods of geological time (Cockell et

al., 2016).

It is important to note that these criteria are based on our current understanding of life as we know it on Earth. However, the concept of habitability is evolving, and future discoveries may expand these criteria or introduce new ones as our knowledge of the possibilities for life in the universe expands.

The solar system harbors a variety of potentially habitable environments, each offering unique possibilities for the existence of life beyond Earth. Among these environments, Europa, one of Jupiter's moons, stands out with its subsurface ocean and the potential for chemical reactions that could sustain life (Russell et al., 2017). Enceladus, a moon of Saturn, exhibits active hydrothermal vents and organic compounds, suggesting a habitable environment beneath its icy surface (Postberg et al., 2018; Waite et al., 2017). Additionally, Titan, Saturn's largest moon has complex organic chemistry and methane lakes (Mackenzie et al., 2021; Mastrogiuseppe et al., 2019). However, in this Thesis, we will focus on Mars as it is the planet most explored by space missions since it is the most accessible and is believe to have hosted multiple habitable environments in its early history.

2. HABITABILITY OF MARS

2.1. CONTINUOUS PLANETARY HABITABILITY OF MARS

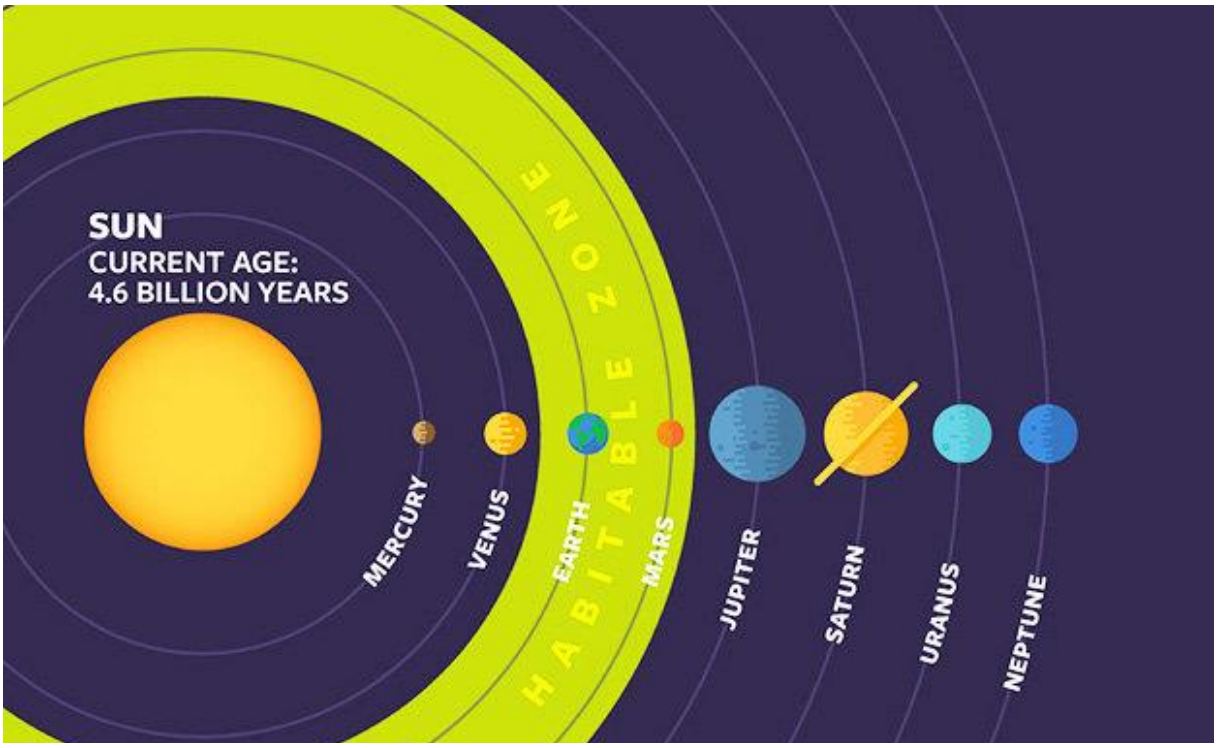

Figure 1 : Current habitability zone (in green) of our Solar system (Image credit: Cornell University)

Mars is the fourth planet from the Sun and is situated in our solar system's "habitable zone" (Figure 1), as its distance from the Sun could allow liquid water on its surface. However, when looking at the planet Mars today, it is cold and dry, which is not favorable conditions to host life. Indeed, Mars does not fulfill the continuous planetary habitability criteria necessary to maintain water on its surface like Earth today. Several factors are responsible. First, Mars is a smaller planet than Earth (6794 km in diameter *vs* 12 756 km, respectively) and therefore has a lower mass ($6.4169.10^{23}$ kg *vs* $5.9722.10^{24}$ kg, respectively) and surface gravity (3.711 $m.s^2$ *vs* 9.81 $m.s^2$, respectively). Both factors influence the velocity (Fox, 1993) and thermal escape (Lammer et al., 2013) of the gases present in a planet's atmosphere so lighter gas molecules, such as hydrogen and helium, escape more readily from Mars' atmosphere than Earth. This phenomenon combined with solar wind erosion (Jakosky, 2022) and the absence of a global magnetic field resulted in the thin atmosphere (6.35 mbar on Mars *vs* 1 bar on

Earth) that we see today and, thus, a limited greenhouse effect leading to colder surface temperatures of ~-60 °C (McKay, 2009). Moreover, the loss of Mars' thicker atmosphere and subsequent pressure drop caused liquid water to either evaporate or freeze, leaving Mars predominantly dry. The phase diagram of water shows that the current atmospheric pressure on Mars is just slightly higher than the triple point, below which liquid water is not possible (Figure 2). Thus, at martian surface pressure, water exists in the liquid phase only for a very small range of temperatures around 0.01 °C, out of which it freezes or evaporates.

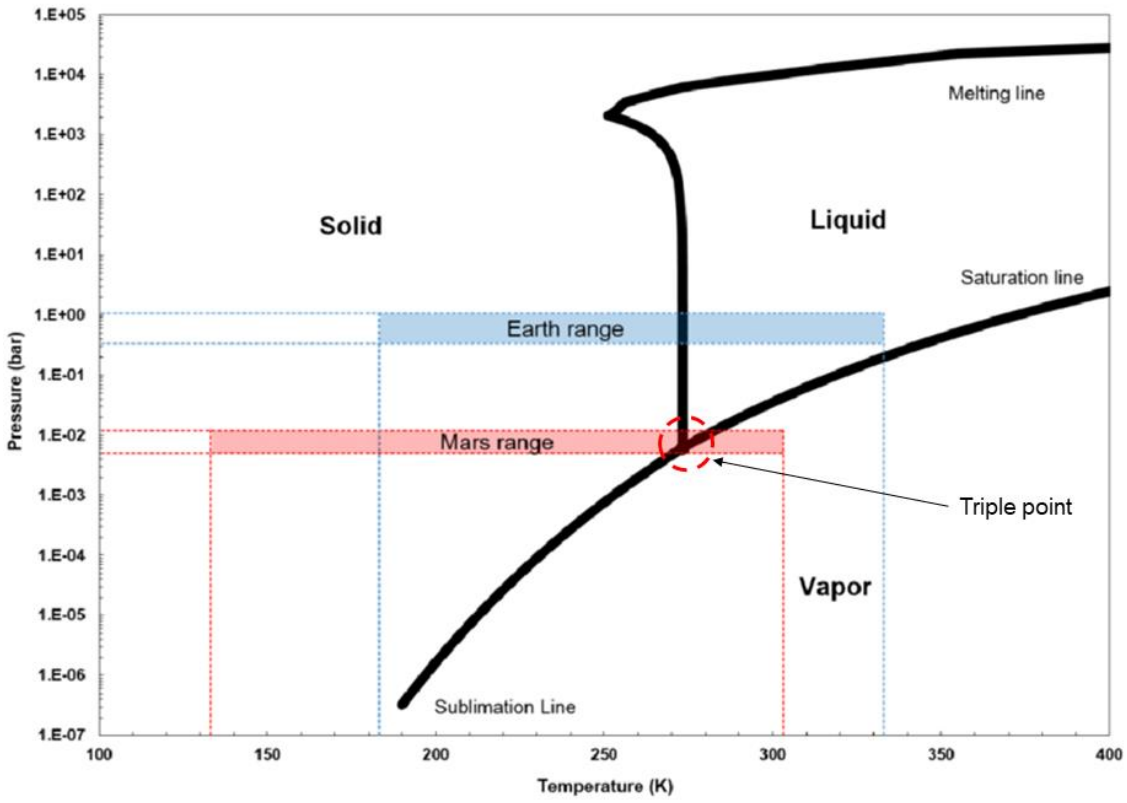

Figure 2 : Phase diagram showing water's state as a function of pressure and temperature. The "Mars range" and "Earth range" boxes indicate the ranges of pressure and temperature found on Mars's and Earth's surfaces, respectively. From Verseux 2018.

2.2. Instantaneous habitability of Mars

Despite today's unwelcoming conditions of its surface, Mars has been the focus of space exploration for extraterrestrial life since the 1960s. This is because, in addition to being the most accessible planet from Earth, Mars, in its early history, had an

environment much more conducive to the emergence, development, and maintenance of life than today, with the presence of **liquid water** and **organic molecules**, therefore fitting the criteria of the instantaneous habitability factors described by Cockell et al. (2016). Moreover, contrary to the Earth, it has preserved the memory of its ancient grounds due to the low tectonic activity (Golombek et al., 2010) and is considered today as a form of an archive of what the Earth was at the time of the appearance of life.

2.2.1. Liquid water

Mars' geology and mineralogy suggest that liquid water has existed on its surface and underground for hundreds of thousands of years (Arvidson, 2016). However, the exact quantity of water on the surface and the significance of underground water reservoirs remain uncertain. Valley networks, which have been documented for several decades, have been extensively mapped across significant portions of Noachian (-4.1 to -3.7 Ga) and some regions of Hesperian (-3.7 to -3.0 Ga) Mars (Hynek et al., 2010). Moreover, the identification of phyllosilicate minerals provides evidence for the existence of perennial liquid water during the Noachian period. These minerals are believed to originate from surface weathering processes caused by the alteration of basaltic crust through the action of water (Bibring et al., 2006; Mustard et al., 2008; Poulet et al., 2005). The most accredited hypothesis to explain the presence of liquid water at the surface of Mars in its early history, is that an intense volcanic activity in the Noachian era might have brought in the atmosphere large amounts of greenhouse gases causing the raise of temperature.

On the other hand, the presence of liquid water on the planet Mars today is still a subject of scientific investigation and debate. In 2015, NASA announced the discovery of Recurring Slope Lineae (RSL) on Mars (Ojha et al., 2015), which are dark streaks that appear to flow down steep slopes during warmer seasons and fade during colder periods. It was hypothesized that these RSL could be caused by the intermittent flow of briny water. Salts can become hydrated by pulling water vapor from the atmosphere,

and this process can form drops of salty water. Seasonal changes in hydration of salt-containing grains might result in some trigger mechanism for RSL grain flows, such as expansion, contraction, or release of some water. Darkening and fading might result from changes in hydration. Subsequent research and observations form orbiters and rovers have provided additional support for the presence of brines and seasonal fluctuations of liquid water (Ojha et al., 2014; Stillman et al., 2017; Stillman et al., 2014; Wang et al., 2019). However, another hypothesis is that they are due to granular flows (Dundas et al., 2017), where grains of sand and dust slip downhill to make dark streaks, rather than the ground being darkened by seeping water. They exist only on slopes steep enough for dry grains to descend the way they do on faces of active dunes.

Moreover, Mars has regions where the subsurface is believed to contain water ice that remains frozen throughout the years (Dundas et al., 2018). Permafrost is commonly found in the polar regions, especially in the northern polar plains, where the Phoenix lander discovered water ice just below the surface (Cull et al., 2010). Additionally, ice-rich deposits have been identified in the transition zone between the Elysium Rise and the Utopia Planitia Basin (Pedersen & Head, 2010) and recent results from ESA Mars Express spacecraft point to a present-day subglacial salty lake of liquid water 20 km across, located 1.5 km beneath the ice at Mars' South Pole (Lauro et al., 2021).

The extent, frequency and duration of liquid water on present-day Mars are still being investigated, and the exact nature of these potential water sources remains a topic of ongoing research and exploration.

2.2.2. Organic matter detection on Mars

Finding organic matter on Mars is the last definitive clue of the habitability of the planet. The presence of organic compounds on the Martian surface is not correlated to the presence of life but it would indicate that the planet has or has had the necessary ingredients for the emergence of life. Organic matter can come from either biological or nonbiological sources, and its detection on Mars would indicate that either life

existed on or was transported to the planet, or that chemical processes that produce organic compounds are occurring.

Furthermore, early Mars should have received the same input of organic compounds as early Earth from the Late Heavy Bombardment (Gomes et al., 2005), and there is ample evidence from Martian meteorites that Mars has been undertaking organic chemistry for most of its history (Steele et al., 2012; Steele et al., 2016). Thus, the emergence of more complex biochemistry from simple organic chemistry and chemical precursors under more Earth-like conditions (e.g. presence of liquid water) is plausible.

If the organic matter is of biological origin, it would change our understanding of the possibility of life beyond Earth. Scientists could study the age and composition of the organic materials found on Mars to identify potential habitats for microbial life in its past. If the organic matter was formed through non-biological processes, it would still provide important information about Mars' geological history. Studying organic molecules on Mars could provide insights into the planet's geological and environmental history, allowing scientists to better understand the processes that have shaped the planet over time.

In order to confirm the presence of organic matter on the Martian surface, landers and rovers equipped with analytical chemistry instrument capable of analyzing the molecular content of Martian soil samples were developed.

2.2.2.1. *In situ* Martian missions and instruments for organic matter detection

2.2.2.1.1. Viking 1 & 2 (1975-1982)

2.2.2.1.1.1. Scientific goals

The NASA Viking mission stands as one of the most significant events in the history of space exploration as it marked the first successful landing of a spacecraft on another planet, a feat that required tremendous engineering and technological advancements.

The primary objectives of the Viking mission was to study the Martian environment and

search for evidence of life on the planet. To achieve these goals, NASA sent two spacecrafts, Viking 1 and 2, to Mars. The Viking mission was far more sophisticated and advanced than previous missions, such as the Mariner and Pioneer missions. The spacecrafts were equipped with cutting-edge instruments, allowing for detailed measurements and analysis of the Martian environment. The two landers carried a suite of instruments, including a gas chromatograph-mass spectrometer (GC-MS) for detecting organic molecules in the soil, a biology experiment to look for metabolic activity and cameras for imaging the surface (Klein, 1979).

Overall, the launch in 1975 of the Viking landers represented a new era for planetary exploration and scientific discovery. It provided valuable insights into Mars' geology, atmosphere, and potential habitability and layed the foundation for future missions.

2.2.2.1.1.2. Landing sites: *Chryse Planitia* and *Utopia Planitia*

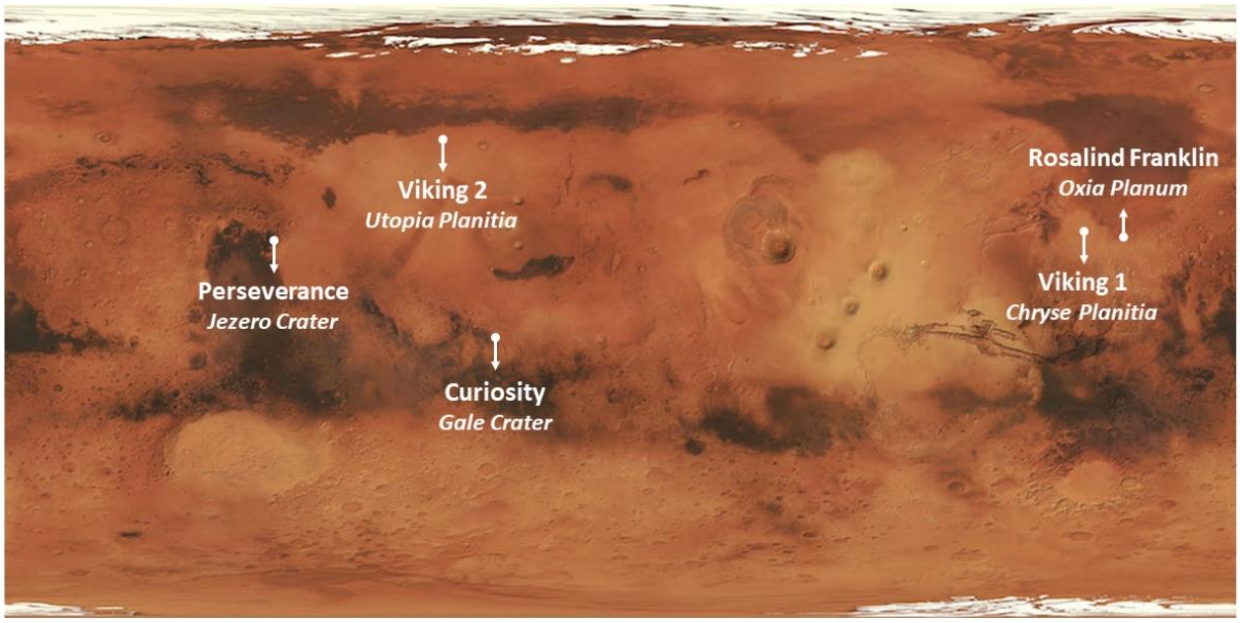

Figure 3: Landing sites of the Viking, Curiosity, Perseverance, and Rosalind Franklin landers on Mars.

The two landing sites chosen for the Viking missions, *Chryse Planitia* and *Utopia Planitia* (Figure 3), were carefully selected based on a number of scientific and engineering considerations.

Chryse Planitia was chosen as the landing site for the Viking 1 lander due to its flat, relatively rock-free terrain and what appeared to be a dry riverbed. The riverbed suggested that liquid water may have once flowed on the surface of Mars, making the site a promising location to search for signs of past or present life (Masursky & Crabill, 1976b). The site was also located near the Martian equator, providing enough sunlight for the lander's solar panels and allowing communication with Earth throughout the day.

For similar reasons, *Utopia Planitia* was chosen as the landing site for the Viking 2 lander. The site had a relatively flat terrain with few large rocks or hazards, making it a safe and stable landing location. The area was also of scientific interest, as it was known to have a thick layer of dust covering the surface, which could provide valuable insights into the planet's geology and history (Masursky & Crabill, 1976a).

2.2.2.1.1.3. Discoveries

Two surface samples were collected from each lander to be analyzed by GC-MS. One of the samples collected from the *Chryse Planitia* region by the Viking Lander 1 (VL-1) revealed traces of chloromethane (15 ppb) and perfluoroethers of the freon E-type (1-50 ppb) (Biemann, 1976). These species were previously encountered in pre-flight and cruise tests on Earth. While the authors emitted no doubt on the terrestrial origin of the freon-E compounds, they agreed that the chloromethane could conceivably be indigenous to Mars. However, the lack of related compounds such as ethyl chloride or methyl bromide, led to the conclusion that the chloromethane came from terrestrial sources as well such as chlorinated solvents or from adsorbed traces of methanol and Hydrogen Chloride (HCl) (Biemann et al., 1977).

Samples collected from the *Utopia Planitia* region by the Viking Lander 2 (VL-2) revealed the presence of chloromethane and perfluoroethers as well as other organic molecules like acetone, benzene, toluene, xylene and alkyl benzene (C_3) (Biemann et al., 1977). All these compounds matched with those detected in the cruise experiments,

at the exception of chloromethane. Their quantities varied but remained at similar levels as in the blank experiment. Therefore, none of the gas-chromatogram peaks observed were considered to be due to compounds indigenous to the Martian soil sample. Moreover, traces of dichloromethane were detected from the second sample analyzed by VL-2, but since this was a common laboratory solvent used in the cleaning of the gas-chromatograph system, it was considered a terrestrial contaminant although it had not been detected at those levels in the blank run.

The authors concluded that no organic endogenous molecules were present in the samples analyzed at both locations. However, the absence of organic matter on Mars came as a surprise. Indeed, even by assuming that no process has ever occurred to generate organic matter at the surface of the planet, or that none of the organic molecules possibly present in the material from the planet's formation survived, one must admit that organic molecules present in exogenous sources (meteoritic material, interplanetary dust particles (IDPs), and larger volatile-rich impactors such as comets or carbonaceous asteroids) must be arriving at the surface of Mars. Ultimately, the conclusion reached by the scientists was that if organic materials were present in the sample analyzed, they must have been below the detection limit of the GC-MS instruments.

However, the Viking landers' GC-MS system, still provided important insights into the chemical composition of the Martian environment. The system was able to provide valuable information about the presence of inorganic compounds in the Martian atmosphere and soil, paving the way for future missions to explore the red planet. Indeed, the GC-MS instrument gave a precise and definitive analysis of the composition of the Martian atmosphere and found previously undetected trace elements. For example, Nitrogen, never before detected, was found to be a significant component of the Martian atmosphere (2.5 %) (Klein, 1979) and surface. This discovery eased the prospects for complex organic chemistry on Mars.

Moreover, other instruments provided information that was later used to explain

results from the Viking GC-MS instrument and to interpret *in situ* data of later mission such as Curiosity (see after). Information concerning the inorganic content of the Martian surface material was also delivered by the Viking X-Ray fluorescence experiment (Toulmin III et al., 1973). Among the inorganic phases detected at both landing sites, three are of particular interest for this thesis: Mg (5%), Ca (3.6 – 4.0 %) and Cl (0.6 – 0.9 %). The overall interpretation of these data were construed as indicating that the Martian surface was a mixture of iron-rich clay (smectite), magnesium sulfate, iron oxides and carbonates (Baird et al., 1976; Toulmin III et al., 1977). The presence of such materials on Mars, in particular clays, was exciting as they have been found to provide effective catalytic properties for the formation of complex organic compounds in laboratory experiments (Paecht-Horowitz, 1971), and that they could ensure the survivability of microorganisms under Martian conditions (Moll & Vestal, 1992). The Gas Exchange (GEX) experiment also suggested the presence of a highly oxidizing substance that releases oxygen when exposed to a water saturated atmosphere (Klein et al., 1976).

Overall, while it found no traces of life or organic matter, Viking 1 and 2 did help better characterize Mars as a cold planet with volcanic soil, a thin, dry carbon dioxide atmosphere and striking evidence for ancient river beds and vast flooding. Certain findings turned out to be critical for the understanding and study of organic matter in future space missions and the interpretation of *in situ* data.

2.2.2.1.1.4. Reconsideration of the Viking data and implications for the future detection of Martian organic content

In 2006, a study by Navarro-Gonzàlez et al., comparing the pyrolysis GC-MS and the total organics for a variety of Mars analogue soils, provided some explanations on why the Viking instruments may have been blind to organics. They showed that organic detectability significantly decreased when processed by pyrolysis due to the catalytic oxidation of the organics in CO_2 by the iron oxides present in the soil. Moreover, the detectability of organic material was reduced by a factor of > 10^3 by pyrolysis

compared with extraction by organic solvents and that for low-volatile compounds, the temperature reached by the Viking instruments (maximum 500 °C) might be inadequate to release refractory substances.

The formation of refractory compounds on Mars that would be mostly undetectable by the Viking GC-MS experiments, was also proposed by Benner et al., in 2000. The authors suggested that the oxidative and radiative environment of the planet would result in non-volatile salts of benzocarboxylic acids such as benzoates or phthalates.

Moreover, motivated by the discovery of perchlorates in the northern plains of the Vastitas Borealis by the Phoenix Lander (0.4 - 0.6 %) (Hecht et al., 2009), Navarro-González et al. (2010) revisited the Viking data and reanalyzed the results. Laboratory experiments on analogue samples mixed with magnesium perchlorate heated at 500 °C led to the formation of chloromethane and dichloromethane. Both species, detected by the Viking landers, have been considered terrestrial contaminants, although they had not been observed at those levels in the blank runs. Navarro-Gonzàlez et al. (2010) study concluded that the detection of chlorohydrocarbons by VL-1 and VL-2 could, therefore, be due to the interaction of perchlorates and organics in the soil sample during pyrolysis-GC-MS analysis. This reinterpretation of the Viking results has significant implications for our understanding of the potential for life on Mars. The presence of organic molecules is a key indicator of the possibility of life, and the fact that they may have been present on Mars all along suggests that the planet may have been habitable in the past. Additionally, the discovery of chlorinated compounds on Mars has important implications for the search for life on other planets. It suggests that the presence of inorganic phases like perchlorates may complicate the detection of organic molecules, and that future missions to Mars will need to take this into account when searching for organic molecules and biosignatures.

Finally, in 2018 the reexamination of the original, microfilm preserved, Viking GC-MS data sets (Guzman et al., 2018) led to the formal identification of chlorobenzene as likely coming from indigenous organic material to the Martian surface. Indeed,

evidences for the presence of the chlorinated organic in VL-2 data at levels corresponding to 0.08 to 0.10 ppbw were detected and the temperature range of the chlorobenzene release coincided with the temperature range where oxychlorine compounds break down, rather than with the temperature range of terrestrial sources. Based on this evidence, and the fact that there was no chlorobenzene detected in the VL-1 GC-MS, which followed the same cleaning procedure, the authors concluded that the source of chlorine in VL-2 was Martian.

2.2.2.1.2. Mars Science Laboratory (MSL) (2011- ongoing)

2.2.2.1.2.1. Scientific goals

The Curiosity rover from NASA's Mars Science Laboratory (MSL) mission was launched in November 2011 with the goal of exploring Mars and assessing the planet's potential to support life, both past and present. Since landing on the Red Planet in 2012, Curiosity has sent back numerous data and images, enabling a detailed understanding of Mars' geological, chemical, and atmospheric makeup.

The MSL mission significantly differs from previous Mars missions regarding its size, scope, and scientific objectives. The rover's size is the most important difference between the MSL mission and its predecessors. Curiosity is the largest and most advanced rover ever sent to another planet. Its size allowed the rover to carry a suite of sophisticated scientific instruments that enabled it to analyze the Martian environment in unprecedented details.

The scientific objectives of the MSL mission were to determine if Mars was, or is, habitable and to assess its geologic history. The rover's primary mission is to explore the Gale Crater. The crater is home to a mountain called Mount Sharp, which is the primary target of the MSL's exploration efforts. Mount Sharp contains sedimentary rocks exposed to erosion, giving scientists a unique window into Mars' geological history. The rover's sophisticated scientific instruments can analyze these rocks' composition and structure to determine their origin and potentially uncover evidence

of past or present microbial life.

The MSL mission has already achieved many significant milestones since its launch, including its successful landing on Mars, and the rover's extensive exploration of the Gale Crater. One of the most notable achievements of the MSL mission was the first certain identification of organic molecules in Martian rocks, indicating that Mars may have had the necessary building blocks for life at some point in its history. The MSL mission also discovered that Mars had a much more hospitable environment in the past, with flowing water and a thicker atmosphere, suggesting that the planet may have been capable of supporting life.

2.2.2.1.2.2. Landing site: Gale Crater

Gale Crater is a large impact crater located near the Martian equator (Figure 3), which provided the rover with sufficient sunlight for its power needs and communication with Earth. The crater is approximately 154 kilometers in diameter and contains a large mountain in the center, known as Mount Sharp or Aeolis Mons. The mountain is of particular scientific interest because it contains layers of sedimentary rock that may provide valuable insights into the history and evolution of Mars (Golombek et al., 2012; Wray, 2013).

The selection of Gale Crater was also based on its geological and environmental characteristics. The crater was chosen because it is thought to have once contained several geologic features such as a large lake, channels and alluvial fans, suggesting that liquid water may have once flowed on the surface thus, providing a habitable environment for microbial life (Golombek et al., 2012).

2.2.2.1.2.3. Discoveries

In 2015, Freissinet et al. reported for the first time the definitive identification of chlorinated organic molecules with the Sample Analysis at Mars (SAM) instrumental suite in the Cumberland (CB) samples from the Sheepbed mudstone at Gale Crater. Organic molecules such as chlorobenzene (150 to 300 parts per billion per weight

(ppbw)) and trace levels of dichloropropane (up to 70 ppbw), dichloroethane and dichlorobutane isomers (below the quantification limit), were identified by GC-MS and Evolved Gas Analysis (EGA). The elevated levels of chlorobenzene and dichloroalkanes could not be solely explained by instrument background sources which indicated that they were indigenous to the Martian surface or from the cross-interaction of Martian chlorine and organic carbon. Furthermore, the release of chlorine-containing hydrocarbons through thermal processes occurred around the same temperature range where an increase in O_2 and HCl was detected, presenting compelling evidence for the existence of an oxychlorine compound, such as perchlorate. Further analysis of the CB samples (Szopa et al., 2020) revealed the detection of new chlorinated molecules (dichlorobenzene isomers and trichloromethylpropane) as well as the confirmation of the detection of chlorobenzene previously reported (Freissinet et al., 2015). Laboratory experiments ruled out the SAM internal background as the origin of those compounds, thereby confirming that the molecules were indeed indigenous to the mudstone sample.

Eigenbrode et al. in 2018, reported the detection of more organic molecules by SAM using EGA and GC-MS. Diverse pyrolysis products, including thiophenic (thiophene, methylthiophene isomers, dimethylsulfide, methanthiol and possibly benzothiophene), aromatic (benzene, alkylbenzene, chlorobenzene and naphthalene) and aliphatic (C_2 to C_5) compounds released at high temperatures (500 to 820 °C) where detected in the lancrustine mudstone at the base of the ~ 3.5 billion-year-old Murray formation at Pahrump Hills in Gale Crater.

Moreover, a derivatization experiment using N-methyl-N-(tert-butyldimethylsilyl) trifluoroacetamide (MTBSTFA), a derivatization reagent (see chapter 2 section 1.4), was conducted by Curiosity when exploring Gale Crater's Vera Rubin Ridge. The sample named Ogunquit Beach (OG) from the Bagnold Dunes area, resulted in the identification of mass spectra belonging to various classes of compounds, including derivatized molecules (M Millan et al., 2022). Among the compounds detected,

chemically derivatized benzoic acid was identified. Benzoic acid is one precursor of chlorobenzene and could have been a contributor to the chlorobenzene detected by SAM in the CB mudstone sample (Freissinet et al., 2015; Szopa et al., 2020). Mass spectra matching derivatized phosphoric acid, phenol and several nitrogen-bearing molecules were also detected such as ammonia, HCN, derivatized isocyanate, isocyanomethane, trifluoroacetonitrile, aceto-nitrile, propenenitrile, propanenitrile, isobutyronitrile, butenenitrile, dimethylaminoacetonitrile and benzonitrile. The sources of these molecules were diverse, including: (1) breakdown products of larger and/or more intricate organic compounds originating from the sample itself, (2) byproducts of organic molecules reacting with inorganic phases like nitrate or phosphate during pyrolysis, (3) degradation products of MTBSTFA and/or DMF, and (4) products of the interaction between MTBSTFA and minerals present in the sample. Overall, this SAM derivatization experiment greatly improved our comprehension of the organic compounds present on the Martian surface.

Finally, the inorganic and organic chemical makeup of seven samples obtained from the clay-bearing unit in Glen Torridon were analyzed (M. Millan et al., 2022). The experiments conducted by SAM identified nitrogen-, oxygen-, and chlorine-containing molecules, as well as polycyclic aromatic hydrocarbons. Furthermore, these analyses revealed a greater variety and abundance of sulfur-containing aliphatic and aromatic organic compounds than previously analyzed samples. Some of these organic compounds were thought to be associated with chemical compounds present in the background of the SAM instrument. Still, the presence of sulfur-bearing organics released at high temperatures (≥600 °C) suggests that they likely originated from Martian or external sources aligning with refractory organic materials in the sample. The measurements carried out by SAM in the Glen Torridon clay-bearing unit helped expand the inventory of organic matter present in the Gale Crater and support the hypothesis that clay minerals played a crucial role in preserving ancient organic matter on Mars.

In conclusion, the discoveries made by the Curiosity rover on Mars have significantly advanced our understanding of the presence of organic matter on the Red Planet. Through the utilization of sophisticated instruments such as the SAM instrument suite, the rover has identified and characterized a diverse range of organic compounds, including the detection of sulfur-bearing aliphatic and aromatic compounds, nitrogen-containing molecules, chlorinated compounds and polycyclic aromatic hydrocarbons. These findings indicate the existence of a complex organic inventory on Mars, with implications for the planet's geological and environmental history, as well as its potential for habitability. Moreover, the rover's observations have provided valuable insights into the preservation of organic matter over long periods of time, particularly in association with clay-bearing units and ancient aqueous environments.

2.2.2.1.3. Mars 2020 (2020-ongoing)

2.2.2.1.3.1. Scientific goals

The NASA Mars 2020 mission to Mars launched on July 30, 2020, and landed successfully on Mars on February 18, 2021.

One of the primary objectives of the Mars 2020 mission with its Perseverance rover, is the search for signs of ancient microbial life. The rover's landing site, Jezero Crater, was chosen based on its potential as a site that once hosted a lake and a river delta. Such environments could have offered the necessary conditions for the emergence and preservation of microbial life. By analyzing the geological and mineralogical characteristics of the crater, Perseverance aims to identify biosignatures indicators of past life or the potential for life within the rock formations and sediments (Farley et al., 2020).

To achieve this objective, the mission is equipped with the Sample Caching System (SCS), a cutting-edge technology designed to collect and store rock and soil samples for future return to Earth (Moeller et al., 2021). Perseverance will gather samples using its drill and coring capabilities, carefully documenting each sample's location and

geological context. These samples will serve as a treasure trove for future analysis in laboratories on Earth, enabling scientists to employ advanced techniques not available *in situ* to search for definitive evidence of ancient microbial life.

In addition to the search for signs of past life, Perseverance aims to understand the geologic history of the planet and its potential for supporting future human exploration. The rover's instruments, including cameras, spectrometers, and ground-penetrating radar, will enable detailed mapping and analysis of the planet's surface, subsurface, and atmosphere (Bell et al., 2021). This information will contribute to our understanding of Mars' climate, water cycle, and the processes that have shaped its landscape over time.

Perseverance also carries a technology demonstration experiment known as MOXIE (Mars Oxygen In-Situ Resource Utilization Experiment) (Hoffman et al., 2022). MOXIE aims to demonstrate the production of oxygen from the thin Martian atmosphere, a crucial step towards enabling human missions to Mars in the future. This technology aims to pave the way for producing oxygen for life support systems, propulsion, and even the production of rocket fuel for return journeys from Mars.

Furthermore, the mission deployed the Ingenuity Mars Helicopter (Balaram et al., 2021), a small rotorcraft designed to test powered flight on another planet. The objective of this technology demonstration has been to assess the feasibility and potential of aerial exploration on Mars, which could revolutionize the way we explore the planet's vast terrains in the future.

2.2.2.1.3.2. Landing site: Jezero Crater

Jezero Crater was selected as the landing site for NASA's Perseverance rover based on several compelling factors (Figure 3). One key reason for choosing Jezero Crater is its geological and astrobiological significance. It is believed that Jezero Crater was once home to a lake and a river delta, making it an intriguing location to investigate the potential for past habitability and the preservation of biosignatures (Horgan et al.,

2020). The presence of these features indicates the past presence of liquid water (Goudge et al., 2015; Schon et al., 2012). The interactions between water, sediments, and minerals in such environments offer excellent opportunities for the accumulation and preservation of evidence related to potential ancient microbial life.

The crater itself also exhibits diverse geological features that are of scientific interest. The varied terrain, including ancient river channels, delta deposits, and exposed bedrock, provides a great opportunity to study the history and processes that shaped Mars' surface.

2.2.2.1.3.3. Discoveries

The first results obtained with the Scanning Habitable Environments with Raman and Luminescence for Organics and Chemicals (SHERLOC) instrument onboard the Perseverance rover, revealed fluorescent signatures consistent with aromatic organic molecules (Scheller et al., 2022). The observed fluorescence patterns in three of the analyzed samples are compatible with aromatic organic compounds containing either one or two fused aromatic rings or aromatic heterocycles. Although it is impossible to conclusively determine the exact organic compounds based on the fluorescence signatures, the results indicate naphthalene and benzene-like structures in the 340 nm and 275-285 nm fluorescence range, respectively. The Raman experiments did not reveal the characteristic bands of organic molecules, such as the C=C stretching mode. The authors suggested that the organic concentrations in the samples were too low to be detected by the instrument as the intensity of Raman scattered light is significantly lower, by several orders of magnitudes, compared to fluorescence. Overall, the conclusion of these first investigations by the SHERLOC instruments was that the presence of fluorescence signatures that align with organic compounds in these materials suggested a complex relationship between igneous rocks, aqueous alteration processes, and organic matter on Mars.

2.2.2.1.4. ExoMars (schedule for 2028)

2.2.2.1.4.1. Delays

The ExoMars mission, a joint venture between the European Space Agency (ESA) and, until recently, the Russian space agency Roscosmos, has been a long and tumultuous journey. Originally planned for a 2011 launch, the mission has experienced multiple delays and setbacks that have pushed back its launch date by several years.

One of the main challenges faced by the ExoMars mission was the development of the necessary technology to make the mission possible. The mission's primary objective is to search for signs of life on Mars, a daunting task that requires advanced scientific instruments and cutting-edge technology. The development of these instruments and the necessary spacecraft components took longer than expected, leading to delays in the mission's launch.

In 2018, the mission suffered another setback when the parachute system designed to slow the lander's descent to the Martian surface failed during a test. This failure resulted in a delay of the second phase of the mission, which was originally scheduled for 2020.

In 2020, the mission's launch was postponed once again due to the COVID-19 pandemic, as travel restrictions and social distancing measures made it difficult for scientists and engineers to work together on the project.

Finally, in 2022, the war opposing Russia and Ukraine led ESA to sever all ties with the Russian Space Agency. Because the lander was constructed by Roscosmos, new plans, possibly with NASA, to build a new lander is under discussion. The mission is again postponed to 2028.

Despite these setbacks, the ExoMars mission remains one of the most ambitious and exciting missions in the history of space exploration. If successful, the ExoMars mission could provide a wealth of information about the history and evolution of our neighbouring planet, and offer valuable insights into the origins and evolution of life

in the universe.

2.2.2.1.4.2. Scientific goals

By studying the chemical composition of the Martian soil and atmosphere, and by analyzing the weather patterns and environmental conditions on Mars, the ExoMars mission hopes to shed light on the potential habitability of Mars and the possibility of finding signs of life on the red planet. The discovery of biosignatures would be a significant step towards this goal.

The ExoMars Rosalind Franklin mission is unique in several ways. Firstly, it is the first Mars mission to be designed and led by the European Space Agency (ESA). Secondly, the mission is the first to be specifically dedicated to the search for biosignatures on Mars. Previous Mars missions, such as NASA's Mars rovers Spirit, Opportunity, and Curiosity, have focused on understanding the geology, climate and habitability of the planet.

In addition to its scientific goals, the ExoMars Rosalind Franklin mission also aims to demonstrate advanced technologies for future space exploration. For example, one of the key features of Rosalind Franklin is its ability to drill to a depth of up to two meters below the Martian surface to collect samples (Vago et al., 2015; Zacny et al., 2008). This is a significant improvement over the capabilities of the other rovers and landers, which could only analyze samples collected from the surface. The Rosalind Franklin's drill system is designed to collect samples from different depths in the Martian regolith, allowing for a better understanding of the geological history of the planet. The drill system can also extract samples from areas that have been shielded from radiation, which may preserve organic molecules that have been destroyed on the surface.

The ExoMars mission is expected to provide a wealth of new information about Mars and its potential for supporting life by analyzing the chemical and mineralogical properties of rocks and soil on the Martian surface and subsurface. The mission will also pave the way for future Mars exploration, demonstrating new technologies and

techniques that will enable more sophisticated missions in the future.

2.2.2.1.4.3. Landing site: *Oxia Planum*

Oxia Planum is located in a region of Mars where multiple channels emptied into the vast lowland plains on Mars (Figure 3). It is an area where layers of clay-rich minerals were formed about four billion years ago, during a wet period, most likely in a large body of standing water. The channels that carried material into the lower-elevation 'sink' region, where the landing ellipse is located, cover an area of approximately 200 km wide terrains (Ivanov et al., 2020). Any of the touchdown points provide access to layers of material that have recently been exposed through erosion, offering a glimpse into the early history of the area, believe to date from the Noachian age.

The minerals found in *Oxia Planum* are similar to those found in a large area surrounding the region, making it possible to gain insights into the conditions experienced on a global scale. This can help constrain the climate and habitability potential of Mars during this period.

A variety of wet episodes occurred in the region, followed by late volcanic activity that covered the clay-rich deposits (Ivanov et al., 2020; Quantin et al., 2016). Some of the lava material has not eroded, which means the underlying materials may have been exposed only recently (Quantin et al., 2016). This initial protection from space radiation and subsequent accessibility to the rover's analytical tools make this region of interest for scientific investigation and the search for signs of past or present microbial life.

In addition to its scientific interest, *Oxia Planum* was chosen for its relatively flat and safe terrain. The site has a low altitude, which reduces the amount of atmosphere that the rover must pass through during landing and therefore reduces the risk of landing complications. The terrain is also relatively free of large rocks and hazards, making it a stable and safe location for the rover to land and operate.

2.2.2.2. Factors influencing the detection of organic matter on Mars

The detection of organic matter on the surface of Mars is a challenging task due to various factors that can complicate the process.

Sample analysis and processing:

Miniaturization, real-time measurements, automation, low power consumption and reliability of operation under extreme conditions are some of the major challenges that analytical chemistry has faced as a result of the technological and scientific requirements of space missions. With time, space exploration has been using increasingly better technology to face increasingly more challenging goals and traditional analytical techniques have been adapted to the era of *in situ* space exploration. However, several factors are still impacting the detection and interpretation of organic molecules *in situ* as seen previously with the Viking (see section 2.2.2.1.1.3.) and MSL (see section 2.2.2.1.2.3.) missions:

- **Chemical reactions.** High-temperature pyrolysis or thermochemistry performed by analytic chemistry laboratories onboard Martian surface probes, can lead to thermal degradation of organic molecules or oxidation. These reactions can occur during sample collection or analysis, leading to the loss or modification of the target molecule.
- **Low concentrations** of organic compounds that are below the sensitivity of the onboard instruments.
- **Contamination**. If organic molecules are found on Mars, it is important to ensure that they are not the result of contamination from Earth. The detection process must be designed to avoid any contact with potential contaminants.
- **Signal Interpretation**. The interpretation of the data can be challenging. Organic molecules can be complex and diverse, making it difficult to determine their origin and significance. Careful analysis and comparison to known standards are crucial for accurate interpretation of the data.

Martian surface conditions:

Moreover, as mentioned previously, today the surface of Mars present much more harsh environmental conditions than in its early history with factors influencing the preservation and survivability of organic molecules.

- **The radiative environment**. Mars is exposed to a complex radiative environment associated with the destruction or transformation of surface organic compounds (e.g. (Fox et al., 2019; Pavlov et al., 2012; Yang et al., 2020).
- **Harsh climate**. Mars has a harsh, dry and cold environment with an average temperature of -60 °C throughout the year (McKay, 2009). This makes it difficult for organic molecules to survive.
- **Thin atmosphere**. Mars has a very thin atmosphere (Jakosky et al., 2017), which is only about 1% of the Earth's atmosphere. This creat challenges in protecting organic molecules from harmful solar radiations and prevents water to persist in its liquid state (Jakosky, 2022).
- **Oxidizing environment**. Mars has a highly oxidizing environment, due to the presence of perchlorates and other oxidizing agents in the soil like iron oxide. This means that organic molecules on the surface of Mars can be easily degraded by oxidation, which can break chemical bonds and alter the structure of the molecules (Lasne et al., 2016). This can pose a greater challenge to detect organic molecules on Mars, as they may be too degraded to be recognizable.
- **Mineralogy**. The mineral composition of the Martian surface can also affect the preservation of organic molecules (Fornaro, Steele, et al., 2018). Some minerals can protect organic molecules from degradation by shielding them from radiation or providing a stable environment. Other minerals can interact with organic molecules and cause them to break down more quickly.

These factors need to be taken into account when analysing the surface of Mars for the detection of organic matter and make accurate interpretation of the *in situ* data collected by the probes.

2.2.2.2.1. The radiative environment on the surface of Mars

A critical factor determining a planet's habitability is its radiation environment, which can affect the stability and formation of organic molecules. These radiation conditions can cause various chemical reactions that either facilitate or hinder the formation and preservation of organic molecules on the Martian surface. Thus, understanding the radiation environment on Mars and its implications for the search for organic matter is crucial for determining the planet's habitability potential.

2.2.2.2.1.1. General context of the Mars radiation environment

Several types of radiative energy impact the Martian surface:

- *Solar radiations* which is the energy that the Sun emits in the form of electromagnetic radiation, including visible light, ultraviolet radiation, and infrared radiation (Appelbaum et al., 1993). Solar radiation is constantly present and varies over time due to the Sun's activity. During its closest approach to the sun (perihelion), Mars receives about twice the amount of solar radiation as it does at its farthest point (aphelion) (Zeitlin et al., 2013). Solar radiation typically penetrate the first surface layers (µm to mm) (Figure 4).
- *Solar Energetic Particles (SEPs)* generated in the solar corona during high-energy events like flares, coronal mass ejections, and their associated shocks. SEP occurrences are infrequent and unpredictable, with onset times lasting minutes to hours and durations of hours to days (Dartnell et al., 2007; Hassler et al., 2013). SEPs travel farther in the Martian layers than solar radiation, up to a meter (Figure 4).
- *Galactic Cosmic Rays (GCRs)*, high-energy particles that originate from outside the solar system. These particles can penetrate deep into the Martian

atmosphere and deposit their energy into the surface materials, creating secondary particles that can contribute to the radiation dose received by equipment on the surface. Unlike solar energetic particles, which are sporadic and short-lived, cosmic rays are a constant source of radiation (Hassler et al., 2013). GCRs can penetrate the Martian surface up to several meters (~2 meters) (Figure 4).

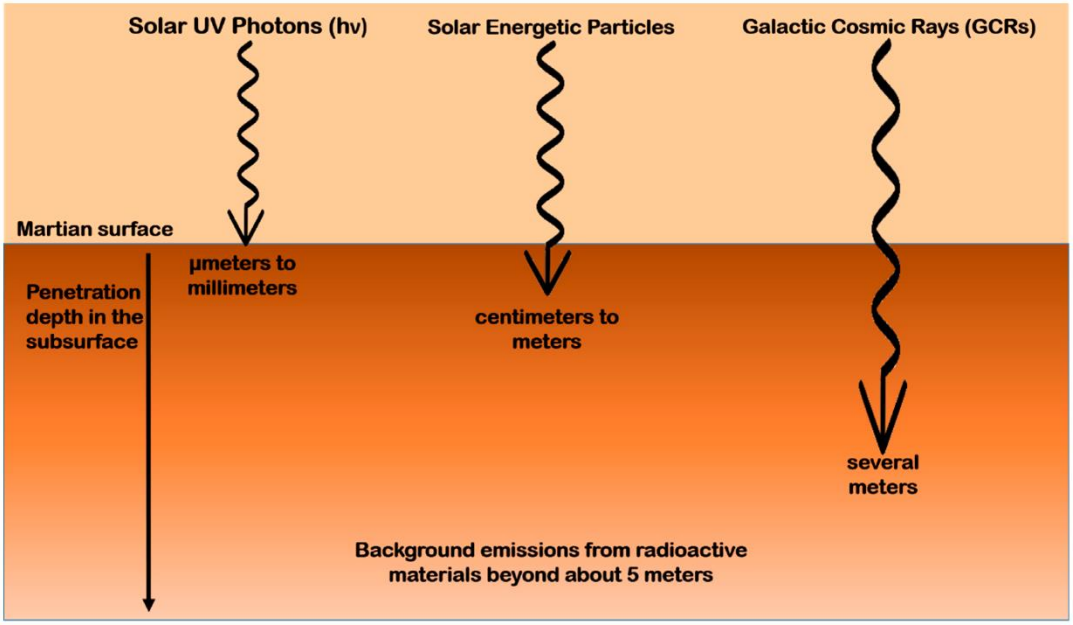

Figure 4: Penetration depths of different kinds of radiation in the near-surface of Mars. From Fornaro et al. (2018).

2.2.2.2.1.2. Implications for the search of organic matter on Mars

In recent years, several studies have been conducted to investigate the effects of these radiations on the formation and preservation of organic molecules. Understanding the chemical evolution of organic species under Martian environmental conditions is essential to target samples for analyses *in situ* during exploration missions.

2.2.2.2.1.2.1. Ultraviolet incidence on organic molecules on Mars

A study by Poch et al. (2014) investigated the chemical and kinetic evolution of several organic molecules under simulated Mars surface UV radiation conditions. The results showed that the UV radiation caused significant changes in the molecular structure and

composition of the organic compounds, with two major evolution pathways leading to the formation of new compounds and the degradation of others. Adsorption of UV photons can be comparable to the bond energy (~ 10 eV) of the target organic compound (Pavlov et al., 2012), causing electronic excitation and photochemical reactions (Fornaro et al., 2020). After the parent molecules undergo photolysis, certain compounds can generate fragments that have the ability to reconfigure or interact with their surroundings, resulting in the formation of new molecules. These findings indicate that certain organic molecules on the surface of Mars can maintain their stability against UV radiation over extended periods. Additionally, solar radiation in the presence of atmospheric oxygen serves as a potent oxidizing agent, leading to the degradation of organic molecules and their conversion into carbon dioxide (Knoevenagel and Himmelreich, 1976).

Other studies have been conducted to simulate SEPs and GCRs radiations by bombarding Mars analogue samples doped with organic compounds with high-energetic particles (Fox et al., 2019). However, previous and ongoing Mars missions have been examining samples from the topmost layer of the surface reaching depths of a few millimeters or centimeters (Abbey et al., 2019; Moeller et al., 2021). This layer is where organic matter is most susceptible to UV light exposure as the SEPs and GCR's radiations are affecting deeper layers of the Martian sub-surface (Figure 4). Consequently, investigations into the effects of UV radiation on organic molecules within the Martian environment have been crucial for interpreting the *in situ* data gathered by these probes. Moreover, the molecular evolution induced by UV radiations occurs at very short time scales on Mars, compare to SEPs and GCRs with a time range of about 100 million years (Gerakines & Hudson, 2013; Pavlov et al., 2012), confirming that UV photons are likely to have a significant impact in the chemical processes occurring at the surface of Mars compared to SEPs and GCRs. In this thesis, we will, therefore, focus on the effect of UV light on organic molecules. That said, interpretation of the future data collected by the Rosalind-Franklin rover will require an understanding of the consequences of these SEPs and GCRs radiations as the rover's

drill will be able to collect samples in deeper layers of the surface, thus likely affected by SEPs and GCRs radiations.

2.2.2.2.1.2.2. Mineral and inorganic compounds influencing the interactions between the radiation and the organics

However, the influence of radiations on organic molecules is also dependent on a multitude of factors that can change the evolution pathway of organic compounds. Among which mineral and inorganic phases in which organics are imbedded on the Martian surface. Several studies, reviewed by Fornaro et al. in 2018, showed that minerals either have catalytic or protective properties towards radiation on organic compounds under Mars-like conditions by changing their reaction pathways.

Combined radiative and oxidative power of solar radiations was suggested to form stable organic salts (Benner et al., 2000; Oró, 1979). Metals associated with organic molecules can act as chemical catalysts, increasing molecular complexity but also contributing to their stability (Fioroni, 2021). These stable organometallic chemical systems could serve as significant intermediates upon which the selection process for future organic life took place. These compounds could thus, play a major role in prebiotic chemistry and the origin of life. However, the low volatility of such stable compounds may interfere with their detection (Benner et al., 2000).

2.2.2.2.2. The effect of the presence of inorganic salts in the detection of the organics

Salt: Salts are ionic compounds that contain positively charged ions (cations) and negatively charged ions (anions) held together by electrostatic forces.

Note: Zwitterions contain an anionic and cationic center in the same molecule but are not considered as salts (*e.g.* amino acids).

In addition to all the factors affecting the determination of organics on Mars, the discovery of chloride salts on the planet by several instruments at Gale Crater, where the rover Curiosity of the NASA's Mars Science laboratory (MSL) mission is exploring,

has made important to determine the influence of these salts on the detectability of organic compounds of astrobiological interest.

Salts are common compounds found in various forms on the surface of Mars. These salts have been a topic of interest, as they can provide valuable information about the planet's geology, chemistry, and potential habitability of the planet. The discovery of salt-rich deposits on the Martian surface points towards past aqueous processes (Glotch et al., 2010). While the current conditions on the Martian surface do not support the existence of liquid water (Haberle et al., 2001), there are processes such as mineral deliquescence that could allow for the formation of liquid water, at least transiently (discussed in section 2.2.1 of this chapter). The salts found on Mars are typically hygroscopic, meaning they can absorb and retain water vapor from the atmosphere (Tang et al., 1977), which has implications for the planet's water cycle and the possibility of liquid water on its surface.

The surface of Mars is known to contain various salts, which have been detected by a variety of orbital and surface probes sent to the red planet (Glavin et al., 2013; Langevin et al., 2005; Osterloo et al., 2008; Squyres et al., 2004; Vaniman et al., 2004). These salts include magnesium sulfate, calcium sulfate, perchlorate salts such as sodium, magnesium, and calcium perchlorates as well as chloride salts. The abundance of these salts varies across the planet and is influenced by factors such as temperature, humidity, and the presence of water.

2.2.2.2.2.1. Interest of chloride salts for Martian organic detection

Chlorine (Cl) has been recognize as an important chemical component of the Martian surface. Its concentration varied from 0.1 wt% at Chryste Planitia to 0.9 wt% at Utopia Planitia as determined by the Viking landers 1 and 2, respectively (Clark, 1981; Clark et al., 1976). At Ares Vallis the Pathfinder rover found Cl at 0.55 wt% (Foley et al., 2003; Wänke et al., 2001). In the equator, at Meridiani Planum, Cl concentrations were measured in the range 0.2 – 2.6 wt% by Opportunity (Rieder et al., 2004). However, so

far, most of the chlorine measurements and studies have been focusing on oxychlorine minerals such as perchlorates and chlorates. Their presence seem ubiquitous on Mars and they are believed to be the precursor of the chlorinated molecules detected on the Martian surface by the Viking landers (Guzman et al., 2018; Navarro-González et al., 2010) and the Curiosity rover (Freissinet et al., 2015; Szopa et al., 2020) (see sections 2.2.2.1.1.4. and 2.2.2.1.2.3., respectively). But recent measurements by the Sample Analysis at Mars (SAM) instrument suite, onboard the Curiosity rover, has brought to light the presence and hence, importance, of another chlorine-bearing mineral phase, chloride salts.

From an astrobiological point of view, chloride salts seem to be ideal targets and could play an important role in the origin and detection of life on Mars. Their crystalline surfaces could act as adsorption sites for the synthesis, concentration, polymerization, and organization of prebiotic molecules. They may also contain inclusions that could trap life and/or biomolecules from the evaporating aqueous phase (Rothschild & Mancinelli, 2001).

In terrestrial environments, continental evaporite ecosystems harbor abundant microbial colonizers that create enduring imprints through processes such as microbial lithification or the formation of minerals associated with microbial metabolisms (Barbieri & Stivaletta, 2011). Martian analogues of these environments could, therefore, be of interest in the search for signs of life on Mars.

One of the key ways in which chloride salts can preserve organic compounds is by lowering the freezing point of water. On Mars, liquid water is not stable on the surface, but it can exist in the form of brines-solutions of water and salts that remain liquid at lower temperatures (Brass, 1980). The presence of chloride salts in these brines can protect organic compounds from degradation by freezing and thawing cycles, which would otherwise destroy them (Heinz et al., 2019). This property can also allow salts to act as time capsules and unravel environmental factors such as temperatures, pH, composition of the brines and most importantly in our study, microorganisms or

biosignature molecules.

Traces of microbial life preserved in ancient salt deposits may be recognized through diagnostic biomarkers such as lipids, alcohol and alkenone fractions, and hydrocarbons (e.g. (Bühring et al., 2009; Fourçans et al., 2004; Jahnke et al., 2008). These biomarkers have a high preservation potential, going back as far as the Archaean (Brocks et al., 1999), and can allow for the recognition of original compounds even after diagenetic alteration (Seewald, 2001). Amino acids and products of amine degradation have been detected in fossil evaporites and could be useful in the search for evidence of life on Mars (Aubrey et al., 2006), especially in cases where biological signatures are expected to be low such as on Mars (Skelley et al., 2005). Furthermore, chloride salts can also protect organic compounds from the harsh radiation environment on Mars (Barbieri & Stivaletta, 2011). This protection can extend the lifetime of organic compounds on the Martian surface, increasing the chances of detecting them with future rovers and landers.

The implications of detecting chloride salts on Mars are not limited to the search for life. These salts are also important for understanding the geochemistry of Mars and its history of water activity.

However, other than the information gathered from environment studied on Earth we do not have much knowledge on the influence of chloride salts on organic molecules in Mars environmental conditions. Moreover, previous studies on other type of chlorine salts, more specifically oxychlorines such as perchlorates and chlorates, demonstrated that the interactions of organic compounds with inorganic material during *in situ* analysis performed by the Martian rovers, influence the comprehension of the results (Millan et al., 2019).

3. OBJECTIVES

The main objective of this Ph.D. thesis is to search for the signatures of organic molecules in *in situ* analyses, identify them and study their fate under Mars

instrumental and surface conditions in the presence of salts. Overall, this thesis will aim to expand our knowledge and comprehension of the possible interactions between organic molecules and salts on Mars.

Specifically, I chose to work on chloride salts as they have been detected on the Martian surface by orbiters (Osterloo et al., 2008) , but also at Gale Crater by the Curiosity rover (Thomas et al., 2019). As described above, they also seem to be excellent candidate for the preservation of organic molecules. The aim of this thesis was to determine the influence of these salts on the survivability and detectability of different organic molecules of astrobiological interest: amino acids, carboxylic acids, and Polycyclic Aromatic Hydrocarbons (PAHs).

In Chapter 3, I first evaluate chloride salts' catalytic/protective behavior towards different organic molecules under UV irradiation. I studied the kinetic degradation profile of characteristic bands of each molecule by infrared spectroscopy. The results of this study intend to help choose potential samples to perform analytical chemistry experiments on. If chloride salts help preserve the integrity of organic molecules under UV radiations, they could constitute good analytical targets for *in situ* analysis. On the other hand, if salts degrade the organic content through photocatalysis, they should be avoided for *in situ* analysis targeting organic matter.

Chapter 4 aims at determining the influence of chloride salts on organic molecules during *in situ* analysis as performed by the analytical chemistry instruments onboard Martian rovers such as Viking, Curiosity, and Rosalind Franklin. Understanding how these inorganic salts behave when interacting with organic compounds during analytical chemistry experiments is crucial. The results are devoted to help interpreting *in situ* data provided by the rover's instruments and offer information on the organic and inorganic content of the samples collected and analyzed *in situ*.

Finally, in Chapter 5, I present pyrolysis- and derivatization-GC-MS experiments conducted on organic salts. Organic salts were suggested to be the product of the

degradation of organic molecules from the radiative and oxidative conditions on Mars. Metal-bound organic complexes are highly interesting as they might form ubiquitously on Mars through several environmental factors. Moreover, if present, their low volatility can make them difficult to detect through *in situ* analysis, hence the importance to understand their behavior under analytical conditions as performed by the Martian rovers.

Laboratory measurements play a critical role in improving our understanding of the Martian environment and the *in situ* measurements provided by rovers. By analyzing samples and conducting experiments in a controlled environment, we can gain insights into the complex interactions between the Martian atmosphere, geology, and chemistry. These measurements allow to better interpret the data collected by rovers on the surface of Mars and to develop more accurate models of the Martian environment. Furthermore, laboratory measurements provide a means to test hypotheses and explore new avenues of research that may not be feasible with current space technology. As we continue to explore Mars and search for signs of past or present life, it is essential that we make use of all available tools to enhance our understanding of this fascinating planet.

REFERENCES

Abbey, W., Anderson, R., Beegle, L., Hurowitz, J., Williford, K., Peters, G., Morookian, J. M., Collins, C., Feldman, J., & Kinnett, R. (2019). A look back: The drilling campaign of the Curiosity rover during the Mars Science Laboratory's Prime Mission. Icarus, 319, 1-13.

Appelbaum, J., Landis, G. A., & Sherman, I. (1993). Solar radiation on Mars—Update 1991. Solar Energy, 50(1), 35-51. https://doi.org/10.1016/0038-092x(93)90006-a

Arvidson, R. E. (2016). Aqueous history of Mars as inferred from landed mission measurements of rocks, soils, and water ice. Journal of Geophysical Research: Planets, 121(9), 1602-1626. https://doi.org/10.1002/2016je005079

Balaram, J., Aung, M., & Golombek, M. P. (2021). The Ingenuity Helicopter on the Perseverance Rover. Space Science Reviews, 217(4). https://doi.org/10.1007/s11214-021-00815-w

Barbieri, R., & Stivaletta, N. (2011). Continental evaporites and the search for evidence of life on Mars. Geological Journal, 46(6), 513-524. https://doi.org/10.1002/gj.1326

Bell, J. F., Maki, J. N., Mehall, G. L., Ravine, M. A., Caplinger, M. A., Bailey, Z. J., Brylow, S., Schaffner, J. A., Kinch, K. M., Madsen, M. B., Winhold, A., Hayes, A. G., Corlies, P., Tate, C., Barrington, M., Cisneros, E., Jensen, E., Paris, K., Crawford, K., Rojas, C., Mehall, L., Joseph, J., Proton, J. B., Cluff, N., Deen, R. G., Betts, B., Cloutis, E., Coates, A. J., Colaprete, A., Edgett, K. S., Ehlmann, B. L., Fagents, S., Grotzinger, J. P., Hardgrove, C., Herkenhoff, K. E., Horgan, B., Jaumann, R., Johnson, J. R., Lemmon, M., Paar, G., Caballo-Perucha, M., Gupta, S., Traxler, C., Preusker, F., Rice, M. S., Robinson, M. S., Schmitz, N., Sullivan, R., & Wolff, M. J. (2021). The Mars 2020 Perseverance Rover Mast Camera Zoom (Mastcam-Z) Multispectral, Stereoscopic Imaging Investigation. Space Science Reviews, 217(1). https://doi.org/10.1007/s11214-020-00755-x

Benner, S. A., Devine, K. G., Matveeva, L. N., & Powell, D. H. (2000). The missing organic molecules on Mars. Proceedings of the National Academy of Sciences, 97(6), 2425-2430. https://doi.org/10.1073/pnas.040539497

Benner, S. A., Ricardo, A., & Carrigan, M. A. (2004). Is there a common chemical model for life in the universe? Current opinion in chemical biology, 8(6), 672-689.

Bibring, J.-P., Langevin, Y., Mustard, J. F., Poulet, F., Arvidson, R., Gendrin, A., Gondet, B., Mangold, N., Pinet, P., & Forget, F. (2006). Global mineralogical and aqueous Mars history derived from OMEGA/Mars Express data. Science, 312(5772), 400-404.

Breezee, J., Cady, N., & Staley, J. (2004). Subfreezing growth of the sea ice bacterium "Psychromonas ingrahamii". Microbial Ecology, 47, 300-304.

Chevrier, V. F., Hanley, J., & Altheide, T. S. (2009). Stability of perchlorate hydrates and their liquid solutions at the Phoenix landing site, Mars. Geophysical Research Letters, 36(10).

Cockell, C. S., Bush, T., Bryce, C., Direito, S., Fox-Powell, M., Harrison, J. P., Lammer, H., Landenmark, H., Martin-Torres, J., & Nicholson, N. (2016). Habitability: a review. Astrobiology, 16(1), 89-117.

Cull, S., Arvidson, R. E., Mellon, M. T., Skemer, P., Shaw, A., & Morris, R. V. (2010). Compositions of subsurface ices at the Mars Phoenix landing site. Geophysical Research Letters, 37(24), n/a-n/a. https://doi.org/10.1029/2010gl045372

Dartnell, L. R., Desorgher, L., Ward, J. M., & Coates, A. J. (2007). Martian sub-surface ionising radiation: biosignatures and geology. Biogeosciences, 4(4), 545-558. https://doi.org/10.5194/bg-4-545-2007

Dundas, C. M., Bramson, A. M., Ojha, L., Wray, J. J., Mellon, M. T., Byrne, S., McEwen, A. S., Putzig, N. E., Viola, D., & Sutton, S. (2018). Exposed subsurface ice sheets in the Martian mid-latitudes. Science, 359(6372), 199-201.

Dundas, C. M., McEwen, A. S., Chojnacki, M., Milazzo, M. P., Byrne, S., McElwaine, J. N., & Urso, A. (2017). Granular flows at recurring slope lineae on Mars indicate a limited role for liquid water. Nature Geoscience, 10(12), 903-907.

Eigenbrode, J. L., Summons, R. E., Steele, A., Freissinet, C., Millan, M., Navarro-González, R., Sutter, B., McAdam, A. C., Franz, H. B., Glavin, D. P., Archer, P. D., Mahaffy, P. R., Conrad, P. G., Hurowitz, J. A., Grotzinger, J. P., Gupta, S., Ming, D. W., Sumner, D. Y., Szopa, C., Malespin, C., Buch, A., & Coll, P. (2018). Organic matter preserved

in 3-billion-year-old mudstones at Gale crater, Mars. Science, 360(6393), 1096-1101. https://doi.org/10.1126/science.aas9185

Farley, K. A., Williford, K. H., Stack, K. M., Bhartia, R., Chen, A., Manuel, Hand, K., Goreva, Y., Herd, C. D. K., Hueso, R., Liu, Y., Maki, J. N., Martinez, G., Moeller, R. C., Nelessen, A., Newman, C. E., Nunes, D., Ponce, A., Spanovich, N., Willis, P. A., Beegle, L. W., Bell, J. F., Brown, A. J., Hamran, S.-E., Hurowitz, J. A., Maurice, S., Paige, D. A., Rodriguez-Manfredi, J. A., Schulte, M., & Wiens, R. C. (2020). Mars 2020 Mission Overview. Space Science Reviews, 216(8). https://doi.org/10.1007/s11214-020-00762-y

Fornaro, T., Steele, A., & Brucato, J. (2018). Catalytic/Protective Properties of Martian Minerals and Implications for Possible Origin of Life on Mars. Life, 8(4), 56. https://doi.org/10.3390/life8040056

Fox, A. C., Eigenbrode, J. L., & Freeman, K. H. (2019). Radiolysis of Macromolecular Organic Material in Mars-Relevant Mineral Matrices. Journal of Geophysical Research: Planets, 124(12), 3257-3266. https://doi.org/10.1029/2019je006072

Fox, J. L. (1993). On the escape of oxygen and hydrogen from Mars. Geophysical Research Letters, 20(17), 1747-1750. https://doi.org/10.1029/93gl01118

Freissinet, C., Glavin, D. P., Mahaffy, P. R., Miller, K. E., Eigenbrode, J. L., Summons, R. E., Brunner, A. E., Buch, A., Szopa, C., Archer, P. D., Franz, H. B., Atreya, S. K., Brinckerhoff, W. B., Cabane, M., Coll, P., Conrad, P. G., Des Marais, D. J., Dworkin, J. P., Fairén, A. G., François, P., Grotzinger, J. P., Kashyap, S., Ten Kate, I. L., Leshin, L. A., Malespin, C. A., Martin, M. G., Martin-Torres, F. J., McAdam, A. C., Ming, D. W., Navarro-González, R., Pavlov, A. A., Prats, B. D., Squyres, S. W., Steele, A., Stern, J. C., Sumner, D. Y., Sutter, B., & Zorzano, M. P. (2015). Organic molecules in the Sheepbed Mudstone, Gale Crater, Mars. Journal of Geophysical Research: Planets, 120(3), 495-514. https://doi.org/10.1002/2014je004737

Golombek, M., Grant, J., Kipp, D., Vasavada, A., Kirk, R., Fergason, R., Bellutta, P., Calef, F., Larsen, K., Katayama, Y., Huertas, A., Beyer, R., Chen, A., Parker, T., Pollard, B., Lee, S., Sun, Y., Hoover, R., Sladek, H., Grotzinger, J., Welch, R., E, Michalski, J., & Watkins, M. (2012). Selection of the Mars Science Laboratory Landing Site. Space Science Reviews, 170(1-4), 641-737. https://doi.org/10.1007/s11214-012-9916-y

Golombek, M. P., Phillips, R. J., Watters, T., & Schultz, R. (2010). Mars tectonics. Planetary tectonics, 11, 183-232.

Goudge, T. A., Mustard, J. F., Head, J. W., Fassett, C. I., & Wiseman, S. M. (2015). Assessing the mineralogy of the watershed and fan deposits of the Jezero crater paleolake system, Mars. Journal of Geophysical Research: Planets, 120(4), 775-808.

Hassler, Cary Zeitlin, 1 Robert F. Wimmer- Schweingruber, 2 Bent Ehresmann, 1 Scot Rafkin, L., J., Eigenbrode, 3 David E. Brinza, 4 Gerald Weigle, 5 Stephan Böttcher, 2, Eckart Böhm, 2 Soenke Burmeister, 2 Jingnan Guo, 2 Jan Köhler, 2, Cesar Martin, 2 Guenther Reitz, 6 Francis A. Cucinotta, Myung-Hee, Kim, 8 David Grinspoon, 9 Mark A. Bullock, 1 Arik Posner, Javier, Gómez-Elvira, 11 Ashwin Vasavada, 4 John P. Grotzinger, MSL, & Team†, S. (2013). Mars' Surface Radiation

Environment with the Mars Science Laboratory's Curiosity Rover. Science. https://doi.org/10.1126/science.1244797

Hoffman, J. A., Hecht, M. H., Rapp, D., Hartvigsen, J. J., SooHoo, J. G., Aboobaker, A. M., McClean, J. B., Liu, A. M., Hinterman, E. D., & Nasr, M. (2022). Mars Oxygen ISRU Experiment (MOXIE)—Preparing for human Mars exploration. Science Advances, 8(35), eabp8636.

Horgan, B. H., Anderson, R. B., Dromart, G., Amador, E. S., & Rice, M. S. (2020). The mineral diversity of Jezero crater: Evidence for possible lacustrine carbonates on Mars. Icarus, 339, 113526.

Hynek, B. M., Beach, M., & Hoke, M. R. (2010). Updated global map of Martian valley networks and implications for climate and hydrologic processes. Journal of Geophysical Research: Planets, 115(E9).

Ivanov, M. A., Slyuta, E. N., Grishakina, E. A., & Dmitrovskii, A. A. (2020). Geomorphological Analysis of ExoMars Candidate Landing Site Oxia Planum. Solar System Research, 54(1), 1-14. https://doi.org/10.1134/s0038094620010050

Jakosky, B. M. (2022). How did Mars lose its atmosphere and water? Physics Today, 75(4), 62-63.

Junge, K., Eicken, H., & Deming, J. W. (2004). Bacterial activity at− 2 to− 20 C in Arctic wintertime sea ice. Applied and Environmental Microbiology, 70(1), 550-557.

Klein, H. P. (1979). The Viking mission and the search for life on Mars. Reviews of Geophysics, 17(7), 1655. https://doi.org/10.1029/rg017i007p01655

Knoevenagel, K., & Himmelreich, R. (1976). Degradation of compounds containing carbon atoms by photooxidation in the presence of water. Archives of environmental contamination and toxicology, 4, 324-333.

Lammer, H., Chassefière, E., Karatekin, Ö., Morschhauser, A., Niles, P. B., Mousis, O., Odert, P., Möstl, U. V., Breuer, D., Dehant, V., Grott, M., Gröller, H., Hauber, E., & Pham, L. B. S. (2013). Outgassing History and Escape of the Martian Atmosphere and Water Inventory. Space Science Reviews, 174(1-4), 113-154. https://doi.org/10.1007/s11214-012-9943-8

Lasne, J., Noblet, A., Szopa, C., Navarro-Gonzalez, R., Cabane, M., Poch, O., Stalport, F., Francois, P., Atreya, S. K., & Coll, P. (2016). Oxidants at the Surface of Mars: A Review in Light of Recent Exploration Results. Astrobiology, 16(12), 977-996. https://doi.org/10.1089/ast.2016.1502

Lauro, S. E., Pettinelli, E., Caprarelli, G., Guallini, L., Rossi, A. P., Mattei, E., Cosciotti, B., Cicchetti, A., Soldovieri, F., & Cartacci, M. (2021). Multiple subglacial water bodies below the south pole of Mars unveiled by new MARSIS data. Nature Astronomy, 5(1), 63-70.

Mackenzie, S. M., Birch, S. P. D., Hörst, S., Sotin, C., Barth, E., Lora, J. M., Trainer, M. G., Corlies, P., Malaska, M. J., Sciamma-O'Brien, E., Thelen, A. E., Turtle, E., Radebaugh, J., Hanley, J., Solomonidou, A., Newman, C., Regoli, L., Rodriguez, S., Seignovert, B., Hayes, A. G., Journaux, B., Steckloff, J., Nna-Mvondo, D., Cornet, T., Palmer, M. Y., Lopes, R. M. C., Vinatier, S., Lorenz, R., Nixon, C., Czaplinski, E., Barnes, J. W., Sittler, E., & Coates, A. (2021). Titan: Earth-like on the Outside,

Ocean World on the Inside. The Planetary Science Journal, 2(3), 112. https://doi.org/10.3847/psj/abf7c9

Mastrogiuseppe, M., Poggiali, V., Hayes, A., Lunine, J., Seu, R., Mitri, G., & Lorenz, R. (2019). Deep and methane-rich lakes on Titan. Nature Astronomy, 3(6), 535-542.

Masursky, H., & Crabill, N. (1976a). Search for the Viking 2 landing site. Science, 194(4260), 62-68.

Masursky, H., & Crabill, N. (1976b). The Viking landing sites: Selection and certification. Science, 193(4255), 809-812.

McKay, C. P. (2009). Planetary ecosynthesis on Mars: restoration ecology and environmental ethics. Exploring the origin, extent, and future of life: Philosophical, ethical, and theological perspectives, 245-260.

Millan, M., Teinturier, S., Malespin, C., Bonnet, J., Buch, A., Dworkin, J., Eigenbrode, J., Freissinet, C., Glavin, D., & Navarro-González, R. (2022). Organic molecules revealed in Mars's Bagnold Dunes by Curiosity's derivatization experiment. Nature Astronomy, 6(1), 129-140.

Millan, M., Williams, A. J., McAdam, A. C., Eigenbrode, J. L., Steele, A., Freissinet, C., Glavin, D. P., Szopa, C., Buch, A., Summons, R. E., Lewis, J. M. T., Wong, G. M., House, C. H., Sutter, B., McIntosh, O., Bryk, A. B., Franz, H. B., Pozarycki, C., Stern, J. C., Navarro-Gonzalez, R., Archer, D. P., Fox, V., Bennett, K., Teinturier, S., Malespin, C., Johnson, S. S., & Mahaffy, P. R. (2022). Sedimentary Organics in Glen Torridon, Gale Crater, Mars: Results From the SAM Instrument Suite and Supporting Laboratory Analyses. Journal of Geophysical Research: Planets, 127(11). https://doi.org/10.1029/2021je007107

Moeller, R. C., Jandura, L., Rosette, K., Robinson, M., Samuels, J., Silverman, M., Brown, K., Duffy, E., Yazzie, A., Jens, E., Brockie, I., White, L., Goreva, Y., Zorn, T., Okon, A., Lin, J., Frost, M., Collins, C., Williams, J. B., Steltzner, A., Chen, F., & Biesiadecki, J. (2021). The Sampling and Caching Subsystem (SCS) for the Scientific Exploration of Jezero Crater by the Mars 2020 Perseverance Rover. Space Science Reviews, 217(1). https://doi.org/10.1007/s11214-020-00783-7

Mustard, J. F., Murchie, S. L., Pelkey, S., Ehlmann, B., Milliken, R., Grant, J. A., Bibring, J.-P., Poulet, F., Bishop, J., & Dobrea, E. N. (2008). Hydrated silicate minerals on Mars observed by the Mars Reconnaissance Orbiter CRISM instrument. Nature, 454(7202), 305-309.

Mykytczuk, N., Foote, S. J., Omelon, C. R., Southam, G., Greer, C. W., & Whyte, L. G. (2013). Bacterial growth at− 15 C; molecular insights from the permafrost bacterium Planococcus halocryophilus Or1. The ISME journal, 7(6), 1211-1226.

Navarro-González, R., Navarro, K. F., Rosa, J. D. L., Iñiguez, E., Molina, P., Miranda, L. D., Morales, P., Cienfuegos, E., Coll, P., Raulin, F., Amils, R., & McKay, C. P. (2006). The limitations on organic detection in Mars-like soils by thermal volatilization–gas chromatography–MS and their implications for the Viking results. Proceedings of the National Academy of Sciences, 103(44), 16089-16094. https://doi.org/10.1073/pnas.0604210103

Navarro-González, R., Vargas, E., De La Rosa, J., Raga, A. C., & McKay, C. P. (2010). Reanalysis of the Viking results suggests perchlorate and organics at

midlatitudes on Mars. Journal of Geophysical Research, 115(E12). https://doi.org/10.1029/2010je003599

Ojha, L., McEwen, A., Dundas, C., Byrne, S., Mattson, S., Wray, J., Masse, M., & Schaefer, E. (2014). HiRISE observations of recurring slope lineae (RSL) during southern summer on Mars. Icarus, 231, 365-376.

Ojha, L., Wilhelm, M. B., Murchie, S. L., McEwen, A. S., Wray, J. J., Hanley, J., Massé, M., & Chojnacki, M. (2015). Spectral evidence for hydrated salts in recurring slope lineae on Mars. Nature Geoscience, 8(11), 829-832.

Osterloo, M., Hamilton, V., Bandfield, J., Glotch, T., Baldridge, A., Christensen, P., Tornabene, L., & Anderson, F. (2008). Chloride-bearing materials in the southern highlands of Mars. Science, 319(5870), 1651-1654.

Pedersen, G. B. M., & Head, J. W. (2010). Evidence of widespread degraded Amazonian-aged ice-rich deposits in the transition between Elysium Rise and Utopia Planitia, Mars: Guidelines for the recognition of degraded ice-rich materials. Planetary and Space Science, 58(14-15), 1953-1970.

Poch, O., Kaci, S., Stalport, F., Szopa, C., & Coll, P. (2014). Laboratory insights into the chemical and kinetic evolution of several organic molecules under simulated Mars surface UV radiation conditions. Icarus, 242, 50-63.

Postberg, F., Khawaja, N., Abel, B., Choblet, G., Glein, C. R., Gudipati, M. S., Henderson, B. L., Hsu, H.-W., Kempf, S., Klenner, F., Moragas-Klostermeyer, G., Magee, B., Nölle, L., Perry, M., Reviol, R., Schmidt, J., Srama, R., Stolz, F., Tobie, G., Trieloff, M., & Waite, J. H. (2018). Macromolecular organic compounds from the depths of Enceladus. Nature, 558(7711), 564-568. https://doi.org/10.1038/s41586-018-0246-4

Poulet, F., Bibring, J.-P., Mustard, J., Gendrin, A., Mangold, N., Langevin, Y., Arvidson, R., Gondet, B., & Gomez, C. (2005). Phyllosilicates on Mars and implications for early Martian climate. Nature, 438(7068), 623-627.

Quantin, C., Carter, J., Thollot, P., Broyer, J., Lozach, L., Davis, J., Grindrod, P., Pajola, M., Baratti, E., & Rossato, S. (2016). Oxia Planum, the landing site for ExoMars 2018. 47th Lunar and Planetary Science Conference Abstracts, Abstract,

Remick, K. A., & Helmann, J. D. (2023). The elements of life: A biocentric tour of the periodic table. In Advances in Microbial Physiology (Vol. 82, pp. 1-127). Elsevier.

Rothschild, L. J., & Mancinelli, R. L. (2001). Life in extreme environments. Nature, 409(6823), 1092-1101.

Russell, M. J., Murray, A. E., & Hand, K. P. (2017). The Possible Emergence of Life and Differentiation of a Shallow Biosphere on Irradiated Icy Worlds: The Example of Europa. Astrobiology, 17(12), 1265-1273. https://doi.org/10.1089/ast.2016.1600

Scheller, E. L., Hollis, J. R., Cardarelli, E. L., Steele, A., Beegle, L. W., Bhartia, R., Conrad, P., Uckert, K., Sharma, S., & Ehlmann, B. L. (2022). Aqueous alteration processes in Jezero crater, Mars− implications for organic geochemistry. Science, eabo5204.

Schon, S. C., Head, J. W., & Fassett, C. I. (2012). An overfilled lacustrine system and progradational delta in Jezero crater, Mars: Implications for Noachian climate. Planetary and Space Science, 67(1), 28-45.

Schulze-Makuch, D., & Irwin, L. N. (2006). The prospect of alien life in exotic forms on other worlds. Naturwissenschaften, 93, 155-172.

Stillman, D. E., Michaels, T. I., & Grimm, R. E. (2017). Characteristics of the numerous and widespread recurring slope lineae (RSL) in Valles Marineris, Mars. Icarus, 285, 195-210.

Stillman, D. E., Michaels, T. I., Grimm, R. E., & Harrison, K. P. (2014). New observations of martian southern mid-latitude recurring slope lineae (RSL) imply formation by freshwater subsurface flows. Icarus, 233, 328-341.

Thomas, N. H., Ehlmann, B. L., Meslin, P. Y., Rapin, W., Anderson, D. E., Rivera-Hernández, F., Forni, O., Schröder, S., Cousin, A., Mangold, N., Gellert, R., Gasnault, O., & Wiens, R. C. (2019). Mars Science Laboratory Observations of Chloride Salts in Gale Crater, Mars. Geophysical Research Letters, 46(19), 10754-10763. https://doi.org/10.1029/2019gl082764

Waite, J. H., Glein, C. R., Perryman, R. S., Teolis, B. D., Magee, B. A., Miller, G., Grimes, J., Perry, M. E., Miller, K. E., & Bouquet, A. (2017). Cassini finds molecular hydrogen in the Enceladus plume: evidence for hydrothermal processes. Science, 356(6334), 155-159.

Wang, A., Ling, Z., Yan, Y., McEwen, A. S., Mellon, M. T., Smith, M. D., Jolliff, B. L., & Head, J. (2019). Subsurface Cl-bearing salts as potential contributors to recurring slope lineae (RSL) on Mars. Icarus, 333, 464-480.

Wells, L. E., & Deming, J. W. (2006). Significance of bacterivory and viral lysis in bottom waters of Franklin Bay, Canadian Arctic, during winter. Aquatic microbial ecology, 43(3), 209-221.

Wray, J. J. (2013). Gale crater: the Mars Science Laboratory/Curiosity Rover Landing Site. International Journal of Astrobiology, 12(1), 25-38. https://doi.org/10.1017/s1473550412000328

Zeitlin, C., Hassler, D., Cucinotta, F., Ehresmann, B., Wimmer-Schweingruber, R., Brinza, D., Kang, S., Weigle, G., Böttcher, S., & Böhm, E. (2013). Measurements of energetic particle radiation in transit to Mars on the Mars Science Laboratory. Science, 340(6136), 1080-1084.

CHAPTER 2: INSTRUMENTATION

1. GAS CHROMATOGRAPHY-MASS SPECTROMETRY (GC-MS)

1.1. OPERATING PRINCIPLES OF GC-MS

Gas chromatography-mass spectrometry (GC-MS) is a powerful analytical technique used to identify and quantify compounds in a sample. The process involves two main steps. Firstly, the sample is vaporized and separated into its individual components using gas chromatography (GC) (Figure 1). This involves passing the sample through a column packed with a stationary phase, which selectively interacts with different components based on their physical and chemical properties. The components are then eluted from the column at different times, result of the separation. Secondly, the separated components are ionized and detected using mass spectrometry (MS). This involves bombarding the separated components with electrons, which causes them to fragment into smaller ions. These ions are then separated and detected based on their mass-to-charge ratio (*m/z*), providing a unique fingerprint for each component.

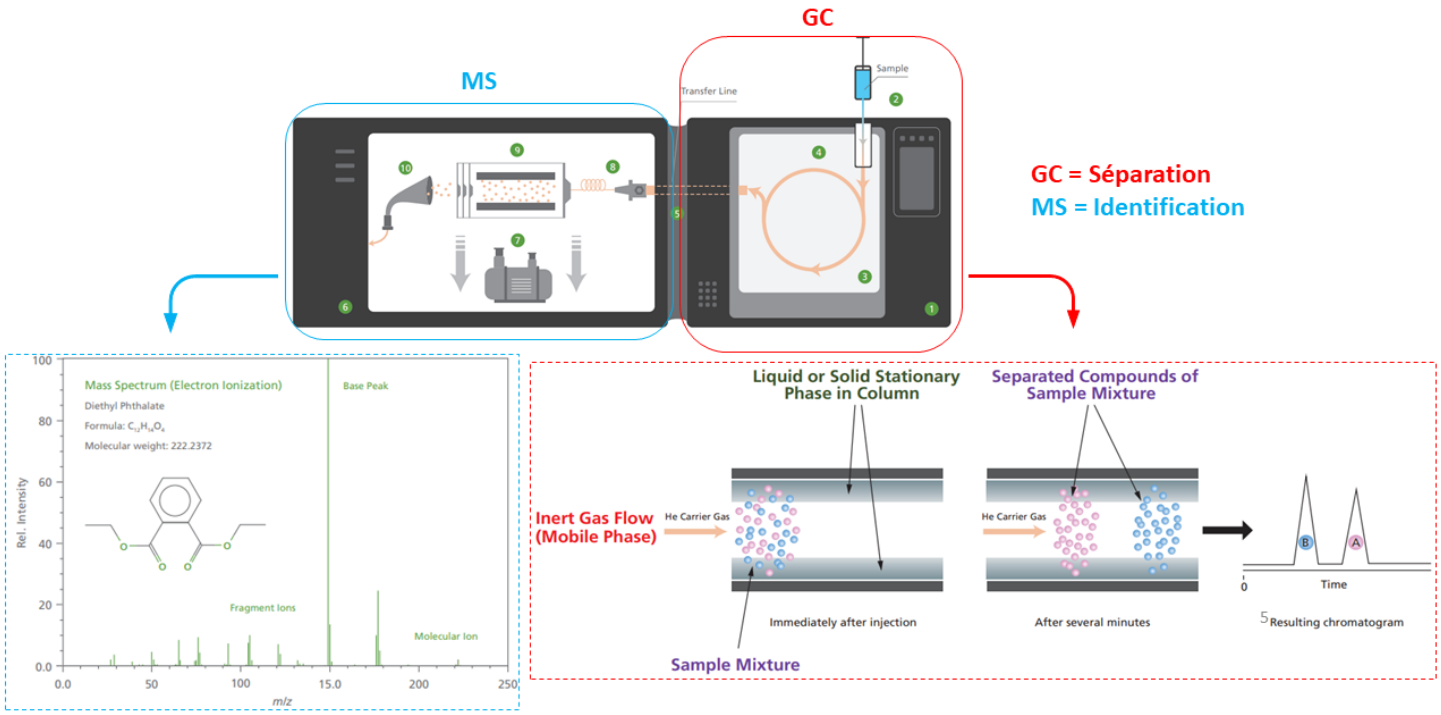

Figure 1: Operating principles of a Gas Chromatograph coupled to a Mass Spectrometer (GC-MS).(Image credit: Shimazu)

By comparing the mass spectra of the separated components to a database of known compounds, GC-MS can identify the individual components of a sample and determine their relative abundance.

1.2. GC-MS FOR SPACE EXPLORATION MISSIONS

1.2.1. Advantages

GC-MS is a technique widely used in space exploration missions because it can help scientists to identify and characterize the organic molecules that are present in extraterrestrial samples such as meteorites, comets, and planetary atmospheres.

Past missions such as the Viking twin landers (Soffen & Young, 1972), Rosetta (Rosenbauer et al., 1999), Cassini-Huygens (Raulin et al., 1998), current missions like Mars Science Laboratory (MSL) (Mahaffy et al., 2012) or future missions like ExoMars (Goesmann et al., 2017) or Dragonfly (Moulay et al., 2023), all have GC-MS instruments.

It is a well-established and reliable analytical technique that has been widely used for decades in laboratories on Earth. Its performance has been extensively tested and validated, and it has a proven track record of providing accurate and reliable results.

GC-MS is also a compact and robust instrument that is well-suited to survive the harsh and challenging conditions of space exploration (Pietrogrande, 2012). It can operate at high temperatures and pressures, and can withstand the shock and vibration of launch and landing (Pietrogrande, 2012).

GC-MS is a versatile technique that can be adapted to analyze a wide range of samples, including solid, liquid, and gaseous samples. This makes it ideal for analyzing the diverse range of extraterrestrial samples that are encountered in space exploration, such as rocks, soils, atmospheres, and cometary dust.

Finally, GC-MS is capable of detecting and identifying a widespray of organic molecules, including those that are relevant to the search for life in the universe. This makes it an invaluable tool for investigating the chemical composition of

extraterrestrial samples and for searching for evidence of biological activity or the building blocks of life.

GC-MS alone is a powerful analytical tool; however, many extraterrestrial samples contain complex mixtures of organic and inorganic compounds that can be difficult to analyze directly by GC-MS. Therefore, in space missions, GC-MS is usually coupled to **pyrolysis** and/or **derivatization** techniques (see below).

1.2.2. Limitations

On the other hand, the spatial requirements of these instruments influence not only their design, but also their operating conditions, with consequences for their analysis capabilities (Szopa et al., 2001).

- Limited analysis time, generally between 10 and 30 minutes, mainly due to the quantity of energy, carrier gas and data storage available.
- Analysis temperature constrained (initial, final and ramp temperatures) by the amount of energy and eventual thermal environment of the instrument.
- A restricted data acquisition frequency to limit the amount of data generated by the analysis and therefore the space occupied by it. This influences chromatogram resolution and hence qualitative and quantitative interpretation.
- The choice of the chromatographic columns (Szopa et al., 2001) oboard the landers instrument payload.

1.3. PYROLYSIS

Pyrolysis is a process in which organic materials are decomposed at high temperatures in the absence of oxygen. The principle of pyrolysis is based on the fact that when organic materials are heated to high temperatures (typically above 400 °C), their molecular bonds begin to break down, causing the material to break into smaller molecules, gases, and other substances. It allows the extraction of volatile molecules and the degradation of the refractory ones into volatile fragments.

Pyrolyzates are the products that are generated from the process of pyrolysis. The

composition and properties of pyrolyzates depend on a variety of factors, such as the type of organic material being pyrolyzed, the temperature and duration of the pyrolysis process, and the presence of other chemicals or catalysts.

1.4. DERIVATIZATION

Derivatization in chemistry refers to the process of chemically modifying a compound to create a derivative that is more amenable to analysis. This is often necessary when the original compound is not easily detectable or quantifiable using standard analytical techniques. The principle of derivatization involves introducing a functional group or other chemical moiety to the original compound to create a new derivative that has different physical or chemical properties (see figure 2). This can make the derivative more volatile, more polar, or more stable, allowing for easier detection or separation using techniques such as GC-MS.

Derivatization can improve the selectivity and sensitivity of GC-MS analysis (Knapp, 1979). By derivatizing a sample, it is possible to selectively target specific classes of compounds, such as amino acids or sugars, and to increase the sensitivity of detection by amplifying the signal produced by each molecule.

Derivatization can also be used to increase the stability of a molecule (He et al., 2020), which is important for space exploration missions.

Finally, derivatization can be used to improve the chromatographic separation of a sample by changing the physicochemical properties of the molecules (Pietrogrande & Basaglia, 2010) , which can increase the resolution and accuracy of GC-MS analysis.

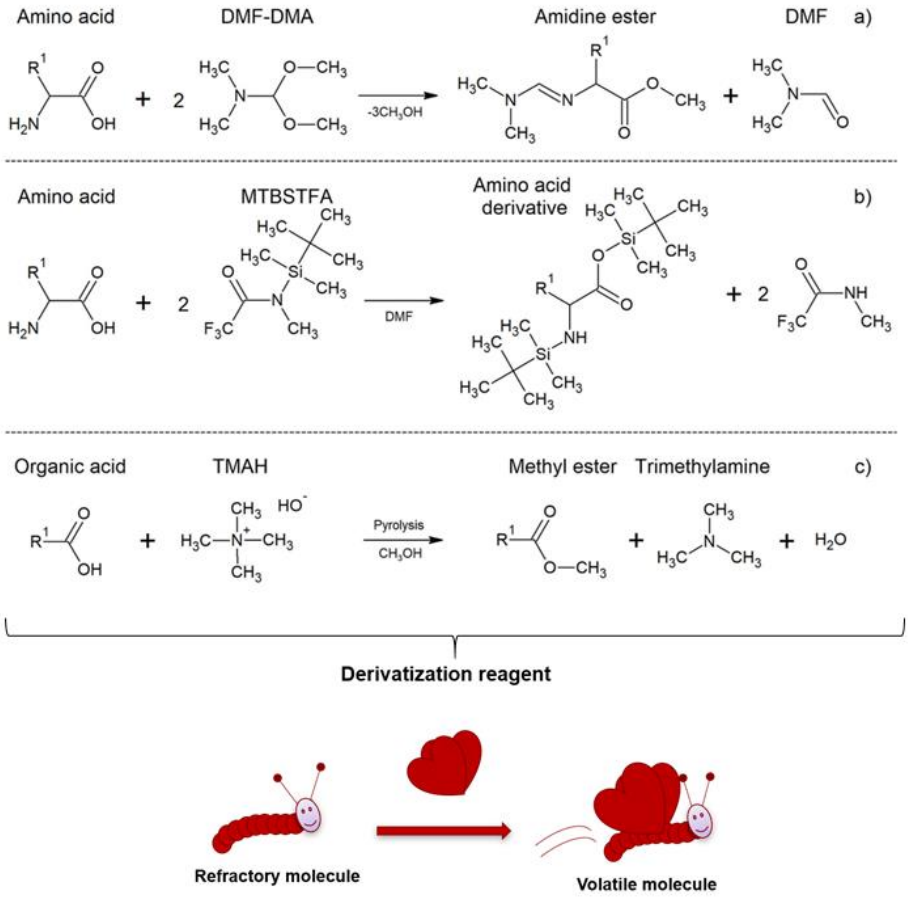

Figure 2 : (a) DMF-DMA derivatization reaction with a chiral amino acid. (b) MTBSTFA silylation reaction on an amino acid. (C) TMAH methylation reaction on a carboxylic acid.

1.5. GC-MS ANALYSIS IN MARTIAN MISSIONS

1.5.1. Viking

The Viking landers' GC-MS system was equipped with a pyrolysis system in addition to the gas chromatograph and mass spectrometer. The pyrolysis system was designed to analyze the composition of solid samples by heating them to high temperatures and breaking them down into their constituent molecules. This technique allowed the Viking GC-MS system to analyze the chemical composition of the Martian soil in more detail than previous missions.

The pyrolysis system consisted of a sample container, a heater, and a gas chromatograph. The sample container was filled with Martian soil, and the heater was used to raise the temperature of the soil to 50 °C, 200 °C, 350 °C, or 500 °C (Rushneck

et al., 1978). The maximum temperature (500 °C) was considered high enough to break the soil down into its individual molecules, but low enough to prevent the destruction of more complex organic molecules that might be present.

The gases released by the pyrolysis process were then sent to the gas chromatograph, where they were separated and analyzed by the mass spectrometer. The mass spectrometer identified the individual components in the sample based on their mass-to-charge ratio, providing information about the chemical composition of the soil with a detection range of 10-100 parts per billion (Soffen & Young, 1972).

1.5.2. Sample Analysis at Mars (SAM)

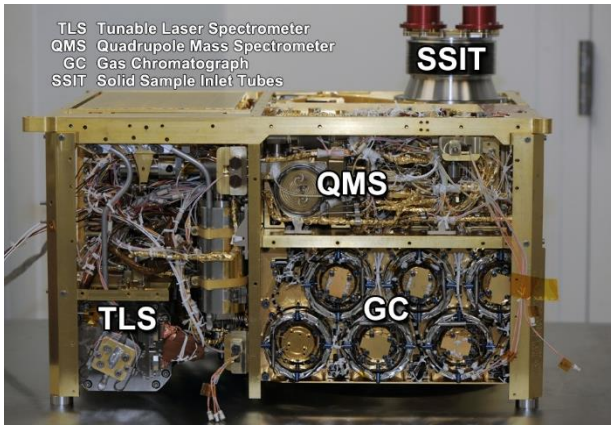

Figure 3: Sample Analysis at Mars (SAM) instrument suite. Image credit: NASA

The Sample Analysis at Mars (SAM) instrument is one of the key instruments onboard the Mars Science Laboratory (MSL) Curiosity rover. SAM is designed to investigate the chemical and isotopic composition of the Martian surface and atmosphere to help answer questions about the history and habitability of Mars (Mahaffy et al., 2012). The SAM instrument is a suite of three instruments that work together to provide complementary information on the same samples: a gas chromatograph (GC), a tunable laser spectrometer (TLS), and a quadrupole mass spectrometer (QMS) (Figure 3). The QMS and the GC can function in tandem in a GC-MS mode for separation (GC) and definitive identification (QMS) of organic molecules. The TLS acquires precise isotope ratios for carbon (C) and Oxygen (O) and measures trace levels of methane and its carbon isotope. However, in this work when talking about SAM we will only refer to the GC-MS sub-system.

After a targeted area is drilled, the powdered samples are sieved to < 150 µm and released from the Curiosity Sample Processing and Handling (SPaH) system. The

material is then delivered into a quartz cup and sealed in its oven for the Evolved Gas Analysis (EGA). In EGA, the sample temperature undergoes a gradual increase (35 °C·min^{-1}) (Mahaffy et al., 2012) to its final temperature (950 °C to 1100 °C) while the QMS is continuously scanned. This technique provides information on the thermal evolution of the species present in the sample and allows a first interpretation of the data. At selected intervals during the EGA ramp, the gas flow can either be redirected through the SAM hydrocarbon (HC) trap for subsequent GC-MS analysis or directed to the TLS.

The Hydrocarbon trap is used for the trapping and transfer of organic compounds to the SAM GC (Mahaffy et al., 2012). To release these adsorbed gases and transport them to the GC columns via helium carrier gas, the trap is heated and the flow direction is reversed.

SAM GC system is equipped with six chromatographic columns to allow for effective separation and identification of a wide-range of organic species (Millan et al., 2019). The GC-MS analysis will normally be performed immediately after the EGA sequence (Figure 4). Following the purging of the selected GC column, the organic compounds are thermally released from the SAM HC trap and captured by a smaller trap known as the injection trap (IT). The IT is either connected at the head of the selected GC column or the analytes are directly injected into the dedicated GC column (3 of the 6 GC columns possess ITs). These injection traps serve the purpose of concentrating the analytes, and subsequently, rapidly (~4 and 10 s) releasing them into the GC columns through flash heating. This fast release enhances the chromatograph's separation capability.

Moreover, one of the unique features of the SAM instrument compare to the Viking missions is its use of derivatization techniques (wet chemistry and thermochemolysis). The SAM instrument can perform a lower temperature (75 - 300 °C) wet chemical processing step prior to GC-MS analysis. Scientists from the SAM team developed a "one-pot" extraction and chemical derivatization protocol using N-methyl-N-(tert-

butyldimethylsilyl) trifluoroacetamide (MTBSTFA) and dimethylformamide (DMF) (Stalport et al., 2012) to facilitate the detection of amino acids and carboxylic acids in a surface soil sample.

SAM also has the ability to identify polar organic molecules that are incorporated within complex molecular structures, such as amino acids in proteins, fatty acids in membranes, or carboxylic acids in non-living macromolecules. This is achieved through thermochemolysis, which involves subjecting the sample to temperatures above 340 °C using a mixture of tetramethylammonium hydroxide (TMAH) and methanol. Thermochemolysis with TMAH is particularly advantageous in aqueous environments as it exhibits greater resistance to the presence of water. It serves as a viable alternative for extracting organic compounds from samples that contain abundant hydrated minerals.

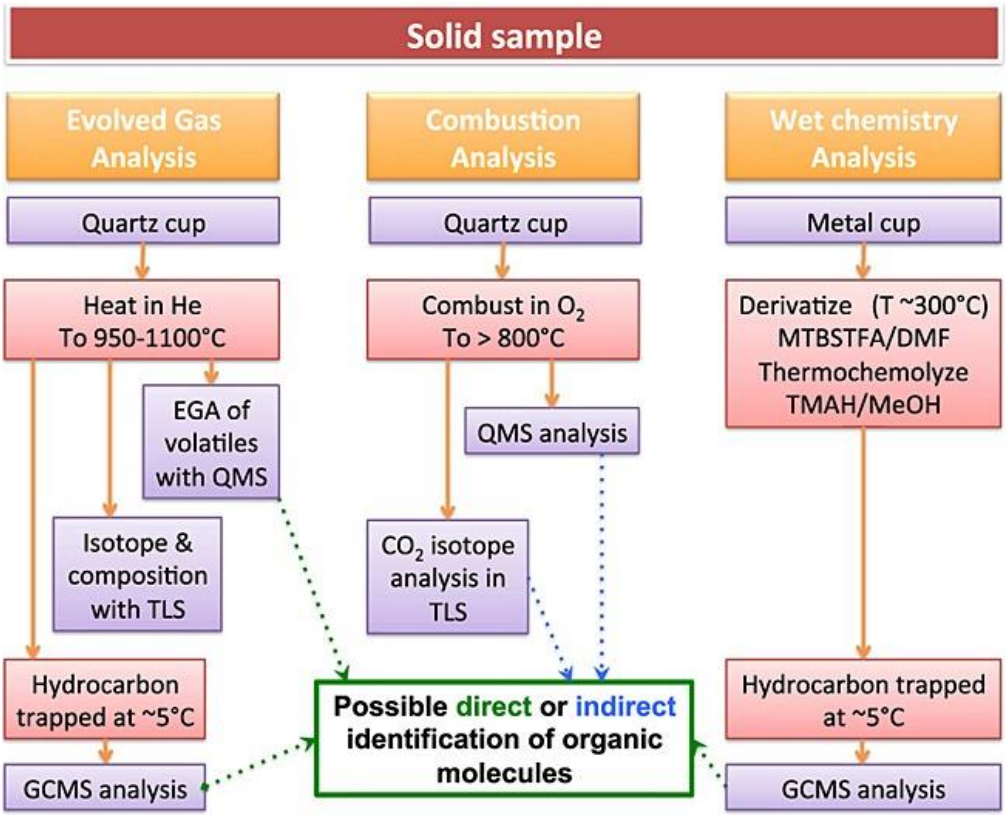

Figure 4: The three different modes of analysis of a solid sample for organic compounds by the SAM instrument. From Freissinet et al. 2015.

Overall, the GC-MS instrument on the SAM suite is a highly advanced analytical tool, capable of detecting trace amounts of organic compounds in the Martian soil and atmosphere. Its pyrolysis capacity and the use of novel derivatization techniques make it a highly sensitive and versatile instrument.

1.5.3. Mars Organic Molecule Analyzer (MOMA)

One of the key instruments onboard the Rosalind Franklin rover is the Mars Organic Molecule Analyzer (MOMA) (Goesmann et al., 2017). MOMA is a state-of-the-art analytical instrument suite designed to search for organic molecules on Mars. The main objective of MOMA is to detect and identify any organic molecules present in the Martian regolith, which could provide evidence of past or present life on the planet. The instrument suite includes a mass spectrometer (MS), a gas chromatograph (GC), and a laser desorption mass spectrometer (LDMS) (Figure 5). In this thesis we will focus only on the GC-MS system.

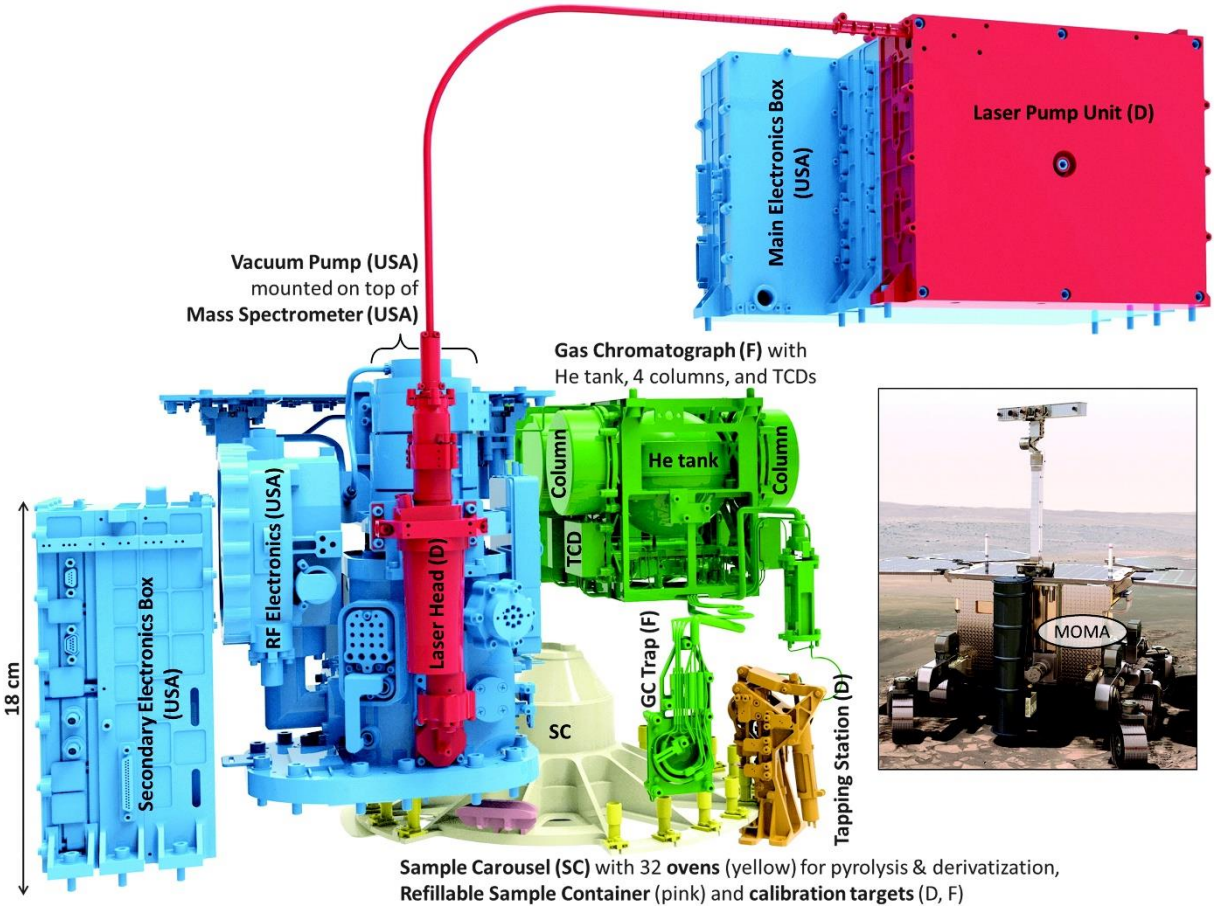

Figure 5: The different parts of MOMA and their contributors (France (F), Germany (D), United States) are displayed in the figure above. The LPU that controls the LH is mounted as a slice on the MEB (top right). Sample carousel (SC) and refillable sample container are not part of MOMA. LH, Laser Head; LPU, Laser Pump Unit; MEB, Main Electronic Box; MOMA, Mars Organic Molecule Analyzer. From Goesman et al. 2017.

As described for SAM, the MOMA GC-MS instrument is designed to perform two critical tasks: pyrolysis and derivatization. These capabilities are essential for detecting and characterizing volatile and refractory organic molecules on the Martian surface.

Samples are pyrolyzed to a maximum temperature of 850 °C in individual ovens with a fast ramp of approximately 200 °C·min^{-1} (Goesmann et al., 2017). As seen in the SAM system, thermal desorption traps are used on MOMA to get the best separation of the analyzed compounds. The MOMA traps' temperature are regulated by a Peltier cooler, maintaining the traps at a temperature ~30 °C lower than the surrounding ambient temperature during the experiment and rapidly (~15 s) heated to 300 °C once trapping

is done. Although not included in the primary investigation, MOMA also possesses the additional capability to conduct EGA (Goesmann et al., 2017).

Moreover, as described previously for SAM, derivatization experiments can also be performed by MOMA with MTBSTFA/DMF and TMAH. However, MOMA, contrary to its predecessors, carries a third derivatization reagent: N,N-Dimethylformamide dimethyl acetal (DMF-DMA). DMF-DMA is a methylation reagent developed for use by the Cometary Sampling and Composition (COSAC) experiment of the Rosetta mission (Szopa et al., 2007). Although it is less efficient than MTBSTFA (detection limit of 1.3 ppm rather than 80 ppb for amino acids) (Goesmann et al., 2017), the instrument remains compatible with the concentration of organic compounds present in micrometeorites due to a enhance response of the mass spectrometer. The key property of DMF-DMA is its capability to facilitate the differentiation and separation of enantiomers when used with an enantioselective GC column (Freissinet et al., 2010). This is important because life on Earth uses only left-handed amino acids and right-handed sugars (Bonner, 1995), and detecting the presence of chiral molecules on Mars could provide evidence for the existence of life.

Table 1: Summary of the analytical capabilities of the Viking, SAM and MOMA instruments.

	Viking	**SAM**	**MOMA**
Maximum oven temperature	500 °C	1100 °C	850 °C
Flash/ramp	Flash	Ramp (35 °C·min^{-1})	Ramp (200 °C·min^{-1})
Carrier gas	Hydrogen	Helium	Helium
Derivatization	N/A	TMAH MTBSTFA/DMF	TMAH MTBSTFA/DMF DMFDMA
EGA	No	Yes	Yes, but not part of the base line investigation
GC columns	Dexsil-Hi-Eff 8-Chromosorb W-HP	MTX-20 MXT-5 Chirasil-β Dex MXT-CLP MXT Q Carbobond	MXT-Q BOND MXT-5 CP Chirasil Dex CB MXT-CLP
Samples drill depth	millimeters to centimeters	millimeters to centimeters	Up to 2 meters

1.6. GC-MS: FROM SPACE TO THE LABORATORY

We developed experimental strategies to work in the laboratory under conditions as close as possible to the Viking, SAM, and MOMA experiments. It should be remembered, however, that there are still differences inherent to the laboratory work which can lead to analytical biases.

The full details on the experimental parameters and protocols used will be described in the method section of chapters 4 and 5.

1.6.1. GC-MS

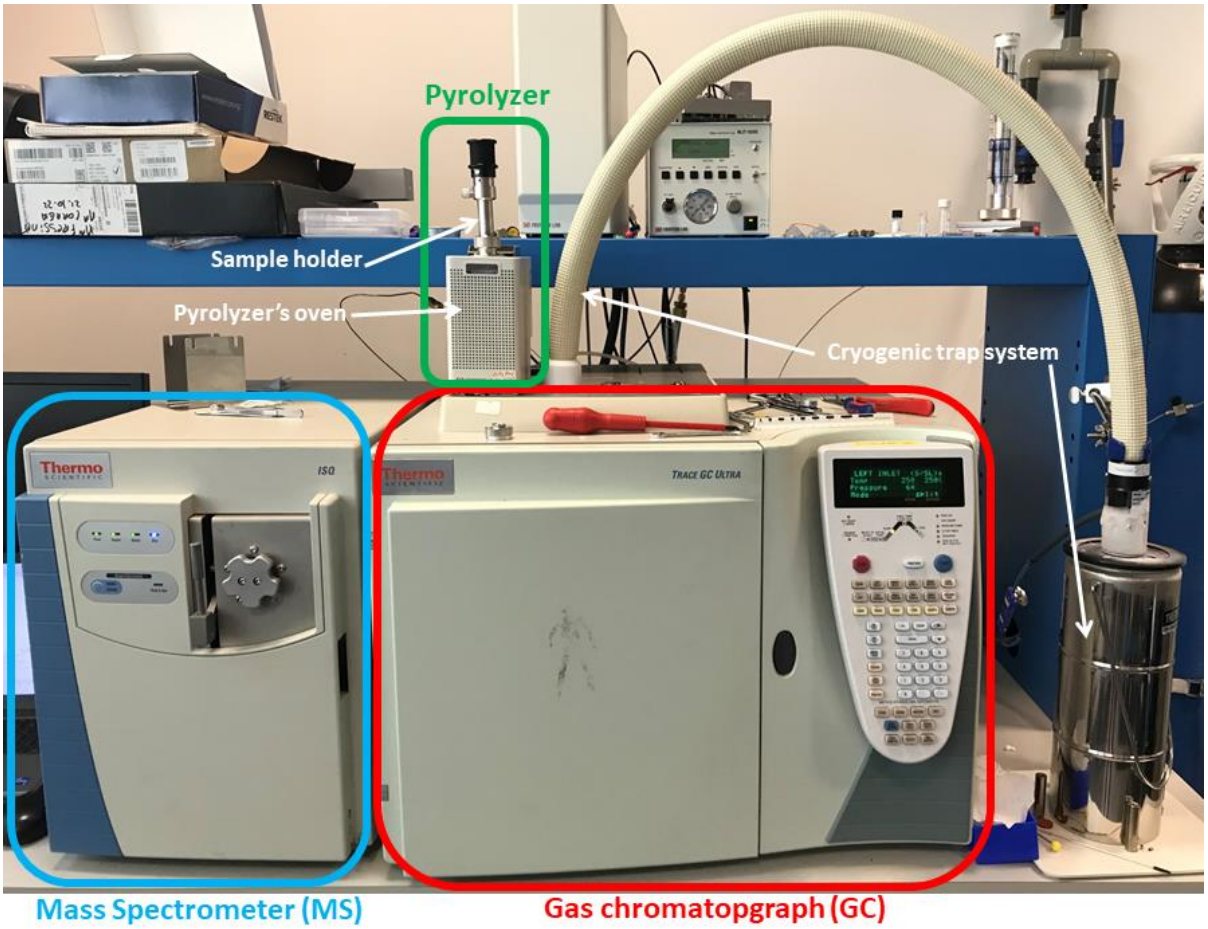

Figure 6: Photo of the experimental set-up used for laboratory analyses.

To perform our GC-MS analysis in the laboratory, we used a Trace 1300 Ultra gas chromatograph (GC) coupled to an ISQ^{TM} quadrupole mass spectrometer (MS) (Figure 6).

The resolution of our commercial instrument is better than the ones from the Martian rovers which are limited by the modification generated by their spatialization (section 1.2.2. of this chapter). Moreover, laboratory software allows us to conveniently subtract background noise from chromatographic peaks or blank runs to eliminate any contamination from the system between analyses. On Mars, gas mixtures containing numerous organic and inorganic species are analyzed, contributing to the overall

background interferences of the chromatograms. Thus, laboratory measures allow us to retrieve more information on the sample studied and help interpret *in situ* data collected by the rovers.

Moreover, because of the differences in atmospheric pressure on Mars and Earth, the pressure applied at the top of the column differs. Indeed, on SAM, the pressure was permanently fixed at 0.9 bar by adjusting a screw located at the entrance of the helium tank. This adjustment was made prior to integrating the instrument suite into the rover, and the pressure cannot be modified thereafter. In the laboratory, it is not possible to work at a sub-atmospheric pressure. However, by utilizing a flow restrictor (further details in Chapter 5), it becomes possible to replicate the carrier gas flow rate used in the SAM experiment and operate at the same pressure level as on Mars. Consequently, the retention times measured in the laboratory can be directly compared to those measured during the flight.

Finally, although the temperatures applied during experiments in the laboratory are the same as those in the flight model, thermal differences remain. On Mars, temperatures vary between -133 and 27 °C, with an average of around -60 °C. These variations can influence the operation of GC-MS systems and SAM components (columns, traps, etc.). Additionally, even with two columns coated with identical stationary phases, there can be slight discrepancies due to variations in their manufacturing process, such as the precise thickness of the stationary phase or column wear. These factors can contribute to slight differences in retention times between the laboratory and flight measurements, as discussed further in Chapter 5.

1.6.2. Pyrolysis

Experiments in the laboratory were conducted using a Frontier Laboratories 3030D multi-shot pyrolizer mounted on the split/spitless injector of the GC-MS instrument (Figure 6). This pyrolyzer allows the analyses of 10 to 100 mg of powdered samples and enables to work in both flash and ramp mode. As mentioned above, both SAM and MOMA reach their final temperature through a ramp (35 and 200 °C·min^{-1},

respectively), whereas Viking works in flash mode. However, the MOMA flight model's temperature ramp is not linear, reaching its highest temperature faster than in the laboratory. This discrepancy led us to apply flash pyrolysis to mimic the MOMA conditions instead of the fast ramp pyrolysis of 200 °C·min^{-1} ramp that the rover on Mars will use.

Moreover, to mimic the function of a chemical trap, present at the head of some of the SAM and MOMA columns (sections 1.5.2. and 1.5.3. of this chapter), the laboratory pyrolyzer is equipped with a cryogenic trap (Figure 6) which, enables the volatile species produced by the sample to be trapped at the head of the column for the duration of the pyrolysis. In our laboratory set-up, the column is inserted through the hole of a cryogenic needle which focuses a cold point (~-180 °C) at the beginning of the column (Figure 7). Once pyrolysis is complete, the trap is reheated and GC-MS analysis begins. However, the temperature of the laboratory trap does not reach cruising temperature as quickly as that of the flight injection trap. Despite this bias, the study of the desorption performance of the injection trap provides a basic understanding of the behavior of the trap in flight. Moreover, the cryogenic trap used in the laboratory does not introduce issues due to the injection system of the flight instruments such the production of secondary byproducts due to the presence of Tenax®, an adsorbant present in the SAM and MOMA's ITs (Buch et al., 2019) or the permanent trapping of organic compounds in the gas processing system as seen on SAM (Millan et al., 2016).

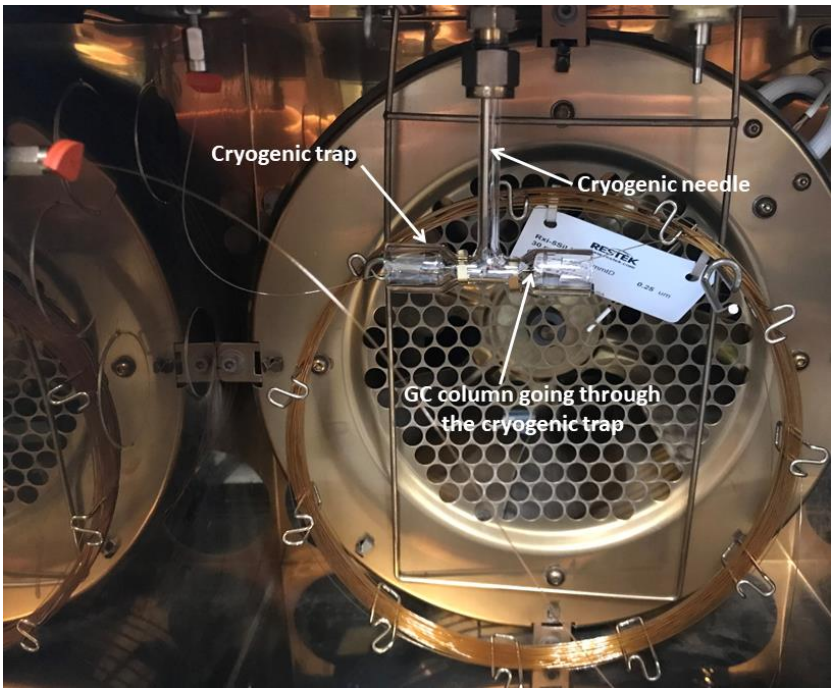

Figure 7: Pyrolyzer cryogenic trap laboratory set up.

1.6.3. Derivatization

Both SAM and MOMA contain capsules dedicated to perform derivatization experiments. In the flight instruments, the derivatization processes (MTBSTFA, DMFDMA and TMAH) all occur in a single step reaction where the sample is directly collected in the capsule containing the derivatization reagent. The capsule is then heated to start the derivatization process and the released gases are transferred directly in the GC-MS system. In the laboratory, this one-step strategy was used only for the TMAH experiments (see chapter 5). The TMAH reagent was added directly in the capsule with the solid sample and flashed pyrolyzed. Indeed, thermochemolysis experiments reach temperatures above 300 °C which can only be attained with our pyrolizer's oven. On the other hand, MTBSTFA/DMF and DMFDMA derivatization were injected in the GC injector via a syringe. The temperature and derivatization time (75 °C for 15 minutes for MTBSTFA and 145 °C for 3 minutes for DMFDMA (Freissinet et al., 2010)) would have required to use the cryogenic trap prior to analysis and although both methods are effective for rapid injection of organic compounds, injection traps present uncertainty in time and release efficiency (see above). As a result, the resolution, and therefore separation capacity, of chromatographic columns may be

slightly overestimated compared with that of flight instruments.

Overall, understanding the distinctions between the flight model and laboratory GC-MS systems is crucial. This knowledge allows us to evaluate analytical biases and consider potential solutions, whether it be resolving them, leveraging them to our advantage, or accommodating them during experiments.

2. DECISION-MAKING PROCESS FOR A GC-MS ANALYSIS ON MARS

Before deciding which sample to analyze with GC-MS on Mars, scientists use a combination of remote sensing and *in situ* measurements to gather information about the Martian environment and select potential sites for sample collection. The following are the decision-making processes and remote sensing analyses that are typically done:

1. Scientists use **remote sensing** instruments, such as cameras, spectrometers, and radar, to study the Martian surface and identify potential sample sites.
    - Imagers: Geology and morphology are the first factors in identifying potential targets for GC-MS analysis. Scientists look for areas where geological processes, such as volcanism or water erosion, have occurred, as these processes can create environments that may be conducive to the preservation of organic molecules.
    - Spectroscopes (X-Ray, Raman, Infrared): Spectroscopy is a technique that measures the absorption or emission of electromagnetic radiation by a sample. On Mars, this technique is used to study the surface mineralogy and composition of the rocks and soils helping scientists identify areas that may contain interesting samples for further study (see chapter 3).
2. Based on the data collected from remote sensing instruments, scientists **prioritize** which samples to analyze with GC-MS.

Overall, the decision-making process for selecting a sample for GC-MS analysis on Mars involves a combination of remote sensing and *in situ* measurements to gather information about the Martian environment and identify potential sites for sample

collection.

REFERENCES

Bonner, W. A. (1995). Chirality and life. Origins of Life and Evolution of the Biosphere, 25(1-3), 175-190. https://doi.org/10.1007/bf01581581

Buch, A., Belmahdi, I., Szopa, C., Freissinet, C., Glavin, D. P., Millan, M., Summons, R., Coscia, D., Teinturier, S., Bonnet, J. Y., He, Y., Cabane, M., Navarro-Gonzalez, R., Malespin, C. A., Stern, J., Eigenbrode, J., Mahaffy, P. R., & Johnson, S. S. (2019). Role of the Tenax® Adsorbent in the Interpretation of the EGA and GC-MS Analyses Performed With the Sample Analysis at Mars in Gale Crater. Journal of Geophysical Research: Planets, 124(11), 2819-2851. https://doi.org/10.1029/2019je005973

Freissinet, C., Buch, A., Sternberg, R., Szopa, C., Geffroy-Rodier, C., Jelinek, C., & Stambouli, M. (2010). Search for evidence of life in space: Analysis of enantiomeric organic molecules by N,N-dimethylformamide dimethylacetal derivative dependant Gas Chromatography–Mass Spectrometry. Journal of Chromatography A, 1217(5), 731-740. https://doi.org/10.1016/j.chroma.2009.11.009

Freissinet, C., Glavin, D. P., Mahaffy, P. R., Miller, K. E., Eigenbrode, J. L., Summons, R. E., Brunner, A. E., Buch, A., Szopa, C., Archer, P. D., Franz, H. B., Atreya, S. K., Brinckerhoff, W. B., Cabane, M., Coll, P., Conrad, P. G., Des Marais, D. J., Dworkin, J. P., Fairén, A. G., François, P., Grotzinger, J. P., Kashyap, S., Ten Kate, I. L., Leshin, L. A., Malespin, C. A., Martin, M. G., Martin-Torres, F. J., McAdam, A. C., Ming, D. W., Navarro-González, R., Pavlov, A. A., Prats, B. D., Squyres, S. W., Steele, A., Stern, J. C., Sumner, D. Y., Sutter, B., & Zorzano, M. P. (2015). Organic molecules in the Sheepbed Mudstone, Gale Crater, Mars. Journal of Geophysical Research: Planets, 120(3), 495-514. https://doi.org/10.1002/2014je004737

Goesmann, F., Brinckerhoff, W. B., Raulin, F., Goetz, W., Danell, R. M., Getty, S. A., Siljeström, S., Mißbach, H., Steininger, H., Arevalo, R. D., Buch, A., Freissinet, C., Grubisic, A., Meierhenrich, U. J., Pinnick, V. T., Stalport, F., Szopa, C., Vago, J. L., Lindner, R., Schulte, M. D., Brucato, J. R., Glavin, D. P., Grand, N., Li, X., Van Amerom, F. H. W., & The Moma Science, T. (2017). The Mars Organic Molecule Analyzer (MOMA) Instrument: Characterization of Organic Material in Martian Sediments. Astrobiology, 17(6-7), 655-685. https://doi.org/10.1089/ast.2016.1551

He, Y., Buch, A., Szopa, C., Williams, A. J., Millan, M., Guzman, M., Freissinet, C., Malespin, C., Glavin, D. P., Eigenbrode, J. L., Coscia, D., Teinturier, S., Pin, L., Cabane, M., & Mahaffy, P. R. (2020). The search for organic compounds with TMAH thermochemolysis: From Earth analyses to space exploration experiments. TrAC Trends in Analytical Chemistry, 127, 115896. https://doi.org/10.1016/j.trac.2020.115896

Knapp, D. R. (1979). Handbook of analytical derivatization reactions. John Wiley & Sons.

Mahaffy, P. R., Webster, C. R., Cabane, M., Conrad, P. G., Coll, P., Atreya, S. K., Arvey, R., Barciniak, M., Benna, M., Bleacher, L., Brinckerhoff, W. B., Eigenbrode, J. L., Carignan, D., Cascia, M., Chalmers, R. A., Dworkin, J. P., Errigo, T., Everson, P., Franz, H., Farley, R., Feng, S., Frazier, G., Freissinet, C., Glavin, D. P., Harpold, D. N., Hawk, D., Holmes, V., Johnson, C. S., Jones, A., Jordan, P., Kellogg, J., Lewis, J., Lyness, E., Malespin, C. A., Martin, D. K., Maurer, J., McAdam, A. C., McLennan, D., Nolan, T. J., Noriega, M., Pavlov, A. A., Prats, B., Raaen, E., Sheinman, O., Sheppard, D., Smith, J., Stern, J. C., Tan, F., Trainer, M., Ming, D. W., Morris, R. V., Jones, J., Gundersen, C., Steele, A., Wray, J., Botta, O., Leshin, L. A., Owen, T., Battel, S., Jakosky, B. M., Manning, H., Squyres, S., Navarro-González, R., McKay, C. P., Raulin, F., Sternberg, R., Buch, A., Sorensen, P., Kline-Schoder, R., Coscia, D., Szopa, C., Teinturier, S., Baffes, C., Feldman, J., Flesch, G., Forouhar, S., Garcia, R., Keymeulen, D., Woodward, S., Block, B. P., Arnett, K., Miller, R., Edmonson, C., Gorevan, S., & Mumm, E. (2012). The Sample Analysis at Mars Investigation and Instrument Suite. Space Science Reviews, 170(1-4), 401-478. https://doi.org/10.1007/s11214-012-9879-z

Millan, M., Szopa, C., Buch, A., Cabane, M., Teinturier, S., Mahaffy, P., & Johnson, S. (2019). Performance of the SAM gas chromatographic columns under simulated flight operating conditions for the analysis of chlorohydrocarbons on Mars. Journal of Chromatography A, 1598, 183-195.

Millan, M., Szopa, C., Buch, A., Coll, P., Glavin, D. P., Freissinet, C., Navarro-Gonzalez, R., François, P., Coscia, D., Bonnet, J. Y., Teinturier, S., Cabane, M., & Mahaffy, P. R. (2016). In situ analysis of martian regolith with the SAM experiment during the first mars year of the MSL mission: Identification of organic molecules by gas chromatography from laboratory measurements. Planetary and Space Science, 129, 88-102. https://doi.org/10.1016/j.pss.2016.06.007

Moulay, V., Freissinet, C., Rizk-Bigourd, M., Buch, A., Ancelin, M., Couturier, E., Breton, C., Trainer, M. G., & Szopa, C. (2023). Selection and Analytical Performances of the Dragonfly Mass Spectrometer Gas Chromatographic Columns to Support the Search for Organic Molecules of Astrobiological Interest on Titan. Astrobiology, 23(2), 213-229.

Pietrogrande, M., & Basaglia, G. (2010). Enantiomeric resolution of biomarkers in space analysis: Chemical derivatization and signal processing for gas chromatography–mass spectrometry analysis of chiral amino acids. Journal of Chromatography A, 1217(7), 1126-1133.

Pietrogrande, M. C. (2012). Gas chromatography in space exploration. In Gas chromatography (pp. 865-874). Elsevier.

Raulin, F., Coll, P., Coscia, D., Gazeau, M., Sternberg, R., Bruston, P., Israel, G., & Gautier, D. (1998). An exobiological view of Titan and the Cassini-Huygens mission. Advances in space research, 22(3), 353-362.

Rosenbauer, H., Fuselier, S., Ghielmetti, A., Greenberg, J., Goesmann, F., Ulamec, S., Israel, G., Livi, S., MacDermott, J., & Matsuo, T. (1999). The COSAC experiment

on the lander of the ROSETTA mission. Advances in space research, 23(2), 333-340.

Rushneck, D. R., Diaz, A. V., Howarth, D. W., Rampacek, J., Olson, K. W., Dencker, W. D., Smith, P., McDavid, L., Tomassian, A., Harris, M., Bulota, K., Biemann, K., Lafleur, A. L., Biller, J. E., & Owen, T. (1978). Viking gas chromatograph-mass spectrometer. Rev Sci Instrum, 49(6), 817. https://doi.org/10.1063/1.1135623

Soffen, G. A., & Young, A. T. (1972). The viking missions to mars. Icarus, 16(1), 1-16.

Stalport, F., Glavin, D. P., Eigenbrode, J., Bish, D., Blake, D., Coll, P., Szopa, C., Buch, A., Mcadam, A., & Dworkin, J. (2012). The influence of mineralogy on recovering organic acids from Mars analogue materials using the "one-pot" derivatization experiment on the Sample Analysis at Mars (SAM) instrument suite. Planetary and Space Science, 67(1), 1-13.

Szopa, C., Goesmann, F., Rosenbauer, H., & Sternberg, R. (2007). The COSAC experiment of the Rosetta mission: Performance under representative conditions and expected scientific return. Advances in space research, 40(2), 180-186.

Szopa, C., Sternberg, R., Rodier, C., Coscia, D., & Raulin, F. (2001). Development and analytical aspects of gas chromatography for space exploration. LC GC EUROPE, 14(2), 114-121.

CHAPTER 3: UNDECANOIC ACID AND L-PHENYLALANINE IN VERMICULITE: DETECTION, CHARACTERIZATION AND UV DEGRADATION STUDIES FOR BIOSIGNATURE IDENTIFICATION ON MARS

ABSTRACT

Solar radiation arriving on the surface of Mars interacts with the organic molecules present in the soil. The radiation can degrade or transform the organic matter and make searching for biosignatures on the planet's surface difficult. Therefore, samples that would be analyzed by the instrument onboard the Martian probes for molecular content should be selectively chosen to have the highest organic preservation content. In order to support the identification of organic molecules on Mars, the behavior under UV irradiation of two organic compounds, undecanoic acid, and L-phenylalanine, in the presence of vermiculite and two chloride salts, NaCl and $MgCl_2$, was studied. The degradation of the molecule's bands was monitored through IR spectroscopy. Our results show that while vermiculite acts as a photoprotective mineral with L-phenylalanine, it catalyses the photodegradation of undecanoic acid molecules. On the other hand, both chloride salts studied decreased the degradation of both organic species, acting as photoprotectors. While these results do not allow us to conclude on the preservation capabilities of vermiculite, it shows that places where chloride salts are present could be good candidates for *in situ* analytic experiments on Mars due to their organic preservation capacity under UV radiation.

1. INTRODUCTION

Over the past decades, one of the primary goals of Martian exploration was to establish if Mars ever fulfilled possible criteria for a habitable planet. Among these criteria, detection of organic matter is key, both for the emergence and the sustainability of life.

The first detection of organic molecules on Mars was performed by the Viking twin landers through the identification of low molecular weight molecules including hydrocarbons and fluorocarbons (Biemann, 1976). The chlorinated compounds were first attributed to terrestrial contaminants. However, the detection of oxychlorines in different regions of Mars (Glavin et al., 2013; Hecht et al., 2009; Meslin et al., 2022) and laboratory experiments reproducing the pyrolytic sequence of the Viking GC-MS, showed that chlorinated compounds are very likely produced from the interaction between Martian hydrocarbons and perchlorates present in the soil during thermal degradation analysis (Guzman et al., 2018; Navarro-González et al., 2010). Since then, different organic molecules have been identified with the Sample Analyzer at Mars (SAM) instrumental suite onboard the Mars Science Laboratory (MSL) Curiosity rover (Eigenbrode et al., 2018; Freissinet et al., 2015; M Millan et al., 2022; Szopa et al., 2020) and the Scanning Habitable Environments with Raman and Luminescence for Organics and Chemicals (SHERLOC) instrument onboard the Mars 2020 Perseverance rover (Scheller et al., 2022). However, organics on the surface of Mars are continuously exposed to the harsh environmental conditions. Among them, the radiation environment on Mars is known for its critical implications on the organic matter present in the soil. The heterogenous ozone spatiotemporal distribution (Perrier et al., 2006) and the overall thin atmosphere of Mars (Jakosky et al., 2017) reduces the atmospheric absorption of Ultraviolet (UV) light, which can penetrate down to a few microns or millimeters depth into the surface (Fornaro, Steele, et al., 2018; Schuerger et al., 2012). UV photons can dissociate molecular bonds, produce ionic species, and excite molecules. These properties mean that UV radiation can stress organic compounds (Sagan, 1973) leading to their decomposition and transformation. The past and current probes on Mars have been analyzing samples at the surface, where organic matter is the most exposed to UV light, and in the first few millimeters or centimeters below the surface (Abbey et al., 2019; Moeller et al., 2021) where UV does not penetrate but can still affect freshly exposed subsurface material in very short timescales. Studies on the impact of UV radiation on organic molecules in the Martian context have, therefore,

been of critical importance to interpret the *in situ* data collected by the probes as well as preparing the missions next analytical targets.

In this effort, understanding the environment in which organic matter evolve on the Martian surface is necessary. Minerals play a crucial role in the processes experienced by organic molecules on Mars, influencing their chemical evolution. The preservation state of organic molecules is often regulated by their interaction with the mineral phase in which they are embedded. Investigations on the catalytic and protective properties of different Martian minerals under Martian-like conditions have been carried out and reviewed by Fornaro et al. (2018)a. The authors concluded that in several paleoenvironments on Earth, long-term preservation of terrestrial biosignature is attributed to sedimentary materials notably phosphates, silica, clays, carbonates and metalliferous materials. However, the straight forward classification of Martian minerals as catalytic or protective is not possible, since the behavior of minerals under Martian conditions depends on the organic molecules involved and their specific interactions with the mineral surface sites. Thus, it is important to investigate the response to UV irradiation of specific molecule-mineral complexes.

The Compact Reconnaissance Imaging Spectrometer for Mars (CRISM) spectra taken at various locations of the landing area chosen for the future ExoMars Rosalind Franklin mission, are consistent with material bearing Fe/Mg-rich clay minerals (Carter et al., 2016). The closest matches are vermiculite, a phyllosilicate phase with a structure intermediate between mica and smectite, and saponite (Mandon et al., 2021). Vermiculite was also detected at Jezero Crater where the Perseverance rover landed in February 2021 (E. Dehouck et al., 2023). Phyllosilicates are characterized by a high organic sequestration and preservation potential (Ehlmann et al., 2008) making them desirable targets for investigations on Mars. Vermiculite is a 2:1 phyllosilicate which means that is composed of tetrahedral sheets $[X_4O_{10}]^{n-}$, where X is Si^{4+}, Al^{3+} and Fe^{3+}, and an octahedral sheet composed of two planes of closely packed O_2^-, OH- anions with the central cations being Mg^{2+}, Fe^{2+} or Fe^{3+}, Al^{3+}. The negative layer charge of

vermiculite results from the substitution of Si^{4+} by trivalent cations in the tetrahedral positions. The general formula can be written as $X_4(Y_{2-3})O_{10}(OH)_2M{\cdot}nH_2O$ where X are the cations in the tetrahedral positions, Y the ones in the octahedral and M refers to the exchangeable cations positioned in the interlayer space that can be Mg^{2+}, Ca^{2+}, Ba^{2+}, Na^{+} and K^{+} (Valášková & Martynkova, 2012). The interlayer space thickness depends on the cations in the interlayer and on the interlamellar water molecules. The hydration properties of vermiculite depends on the interlayer cations, especially in Mg^{2+} for being the major cation and to a lesser extent in the minor ones Ca^{2+}, Na^{+} and K^{+} (Valášková & Martynkova, 2012). This structure confers to vermiculite several properties that promote the adsorption of biomolecules such as its high surface area to interact with, through electrostatic interactions, hydrophobic interactions or Van der Waal's forces. Its structure also provides a good cation exchange capacity as the interlayer cations can be exchanged by some organic cations. Finally, this structure allows other kinds of intercalation of molecules in the mineral interlayers. Water molecules in the interlayer space of vermiculites can be displaced by polar molecules and some neutral organic ligands can form complexes with the interlayer cations (Lagaly et al., 2013).

Among the inorganic species present in the Martian soil, salts are important components of the fine-grained regolith on Mars which presence may affect also the preservation of the organic molecules. Among which, chloride salts have been identified on Mars through infrared spectrometry (Osterloo et al., 2008) and at Gale Crater, where the Curiosity rover operates, with the ChemCam instrument (Thomas et al., 2019). Moreover, a change in the oxychlorine signature along the path of Mount Sharp, advocates for the presence of chloride-bearing material among the chemical phases (Clark et al., 2020). Geologic environments containing saline minerals are potential areas of biological activity. Although the long-term viability of microorganisms within salt is still questioned, salt crystals and brine inclusions appear to provide excellent environments for the long-term preservation of biomolecules (Farmer & Des Marais, 1999). For these reasons, this study aims at understanding the

possible effect of the presence of two types of chloride salts, magnesium chloride ($MgCl_2$) and sodium chloride (NaCl), in the detection and preservation of the organics adsorbed on the mineral. Sodium and magnesium were identified as important elements in the soils at all landing sites, with mass fractions ranging from 0.5 to 5% (Karunatillake et al., 2007). The adsorption of molecules onto minerals is a complex process in which a variety of physical and chemical interactions, such as cation exchange, electrostatic interactions, hydrophobic/hydrophilic affinity, hydrogen bonding and Van der Waals forces, can take part (Yu et al., 2013). The adsorption of amino acids by minerals is also likely affected by ionic strength and interactions between different salts (Zaia, 2012). For example, in the case of electrostatic adsorptions, the increase of the ionic strength would bring a competitive ion exchange resulting in a decrease of the adsorption. However, ion strength has no influence on covalent bonding. On the other hand, salt ions can destroy the hydration layers around the molecules increasing the exposure of the hydrophobic groups and thus, increasing the hydrophobic interaction and adsorption (Yu et al., 2013).

In this work, the interaction, stability and detection of two organic compounds, undecanoic acid and L-phenylalanine in vermiculite are studied by means of Fourier Transform Infrared spectroscopy (FTIR). Undecanoic acid was chosen as a biomarker as it belongs to the fatty acid family, constituents of cell membranes (Nagy & Tiuca, 2017), and crucial sources of metabolic energy for life as we know it (Schoors et al., 2015). Moreover, carboxylic acids are the most likely oxidation products of organic molecules on Mars surface environmental conditions (Benner et al., 2000). Amino acids such as L-phenylalanine play a crucial role in the structure, metabolism, and physiology of cells as constituents of peptides and proteins. Interestingly, amino acids were detected in several meteorites and comets (Burton et al., 2012; Cronin & Pizzarello, 1983), making their presence through exogenous sources on the surface of Mars likely and therefore of high astrobiological interest (Fornaro et al., 2013). In this work, the catalytic/protective behaviour of vermiculite and chloride salts over undecanoic acid and L-phenylalanine under UV irradiation is studied monitoring the IR spectra changes

and a degradation half-lifetime coefficient is calculated for each IR band. The results are extrapolated to calculate the half-lifetime degradation of the molecule under the Martian UV flux. Density Functional Theory simulations were used to help with the vibrational modes assignments of IR bands, and other techniques such as X-Ray Powder Diffraction (XRPD) and Time-of-Flight Secondary Ion Mass Spectrometer (ToF-SIMS) were used to assist with the interpretation of the results.

2. MATERIALS AND METHOD

2.1. SAMPLE PREPARATION

Germen and bacteria free vermiculite was purchase from Sigma-Aldrich in a solid form of 2-3 mm grains. To favor molecular adsorption, the vermiculite was ground in a Planetary Ball Mill PM100 from Retsch for 30 minutes, using a velocity of rotation of 200 rpm and intervals of 2 minutes.

The vermiculite was then baked in an oven at 500 °C for over three hours to pyrolyze the natural organic compounds present in it.

The undecanoic acid (purity > 97 % - Sigma-Aldrich) and the L-phenylalanine (purity > 99.5 % - Sigma-Aldrich) were then adsorbed onto vermiculite by mixing the vermiculite powder with a solution of undecanoic acid or L-phenylalanine solubilized in ethanol (Analar Normapur 96% v/v) and milli-Q water, respectively. Each sample was prepared to contain 10 wt.% of the organic molecule in order to be able to differentiate the band in the IR analyses and to study the degradation of these bands under UV irradiation. Moreover, to study the effect of the salts, sodium or magnesium chloride (purity > 97 % - Sigma-Aldrich) dissolved into milli-Q water were added to some of the samples (10 wt.%). The suspensions were kept for three hours on a stirring plate to favour the establishment of physico-chemical interactions between the organic molecules and the mineral phase (Fornaro, Boosman, et al., 2018). The samples were then dried in an oven at 50 °C.

2.2. SAMPLE CHARACTERIZATIONS

In order to understand and explain the UV degradations or preservations of organic molecules adsorbed onto the mineral matrices, it is essential to identify the IR bands of the organic compounds that can be detected in the studied sample. Then, it is crucial to assign the vibrational modes involved in these bands and to study if there is a shift in their position with respect to the pure organic to understand the interactions between the organic molecules and the mineral.

2.2.1. Infrared measurements

The characterization of the samples was performed using a VERTEX 70v FT-IR spectrometer (Bruker) equipped with a Praying Mantis™ Diffuse Reflection Accessory (Harrick) to carry out Diffuse Reflectance InfraRed Fourier Transform Spectroscopy (DRIFTS) analysis in the Mid-Infrared (MIR) range (8000 to 400 cm^{-1}) using 200 scans for each spectrum with an instrumental resolution of 4 cm^{-1}. The samples were analyzed in a chemically inert environment with a constant flux of dinitrogen (N_2) to avoid disturbances in the spectra from atmospheric CO_2 and O_2.

2.2.2. Density Functional Theory (DFT) simulations

Assignment of the Near Infrared (NIR) spectra was supported by anharmonic computations, allowing to predict frequencies and intensities of overtones and combination bands, employing the Generalized second-order Vibrational Perturbation Theory approach (GVPT2) (Barone, 2005; Barone et al., 2014; Bloino, 2015; Bloino et al., 2015). All computations have been performed by means of Density Functional Theory (DFT) employing the B3LYP functional (Becke, 1993) with the double-zeta basis sets SNSD (Barone et al., 2014), and including Grimme's dispersion correction D3 (in conjunction with Becke-Johnson damping) (Ehrlich et al., 2011; Grimme et al., 2010; Grimme et al., 2011). This approach has been well tested for structural and spectroscopy properties of biological molecules of astrochemical interest (Biczysko et al., 2018; Fornaro et al., 2014; Fornaro, Boosman, et al., 2018; Fornaro et al., 2015; Zhao et al., 2021).

In GVPT2 computations, the recommendations outlined in Bloino et al. (2016) have been followed and default criteria for anharmonic resonances have been exploited. Moreover, the Large Amplitude-Motion (LAM) vibrations, have been excluded from VPT2 by means of LAM-free VPT2 scheme (Biczysko et al., 2018). Vibrations with harmonic frequencies below 100 cm^{-1} have been considered as LAMs.

All calculations were performed with Gaussian 16 suite of computer codes (Frisch et al., 2016) and using GaussView to visualize the normal modes and analyze in detail the outcome of vibrational computations and IR spectra. The DFT simulations were performed for the NIR assignments of undecanoic acid in this work and were previously performed in the same way for L-phenylalanine in a former work by Fornaro et al., 2020.

2.2.3. X-Ray Powder Diffraction (XRPD)

The powders for the XRPD analysis were ground in an agate mortar and left into a stove at 363 K for several days, in order to eliminate the eventual moisture absorbed by the vermiculite. The powders were compacted with paraffin oil inside the stove and modelled as a ball of Ca. 0.45 mm diameter (less than the diameter of the X-ray beam). Each ball was glued on a glass capillary and mounted on the goniometer head of the instrument. The X-ray Powder Diffraction patterns (XRPD) were collected at room temperature with the Atlas S2 Rigaku-Oxford Diffraction Gemini R-Ultra diffractometer equipped with a mirror monochromatized Cu-Kα (1.5418 Å) radiation. Each powder pattern was collected by rotating 100 degrees the sample, with an exposure time of 100 seconds.

2.2.4. TOF-SIMS

The non-radiated samples, sitting in the radiation holder, were mounted directly on the Time-of-Flight Secondary Ion Mass Spectrometer (ToF-SIMS) sample holder by clamps, using cleaned tweezers (heptane, acetone and ethanol, in that order) in a laminar flow hood. After mounting of the samples, the sample holder was then directly introduced into the ToF-SIMS.

Analysis of samples were performed in a ToF-SIMS IV instrument (ION-TOF GmbH,

Germany) located at RISE Research Institute of Sweden in Borås in Sweden. Samples were analysed by rastering a 25 keV Bi^{3+} beam over an 200x200 μm^2 area for 250 s. The analyses were performed in both positive and negative mode at high mass resolution (bunched mode: m/Δm ≥ 5000 at *m/z* 30, Δl ~ 5μm) with a pulsed current of 0.1 pA. As the samples were insulating, the sample surface was flooded with electrons for charge compensation.

2.3. ULTRAVIOLET (UV) IRRADIATION EXPERIMENTS

2.3.1. UV measurements

The UV irradiation experimental setup is constituted by a Newport Oriel 300W Xenon arc discharge lamp with a spectral range between 200 to 930 nm. The light is focused directly on the sample through an optical fibber of 800 μm spot size inserted into the sample compartment to monitor the infrared spectra *in situ* during the UV irradiation. With this setup, the irradiated spot on the sample present an area of 7.07 mm^2 and the UV flux on the sample is of $2.75 \cdot 10^{17}$ photons/s·cm^2 in the 200-400 nm spectral range as measured through a single monochromator Spectro 320 scanning spectrometer (Instrument System). This experimental setup allows to monitor the degradation kinetics *in situ* by infrared spectroscopy analysis as described above.

2.3.2. UV data treatment

The L-phenylalanine samples were irradiated for a total of one hour and ten minutes (4200 s), and the undecanoic acid samples were irradiated for a total of five hours and a half (19800 s). These total irradiations times were selected after previous longer irradiation experiments. They are the maximum time after which longer irradiation times did not change the degradation evolution of the studied bands for each molecule. For each sample, the bands corresponding to the molecule (L-phenylalanine and undecanoic acid) were integrated with the integration tool available in the OPUS software (Bruker) and normalized to obtain the relative area of the band after each irradiation time.

The degradation curves obtained for each band were fitted using a first-order kinetics

function (eq.1):

$$\frac{A(t)}{A_M} = a \cdot e^{-b \cdot t} + c \text{ (eq.1)}$$

Where A(t) is the area of a band at irradiation time t, A_M is the area of the band pre-irradiation, b is the degradation rate, a corresponds to the fraction of molecules affected by the UV flux, whereas c refers to the fraction molecules that are not affected by the UV flux. This is due to the fact that the beam of the IR laser is penetrating more than UV radiation of the lamp.

From the degradation rate obtained for each band (b in equation 1), the half-lifetimes ($t_{1/2}$) of degradation for the different bands of the pure organic molecules and for the organic molecules adsorbed in the mineral were calculated according to equation 2:

$$t_{1/2}=\ln 2/b \text{ (eq.2)}$$

The degradation cross section (σ) was calculated from the degradation coefficient (b) and the total flux per area of irradiation of the UV lamp used for irradiation (φ) according to equation 3:

$$\sigma=b/\varphi \text{ (eq.3)}$$

The degradation cross section (σ) obtained for each band of the organic compounds in the different analysed samples is a characteristic parameter of the molecule that can be used to estimate the degradation half-lifetimes under Martian conditions. Assuming a Martian flux per area of $1.4 \cdot 10^{15}$ photons/s·cm^2 (Patel et al., 2002) in the 190–325 nm spectral range as the Martian φ, the Martian b can be calculated from equation 3. Finally, from the obtained Martian b, the half-lifetimes of degradation on Mars ($t_{1/2}$ Mars) can be estimated for the molecular bands.

3. RESULTS AND DISCUSSION

3.1. UNDECANOIC ACID ON VERMICULITE

3.1.1. Influence of interaction with vermiculite on the Infrared vibrational features of undecanoic acid

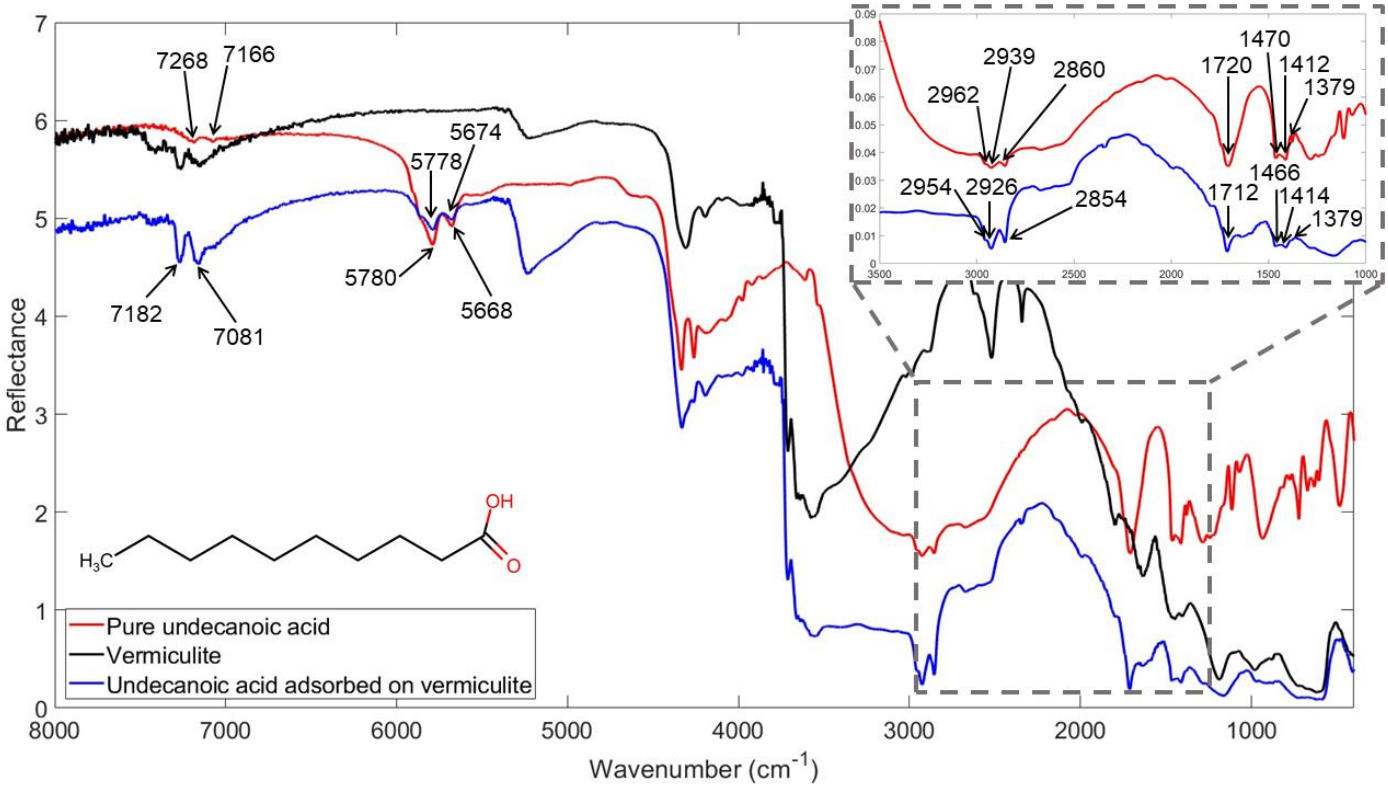

Figure 1: Infrared spectra of vermiculite (black), pure undecanoic acid (red) and 10 wt.% undecanoic acid adsorbed on vermiculite (blue) with the wavenumbers marked for the bands of the undecanoic acid detected in both samples.

As shown in figure 1, when undecanoic acid is adsorbed on vermiculite, some of the characteristic bands of the pure molecule cannot be detected. Among the bands of the pure undecanoic acid that can still be observed in the adsorbed sample, four bands due to non-fundamental vibrational modes in the region > 4000 cm^{-1} and seven bands due to fundamental vibrational modes in the 3000 to 1380 cm^{-1} range were observed. The Near Infrared region (> 3000 cm^{-1}) is of special interest for Mars rover exploration missions as the SuperCam infrared spectrometer on board the NASA Mars 2020 Perseverance rover is analyzing rocks at Jezero crater in the 7692- 3846 cm^{-1} spectral range (Fouchet et al., 2022), and the MicrOmega and Ma-MISS (Mars Multispectral Imager for Subsurface Studies) instruments on board the future ESA ExoMars Rosalind

Franklin rover will investigate the vibrational properties in the 10526-2740 cm^{-1} (Bibring et al., 2017) and 22000-4000 cm^{-1} (Coradini et al., 2001) spectral ranges, respectively, of Martian samples acquired at various depths in the subsurface.

Based on the Near-InfraRed (NIR) study on saturated and unsaturated carboxylic acids by Grabska et al (2017), as well as the NIR computations from this work, the 5780 cm^{-1} and 5668 cm^{-1} bands observed (Figure 1) are assigned to the first overtones and binary combinations of symmetric stretching modes of the respective CH_3 and CH_2 groups, as well as to the contribution from the combination mode of asymmetric CH_2 stretching in this region (Table 1). NIR simulations yield the doublet with band maxima at 5760 cm^{-1} and 5800 cm^{-1} which originated from several normal modes related to C-H stretches.

In the 3000 – 2850 cm^{-1} region, the following bands, 2962 cm^{-1}, 2939 cm^{-1}, and 2860 cm^{-1}, are assigned to the asymmetric stretching of the CH_3 and CH_2 groups and to the symmetric stretching of the CH_2, respectively (Filopoulou et al., 2021). The band at 1720 cm^{-1} can be assigned to the C=O stretching vibrational mode corresponding to the carboxylic functional group of the undecanoic acid (Chapman, 1965). The position of the band at 1720 cm^{-1} is also indicative of the acidic form of the undecanoic acid (-RCOOH) (Yariv & Shoval, 1982) as expected for the pure solid. Finally, the bands appearing in the 1500 - 1350 cm^{-1} region are related to the bending vibrational modes of the C-H groups. More specifically, the 1470 cm^{-1} and 1412 cm^{-1} bands are evidence of CH_2 bending while the 1379 cm^{-1} band corresponds to the CH_3 symmetric bending (Filopoulou et al., 2021). All these assignments are also confirmed by the GVPT2 computations and are listed in the Table 1.

Table 1: Band wavenumbers (ṽ) and vibrational mode assignments for pure undecanoic acid, undecanoic acid adsorbed on vermiculite, and adsorbed on vermiculite in the presence of sodium chloride (NaCl) or magnesium chloride ($MgCl_2$), along with wavenumber shifts (Δṽ)a with respect to the pure undecanoic acid and (Δṽ)b with respect to undecanoic acid adsorbed on vermiculite. ν, stretching; δ, bending; s, symmetric; as, asymmetric.

GVPT2	Pure undecanoic acid	Undecanoic acid on vermiculite		Undecanoic acid on vermiculite + NaCl		Undecanoic acid on vermiculite + $MgCl_2$		Assignment
ṽ (cm^{-1})	ṽ (cm^{-1})	ṽ (cm^{-1})	Δ_aṽ (cm^{-1})	ṽ (cm^{-1})	Δ_bṽ (cm^{-1})	ṽ (cm^{-1})	Δ_bṽ (cm^{-1})	
5800	5780	5778	-2	5784	+6	5782	+4	$\nu_sCH_3 + \nu_sCH_2; \nu_{as}CH_2$
5760	5668	5674	+6	5678	+4	5676	+2	$\nu_sCH_3 + \nu_sCH_2; \nu_{as}CH_2$
2960	2962	2954	-8	2955	+1	2957	+3	$\nu_{as}CH_3$
2937	2939	2926	-13	2924	-2	2924	-2	$\nu_{as}CH_2$
2890	2860	2854	-6	2855	+1	2855	+1	ν_sCH_2
1781	1720	1712	-6	1645/1587	-78	1634/1587	-78	νC=O
1471	1470	1466	-4	1466	0	1466	0	δCH_2
1415	1412	1414	+2	1412	-2	1412	-2	δCH_2
1375	1379	1379	0	1381	+2	1381	+2	δ_sCH_3

For the pure undecanoic acid, a good agreement was observed between the observed band positions and the ones reported in the literature, while shifts on the vibrational frequencies of some non-fundamental bands were observed when comparing the IR spectra of the pure undecanoic acid and the one adsorbed on vermiculite. Specifically, the non-fundamental bands at 5668 cm^{-1} present a shift to higher wavenumbers of 6 cm^{-1}. However due to the complex nature of the band, this shift cannot be simply related to the modification of bonds strength involved in these vibrational modes upon acid adsorption in the mineral. On the other hand, the bands at 2962 cm^{-1}, 2939 cm^{-1}, 2860 cm^{-1} corresponding to the C-H stretching vibrational modes and the band at 1720 cm^{-1} corresponding to the C=O stretching present shifts to lower vibrational frequencies (see Table 1). These observations indicate that the molecular bonds

become weaker, probably due to their participation in the interaction with the mineral.

Lagaly et al. (2013) observed that the arrangement and orientation of intercalated long-chain compounds between mineral layers are dependent on the Van der Waal´s forces established between the alkyl chains. These forces can be strong enough to shift the ending polar groups out of position to form optimal hydrogen bonds. As a consequence, the orientation of the acids with short alkyl chains (< C_9) is mainly determined by the interactions of the polar groups with the silicate layer while the longer alkyl chains (> C_9) and therefore stronger Van der Waal's forces present paraffin type arrangements (Lagaly et al., 2013). Similarly, the long chain in the undecanoic acid (C_{11}) when adsorbed in vermiculite may be subjected to these Van der Waal´s forces which could explain the shifts observed for the C-H bands at 2962 cm^{-1}, 2939 cm^{-1}, and 2860 cm^{-1}. Moreover, acids can be intercalated in vermiculite by displacing the water molecules of the hydrated vermiculite. The OH- and C=O groups of the acid can relocate the water molecules around hard cations such as Na^+, Mg^{2+} and Ca^{2+} to directly interact with them (Lagaly et al., 2013). According to the work by Yariv and Shoval (1982), there are different possible associations in the interlayer for the fatty acids. The COOH group can interact with the oxygen of a silicate sheet of the mineral or with the structured water (Figure. A and B). The COOH group can interact with an exchangeable cation through a water bridge (Figure 2. C1 and C2) or directly with the metal (Figure 2. D1 and D2). Finally, the COO- group can also interact directly or through a water bridge with the exchangeable cation (Figure 2. E1, E2, and F1, F2 respectively). The predominant associations are highly conditioned by the exchangeable cations and the nature of the fatty acid (Yariv & Shoval, 1982). The absence of bands corresponding to the vibrations of the RCOOH or OH groups in the IR spectra of undecanoic acid adsorbed on vermiculite does not allow to conclude on the mechanisms taking place between the mineral phase and the functional groups of the molecule. Only the interactions through the C=O functional group observed at 1712 cm^{-1} (Figure 2 . C2, D1, D2, E1, F1) can be inferred due to the shift present for this band in the acid adsorbed on the mineral. Among these possible interactions of the

carbonyl group, the most likely is the C2, since a direct interaction with the metal would have resulted in a much larger shift and appearance of a new band.

The deviations under the resolution of the instrument of 4 cm^{-1} for the rest of the bands indicate no changes in those vibrational modes when the molecule is adsorbed in the mineral.

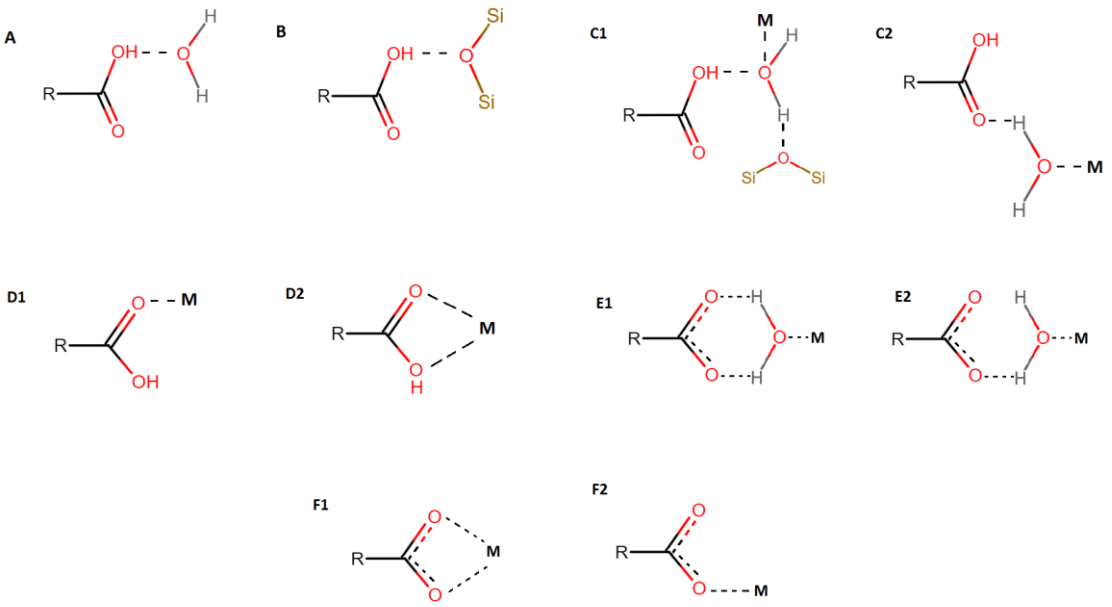

Figure 2: Different associations that can take place in the interlayer of the mineral for the fatty acids.

To understand the interaction of the undecanoic acid compounds with vermiculite, XRPD measurements were performed. As described above, the intercalation of the undecanoic acid between mineral layers could cause two effects on the crystal structure of the vermiculite: the distortion of the crystal lattice resulting in the enlargement of the cell or the displacement of the water molecules without the modification of the vermiculite skeleton. In the first case, a sensible shift of the peaks in XRPD patterns should be observed together with a change in their relative intensities. In the second one, only differences in the relative intensities are expected. Since the undecanoic acid is present in the structure at low quantities, we do not expect large modifications in the patterns, but they should be significant enough to be observed. In Figure 3 are

reported the XRPD patterns of the vermiculite (black) and the 10 wt.% undecanoic acid adsorbed on vermiculite (red).

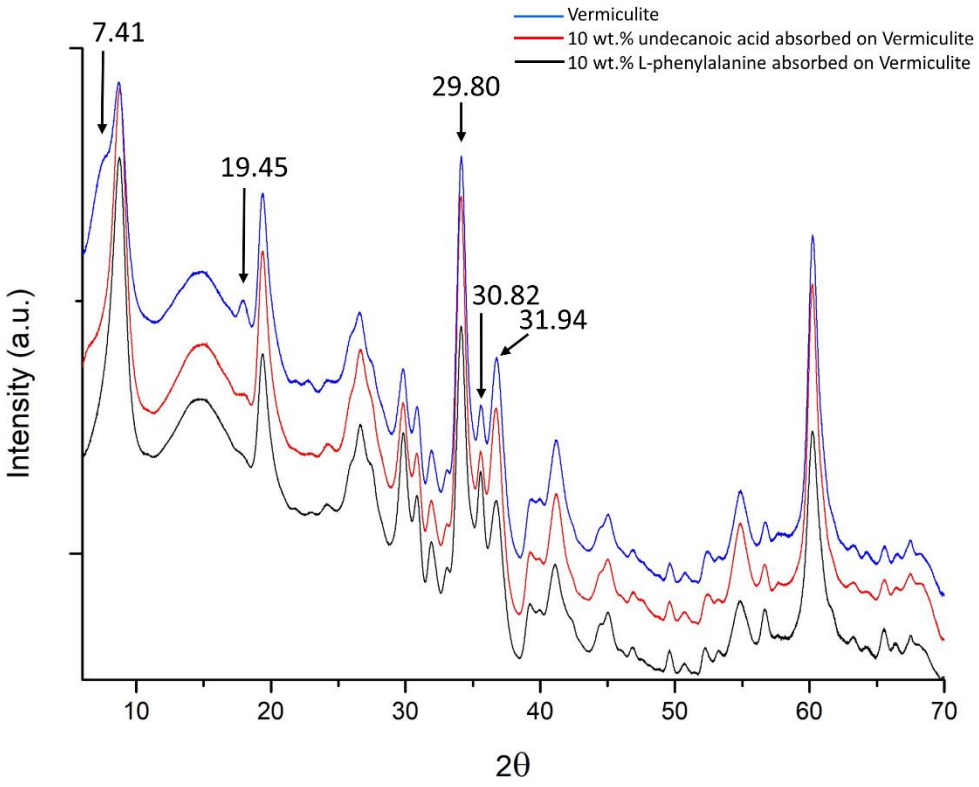

Figure 3: XRPD patterns of pyrolyzed Vermiculite (black), 10 wt.% undecanoic acid absorbed on Vermiculite (red), 10 wt.% L-phenylalanine absorbed on Vermiculite.

No modification in the peaks' position is observed in the XRPD patterns of vermiculite with and without undecanoic acid. In contrast, small differences in the relative intensity of many peaks are perceptible, especially those at 2θ values of 29.80, 30.82, and 31.94 degrees. Thus, we can conclude that the molecules of undecanoic acid were introduced into the structure of the vermiculite without any modification of the mineral skeleton, *i. e.* they substituted some water molecules that lay between the layers and interacting with the metal ions present in the interlayers of the vermiculite according to one of the mechanisms shown in Figure 2. This is consistent with the small shift variations observed in the IR spectra between the pure undecanoic acid and the undecanoic acid on vermiculite.

3.1.2. Influence of chloride salts on the spectroscopic features of undecanoic acid adsorption on vermiculite

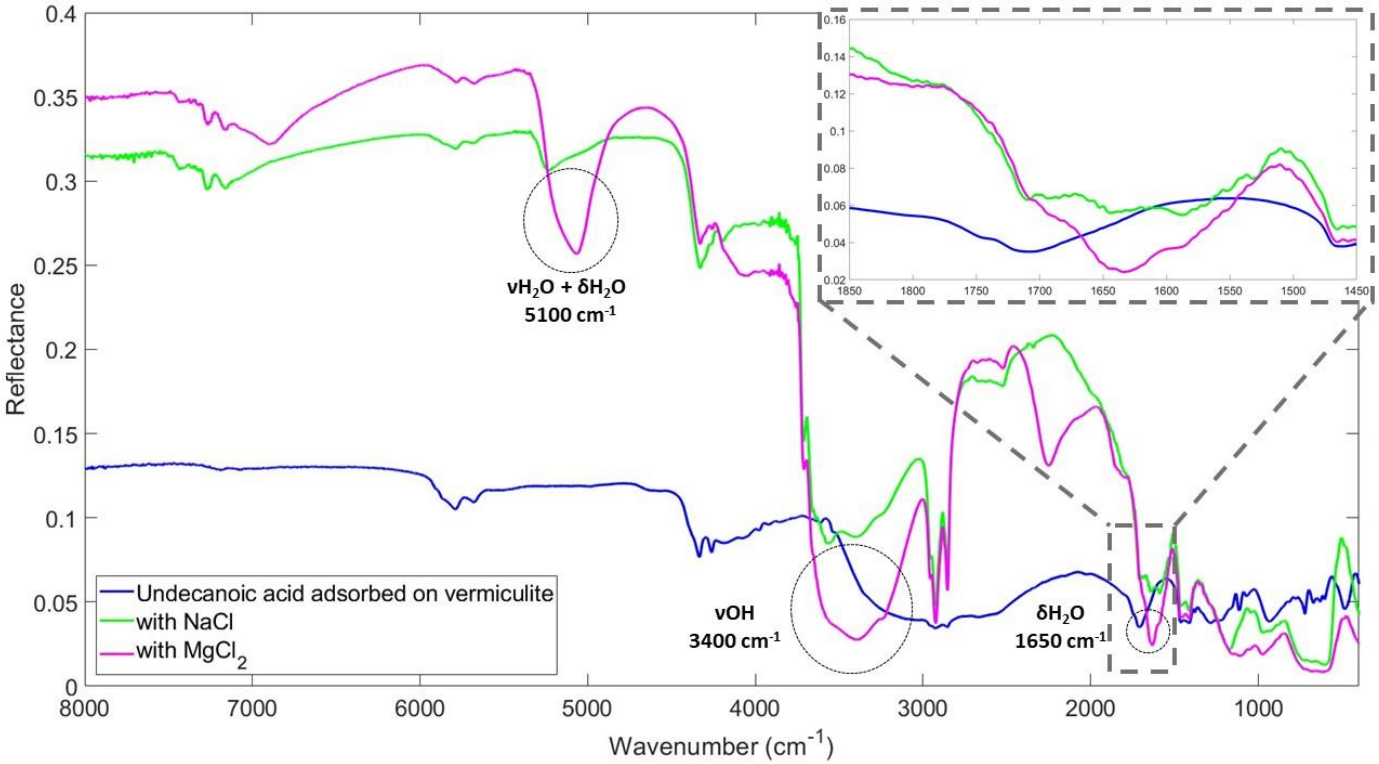

Figure 4: Infrared spectra of 10 wt.% undecanoic acid adsorbed on vermiculite (blue), adsorbed on vermiculite in the presence of sodium chloride (NaCl) (green), and in the presence of magnesium chloride ($MgCl_2$) (magenta).

In presence of chloride salts, as shown in Figure 4, the dominating feature of the IR spectrum is the water band located at 3400 cm^{-1} (Brubach et al., 2005) which corresponds to the stretching mode of the covalent O-H bonds. We also observed a broad band at 5100 cm^{-1} due to a combination of the stretching and bending modes of the H-O-H group. Finally, the band at 1650 cm^{-1} corresponding to the H-O-H bending mode is present. The water bands are much more prominent in the presence of $MgCl_2$, due to its higher hygroscopic nature than NaCl.

The presence of chloride salts during the adsorption process of the undecanoic acid in vermiculite also caused different shifts in the vibrational frequencies of some of the bands of undecanoic acid, as reported in Table 1. When chloride salts are present in

the sample, small shifts of the non-fundamental bands are observed with respect to their position in the spectrum of undecanoic acid adsorbed on vermiculite. A 6 cm^{-1} high-frequency shift of the band at 5778 cm^{-1} in presence of NaCl can be appreciated. However, the spectral region most affected by the presence of salts is between 1700 and 1500 cm^{-1} where a significant low-frequency shift (~78 cm^{-1}) and splitting of the band originally reported at 1712 cm^{-1} in the sample without salt is observed (Figure 4). Specifically, it splits into two main bands at 1634 and 1587 cm^{-1} in the sample adsorbed in the presence of $MgCl_2$, and 1645 and 1587 cm^{-1} in the sample adsorbed in the presence of NaCl. These bands are assigned to the stretching of the undecanoic acid carbonyl (C=O) group and their splitting in multiple features can be explained considering that in such a multicomponent system the carbonyl groups of undecanoic acid molecules can be involved in different kinds of interactions. The significant low-frequency shift of this band indicates that the carbonyl group is involved in very strong interactions, such as hydrogen bonds (Fornaro et al., 2016; Fornaro, Brucato, et al., 2018) with vermiculite, while the broadening may more likely be caused by the presence of water and to the contribution of the bending H-O-H mode in that region (Brubach et al., 2005).

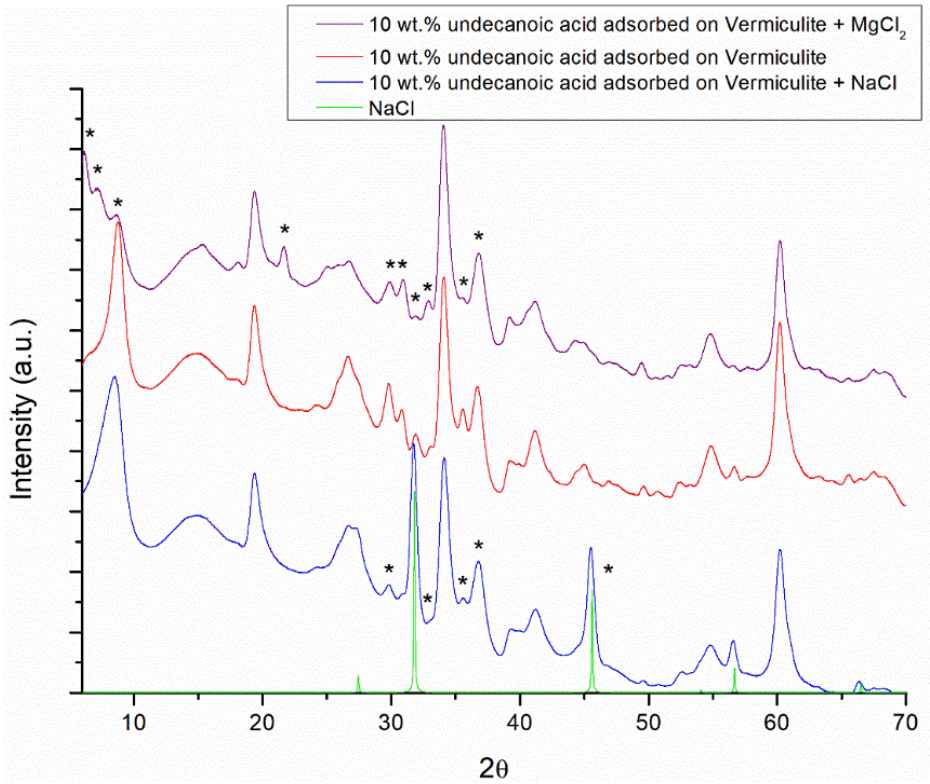

Figure 5: XRPD patterns of 10 wt.% undecanoic acid adsorbed on vermiculite (red), adsorbed on vermiculite in presence of sodium chloride (NaCl) (blue), and in presence of magnesium chloride ($MgCl_2$) (purple). The XRPD pattern of free NaCl (green) is also reported.

Moreover, chloride salts can also change the structure of the vermiculite by their incorporation or even complex the organics and drive them into vermiculite, thus changing the organic-mineral interactions. The XRPD pattern of undecanoic acid adsorbed on vermiculite in presence of NaCl (Figure 5) shows evidences of free solid NaCl mixed with the vermiculite sample. Moreover, the pattern is slightly modified in the relative intensities, especially in the 2θ range between 28 and 38 degrees (peaks evidenced with the stars in Figure 5). This suggests that the presence of NaCl can have a role in the absorption of the undecanoic acid on vermiculite. On the other hand, the free $MgCl_2$ is not visible in the XRPD pattern, and the whole pattern is greater modified with respect to the pattern without the salt. In addition to the relative intensities of the peaks between 28 and 38 degrees, there is a significant modification of the pattern at low angle and a new small peak at 2θ=21.6°. Thus, we can conclude that $MgCl_2$ interacts

stronger with the vermiculite compared to NaCl, and consequently, it can be hypothesized that $MgCl_2$ has a stronger influence on the adsorption of the undecanoic acid.

The same results can be concluded from the IR spectroscopy by comparing the pure vermiculite IR spectrum with the vermiculite treated with the chloride salts (Figure S1). In the case of the vermiculite in presence of NaCl, no significant changes can be appreciated in the bands related to vermiculite. The only changes are due to the presence of the undecanoic acid and one band at 3400 cm^{-1} attribuable to pure NaCl co-precipitated with vermiculite. These outcomes indicate that part of the Na^+ is incorporated with the mineral phase, but a large amount of crystalline NaCl does not interact with the vermiculite. On the other hand, in the presence of $MgCl_2$ changes in the spectra can be appreciated in the bands related to the structure of the vermiculite in the 1300-1000 cm^{-1} ranges (Figure S2) indicating that the Mg^{2+} ions of the magnesium chloride are incorporated in the vermiculite layers.

3.1.3. UV irradiation

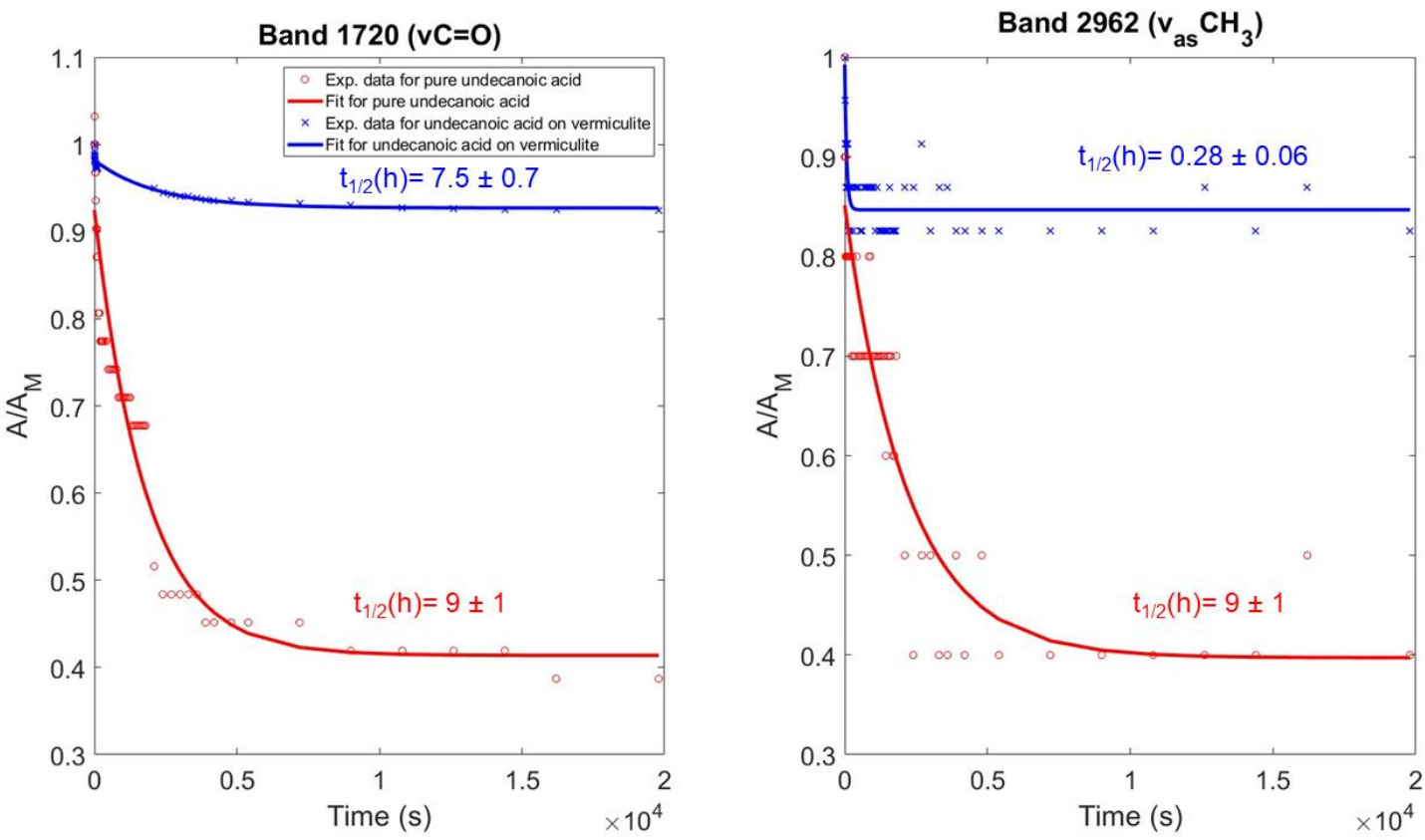

Figure 6: Degradation kinetics curves for bands at 1720 cm^{-1} (ν C=O) and 2962 cm^{-1} (ν_{as} CH_3) of pure undecanoic acid (red) and undecanoic acid adsorbed on vermiculite (blue) and the corresponding half-lifetimes of degradation under Martian UV flux expressed in hours.

The IR bands studied for the UV irradiation experiments were those of the undecanoic acid that were distinguished when adsorbed onto vermiculite and studied in the previous section. In Table 2, the calculated degradation coefficients (b), and the degradation half lifetimes ($t_{1/2}$) under laboratory conditions for the bands mentioned are shown together with the obtained degradation cross section values employed to extrapolate and obtained the results under the Martian UV flux.

Among the bands of undecanoic acid that could be appreciated both in the spectrum of the pure molecule and the spectrum of the molecule adsorbed on vermiculite, only two were reported to decrease due to the effect of UV radiation in both cases; the one at 1720 cm^{-1} assigned to the stretching of C=O and the one at 2962 cm^{-1} assigned to the asymmetric stretching of CH_3. The degradation kinetics of these two bands for pure

undecanoic acid and adsorbed on vermiculite are shown in figure 6. For both bands of undecanoic acid, the degradation curves as a function of time reach a plateau faster when the acid is adsorbed on the mineral matrix. The calculated half-lifetime of degradation under Martian flux showed in figure 6 and Table 2, are lower in the adsorbed samples, meaning that the acid degrades faster when adsorbed in the vermiculite phase than the pure molecule. This shows that vermiculite has a photocatalizing effect on undecanoic acid under UV irradiation conditions. The band at 1470 cm^{-1} assigned to the bending of CH_2 shows the same tendency in the obtained degradation coefficients (see Table 2) for the pure and the adsorbed sample.

Other bands (5780 cm^{-1}, 5668 cm^{-1} and 1412 cm^{-1}) show a decrease in the sample with vermiculite whereas there is no appreciable change over the resolution of the instrument in the bands of the pure undecanoic acid. This reinforces the hypothesis that vermiculite acts as a photocatalizer for undecanoic acid molecules. Finally, the bands 2939 and 2860 cm^{-1} assigned to the asymmetric and symmetric stretching of CH_2 respectively did not show any decrease neither in the pure nor in the adsorbed sample. The band at 1379 cm^{-1} assigned to the bending of CH_3 showed no degradation in the pure acid but the band was too small in the acid adsorbed to be integrated, therefore no comparison could be performed.

Table 2 : Degradation cross section (σ), degradation coefficients (b) and degradation half-life times ($t_{1/2}$) values calculated for some IR bands of undecanoic acid and L-phenylalanine samples after UV irradiation experiments under laboratory conditions and the extrapolated results under Martian conditions.

				Terrestrial			Martian		
Molecule	**Band (cm^{-1}) and assignement**	**Molecule form**	**σ (cm^{-2})**	**b (s^{-1})**	**$t_{½}$ (s)**	**$t_{½}$ (h)**	**b (s^{-1})**	**$t_{½}$ (s)**	**$t_{½}$ (h)**
Undecanoic Acid	5780 $\nu_s CH_3 + \nu_s CH_2$; $\nu_{as} CH_2$	Pure	No appreciable degradation						
		Adsorbed on vermiculite	$(3.8\pm0.5)\cdot10^{-20}$	$(1.2\pm0.1)\cdot10^{-3}$	583±73	0.16±0.02	$(5.4\pm0.7)\cdot10^{-5}$	12732±1587	3.5±0.4
		With NaCl	$(3.9\pm0.7)\cdot10^{-20}$	$(1.2\pm0.2)\cdot10^{-3}$	584±111	0.16±0.03	$(5.4\pm1.0)\cdot10^{-5}$	12754±2417	3.5±0.7
	5668 $\nu_s CH_3 + \nu_s CH_2$; $\nu_{as} CH_2$	Pure	No appreciable degradation						
		Adsorbed on vermiculite	$(3.8\pm0.5)\cdot10^{-20}$	$(0.1\pm0.02)\cdot10^{-2}$	652±100	0.18±0.03	$(4.9\pm0.7)\cdot10^{-5}$	14242±2195	3.5±0.7
		With NaCl	$(5.7\pm1.6)\cdot10^{-20}$	$(0.2\pm0.05)\cdot10^{-2}$	396±112	0.11±0.03	$(8.0\pm2.3)\cdot10^{-5}$	8656±2451	2.4±0.7
	2962 $\nu_{as} CH_3$	Pure	$(1.5\pm0.2)\cdot10^{-20}$	$(4.5\pm0.6)\cdot10^{-4}$	1500±200	0.42±0.05	$(21\pm3)\cdot10^{-6}$	33000±4000	9±1
		Adsorbed on vermiculite	$(50\pm10)\cdot10^{-20}$	$(1.5\pm0.3)\cdot10^{-2}$	46±9	0.013±0.002	$(7\pm1)\cdot10^{-4}$	1000±200	0.28±0.06
	1720 ν C=O	Pure	$(1.5\pm0.2)\cdot10^{-20}$	$(4.5\pm0.6)\cdot10^{-4}$	1500±200	0.42±0.06	$(21\pm3)\cdot10^{-6}$	33000±5000	9±1
		Adsorbed on vermiculite	$(1.8\pm0.2)\cdot10^{-20}$	$(5.6\pm0.5)\cdot10^{-4}$	1200±100	0.34±0.03	$(25\pm2)\cdot10^{-6}$	27000±3000	7.5±0.7
	1470 δCH_2	Pure	$(5.1\pm2.3)\cdot10^{-20}$	$(1.5\pm0.7)\cdot10^{-3}$	447±207	0.12±0.06	$(7.1\pm3.3)\cdot10^{-5}$	9754±4514	2.7±1.2
		Adsorbed on vermiculite	$(21\pm3.1)\cdot10^{-20}$	$(6.5\pm1.0)\cdot10^{-3}$	106±16	0.029±0.004	$(30\pm4)\cdot10^{-5}$	2321±342	0.64±0.09
	1412 δCH_2	Pure	No appreciable degradation						
		Adsorbed on vermiculite	$(1.8\pm0.2)\cdot10^{-20}$	$(0.6\pm0.07)\cdot10^{-2}$	124±16	0.03±0.004	$(25\pm3)\cdot10^{-5}$	2700±348	0.75±0.09
L-phenylalanine	1510 δNH_3^+	Pure	$(73\pm9)\cdot10^{-20}$	$(2.2\pm0.3)\cdot10^{-2}$	31±4	0.009±0.001	$(1.0\pm0.1)\cdot10^{-3}$	680±90	0.19±0.02
		Adsorbed on vermiculite	$(2.5\pm1)\cdot10^{-20}$	$(1.7\pm0.3)\cdot10^{-3}$	410±70	0.11±0.02	$(8\pm1)\cdot10^{-5}$	9000±2000	2.5±0.4
		With NaCl	$(2.1\pm1)\cdot10^{-20}$	$(6.5\pm3)\cdot10^{-4}$	1068±499	0.29±0.14	$(3\pm1)\cdot10^{-5}$	23334±10894	6.5±3.0

The photocatalytic decomposition of carboxylated molecules have been studied by Shkrob et al. (2010) who proposed that the occurrence of photo-Kolbe reactions at the surface of semiconducting iron(III) oxides initiated by the absorption of UV light was at the origin the catalytic degradation of the molecules. The exchangeable cations positioned in the interlayer space of the vermiculite could have acted as semiconductors (Bish et al., 2013; Fox et al., 2019) inducing a decarboxylation of the acid. The degradation observed for the C=O stretching band could, therefore, be due to the decarboxylation of the undecanoic acid molecules.

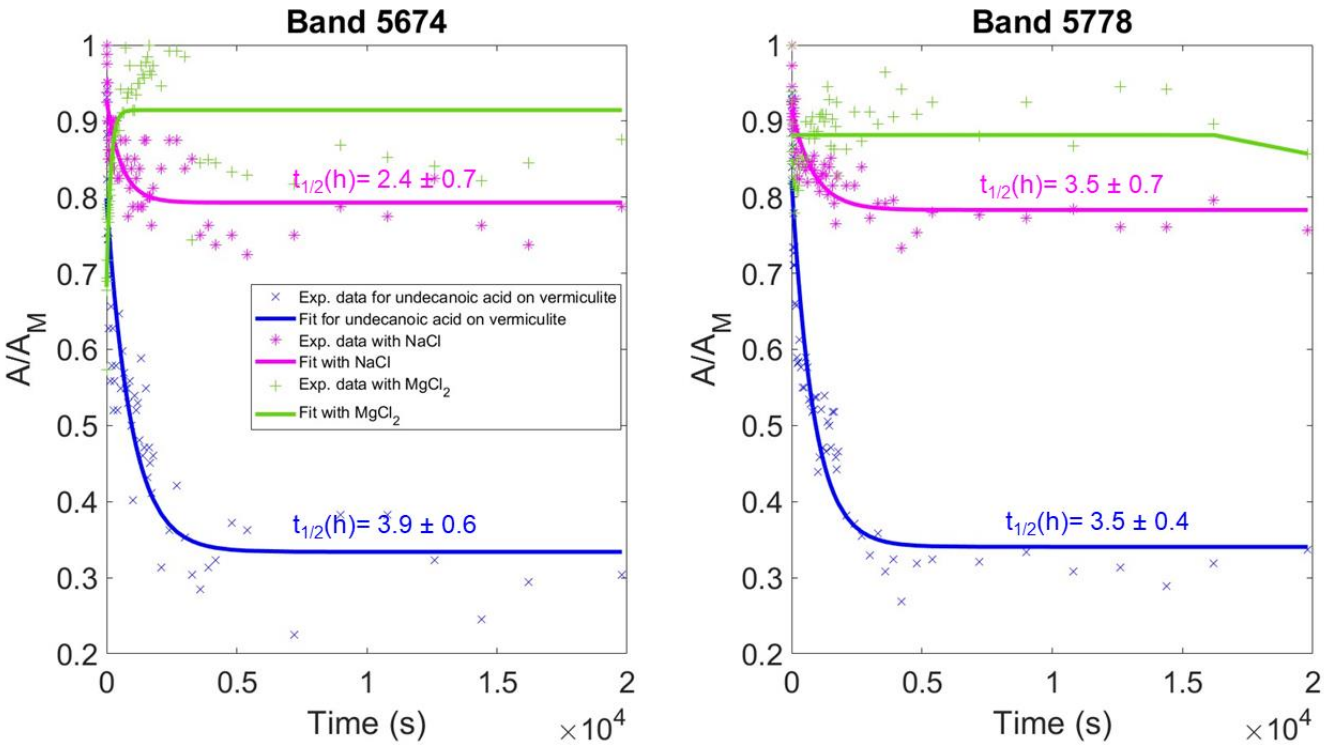

Figure 7: Degradation kinetics curves for bands at 5674 and 5778 cm^{-1} of undecanoic adsorbed on vermiculite (blue), with NaCl (green), with $MgCl_2$ (magenta).

In presence of chloride salts, no bands were found to decrease in presence of $MgCl_2$, thus no degradation of the acid was observed after the UV light exposure. Instead some of them were found to increase (Figure 7). The reason for this behavior could be explained by the evaporation of water present in the sample caused by exposure to UV. Indeed, molecular bands falling within the broad water bands are revealed as the intensity of the water band decreases due to water desorption, reaching a plateau after all the water disappears. Since no decrease of molecular bands was observed in presence of $MgCl_2$, an overall photoprotection behavior can be inferred for undecanoic acid in such mineral matrix. When NaCl was present, in most of the bands no degradation was observed, and the same increasing pattern than in $MgCl_2$ appeared. However, two combination bands (5674 and 5778 cm^{-1}) showed a decrease after the UV irradiation. The band at 5674 cm^{-1} showed a degradation with a lower half-lifetime than in the sample where the salt is absent (t1/2= 2.40 ± 0.7 hours with NaCl and t1/2= 3.96 ± 0.6 hours without salt) which would point at a photocatalyzing effect of NaCl

over this band. It is important to notice that the intervals almost overlap and that the photocatalyzing effect is very small. The band at 5778 cm^{-1}, in contrast, has the same half-lifetime than the band adsorbed on vermiculite without salt. Taking these data into account it can be said that both salts present mainly a photoprotecting behavior for the undecanoic acid adsorbed onto vermiculite.

UV degradation kinetics study revealed that the two inorganic chloride salts are capable of protecting undecanoic acid against UV irradiation. However, the exact mechanism of the protection is not clearly understood. A study by Chang in 1982 on the photoprotective properties of inorganic chloride salts on wood speculated that the incorporation of inorganic ions on wood could result in organic-ion complex systems capable of emitting effective light energy by absorbing and reemitting light through some photophysical decay process. Accordingly, less energy will be absorbed by the organic to initiate photoreactions. Moreover, the newly formed complex system could shift the absorbing zone to a shorter wavelength, which could also interfere with the photochemical reaction (Chang, 1982). A similar reaction pathway could be inferred for undecanoic acid adsorbed on vermiculite in presence of $MgCl_2$ and NaCl.

Another possibility is that the organic molecules are physically protected by the recrystallized chloride salts as they form a barrier protecting them from UV light. Indeed, most mineral that precipitate from aqueous solution incorporate fluid inclusion during growth. These fluid inclusions can capture molecules attached to the crystal surface. During sample preparation, undecanoic acid molecules could have been entrapped as inclusions in magnesium and sodium chloride salts, thus forming a protective cage which prohibits UV light to interact with the organic molecules.

3.2. PHENYLALANINE IN VERMICULITE

3.2.1. Influence of interaction with vermiculite on the Infrared vibrational features of L-phenylalanine

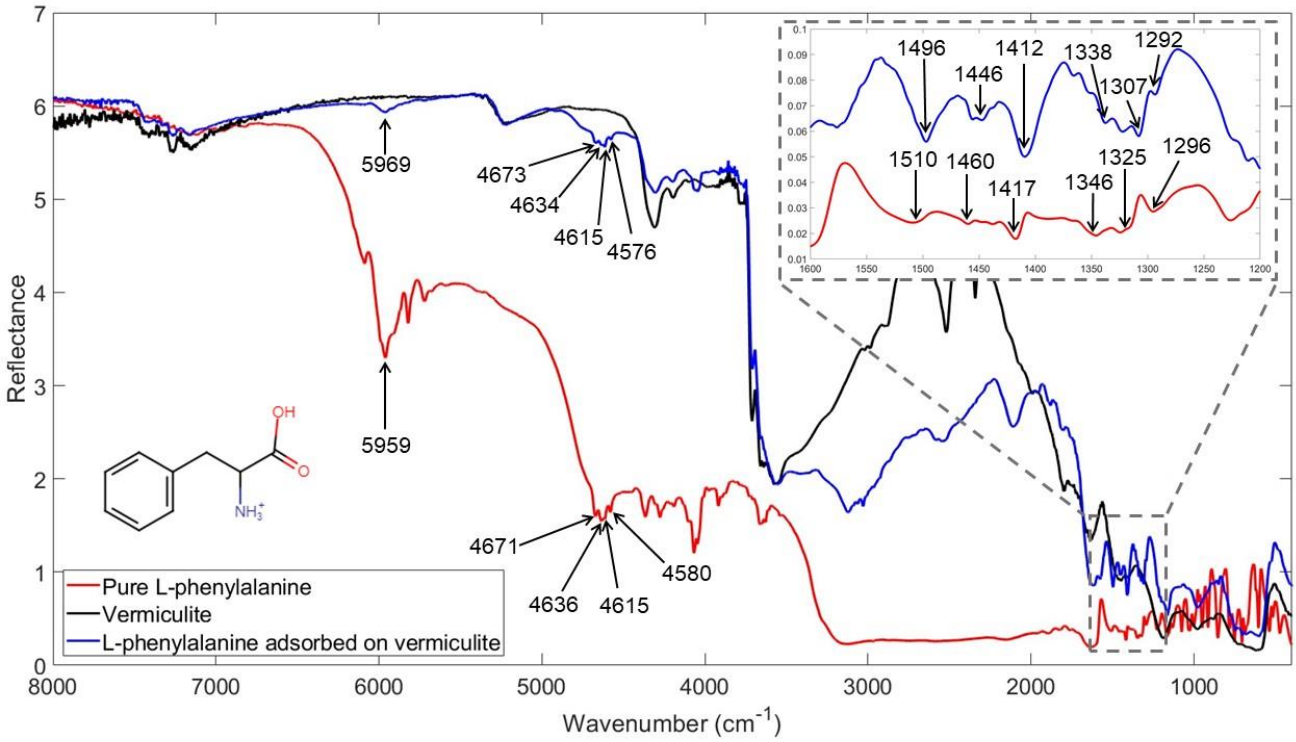

Figure 8: Infrared spectra of vermiculite (black), pure L-phenylalanine (red) and 10 wt.% L-phenylalanine adsorbed on vermiculite (blue) with the wavenumbers marked for the bands of the amino acid detected in both samples.

When L-phenylalanine is adsorbed on vermiculite, most of the characteristic bands of the pure molecule are not detectable due to the high absorption of the vermiculite. In figure 8 are marked the bands of the pure L-phenylalanine that can still be appreciated when the amino acid is adsorbed on vermiculite.

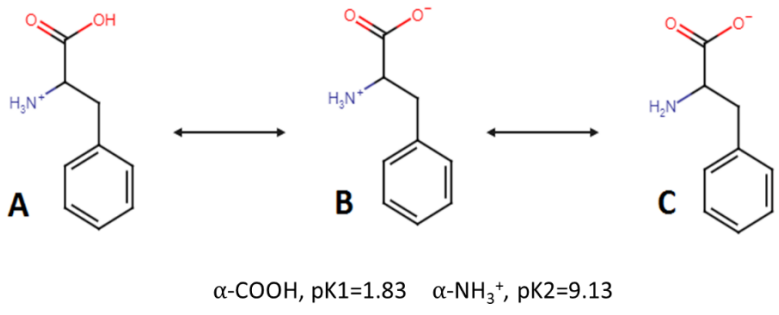

Figure 9: A) Cation form of L-phenylalanine, B) Zwitterionic form of L-phenylalanine, C) Anion form of L-phenylalanine.

L-phenylalanine is expected to be in its zwitterionic form (Figure 9B) in the solid state as well as during the adsorption process of the amino acid onto the mineral when it was dissolved in water (Olsztynska et al., 2001). During the preparation of the sample, the pH was measured at the beginning and at the end of the adsorption process into the vermiculite. The pH slightly varied from 8.21±0.01 to 8.32±0.01, therefore the adsorption process took place at the pH range where the zwitterionic form is predominant. The zwitterionic form of L-phenylalanine presents the amino group in the protonated state, NH_3^+, and the carboxylic group in the deprotonated state, COO-.

In the range > 4000 cm^{-1} five bands due to non-fundamental vibrational modes can be appreciated when the L-phenylalanine is adsorbed on the mineral. In the region 1600 to 1300 cm^{-1}, six bands due to fundamental vibrational modes of the amino acid can be distinguished.

Tentative assignment of experimental NIR bands of pure L-phenylalanine was previously done by Fornaro et al., in 2020. The band at 5959 cm^{-1} was attributed to overtone binary combination of C-H stretching in the aromatic ring, whereas the bands at 4671, 4636 and 4580 cm^{-1} were all attributed to contributions from the combination modes of stretching of the ring and C-H stretching of the aromatic group. Moreover, the band at 1510 cm^{-1} can be attributed to the in plane bending of the NH_3^+ (Griffith & Vaida, 2013; Olsztynska et al., 2001) and is indicative of the ionic form of the nitrogen group in the molecule. No band for the neutral NH_2 group in the anionic form of L-phenylalanine was observed in the IR analysis performed, and the NH_3^+ group for the cationic form of the molecule adsorbs at higher wavenumbers (~1530 cm^{-1}) (Olsztynska et al., 2001). The position of the amine group of L-phenylalanine at 1510 cm^{-1} is therefore, confirming the existence of the molecule in its zwitterionic form.

The band at 1460 cm^{-1} can be assigned to the C-C stretching of the aromatic ring with a possible contribution of the in plane bending of CH_2 and the band at 1417 cm^{-1} can be attributed to the symmetric stretching of the COO- functional group (de Araújo et al., 2021; Olsztynska et al., 2001). The band at 1325 cm^{-1} is assigned to the out of plane

bending of the CH_2 group (Cao & Fischer, 2000; Olsztynska et al., 2001). Finally, the band at 1292 cm^{-1} is assigned to a stretching of a C-C bond by Cao and Fischer. All the assignments are summarized in Table 3.

Table 3 : Band wavenumbers (ṽ) and vibrational mode assignments for pure L-phenylalanine, L-phenylalanine adsorbed on vermiculite, and adsorbed on vermiculite in the presence of sodium chloride (NaCl) or magnesium chloride ($MgCl_2$), along with wavenumber shifts (Δṽ)a with respect to the pure L-phenylalanine and (Δṽ)b with respect to L-phenylalanine adsorbed on vermiculite. ν, stretching; δ, bending; s, symmetric; R, ring, i.p., in plane; o.p., out of plane.

L-phenylalanine	L-phenylalanine on vermiculite		L-phenylalanine on vermiculite + NaCl		L-phenylalanine on vermiculite + $MgCl_2$		Assignment
ṽ (cm^{-1})	ṽ (cm^{-1})	Δ_aṽ (cm^{-1})	ṽ (cm^{-1})	Δ_bṽ (cm^{-1})	ṽ (cm^{-1})	Δ_bṽ (cm^{-1})	
5959	5969	+10	5971	+2	5966	-3	Overtone: $2\nu CH_{aromatic}$
4671	4673	+2	4673	0	4673	0	Combination: $\nu R + \nu CH_{aromatic}$
4636	4634	-2	4641	+7	No band	N/A	Combination: $\nu R + \nu CH_{aromatic}$
4615	4615	0	4615	0	4614	-1	-
4580	4576	-4	4579	+3	4573	-3	Combination: $\nu R + \nu CH_{aromatic}$
1510	1496	-14	1497	+1	1497	+1	i.p. δNH_3^+
1460	1446	-14	1456	+10	1456	+10	ν R/ i.p. δCH_2
1417	1412	-5	1414	+2	1421	+9	$\nu_s COO^-$
1346	1338	-8	1340	+2	1344	+6	-
1325	1307	-18	1308	+1	1304	-3	o.p. δCH_2
1296	1292	-4	No band	N/A	No band	N/A	ν C-C

The band positions observed for the pure L-phenylalanine are shifted when the molecule is adsorbed on vermiculite (see Table 3). The biggest shift appears for the band at 1325 cm^{-1} related with the in plane bending of CH_2 functional group which presents a shift of 18 cm^{-1} to lower wavenumbers when the L-phenylalanine is adsorbed on vermiculite. Both the band at 1510 cm^{-1} related to the in-plane bending

of the NH_3^+ functional group and the band at 1460 cm^{-1} related to the aromatic ring group present a shift of 14 cm^{-1} to lower wavenumbers when the amino acid is adsorbed in the mineral. A much smaller shift of 5 cm^{-1} is observed for the band at 1417 cm^{-1} assigned to the COO- group. These shifts indicate that the functional groups are interacting with the vermiculite mineral phase. In all cases, the shifts are to lower wavenumbers which means that the vibration mode required lower energies, thus indicating a weakening of the bonds due to the interaction with the mineral. In this case, and considering that the shift observed for the COO- functional group is so small that is closed to the resolution of the instrument (4 cm^{-1}), it seems that the molecule is interacting through the positively charged group of the amino acid and through the hydrophobic parts like the CH_2 and the benzene ring. This is pointing out the existence of multiple kinds of interactions in the adsorption mechanisms of L-phenylalanine to vermiculite.

There are many adsorption mechanisms that have been observed for amino acids on clays. For example, the zwitterion form of lysine likely adsorbs on the planar surface of montmorillonite thanks to Van der Waal´s forces (Rao et al., 1980). The existence of Van der Waal´s forces in the adsorption of L-phenylalanine would explain the shift observed for the band at 1325 cm^{-1} of the CH_2 group. Van der Waal´s forces can also result from the polarization of the aromatic ring, which could also explain the important shift observed for the band at 1460 cm^{-1} related to the aromatic ring in the adsorption of L-phenylalanine. In addition, the adsorption of planar aromatic molecules may be assisted by the interaction of the π electrons of an aromatic system with the surface oxygens of the clay, which would also explain the shift observed for the band related to the aromatic ring. However, the L-phenylalanine CH_2-CNH_3^+-COO- group is not planar and it complicates the approximation of the aromatic system to the mineral surface. Other works suggest that both the amino and the carboxylic groups are involved in the adsorption of amino acids (Hashizume, 2012). Cloos et al. (1966) suggested that there are two different types of adsorption of amino acids onto montmorillonite, also a 2:1 layer clay mineral. A strong adsorption can take place

between the cationic amino group and the negatively-charged interlayer sites of the clay surfaces and another weaker adsorption of the amino group can occur though the carboxyl group of another amino acid already strongly adsorbed to the mineral surface (Cloos et al., 1966). This would explain both shifts observed for the band at 1510 cm^{-1} related to NH_3^+ and the small shift for the band at 1417 cm^{-1} related to the COO-. Finally, other studies observed the complexation of the interlayer cations of the mineral by the carboxylate group of the zwitterion (Lagaly et al., 2013).

The XRPD pattern of vermiculite with 10 wt.% of L-phenylalanine absorbed is reported in figure 3 (blue line). Comparing this pattern with the one of "free" vermiculite (black), the absorption of the amino acid molecules does not cause the shift of the peaks in the pattern. In contrast, some significant differences in the relative peaks' intensities are detectable, as already observed for the vermiculite with the absorbed undecanoic acid. Furthermore, it is also remarkable to note that the presence of a shoulder at 2θ value of 7.41 and a small peak at 19.45 degrees that is scarcely perceptible in the vermiculite with the absorbed undecanoic acid and almost non-existent in the "free" vermiculite. Thus, also, in this case, we can conclude that the L-phenylalanine molecules are incorporated in the layers of the vermiculite, probably substituting water molecules, with no modification of the vermiculite skeleton. These observations support the existence of several mechanisms that involve the interaction between the cationic amino group and the negatively charged interlayers of the surface or the complexation of the interlayer cations by the carboxylate group of the zwitterion, both functional groups with shifts in the IR spectrum.

3.2.2. Influence of chloride salts on the spectroscopic features of L-phenylalanine adsorption on vermiculite

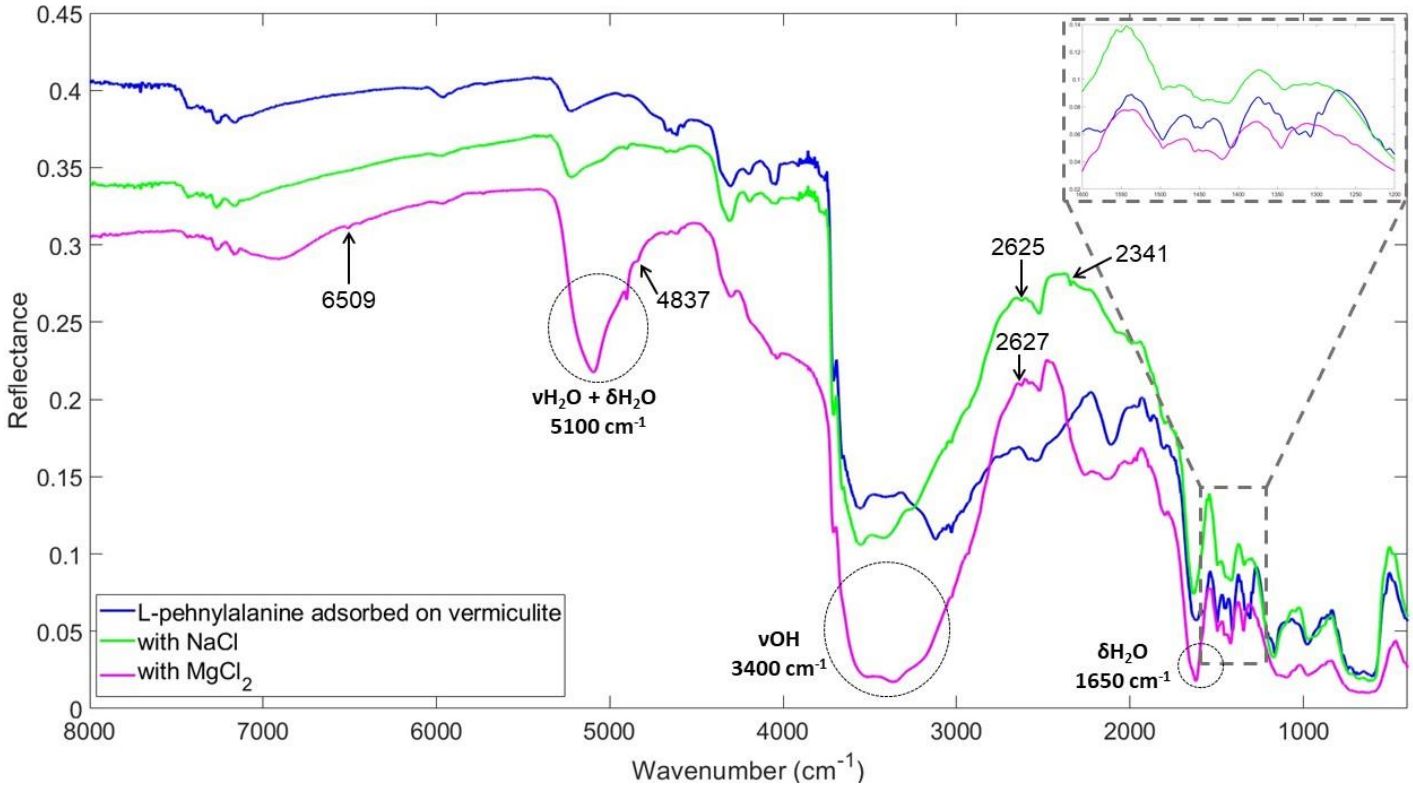

Figure 10: Infrared spectra of 10 wt.% L-phenylalanine adsorbed on vermiculite (blue), adsorbed in the presence of sodium chloride (NaCl) (green), and in the presence of magnesium chloride ($MgCl_2$) (magenta). New bands appearing in the presence of salts are indicated with their wavenumber.

As previously described, the dominating feature of the spectra when chloride salts are added to the samples is water bands due to the high hygroscopic nature of NaCl and $MgCl_2$. Moreover, the presence of chloride salts in the adsorption of L-phenylalanine on vermiculite caused shifts in some of the vibrational frequencies of the adsorbed L-phenylalanine with respect to the ones observed when the adsorption took place without the presence of the salts. Specifically, when sodium chloride was added to the sample, 7 cm^{-1} and 10 cm^{-1} shifts to higher frequency of the bands at 4634 cm^{-1} and 1446 cm^{-1} were observed with respect to their positions in the spectrum of L-phenylalanine adsorbed on vermiculite without any addition of chloride salts. Since the 4634 cm^{-1} band is a combination of ring stretching and aromatic CH stretching and the

band at 1446 cm^{-1} is a ring stretching, these high-frequency shifts suggest a strengthening of the ring, which may mean a lower interaction between the aromatic ring and the mineral. The same shift was observed for this group when the adsorption of L-phenylalanine was performed in the presence of $MgCl_2$. This would agree with the observations of some works where the adsorption onto minerals is generally decreased with the increasing concentrations of salts (Farias et al., 2014; Norén et al., 2008). Moreover, when the adsorption of L-phenylalanine was performed increasing the ionic strength by substituting the NaCl by $MgCl_2$ in the same concentration, a new shift to higher wavenumbers was observed for the band related to the C=O functional group at 1412 cm^{-1}: 2 cm^{-1} for NaCl (under the resolution of the instrument) and 9 cm^{-1} for $MgCl_2$. The shift to higher wavenumbers implies an absorption of a higher energy radiation and therefore a strengthening of the C=O bond, probably due to its lower participation in the adsorption with the mineral. This observation would agree with the fact that the higher the ionic strength, the lower the electrostatic interactions with the mineral (Zaia, 2012).

Moreover, new bands appeared when sodium and magnesium chlorides were added to the L-phenylalanine adsorbed on vermiculite samples. Specifically, three new bands at 6509 cm^{-1}, 4837 cm^{-1}, and 2627 cm^{-1}, indicated in Figure 10, appeared when magnesium chloride was added to the adsorption process, whereas two new bands appeared at 2625 cm^{-1} and 2341 cm^{-1} in the presence of sodium chloride. These bands were not identified in the pure L-phenylalanine, nor in the adsorbed samples without the salts. These new bands may indicate the formation of news bonds, likely mediated by the presence of the Na^+ and Mg^{2+} cations which might have acted as bridges for molecular adsorption on vermiculite. The cross-interaction between NaCl or $MgCl_2$ and L-phenylalanine could have led to the chlorination of the amino acid through the substitution on the aromatic ring of a chlorine, however, this would have led to the appearance of a new band between 690 and 770 cm^{-1} which is not observed in the spectra. The formation of an acid chloride with the substitution of the OH group by a Cl is also not plausible as the band would be situated at lower wavenumber between

1800 and 1770 cm^{-1}.

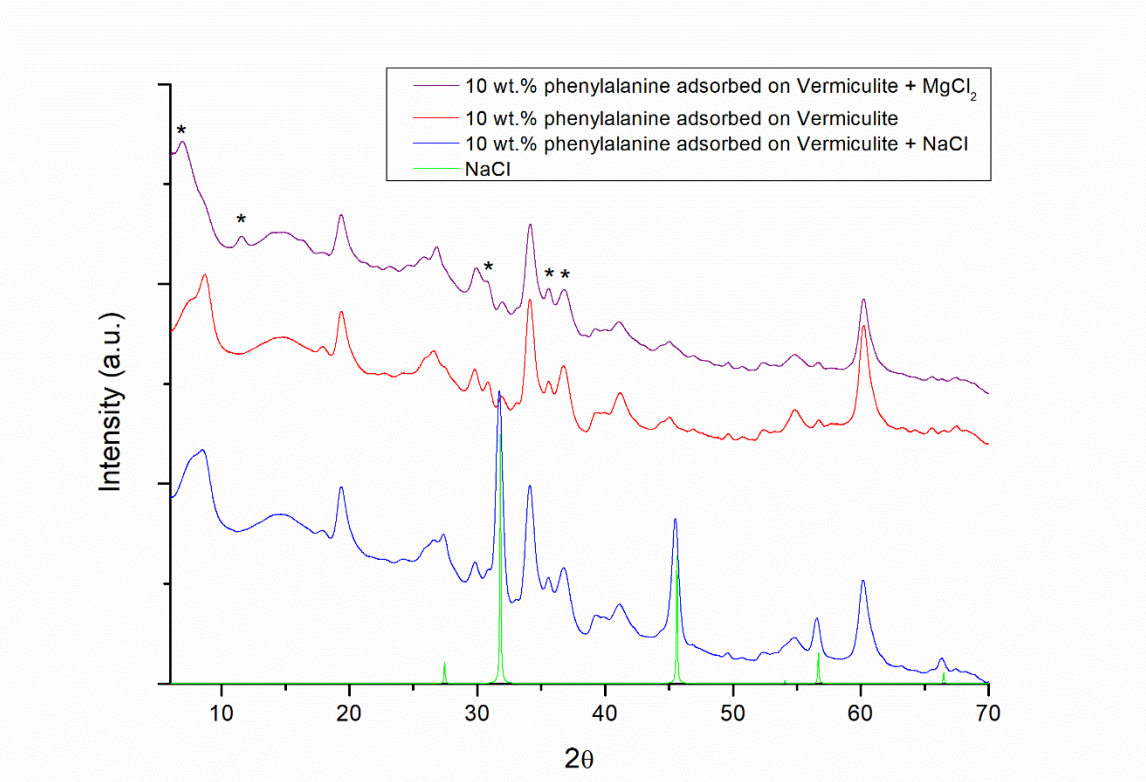

Figure 11: XRPD patterns of 10 wt.% phenylalanine adsorbed on vermiculite (red), adsorbed on vermiculite in presence of sodium chloride (NaCl) (blue), and in presence of magnesium chloride ($MgCl_2$) (purple). The XRPD pattern of free NaCl (green) is also reported.

The XRPD pattern of phenylalanine adsorbed on vermiculite in presence of NaCl (Figure 11) show evidences of free solid NaCl mixed to the vermiculite sample, as already observed for the corresponding undecanoic acid sample. However, in this case the pattern is not modified in the relative intensities of the peaks with respect to the phenylalanine adsorbed in absence of NaCl. In fact, apart for the presence of the NaCl peaks, the pattern is identical to the one of the phenylalanine adsorbed on vermiculite in absence of salts. Thus, the presence of NaCl seems not to have a role in the interlayer absorption of the phenylalanine on vermiculite. However, as described above, the IR spectrum showed changes in the C-H and ring stretching bands of the molecule. Both functional groups interact with the surface of the mineral. The addition of NaCl is, therefore, only affecting the surface interactions with vermiculite. Moreover, if we

compare the spectra of pure vermiculite and the sample with NaCl, we can identify the presence of pure NaCl at 3400 cm^{-1} (see Figure S3).

As for the undecanoic sample, the free $MgCl_2$ is not visible in the XRPD pattern, but some differences in the peak intensities are observed with respect to the pattern without the salt (peaks evidenced with stars in Figure 11). Thus, in the case of phenylalanine absorbed on vermiculite in presence of $MgCl_2$, we can conclude that the salt interacts slightly with the vermiculite, and consequently it can be hypothesized that it could have a role in the adsorption of the organic molecule in the interlayer of the mineral. However, according to the IR observations, $MgCl_2$ is not favoring the interaction between the organic molecule and the vermiculite as seen by the shift to higher wavenumbers of the C=O bond. Therefore, the observed changes in the relative intensities of the XRPD patterns could be due to a smaller amount of organic molecules in the vermiculite interlayer substituting the water molecules.

3.2.3. UV irradiation

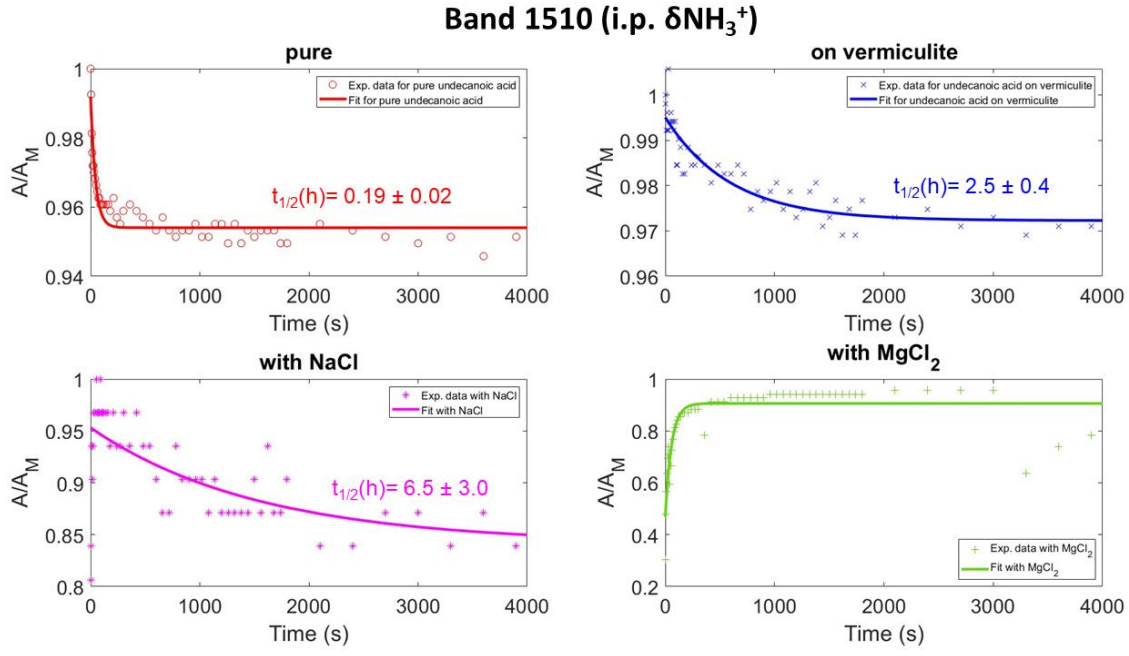

Figure 12: Degradation kinetics curve for the band at 1510 cm^{-1} (i.p. δ NH_3^+) of pure L-phenylalanine (red) and L-phenylalanine adsorbed on vermiculite (blue), in presence of NaCl (magenta) and in presence of $MgCl_2$ (green), and the corresponding half-lifetimes of degradation under Martian UV flux expressed in hours.

For the UV irradiation experiments performed over pure L-phenylalanine and L-phenylalanine adsorbed on vermiculite, only the band at 1510 cm^{-1} corresponding to the in plane bending of the amino group, is showing a decrease after the UV irradiation for both the pure molecule and the molecule adsorbed on the mineral (Figure 12). The degradation coefficients for the calculated laboratory and extrapolated Martian conditions and the cross section for this band are shown in Table 2. The degradation kinetics curve and the calculated half-lifetime of degradation for the pure and the adsorbed amino acid indicate that the molecule is degrading faster in the pure state than when adsorbed on the mineral. This means that, vermiculite is acting as a photoprotector for L-phenylalanine against UV radiation.

The rest of the bands of the pure L-phenylalanine showed no degradation showing a good stability of the amino acid against UV. Considering that the stability of the amino acid could have complicated the study of the role of vermiculite, it was decided to extend the irradiation time from 1h10 to up to 10h30. However, no further degradation in the pure L-phenylalanine bands was observed. Moreover, the bands detected in the spectra of L-phenylalanine adsorbed on vermiculite also do not show any changes that can be appreciated under the resolution of the instrument, therefore indicating that they may not be degrading under UV light or at a rate that cannot be detected with our experimental setup. In some other cases for the amino acid adsorbed onto the mineral, the increasing pattern also appeared (bands 1417 and 1296 cm^{-1}) due to the evaporation of atmospheric water.

Taking these data into account, it seems that the L-phenylalanine is stable under UV light, and according to the band 1510 cm^{-1} for which a degradation could be appreciated, the vermiculite seems to have a photoprotecting nature for L-phenylalanine. Different studies have previously shown the photoprotective effect of clay minerals on the evolution of the amino acids under UV radiation (dos Santos et al., 2016; Ertem et al., 2017; Kate et al., 2005; Poch et al., 2015). Several mechanisms explaining this phenomenon were proposed such as mechanical shielding but also a

stabilizing molecule-mineral interaction that could allow a more efficient energy dissipation (Poch et al., 2015). Moreover, the overall low degradation of L-phenylalanine suggests its high stability. The stability of the radical is dependent on the substituents bonded to the α-carbon atom. A study by (Kate et al., 2005) showed that alkyl substituent groups attached to the α-carbon atom contribute towards the stability of the resulting alkyl amine radical that forms after UV-induced decarboxylation and prolong the life of the amino acid. We infer a similar reasoning for aromatic amino acids such as L-phenylalanine, where the highly stable aromatic phenyl group should contribute to the stability of the molecule and therefore, its photoprotection. Moreover, Poch et al. (2014) results indicate that aromatic molecules are at least ten times more resistant to Martian UV compared to non-aromatic molecules.

Moreover, in figure 13 the ToF-SIMS images obtained for L-phenylalanine and undecanoic acid adsorbed on vermiculite are shown. In this figure, areas where L-phenylalanine molecules are agglomerating are observed, whereas the undecanoic acid is overall homogenously distributed on the vermiculite. Fornaro et al. (2018) suggested that the formation of molecular aggregates in which some molecules are directly exposed to radiation while others are covered and more protected could also be a mechanism of photoprotection.

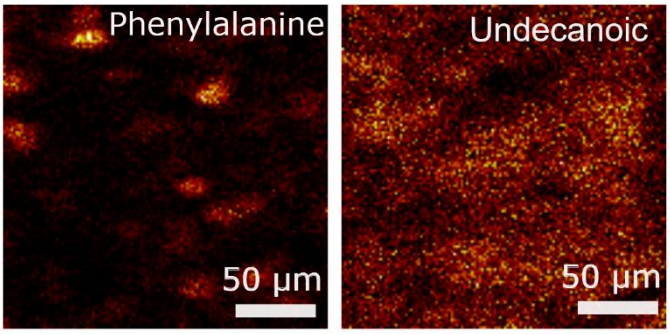

Figure 13: ToF-SIMS image of L-phenylalanine ($C_9N_{12}O_2^+$, m/z 166.09) and undecanoic acid ($C_{11}H_{21}O_2^-$, m/z 185.15) adsorbed on vermiculite.

In the presence of NaCl, the band at 1496 cm^{-1} decreases much more slowly ($t_{1/2}$= 6.48±3.00 h) than in the pure ($t_{1/2}$= 0.19±0.02 h) and in the sample adsorbed onto vermiculite $t_{1/2}$= (2.5±0.4 h) (Figure 12), pointing at a photoprotective behavior of sodium chloride. In presence of $MgCl_2$, an increase in the kinetics curve of the band is observed (Figure 12). These data indicate that chloride salts protect the amino acid from degradation under UV light, exhibiting a photoprotective behavior towards L-phenylalanine. As previously described, adsorption of L-phenylalanine on vermiculite in the presence of chloride salts could have generated cross-reactions between the amino acid and the salt leading to the formation of complexes decreasing the effects of UV lights on the molecules or through crystalline salt shelters protecting the molecules from the radiations.

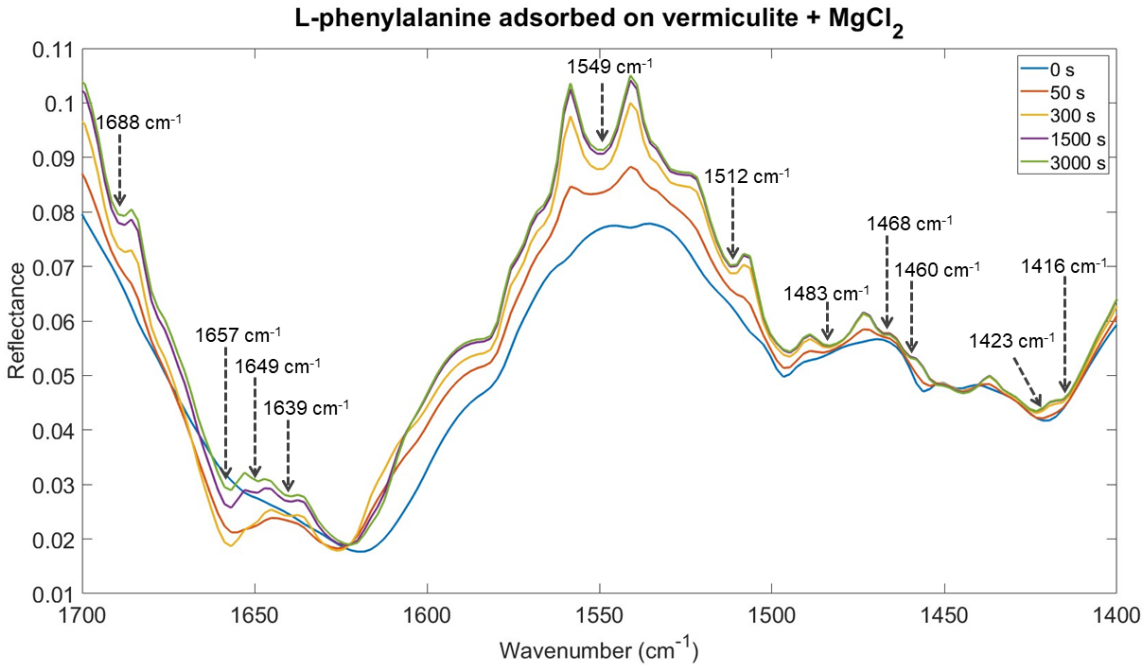

Figure 14: IR spectra of L-phenylalanine adsorbed on vermiculite with $MgCl_2$ at different irradiation times. New bands are indicated by their wavenumber.

Moreover, as can be observed in Figure 14, in the case of L-phenylalanine adsorbed on vermiculite in the presence of magnesium chloride, new bands in the 1700-1400 cm^{-1} range formed during UV irradiation. These bands appear at 1657 cm^{-1}, 1649 cm^{-1}, and 1639 cm^{-1} and are situated within the broad water bending band at 1650 cm^{-1}

described above (Figure 10). They could have appeared due to the decrease in the water content of the sample during the irradiation process where water molecules are cleaved to form radicals or simply evaporated due to a rise in temperature on the sample by the heating of the UV lamp. The emergence of new bands in the 1550-1400 cm^{-1} region is indicative of the formation of new molecules from the interaction of the adsorbed L-phenylalanine on vermiculite and magnesium chloride under UV irradiation, possibly formed through the reactivity of radicals coming from the water adsorbed by the salt which would form new molecules when interacting with L-phenylalanine, or through catalytic effect of Mg^{2+}. It has been shown that following the photolysis of a parent molecule, the produced fragments can rearrange or react with their environment to form new molecules (Poch et al., 2014).

4. CONCLUSION

In this work, the undecanoic acid and L-phenylalanine adsorbed onto vermiculite with and without the presence of chloride salts was studied by means of FTIR spectroscopy to assist the Martian exploration missions to detect and identify organic molecules by showing the changes on the IR spectra of organic molecules due to the different adsorptions. The presence of chloride salts plays a role in the adsorption process of the organic molecules onto the vermiculite matrix. We observed that $MgCl_2$ favors adsorption of the organic species more than NaCl as seen as seen in XRPD. Moreover, this work also studied the stability of these two organic molecules against UV irradiation, an important degradation factor that may be affecting the presence of organic molecules on the surface of Mars. The irradiation laboratory simulations performed in this work showed that vermiculite can act as a photocatalyzer for the undecanoic acid and as a photoprotector for L-phenylalanine and that the degradation due to the UV radiation can be abated by the presence of sodium or magnesium chlorides. This study confirms that, the straight forward classification of Martian minerals as photocatalytic or photoprotective is not possible, since the behavior of minerals under Martian conditions may depend on the organic molecules involved and

their specific interactions with the mineral surface sites. However, from this study it turns out that chloride salts could preserve the integrity of organic molecules such as amino acids or fatty acids by protecting them from photocatalysis and therefore be interesting targets for the detection of organic matter by current and future missions performing *in situ* measurements.

REFERENCES

Abbey, W., Anderson, R., Beegle, L., Hurowitz, J., Williford, K., Peters, G., Morookian, J. M., Collins, C., Feldman, J., & Kinnett, R. (2019). A look back: The drilling campaign of the Curiosity rover during the Mars Science Laboratory's Prime Mission. Icarus, 319, 1-13.

Barone, V. (2005). Anharmonic vibrational properties by a fully automated second-order perturbative approach. The Journal of chemical physics, 122(1), 014108.

Barone, V., Biczysko, M., & Bloino, J. (2014). Fully anharmonic IR and Raman spectra of medium-size molecular systems: accuracy and interpretation. Physical Chemistry Chemical Physics, 16(5), 1759-1787.

Benner, S. A., Devine, K. G., Matveeva, L. N., & Powell, D. H. (2000). The missing organic molecules on Mars. Proceedings of the National Academy of Sciences, 97(6), 2425-2430. https://doi.org/10.1073/pnas.040539497

Bibring, J.-P., Hamm, V., Pilorget, C., & Vago, J. L. (2017). The micrOmega investigation onboard ExoMars. Astrobiology, 17(6-7), 621-626.

Biczysko, M., Bloino, J., & Puzzarini, C. (2018). Computational challenges in Astrochemistry. Wiley Interdisciplinary Reviews: Computational Molecular Science, 8(3), e1349.

Biemann, K. O., J., Toulmin, P., Orgel, L. E., Nier, A. O., Anderson, D. M., ... & Biller, J. A. (1976). Search for Organic and Volatile Inorganic Compounds in Two Surface Samples from the Chryse Planitia Region of Mars. Science, 194(4260), 72-76.

Bish, D. L., Blake, D., Vaniman, D., Chipera, S., Morris, R., Ming, D., Treiman, A., Sarrazin, P., Morrison, S., & Downs, R. (2013). X-ray diffraction results from Mars Science Laboratory: Mineralogy of Rocknest at Gale crater. Science, 341(6153), 1238932.

Bloino, J. (2015). A VPT2 route to near-infrared spectroscopy: the role of mechanical and electrical anharmonicity. The Journal of Physical Chemistry A, 119(21), 5269-5287.

Bloino, J., Baiardi, A., & Biczysko, M. (2016). Aiming at an accurate prediction of vibrational and electronic spectra for medium-to-large molecules: an overview. International Journal of Quantum Chemistry, 116(21), 1543-1574.

Bloino, J., Biczysko, M., & Barone, V. (2015). Anharmonic effects on vibrational spectra intensities: infrared, Raman, vibrational circular dichroism, and Raman optical activity. The Journal of Physical Chemistry A, 119(49), 11862-11874.

Brubach, J.-B., Mermet, A., Filabozzi, A., Gerschel, A., & Roy, P. (2005). Signatures of the hydrogen bonding in the infrared bands of water. The Journal of chemical physics, 122(18), 184509.

Burton, A. S., Stern, J. C., Elsila, J. E., Glavin, D. P., & Dworkin, J. P. (2012). Understanding prebiotic chemistry through the analysis of extraterrestrial amino acids and nucleobases in meteorites. Chemical Society Reviews, 41(16), 5459-5472.

Cao, X., & Fischer, G. (2000). The infrared spectra and molecular structure of zwitterionic L-β-phenylalanine. Journal of Molecular Structure, 519(1-3), 153-163.

Carter, J., Quantin, C., Thollot, P., Loizeau, D., Ody, A., & Lozach, L. (2016). Oxia planum: A clay-laden landing site proposed for the ExoMars rover mission: Aqueous mineralogy and alteration scenarios. Lunar and planetary science conference,

Chang, S.-T. (1982). Photodegradation and photoprotection of wood surfaces. US Forest Products Laboratory.

Chapman, D. (1965). Infrared spectroscopy of lipids. Journal of the American Oil Chemists' Society, 42(5), 353-371.

Clark, J. V., Sutter, B., McAdam, A. C., Rampe, E. B., Archer, P. D., Ming, D. W., Navarro-Gonzalez, R., Mahaffy, P., & Lapen, T. J. (2020). High-Temperature HCl Evolutions From Mixtures of Perchlorates and Chlorides With Water-Bearing Phases: Implications for the SAM Instrument in Gale Crater, Mars. Journal of Geophysical Research: Planets, 125(2). https://doi.org/10.1029/2019je006173

Cloos, P., Calicis, B., Fripiat, J., & Makay, K. (1966). Adsorption of amino-acids and peptides by montmorillonite. I. Chemical and X-ray diffraction studies. Proceedings of the International Clay Conference, Jerusalem, Israel,

Coradini, A., Piccioni, G., Amici, S., Bianchi, R., Capaccioni, F., Capria, M., De Sanctis, M., Di Lellis, A., Espinasse, S., & Federico, C. (2001). MA_MISS: Mars multispectral imager for subsurface studies. Advances in space research, 28(8), 1203-1208.

Cronin, J., & Pizzarello, S. (1983). Amino acids in meteorites. Advances in space research, 3(9), 5-18.

de Araújo, D. T., Ciuffi, K. J., Nassar, E. J., Vicente, M. A., Trujillano, R., Rives, V., Bernal, E. P., & de Faria, E. H. (2021). Grafting of L-proline and L-phenylalanine amino acids on kaolinite through synthesis catalyzed by boric acid. Applied Surface Science Advances, 4, 100081.

dos Santos, R., Patel, M., Cuadros, J., & Martins, Z. (2016). Influence of mineralogy on the preservation of amino acids under simulated Mars conditions. Icarus, 277, 342-353.

E. Dehouck, O. F., C. Quantin-Nataf, P. Beck,, N. Mangold, C. R., E. Clavé, O. Beyssac, J. R. Johnson, L. Mandon, F. Poulet, S. Le Mouélic, G. Caravaca, H. Kalucha,, E. Gibbons, G. D., P. Gasda, P.-Y. Meslin, S. Schroeder, A. Udry, R. B. Anderson, S. Clegg, A. Cousin, T. S., Gabriel, J. L., T. Fouchet, P. Pilleri, C. Pilorget, J. Hurowitz, J. Núñez, A. Williams, P. Russell, J. I. Simon, S., & Maurice, R. C. W. (2023). Overview of the bedrock geochemistry and mineralogy observed by SuperCam during Perseverance's delta front campaign 54th Lunar and Planetary Science Conference 2023,

Ehlmann, B. L., Mustard, J. F., Fassett, C. I., Schon, S. C., Head III, J. W., Des Marais, D. J., Grant, J. A., & Murchie, S. L. (2008). Clay minerals in delta deposits and organic preservation potential on Mars. Nature Geoscience, 1(6), 355-358.

Ehrlich, S., Moellmann, J., Reckien, W., Bredow, T., & Grimme, S. (2011). System-dependent dispersion coefficients for the DFT-D3 treatment of adsorption processes on ionic surfaces. ChemPhysChem, 12(17), 3414-3420.

Eigenbrode, J. L., Summons, R. E., Steele, A., Freissinet, C., Millan, M., Navarro-González, R., Sutter, B., McAdam, A. C., Franz, H. B., Glavin, D. P., Archer, P. D., Mahaffy, P. R., Conrad, P. G., Hurowitz, J. A., Grotzinger, J. P., Gupta, S., Ming, D. W., Sumner, D. Y., Szopa, C., Malespin, C., Buch, A., & Coll, P. (2018). Organic matter preserved in 3-billion-year-old mudstones at Gale crater, Mars. Science, 360(6393), 1096-1101. https://doi.org/10.1126/science.aas9185

Ertem, G., Ertem, M., McKay, C., & Hazen, R. (2017). Shielding biomolecules from effects of radiation by Mars analogue minerals and soils. International Journal of Astrobiology, 16(3), 280-285.

Farias, A. P. S., Tadayozzi, Y. S., Carneiro, C. E., & Zaia, D. A. (2014). Salinity and pH affect Na+-montmorillonite dissolution and amino acid adsorption: a prebiotic chemistry study. International Journal of Astrobiology, 13(3), 259-270.

Farmer, J. D., & Des Marais, D. J. (1999). Exploring for a record of ancient Martian life. Journal of Geophysical Research: Planets, 104(E11), 26977-26995. https://doi.org/10.1029/1998je000540

Filopoulou, A., Vlachou, S., & Boyatzis, S. C. (2021). Fatty Acids and Their Metal Salts: A Review of Their Infrared Spectra in Light of Their Presence in Cultural Heritage. Molecules, 26(19), 6005.

Fornaro, T., Biczysko, M., Bloino, J., & Barone, V. (2016). Reliable vibrational wavenumbers for C [double bond, length as m-dash] O and N–H stretchings of isolated and hydrogen-bonded nucleic acid bases. Physical Chemistry Chemical Physics, 18(12), 8479-8490.

Fornaro, T., Biczysko, M., Monti, S., & Barone, V. (2014). Dispersion corrected DFT approaches for anharmonic vibrational frequency calculations: nucleobases and their dimers. Physical Chemistry Chemical Physics, 16(21), 10112-10128.

Fornaro, T., Boosman, A., Brucato, J. R., Ten Kate, I. L., Siljeström, S., Poggiali, G., Steele, A., & Hazen, R. M. (2018). UV irradiation of biomarkers adsorbed on minerals under Martian-like conditions: Hints for life detection on Mars. Icarus, 313, 38-60. https://doi.org/10.1016/j.icarus.2018.05.001

Fornaro, T., Brucato, J. R., Pace, E., Guidi, M. C., Branciamore, S., & Pucci, A. (2013). Infrared spectral investigations of UV irradiated nucleobases adsorbed on mineral surfaces. Icarus, 226(1), 1068-1085.

Fornaro, T., Brucato, J. R., Poggiali, G., Corazzi, M. A., Biczysko, M., Jaber, M., Foustoukos, D. I., Hazen, R. M., & Steele, A. (2020). UV irradiation and near infrared characterization of laboratory Mars soil analog samples. Frontiers in Astronomy and Space Sciences, 7, 539289.

Fornaro, T., Burini, D., Biczysko, M., & Barone, V. (2015). Hydrogen-bonding effects on infrared spectra from anharmonic computations: uracil–water complexes and uracil dimers. The Journal of Physical Chemistry A, 119(18), 4224-4236.

Fornaro, T., Steele, A., & Brucato, J. (2018). Catalytic/Protective Properties of Martian Minerals and Implications for Possible Origin of Life on Mars. Life, 8(4), 56. https://doi.org/10.3390/life8040056

Fornaro, T., Brucato, J. R., Feuillie, C., Sverjensky, D. A., Hazen, R. M., Brunetto, R., d'Amore, M., & Barone, V. (2018). Binding of nucleic acid components to the serpentinite-hosted hydrothermal mineral brucite. Astrobiology, 18(8), 989-1007.

Fouchet, T., Reess, J.-M., Montmessin, F., Hassen-Khodja, R., Nguyen-Tuong, N., Humeau, O., Jacquinod, S., Lapauw, L., Parisot, J., & Bonafous, M. (2022). The SuperCam infrared spectrometer for the perseverance rover of the Mars2020 mission. Icarus, 373, 114773.

Fox, A. C., Eigenbrode, J. L., & Freeman, K. H. (2019). Radiolysis of Macromolecular Organic Material in Mars-Relevant Mineral Matrices. Journal of Geophysical Research: Planets, 124(12), 3257-3266. https://doi.org/10.1029/2019je006072

Freissinet, C., Glavin, D. P., Mahaffy, P. R., Miller, K. E., Eigenbrode, J. L., Summons, R. E., Brunner, A. E., Buch, A., Szopa, C., Archer, P. D., Franz, H. B., Atreya, S. K., Brinckerhoff, W. B., Cabane, M., Coll, P., Conrad, P. G., Des Marais, D. J., Dworkin, J. P., Fairén, A. G., François, P., Grotzinger, J. P., Kashyap, S., Ten Kate, I. L., Leshin, L. A., Malespin, C. A., Martin, M. G., Martin-Torres, F. J., McAdam, A. C., Ming, D. W., Navarro-González, R., Pavlov, A. A., Prats, B. D., Squyres, S. W., Steele, A., Stern, J. C., Sumner, D. Y., Sutter, B., & Zorzano, M. P. (2015). Organic molecules in the Sheepbed Mudstone, Gale Crater, Mars. Journal of Geophysical Research: Planets, 120(3), 495-514. https://doi.org/10.1002/2014je004737

Frisch, M., Trucks, G., Schlegel, H., Suzerain, G., Robb, M., Cheeseman Jr, J., Montgomery, J., Vreven, T., Kudin, K., & Burant, J. (2016). Gaussian 09 (now Gaussian 16). Gaussian Inc., Wallingford (CT).

Grabska, J., Ishigaki, M., Bec, K. B., Wójcik, M. J., & Ozaki, Y. (2017). Correlations between structure and near-infrared spectra of saturated and unsaturated carboxylic acids. Insight from anharmonic density functional theory calculations. The Journal of Physical Chemistry A, 121(18), 3437-3451.

Griffith, E. C., & Vaida, V. (2013). Ionization state of L-phenylalanine at the air–water interface. Journal of the American Chemical Society, 135(2), 710-716.

Grimme, S., Antony, J., Ehrlich, S., & Krieg, H. (2010). A consistent and accurate ab initio parametrization of density functional dispersion correction (DFT-D) for the 94 elements H-Pu. The Journal of chemical physics, 132(15), 154104.

Grimme, S., Ehrlich, S., & Goerigk, L. (2011). Effect of the damping function in dispersion corrected density functional theory. Journal of computational chemistry, 32(7), 1456-1465.

Guzman, M., McKay, C. P., Quinn, R. C., Szopa, C., Davila, A. F., Navarro-González, R., & Freissinet, C. (2018). Identification of Chlorobenzene in the Viking Gas

Chromatograph-Mass Spectrometer Data Sets: Reanalysis of Viking Mission Data Consistent With Aromatic Organic Compounds on Mars. Journal of Geophysical Research: Planets, 123(7), 1674-1683. https://doi.org/10.1029/2018je005544

Hashizume, H. (2012). Role of clay minerals in chemical evolution and the origins of life. Clay Minerals in Nature—Their characterization, modification and application.

Jakosky, B. M., Slipski, M., Benna, M., Mahaffy, P., Elrod, M., Yelle, R., Stone, S., & Alsaeed, N. (2017). Mars' atmospheric history derived from upper-atmosphere measurements of 38Ar/36Ar. Science, 355(6332), 1408-1410.

Karunatillake, S., Keller, J. M., Squyres, S. W., Boynton, W. V., Brückner, J., Janes, D. M., Gasnault, O., & Newsom, H. E. (2007). Chemical compositions at Mars landing sites subject to Mars Odyssey Gamma Ray Spectrometer constraints. Journal of Geophysical Research: Planets, 112(E8). https://doi.org/10.1029/2006je002859

Kate, I. L., Garry, J. R. C., Peeters, Z., Quinn, R., Foing, B., & Ehrenfreund, P. (2005). Amino acid photostability on the Martian surface. Meteoritics & Planetary Science, 40(8), 1185-1193. https://doi.org/10.1111/j.1945-5100.2005.tb00183.x

Lagaly, G., Ogawa, M., & Dékány, I. (2013). Clay mineral–organic interactions. In Developments in clay science (Vol. 5, pp. 435-505). Elsevier.

Mandon, L., Parkes Bowen, A., Quantin-Nataf, C., Bridges, J. C., Carter, J., Pan, L., Beck, P., Dehouck, E., Volat, M., Thomas, N., Cremonese, G., Tornabene, L. L., & Thollot, P. (2021). Morphological and Spectral Diversity of the Clay-Bearing Unit at the ExoMars Landing Site Oxia Planum. Astrobiology, 21(4), 464-480. https://doi.org/10.1089/ast.2020.2292

Meslin, P.-Y., Forni, O., Beck, P., Cousin, A., Beyssac, O., Lopez-Reyes, G., Benzerara, K., Ollila, A., Mandon, L., & Wiens, R. (2022). Evidence for perchlorate and sulfate salts in jezero crater, mars, from supercam observations. Lunar and Planetary Science Conference,

Millan, M., Teinturier, S., Malespin, C., Bonnet, J., Buch, A., Dworkin, J., Eigenbrode, J., Freissinet, C., Glavin, D., & Navarro-González, R. (2022). Organic molecules revealed in Mars's Bagnold Dunes by Curiosity's derivatization experiment. Nature Astronomy, 6(1), 129-140.

Moeller, R. C., Jandura, L., Rosette, K., Robinson, M., Samuels, J., Silverman, M., Brown, K., Duffy, E., Yazzie, A., Jens, E., Brockie, I., White, L., Goreva, Y., Zorn, T., Okon, A., Lin, J., Frost, M., Collins, C., Williams, J. B., Steltzner, A., Chen, F., & Biesiadecki, J. (2021). The Sampling and Caching Subsystem (SCS) for the Scientific Exploration of Jezero Crater by the Mars 2020 Perseverance Rover. Space Science Reviews, 217(1). https://doi.org/10.1007/s11214-020-00783-7

Nagy, K., & Tiuca, I.-D. (2017). Importance of Fatty Acids in Physiopathology of Human Body. In. InTech. https://doi.org/10.5772/67407

Navarro-González, R., Vargas, E., De La Rosa, J., Raga, A. C., & McKay, C. P. (2010). Reanalysis of the Viking results suggests perchlorate and organics at midlatitudes on Mars. Journal of Geophysical Research, 115(E12). https://doi.org/10.1029/2010je003599

Norén, K., Loring, J. S., & Persson, P. (2008). Adsorption of alpha amino acids at the water/goethite interface. Journal of colloid and interface science, 319(2), 416-428.

Olsztynska, S., Komorowska, M., Vrielynck, L., & Dupuy, N. (2001). Vibrational spectroscopic study of L-phenylalanine: Effect of pH. Applied Spectroscopy, 55(7), 901-907.

Osterloo, M., Hamilton, V., Bandfield, J., Glotch, T., Baldridge, A., Christensen, P., Tornabene, L., & Anderson, F. (2008). Chloride-bearing materials in the southern highlands of Mars. Science, 319(5870), 1651-1654.

Patel, M., Zarnecki, J., & Catling, D. (2002). Ultraviolet radiation on the surface of Mars and the Beagle 2 UV sensor. Planetary and Space Science, 50(9), 915-927.

Perrier, S., Bertaux, J. L., Lefèvre, F., Lebonnois, S., Korablev, O., Fedorova, A., & Montmessin, F. (2006). Global distribution of total ozone on Mars from SPICAM/MEX UV measurements. Journal of Geophysical Research, 111(E9). https://doi.org/10.1029/2006je002681

Poch, O., Jaber, M., Stalport, F., Nowak, S., Georgelin, T., Lambert, J.-F., Szopa, C., & Coll, P. (2015). Effect of nontronite smectite clay on the chemical evolution of several organic molecules under simulated martian surface ultraviolet radiation conditions. Astrobiology, 15(3), 221-237.

Poch, O., Kaci, S., Stalport, F., Szopa, C., & Coll, P. (2014). Laboratory insights into the chemical and kinetic evolution of several organic molecules under simulated Mars surface UV radiation conditions. Icarus, 242, 50-63.

Rao, M., Odom, D., & Oro, J. (1980). Clays in prebiological chemistry. Journal of Molecular Evolution, 15(4), 317-331.

Sagan, C. (1973). Ultraviolet selection pressure on the earliest organisms. Journal of theoretical biology, 39(1), 195-200.

Scheller, E. L., Hollis, J. R., Cardarelli, E. L., Steele, A., Beegle, L. W., Bhartia, R., Conrad, P., Uckert, K., Sharma, S., & Ehlmann, B. L. (2022). Aqueous alteration processes in Jezero crater, Mars− implications for organic geochemistry. Science, eabo5204.

Schoors, S., Bruning, U., Missiaen, R., Queiroz, K. C., Borgers, G., Elia, I., Zecchin, A., Cantelmo, A. R., Christen, S., & Goveia, J. (2015). Fatty acid carbon is essential for dNTP synthesis in endothelial cells. Nature, 520(7546), 192-197.

Schuerger, A. C., Golden, D., & Ming, D. W. (2012). Biotoxicity of Mars soils: 1. Dry deposition of analog soils on microbial colonies and survival under Martian conditions. Planetary and Space Science, 72(1), 91-101.

Sharma, S., Roppel, R. D., Murphy, A. E., Beegle, L. W., Bhartia, R., Steele, A., Hollis, J. R., Siljeström, S., McCubbin, F. M., Asher, S. A., Abbey, W. J., Allwood, A. C., Berger, E. L., Bleefeld, B. L., Burton, A. S., Bykov, S. V., Cardarelli, E. L., Conrad, P. G., Corpolongo, A., Czaja, A. D., Deflores, L. P., Edgett, K., Farley, K. A., Fornaro, T., Fox, A. C., Fries, M. D., Harker, D., Hickman-Lewis, K., Huggett, J., Imbeah, S., Jakubek, R. S., Kah, L. C., Lee, C., Liu, Y., Magee, A., Minitti, M., Moore, K. R., Pascuzzo, A., Rodriguez Sanchez-Vahamonde, C., Scheller, E. L., Shkolyar, S., Stack, K. M., Steadman, K., Tuite, M., Uckert, K., Werynski, A., Wiens, R. C.,

Williams, A. J., Winchell, K., Kennedy, M. R., & Yanchilina, A. (2023). Diverse organic-mineral associations in Jezero crater, Mars. Nature. https://doi.org/10.1038/s41586-023-06143-z

Shkrob, I. A., Chemerisov, S. D., & Marin, T. W. (2010). Photocatalytic decomposition of carboxylated molecules on light-exposed martian regolith and its relation to methane production on Mars. Astrobiology, 10(4), 425-436.

Szopa, C., Freissinet, C., Glavin, D. P., Millan, M., Buch, A., Franz, H. B., Summons, R. E., Sumner, D. Y., Sutter, B., Eigenbrode, J. L., Williams, R. H., Navarro-González, R., Guzman, M., Malespin, C., Teinturier, S., Mahaffy, P. R., & Cabane, M. (2020). First Detections of Dichlorobenzene Isomers and Trichloromethylpropane from Organic Matter Indigenous to Mars Mudstone in Gale Crater, Mars: Results from the Sample Analysis at Mars Instrument Onboard the Curiosity Rover. Astrobiology, 20(2), 292-306. https://doi.org/10.1089/ast.2018.1908

Thomas, N. H., Ehlmann, B. L., Meslin, P. Y., Rapin, W., Anderson, D. E., Rivera-Hernández, F., Forni, O., Schröder, S., Cousin, A., Mangold, N., Gellert, R., Gasnault, O., & Wiens, R. C. (2019). Mars Science Laboratory Observations of Chloride Salts in Gale Crater, Mars. Geophysical Research Letters, 46(19), 10754-10763. https://doi.org/10.1029/2019gl082764

Valášková, M., & Martynkova, G. S. (2012). Vermiculite: structural properties and examples of the use. Clay Minerals in Nature–Their Characterization, Modification and Application, 209-238.

Yariv, S., & Shoval, S. (1982). The effects of thermal treatment on associations between fatty acids and montmorillonite. Israel Journal of Chemistry, 22(3), 259-265.

Yu, W. H., Li, N., Tong, D. S., Zhou, C. H., Lin, C. X. C., & Xu, C. Y. (2013). Adsorption of proteins and nucleic acids on clay minerals and their interactions: A review. Applied Clay Science, 80, 443-452.

Zaia, D. A. (2012). Adsorption of amino acids and nucleic acid bases onto minerals: a few suggestions for prebiotic chemistry experiments. International Journal of Astrobiology, 11(4), 229-234.

Zhao, Y., Hochlaf, M., & Biczysko, M. (2021). Identification of DNA Bases and Their Cations in Astrochemical Environments: Computational Spectroscopy of Thymine as a Test Case. Frontiers in Astronomy and Space Sciences, 8, 757007.

SUPPLEMENTARY MATERIALS

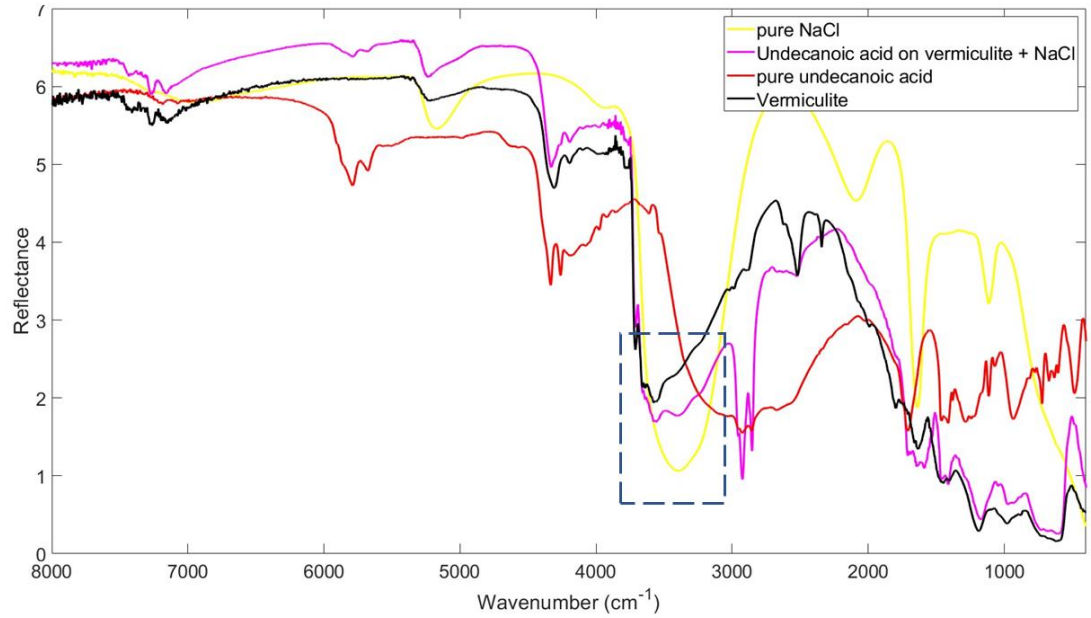

Figure S1: Infrared spectra of pure NaCl (yellow), pure undecanoic acid (red), vermiculite (black) and 10 wt.% undecanoic acid adsorbed on vermiculite in the presence of sodium chloride (NaCl) (magenta). The square identifies the band of pure NaCl.

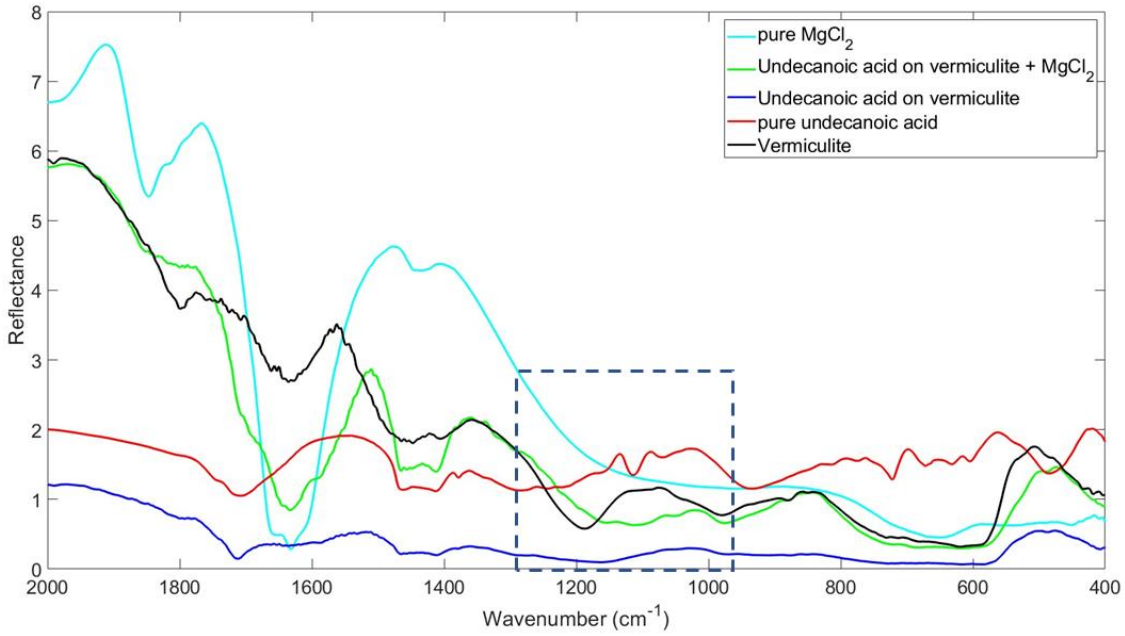

Figure S2: Infrared spectra of pure $MgCl_2$ (cyan), pure undecanoic acid (red), vermiculite (black) and 10 wt.% undecanoic acid adsorbed on vermiculite in the presence of magnesium chloride ($MgCl_2$) (green). The square identifies the regions of the IR spectra where differences from the vermiculite spectrum and the sample with $MgCl_2$ were identified.

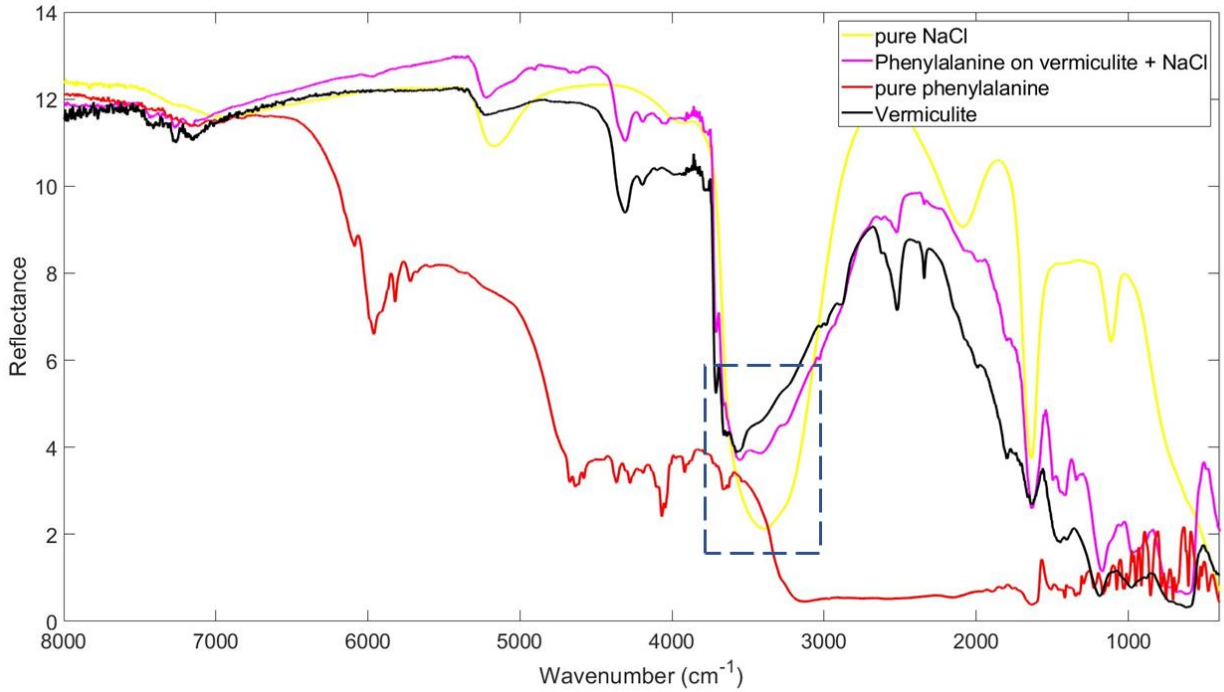

Figure S3: Infrared spectra of pure NaCl (yellow), pure L-phenylalanine (red), vermiculite (black) and 10 wt.% L-phenylalanine adsorbed on vermiculite in the presence of sodium chloride (NaCl) (magenta). The square identifies the band of pure NaCl.

Chapter 4: Thermal reactivity of organic molecules in the presence of chloride salts: implications for the *in situ* Gas Chromatography-Mass Spectrometry analyses on Mars

Abstract

Chlorine-bearing phases, like perchlorates and chlorates, are known to interact with the organic molecules during their thermal extraction from a sample. This was shown with *in situ* analysis of Mars surface solid samples performed by the Sample Analysis at Mars (SAM) instrument suite onboard the Curiosity rover (Glavin et al., 2013), and likely by the GC-MS instrument onboard the Viking landers (Guzmman et al., 2018). The interaction of perchlorates with organic molecules endogenous to the Martian surface produced aliphatic and aromatic organo-chlorine compounds (Freissinet et al., 2015, Szopa et al., 2020). The detection of a new chlorine signature corresponding to chloride salts along Curiosity's traverse is of high interest for astrobiology because these salts could preserve organic molecules from the degradation of solar radiations at Mars surface, as shown in Chapter 3. This would make the environment containing chloride salts good analytical targets for *in situ* analysis. However, knowing the effect of chlorates and perchlorates on organic molecules when analyzed by pyrolysis-GC-MS (Millan et al., 2019), it is legitimate to wonder if chloride salts could influence the detection and identification of organic molecules. Therefore, in Chapter 4, I present a systematic laboratory study that aims at assessing the influence of three chloride salts likely to be present on Mars ($MgCl_2$, $CaCl_2$, and NaCl), on organic molecules when analyzed in pyrolysis-GC-MS as performed by several Martian surface exploration probes like Viking, Curiosity, and Rosalind Franklin. This work aims to understand the effect these salts can

have on the detection of organic compounds during GC-MS analysis and, therefore, support the interpretion the *in situ* data provided or to be provided, by the rovers.

The main results indicate that the thermal degradation of the salts through the release of hydrogen chloride (HCl) from the sample influenced the nature, number, and intensity of pyrolysis products detected in the chromatograms. In addition, we show that some of the organic molecules and chloride salts targeted could be the precursor of the chlorohydrocarbons detected on Mars by the SAM and Viking instruments.

1. INTRODUCTION

In 1976, the Viking probes 1 and 2 landed at the Martian surface to search for clues of life and habitability. The regolith samples collected by the landers were pyrolyzed and analyzed with Gas Chromatography-Mass Spectrometry (GC-MS) to investigate the chemical composition of the soil and to question the presence of organic molecules which are key componenets of living materials. Methyl chloride and fluorocarbons were detected at 1 to 50 parts per billion (ppb) but their presence was attributed to terrestrial contaminants as these species are essentially produced by anthropic activity on Earth. The ultimate conclusion drawn from the Viking GC-MS data at that time was that the organic molecules were not present at the Martian surface above the detection limit of the instrument, and had been destroyed by the planet's harsh oxidative and radiative conditions (Biemann et al., 1977; Oró, 1979; Oró & Holzer, 1979). For these reasons, Mars was considered a barren planet for life. The discovery of perchlorates, highly reactive molecules, in the Martian soil by the Phoenix lander in 2009 at high latitudes (Hecht et al., 2009) motivated reinterpretations of the Viking results. Several studies concluded that the chlorohydrocarbons detected by the GC-MS experiments of the Viking landers could be due to the combined presence of perchlorate and organic molecules present in the Martian regolith or in the instrument, that reacted together during the pyrolysis process (Navarro-González et al., 2010).

The data obtained with the Sample Analysis at Mars (SAM) pyrolyzer GC-MS instrument onboard the Curiosity rover revealed for the first time the presence of organic molecules in Martian rock samples collected and analyzed in Gale Crater, through the detection of chlorobenzene and dichloroalkanes (Freissinet et al., 2015) and the detection of dichlorobenzene isomers and trichloromethylpropane (Szopa et al., 2020). The authors concluded that the chlorinated hydrocarbons detected were reaction products between chlorine and organic carbon indigenous to the sample derived from endogenous or exogenous sources. These detection encouraged a directed analysis of Viking GC-MS data that revealed the presence of chlorobenzene, not originally reported in the instrument signal. This detection strengthen the assumption that the Viking instruments could have detected organic materials endogenous to the Martian samples (Gusman et al., 2018). Since this discovery, studies have been conducted to understand the influence of oxychlorines and more specifically perchlorate on organic molecules and allowed to better constrain the precursors of the Martian chlorohydrocarbons (Millan et al., 2020). However, perchlorates/chlorates are not the only chlorine-bearing molecules present in Martian soil. In 2008, chloride salts were identified through infrared spectrometry in the southern region of Mars (Osterloo et al., 2008) with the larger occurrence of chlorides identified in the *Terra Sirenum* region (Glotch et al., 2010); later, chloride salts in Gale Crater were reported along the Curiosity rover's traverse from measurements with the ChemCam instrument (Thomas et al., 2019). In order to constrain the origin of Hydrogen Chloride (HCl) detected by the Sample Analysis at Mars (SAM) instrument, Evolved Gas Analysis (EGA) laboratory studies on high-temperature HCl released from perchlorate and chloride salts were investigated by Clark et al. in 2020. Detection of perchlorate on Mars is done by correlating the Cl and oxygen release in the EGA data (Glavin et al., 2013). The authors concluded that the production of HCl without the concurrence of O_2 release at temperatures above 600 °C could be attributed to chloride salts on Mars. These laboratory results were compared to SAM flight data obtained from samples collected at different sites on Mars and the data were consistent with the presence of chloride salts in the Martian soil at some locations.

Recent analyses performed with the Curiosity's instruments collected in Gale Crater showed that chlorine is still present (Litvak et al., 2023; Szopa et al., 2020). However, in the recent layers examined by Curiosity, there is no apparent correlation between Cl and O, which means that Cl is not associated with oxygen. Thus, perchlorate or chlorate presence is less likely and that chlorides are the most likely salts present among the chemical phases.

Although the nature of the cation(s) from the salts is generally unknown, calcium, sodium, and magnesium have been suggested as possible candidates to form chloride brines on Mars based on geochemical measurements (Clark, 1981). From these data and additional work by Hecht et al. (2009), Mg^{2+} and Na^{+} could be the most available cations in the Martian soil. These ions were identified as important elements in the soils at all landing sites of Martian rovers, with mass fractions ranging from 0.5 to 5 % (Karunatillake et al., 2007). The presence of sodium chloride (NaCl) is also supported by a correlation between the sodium and chlorine observed by Curiosity's ChemCam instrument (Thomas et al., 2019). The Mars Odyssey Thermal Emission Imaging System (THEMIS) spectra of salt deposits is also consistent with the presence of halite (NaCl) on the surface of the planet (Glotch et al., 2016).

Our study aims at assessing the interactions between organic molecules potentially present in the Mars' samples and chloride salts assumed to be present as well. The objectives are (1) to assess the influence of chlorides on the detection of organic molecules using pyrolysis, (2) to look for potential signatures of chloride salts in the laboratory chromatographs acquired with these experiments and (3) to identify potential precursors of chlorinated organic molecules as detected on Mars. This study presents the results obtained after systematic pyrolysis of chloride salts in the presence of selected organic molecules within the analytical conditions of the Viking-, SAM-, and MOMA-flight pyrolysis.

2. Material and Method

2.1. Studied analytes

2.1.1. Chloride salts

Three types of chloride salts were selected for this study: magnesium chloride ($MgCl_2$), calcium chloride ($CaCl_2$), and sodium chloride (NaCl). The chloride salt standards were purchased from the Merck company, and were of high purity grade (> 98%) and anhydrous.

2.1.2. Organic molecules

Three molecular families were targeted: amino acids, Polycyclic Aromatic Hydrocarbons (PAHs), and carboxylic acids (Table 1). The organic chemical standards (> 97%) were supplied by the Sigma-Aldrich company.

Carboxylic acids- Benzoic acid and undecanoic acid were chosen because of their relevance to the Mars surface exploration.

Benzoic acid is one of the most likely oxidation products of complex organic molecules in the Mars surface environmental conditions and has been proposed by Benner et al. (2000) to be a metastable intermediate of Polycyclic Aromatic Hydrocarbons (PAHs) potentially brought from exogenous sources. Chemically derivatized benzoic acid has also been detected with the SAM instrument in samples collected in the Bagnold Dune's and anaylized using the N-Methyl-N-(tert-butyldimethylsilyl)trifluoroacetamide (MTBSTFA) derivatization experiment (M Millan et al., 2022) and in samples from the Mary Anning site analyzed with the first Tetramethylammonium hydroxide (TMAH) wet chemistry experiment (Williams et al., 2021), thus making its presence very likely at the surface of Mars. Moreover, benzoic acid is a likely precursor from chlorohydrocarbons detected on Mars (Freissinet et al., 2020).

Long-chained carboxylic acids such as undecanoic acid are of astrobiological interest as they are the major constituents of cell membranes (Nagy & Tiuca, 2017) and crucial energy sources for life on Earth (Schoors et al., 2015). Moreover, although terrestrial contamination cannot be excluded, long-chained carboxylic acids have been detected

in carbonaceous chondrites (*e.g.*, Murchison) (Deamer & Pashley, 1989) and Asuka-881458 with chain length of 2 to 12 carbon atoms (Naraoka et al., 1999a) including undecanoic acid (C_{11}) and may thus, have been deposited at the surface of planetary bodies. MTBSTFA wet chemistry derivatization of the Cumberland (CB) sample in a "opportunistic derivatization" (OD) experiment with the SAM instrument suite also revealed the potential presence of long-chained carboxylic acids on Mars (Freissinet et al., 2019). Specifically, the decane detected on Mars is hypothetized to be coming from decarboxylation of its carboxylic acid counterpart, undecanoic acid.

Finally, Benzoic acid is aromatic whereas undecanoic acid is linear which will allow to investigate the influence of the molecular structure on the interaction with chloride salts.

Polycyclic Aromatic Hydrocarbons (PAHs)- PAHs are thought to have been brought to Mars through exogenous sources such as meteorites (Basile et al., 1984; Naraoka et al., 1999b; Sephton, 2002) and micrometeorites (Pizzarello et al., 2006). They have been detected in abundance in carbonaceous chondrites representing up to 80 % of their mass (Botta & Bada, 2002). PAHs can also be synthesized endogenously during the decomposition of organic matter of biotic or abiotic origin in the image of terrestrial PAHs (Zolotov & Shock, 1999). Naphthalene and 9-methylanthracene were selected to study the influence of the size of the molecule as well as the alkyl ramification in the pyrolysis process and interaction with the salts.

Amino acids- Amino acids play a crucial role in the structure, metabolism, and physiology of the cells as main constituents of peptides and proteins. Furthermore, although amino acids synthesis can be non-biological, the recognition of homochirality, a common structural feature of biomolecules in nature (Blackmond, 2010), is an unambiguous property indicating their origin via biological processes, thus making them appealing molecules in the search for life on Mars. Amino acids were also detected in several meteorites and comets up to 52 in the Murchison meteorite (Cronin & Pizzarello, 1983),

thus, their presence as compounds brought by exogenous sources at the surface of Mars is likely (Fornaro et al., 2013). Finally, because amino acids can be detected in very low abundance (Skelley et al., 2005), they might be a valuable tool in the search for evidence of life where biological signatures, if any, are expected to be particularly low as is on Mars. Glycine, glutamic acid, and phenylalanine were all identified in meteorites (Burton et al., 2012) and were selected in this study for the diversity of their functional groups.

Table 1: Structure and main properties of the organic standards targeted in this study.

Chemical family	**Coumpound**	**Raw formula**	**Chemical structure**	**Molecular weight ($g.mol^{-1}$)**	**Purity**
Carboxylic acids	Benzoic acid	$C_7H_6O_2$	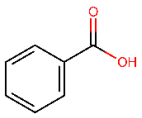	122.12	99.5%
	Undecanoic acid	$C_{11}H_{22}O_2$	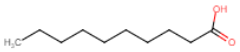	186.29	≥ 97%
PAHs	Naphthalene	$C_{10}H_8$	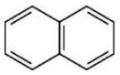	128.17	99%
	Methylanthracene	$C_{15}H_{12}$	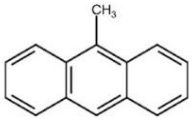	192.25	98%
Amino acids	Glycine	$C_2H_5NO_2$	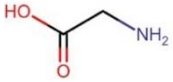	75.06	≥ 99%
	Glutamic acid	$C_5H_9NO_4$	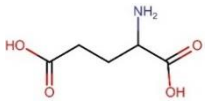	147.13	99.5%
	Phenylalanine	$C_9H_{11}NO_2$	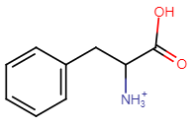	165.19	99.5%

2.2. SAMPLE PREPARATION

Chloride salts and organic molecules are most likely present as trace components in the Martian soil (up to ~ 300 ppbw (Freissinet et al., 2015; M Millan et al., 2022)), including a high concentration of amorphous and crystalline inorganic phases (15–73 wt.%) (Rampe et al., 2020). Therefore, in order to simulate low concentrations in our experiments, the organic standards and chloride salts were mechanically incorporated and diluted in a supposedly chemically inert matrix of fused synthetic silica quartz (Schlten & Leinweber, 1993) (~44 µm grain size powder, supplied by Sigma-Aldrich) prior to pyrolysis. Before the sample preparation, the fused silica was conditioned at 1000 °C for 24 hours in a muffle furnace in order to remove any potential organic contamination.

Each organic compound and chloride salt were individually diluted and crushed in silica in their solid form at 1:100 (10 000 ppm) and 3:100 mixing ratios (30 000 ppm) in weight, respectively. These concentrations were chosen to ensure the detection of all the decomposition products and ease experimental manipulation, while keeping the concentration lower than pure standards. However, it is important to note that the concentration values of organic content detected in Mars samples are much lower: the concentration of chlorobenzene ranges from 150 to 300 ppbw, and dichloroalkanes are up to 70 ppbw (Freissinet et al., 2015), respectively. The highest concentration of organic found was during the wet chemistry experiment performed on the Glen Etive sample from the Glen Torridon region in Gale crater which helped extract sulfur-bearing organic compounds with concentrations up to ~5937 and 1430 ppbw for ethanethiol and thiophene, respectively (M Millan et al., 2022) which is still much lower compared to the concentrations used in the experiments presented in this study. This quantitative effect will have to be taken into account when interpreting the data obtained on Mars.

The powder was mixed and ground in an organically cleaned porcelain mortar and pestle which has been solvent-cleaned with ethanol (99.9%, Merck) and baked at 500 °C

for two hours before sample preparation. Prior to analysis, the samples were weighed out in a stainless-steel Eco-Cups (Frontier Lab) cleaned with ethanol and heated red with a burner (~1400 °C) to remove any potential organic contamination. ~5 mg of the organic/silica mixture plus ~5 mg of the chloride salts/silica mixture were deposited into the cup (10 mg total) and weighted using a scale (Mettler Toledo, precision 0.001 mg). Each sample was analyzed in duplicates to evaluate the uncertainty introduced by this sample preparation method. The sample preparation procedure was identical for all the analytical methods used in this study and described below.

2.3. ANALYTICAL MATERIAL AND METHODS

2.3.1. Instrumentation

All instrumental procedures were performed using a Frontier Laboratories 3030D multi-shot pyrolyzer (Frontier Lab) mounted on the split/spitless injector of a Trace 1300 Ultra gas chromatograph coupled to an ISQTM quadrupole mass spectrometer (both from ThermoFisher). Since the pyrolyzer's heating chamber is within the carrier gas (Helium, purity > 99.999 %, Air Liquide) flow pathway, all the gaseous species produced in the chamber are instantaneously transferred to the injector.

The SAM experimental set-up allows two types of pyrolysis analyses: 1/ Evolved Gas Analysis (EGA), where the gases released through the heating of the sample are directly sent to the mass spectrometer for analysis. EGAs were not performed in the Viking and MOMA conditions as this technique was not applied and not part of the baseline experiments for the mission, respectively. 2/ Gas Chromatography (GC), where the gases are first separated through a chromatographic column before detection by the mass spectrometer.

2.3.2. Evolved Gas Analysis (EGA)

The EGA experiments were conducted using an inert Ultra ALLOY-DTM metallic chromatographic column (2.5 m long; 0.15 mm internal diameter) (Frontier Lab) which was connected to the mass spectrometer with a fused silica transfer line (0.4 m long; 0.25 mm). The short length of the column and absence of stationary phase allowed to

minimize the duration of transfer of the gases from the injector to the mass spectrometer (~10 s). The chromatographic column and the transfer line were maintained at a constant temperature of 250 °C throughout the analysis. The ion source and transfer line temperatures of the MS were both set at 300 °C and ions produced by electron impacts (energy of 70 eV) were scanned in the mass to charge ratios (*m/z*) range of 10 to 400.

The samples were introduced manually by lowering the cup into the pyrolyzer's oven. The samples were heated from 80 to 800 °C with a temperature ramp rate of 35 °C·min^{-1} in order to reproduce the pyrolysis conditions used in the SAM instrument. The time scale given by the chromatographic analysis was converted into temperature scale for EGA by using the heating rate of the pyrolysis and the known time of transfer between the pyrolyzer and the MS.

However, differences between the experimental conditions of the SAM flight model and our laboratory analyses have to be noted. The helium carrier gas was used in the lab at a constant flow of 1 mL·min^{-1}, whereas the flight model is used at a constant pressure of 25 mbar and 0.8 mL·min^{-1} flow rate (Glavin et al., 2013). In addition, our study was conducted with an injection split ratio of 20:1 versus 800:1 on SAM and stainless steel cups were used instead of quartz cups (Glavin et al., 2013). These discrepancies can introduce variations in the relative abundances of some pyrolysis products detected with both the laboratory instrument and the SAM flight model, but should not alter the qualitative results. This should be kept into consideration when interpreting the laboratory data towards SAM flight data.

Blank analyses, where the same procedure was done with an empty capsule, were performed between each analysis in order to ensure the absence of cross-contaminations. When a possible contamination was detected, the pyrolyzer GC-MS chain was cleaned by heating the whole sample pathway within the instrument to the maximum temperature of the oven (800 °C).

2.3.3. Pyrolysis Gas Chromatography-Mass Spectrometry

The same sample preparation process was applied for the GC-MS experiments as described above for the EGA.

Three different sets of pyrolysis conditions were used to reproduce as closely as possible those used in the Viking-GC-MS, MOMA, and SAM space experiments.

To simulate the SAM pyrolysis in the laboratory, the samples were heated in the pyrolyzer's furnace starting at 80 °C, then heated at a 35 °C·min^{-1} ramp up to 800 °C. The sample released volatile substances continuously throughout the entire duration of the pyrolysis (~22 minutes). To mimic the functionality of the chemical traps used on SAM, which concentrates the analytes and enhances the separation capacity of the chromatograph (Mahaffy et al., 2012), we used a cryogenic trap to condense the gases at the inlet of the GC column during the entire pyrolysis phase. This trap utilized a liquid nitrogen cooling system (~-180 °C) provided by FrontierLab directly connected to the pyrolyzer's control system. Once the pyrolysis finished, the cryogenic trap was stopped, causing the condensates to quickly vaporize and flow through the chromatographic column for separation and detection.

For the experiments related to MOMA, the flight instrument performs a rapid temperature increase (~200 °C·min^{-1}) of the sample (Goesmann et al., 2017). However, the heating profile is non-linear making it challenging to replicate accurately in our laboratory setup. Consequently, we conducted experiments using flash pyrolysis, where the samples were directly heated to the maximum temperature achievable by the MOMA oven (800 °C) for a few minutes. In the flash heating mode, the chromatographic analysis started as soon as the sample was introduced into the pyrolyzer, and the gases were generated and transferred immediately to the chromatograph.

Lastly, the experiments related to Viking GC-MS analyses involved a rapid heating the samples (within seconds) to 500 °C (Rushneck et al., 1978), holding them at this

temperature for thirty seconds.

For all chromatographic analyses, we used a Zebron 5MS Plus column (30 m long, 0.25 mm internal diameter, 0.25 µm stationary phase thickness) (Phenomenex®) equipped with a 5-meter-long integrated guard line which protects the analytical column from contamination and fast degradation, specifically in the presence of inorganic salts. The injector temperature was set at 250 °C. The column temperature program started at an initial temperature of 40 °C followed by a 10 °C·min^{-1} ramp up to a final temperature of 300 °C held for 10 minutes in order to separate both light and heavy molecules and keeping a reasonable analytical time. These analytical conditions do not reproduce any of the three space experiments studied but help understand the overall reactivity of the organic molecules with chloride salts. The MS settings were identical to those used for the EGA experiments and two replicas for each sample were performed in order to avoid potential data misinterpretation due to contamination.

3. RESULTS

3.1. EGA

In order to understand the interaction mechanisms between the chloride salts and the targeted organic molecules, we first analyzed the temperature of decomposition of each molecule individually using EGA within the SAM temperature range (80-800 °C). The EGA experiments allowed to track the main species released from each of the compounds studied as a function of their temperature.

3.1.1. Chloride salts

The thermal decomposition of chloride salts produces hydrogen chloride (HCl) (*m/z* 36) and water (*m/z* 18) if hydrated.

Here we show that the thermal decomposition of the three chloride salts diluted in silica leads to the release of water (*m/z* 18) throughout the run, with a significant release at low temperatures (between 80 and 300 °C) (Figure 1). Some of this water can be attributed to water from the laboratory atmosphere adsorbed on the silica beads

used to dilute the samples. This is confirmed by the EGA of pure silica which shows the release of water from 80 to 800 °C with a main release at 110 °C (Figure 1).

The higher temperature water peaks observed in the EGA of the salts (>110 °C) can be explained by the extraction of water from the hydration sphere of the salts and by the fact that chloride salts are highly hygroscopic minerals and can spontaneously adsorb water on the surface of their crystal. Deliquescence occurs at a characteristic relative humidity for each salt (75 % for NaCl, 33 % for $CaCl_2$, and 28-31 % for $MgCl_2$) (Cohen et al., 1987; Greenspan, 1977). The hygroscopic capacity of each salt matches the amount of water released in the EGA experiments ($MgCl_2$ > $CaCl_2$ > NaCl).

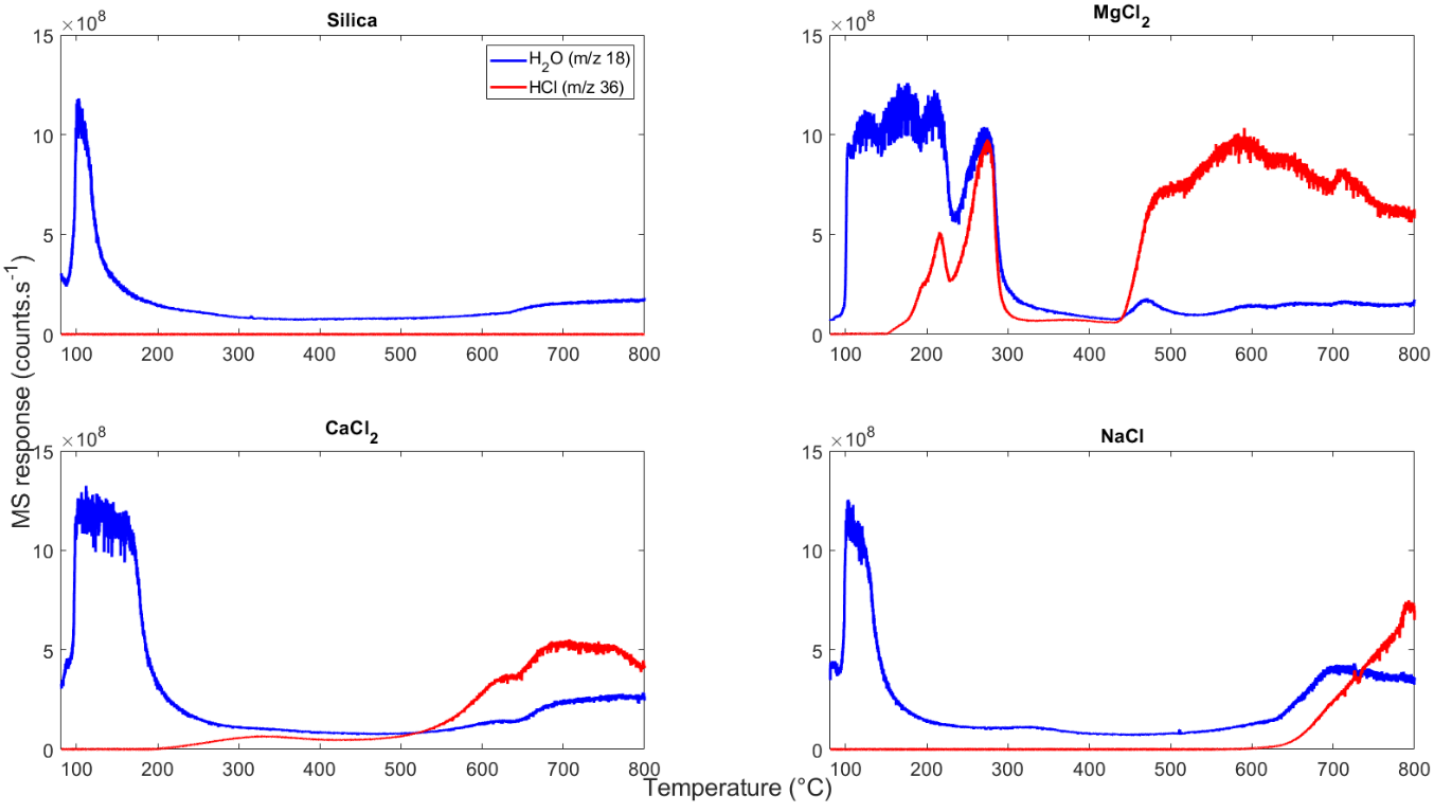

Figure 2: Evolved gas profile of HCl (m/z 36) in red and H_2O (m/z 18) in blue versus the temperature of pure fused silica, magnesium chloride ($MgCl_2$), calcium chloride ($CaCl_2$) and sodium chloride (NaCl), under SAM-like EGA conditions (35 °C·min^{-1} ramp). Each chloride salts were diluted at 3 wt% in silica.

Furthermore, chloride salts release hydrogen chloride (HCl) (*m/z* 36), which vaporization temperature significantly differs for the three targeted salts (Figure 1).

$MgCl_2$ – Magnesium chloride evolves HCl from 150 to 800 °C with two distinct temperature ranges: the first between 150 and 300 °C where HCl co-evolves with water and the second from 450 to 800 °C (Figure 1, top right). Anhydrous magnesium chloride has a high affinity for water and can form several hydrates ($MgCl_2.nH_2O$, n=1, 2, 4, 6, 8, 12) (Kipouros & Sadoway, 2001). The lower temperature release of water and HCl is, thus, related to the direct dehydration of the salt and production of MgOHCl (solid) and HCl (gas) (Clark et al., 2020; Huang et al., 2011) as the salt was exposed to atmospheric moisture. The second HCl release is due to the decomposition of MgOHCl into MgO (solid) and HCl (gas) (Clark et al., 2020).

$CaCl_2$ – The thermal decomposition of anhydrous calcium chloride produces a broad HCl peak between 200 and 800 °C, with a first release between 250 and 450 °C and a relatively higher peak from 500 to 800 °C (Figure 1, bottom left). Calcium chloride is highly hygroscopic and can form several hydrates ($CaCl_2$. nH_2O, n=1, 2, 4, 6) (Handbook, 2003). Fraissler et al. (2009) showed that under humid gas atmosphere conditions, the thermal decomposition of calcium chloride usually occurs in two distinct phases. First, the decomposition of hydrates induces a mass loss at low temperatures. The higher the hydration state of the calcium chloride, the lower the thermal decomposition of the salt. Based on the temperature of decomposition suggested by Fraissler et al. (2009), calcium chloride from our samples seem to be monohydrated and following reaction (1).

$$CaCl_2.H_2O\ (s) \rightarrow CaCl_2\ (s) + H_2O\ (g)\ (1)$$

From this reaction, anhydrous calcium chloride is formed. The second phase of the degradation of calcium chloride is a chlorine release which occurs above the melting temperature of the salt by reaction between calcium chloride with oxygen and HCl. Among the possible pathways of chlorine release from anhydrous calcium chloride, the reaction of $CaCl_2$ with water vapor is the most likely (reaction (2)).

$$CaCl_2\ (s) + H_2O \rightarrow Ca(OH)Cl\ (s) + HCl\ (g)\ \ (2)$$

The differences observed in the release temperature of HCl at high temperature in this study compared to Fraissler et al. (2009) can be explained by the presence of silica in our samples. Silica can shift the observed sublimation of molecules toward higher temperatures. This phenomenon has been observed in previous studies and can be explained by partial absorption of the heat by the silica matrix, thus delaying the heating of the molecule resulting in an increase of the observed temperature of sublimation in the EGA (Millan et al., 2020).

NaCl – Finally, sodium chloride releases gaseous HCl at higher temperature compare to the other salts, starting at 620 °C to the highest temperature of the pyrolysis program used (800 °C)(Figure 1, bottom right). A similar behavior was observed by (Clark et al., 2020) in which the evolution of HCl is showed at high-temperature during the thermal decomposition of sodium chloride with water-bearing phases. One explanation given by Clark et al. (2020) is that the NaCl mixture in silica evolved HCl after the melting point of NaCl due to evolved water reacting with the melting chloride.

3.1.2. Thermal behavior of organic molecules

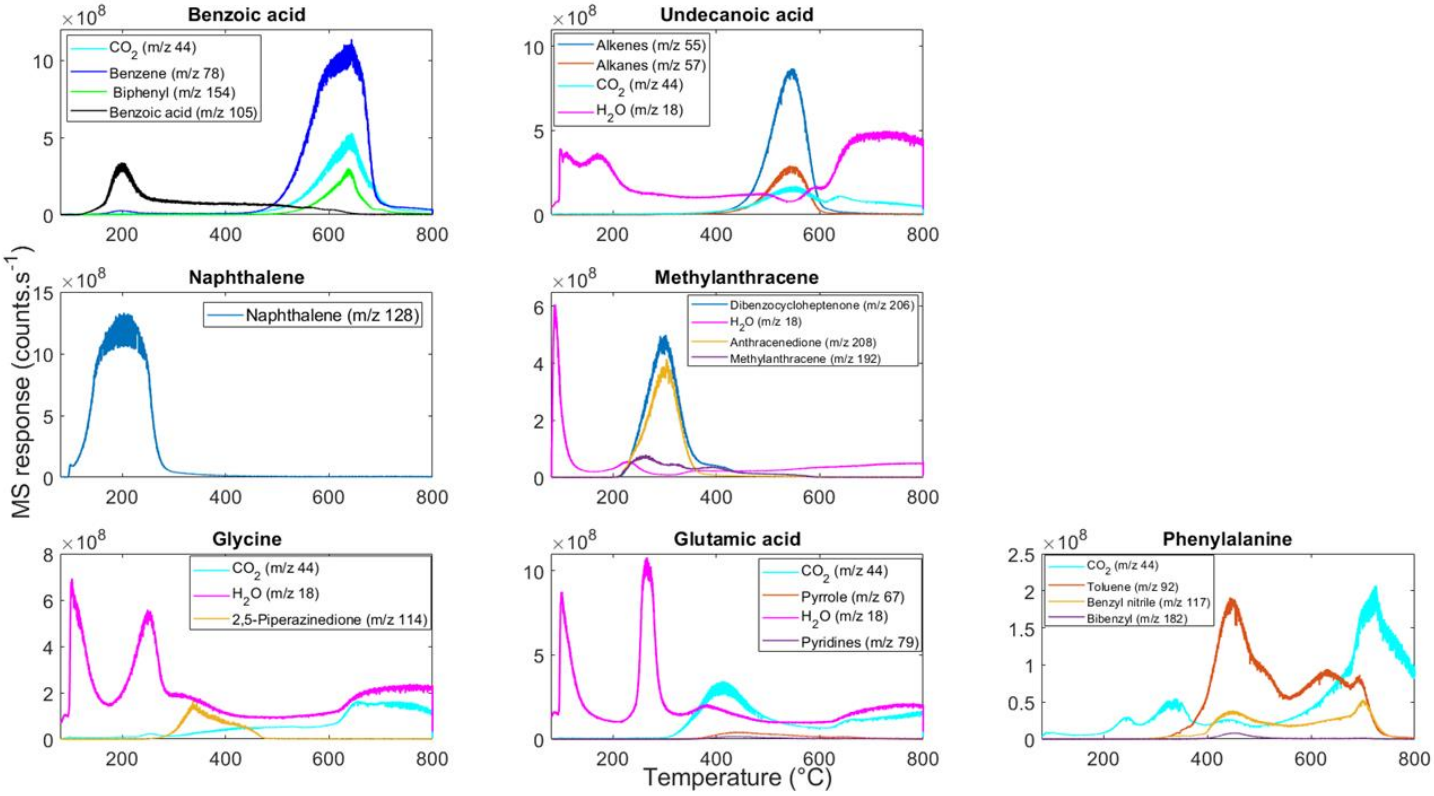

Figure 3 : Evolved gas profile of m/z fragments versus temperature as obtained in SAM-like EGA conditions (35 °C·min^{-1} ramp) of the organic compounds of interest dispersed in 1:100 silica matrix.

EGA were performed in SAM pyrolysis conditions (35 °C·min^{-1}) for each organic compound at 1 wt.% into fused silica, and the evolution of their main molecular fragments as a function of the temperature is presented in **Error! Reference source not found.**.

Benzoic acid – Results indicate that benzoic acid evolves within two distinct temperature ranges: the first release occurs at 110 °C and reached a maximum around 200 °C with a tail reaching up to 620 °C. The corresponding organic compound is benzoic acid itself characterized by its parent molecular ion *m/z* 105. The second gas release occurs at higher temperatures and ranged from 470 °C to 800 °C, with a maximum at ~ 630 °C. Three ions contributed to this peak with *m/z* 44, *m/z* 78 and *m/z* 154. These ions correspond to the release of CO_2, benzene and biphenyl, respectively. CO_2 and benzene are the decarboxylation products of benzoic acid and biphenyls are

formed by cross-reactions of benzene rings (Moldoveanu, 2010).

Undecanoic acid – Apart from water, a single outgassing peak is observed at 550 °C. CO_2 (*m/z* 44) from the decarboxylation of the acid evolved from 400 to 800 °C with a maximum at 550 °C. At 550 °C we observe ions characteristic to hydrocarbons such as alkenes (*m/z* 55) and alkanes (*m/z* 57) formed through the common decarboxylation and dehydration of linear carboxylic acids (Moldoveanu, 2010). Undecanoic acid itself seems to have been entirely degraded as no ions related to the acid itself is observed above the noise level in the EGA signal. Moreover, undecanoic acid is a highly hygroscopic molecule and has adsorbed atmospheric water during sample preparation as shown by the release of water (*m/z* 18) throughout the analysis.

Naphthalene – The sublimation of naphthalene can be tracked by its molecular ion *m/z* 128 which is detected at 200 °C. No other chemical species is observed above the noise level. Naphthalene is very stable within the range of temperature studied and is therefore not affected by the pyrolysis condition.

Methylanthracene – The sublimation of methylanthracene (*m/z* 192) is observed at 250 °C with a tail reaching 600 °C. However, methylanthracene is not the major species detected. A peak at 300 °C reveals the formation and release of heavy polyaromatic species with oxygen-bearing functional groups illustrated in Figure 3 by *m/z* 206 which is a characteristic ion of dibenzocycloheptenone and *m/z* 208 characteristic of anthracenedione. The water contained in the sample (*m/z* 18) can be cleaved into free radicals (H^+ and HO^+) at low temperature and pressure ((125-320 °C) and pressure (0.5-20 MPa) (Mishra et al., 1995)) consistent with the experimental condition applied. These free radicals can then oxidize methylanthracene which further transforms into alcohols, aldehydes, ketones or carboxylic acids species (Benner et al., 2000).

Glycine – The products evolved in EGA showed the formation of 2,5-Piperazinedione (*m/z* 114) (Figure 3), a diketopiperazines (DKP) commonly formed through the dehydration followed by the intermolecular condensation of glycine molecules

(Moldoveanu, 2009). The sublimation of 2,5-Piperazinedione takes place at 340 °C. Two main peaks of water (*m/z* 18) are detected: the first one at 120 °C likely related to the dehydration of the silica matrix (Figure 2), and the second one at 250 °C tailing to 800 °C from the dehydration of glycine during pyrolysis. The release of CO_2 (*m/z* 44) is coming from the decarboxylation of glycine (Moldoveanu, 2009).

Glutamic acid – The EGA results shows four water releases at 120, 270, 400, and between 600-800 °C, with the third and fourth water peaks co-evolving with CO_2 release. The first water peak corresponds to the water released from the silica whereas the second one is likely related to water loss from glutamic acid (Moldoveanu, 2009). The dehydration of glutamic acid molecule usually leads to the formation nitrogen- and oxygen-bearing aromatic compounds (Moldoveanu, 2009) such as pyridines (*m/z* 79) which are indeed released around 450 °C. The decarboxylation of glutamic acid (CO_2 release > 400 °C) led to the formation of pyrrole (*m/z* 67) detected between 440 and 700 °C (Moldoveanu, 2009).

Phenylalanine – The pyrolysis of phenylalanine led to its decarboxylation. CO_2 is released throughout the analysis with two peaks at 240 and 340 °C and a relatively higher peak around 730 °C. The decarboxylation process resulted in the formation of nitrogen-bearing compounds, among which *m/z* 117 characterizing benzyl nitrile and detected as a broad peak in EGA between 300 and 750 °C. Other pyrolyzates of phenylalanine are detected such as toluene (*m/z* 92) between 300 and 750 °C with a maximum sublimation peak at 440 °C and bibenzyl (*m/z* 182) released between 400 and 500°C (Moldoveanu, 2009).

3.2. GAS CHROMATOGRAPHY

In order to infer the influence of each chloride salt on the targeted organic molecules, we compared the Total Ion Current (TIC) chromatograms of each organic molecule with and without the different chloride salts and inventoriated all the compounds detected above the noise level of the instrument.

3.2.1. Influence of chloride salts on the SAM-like pyrolysis of organic molecules in the presence of Silica

3.2.1.1 Benzoic acid

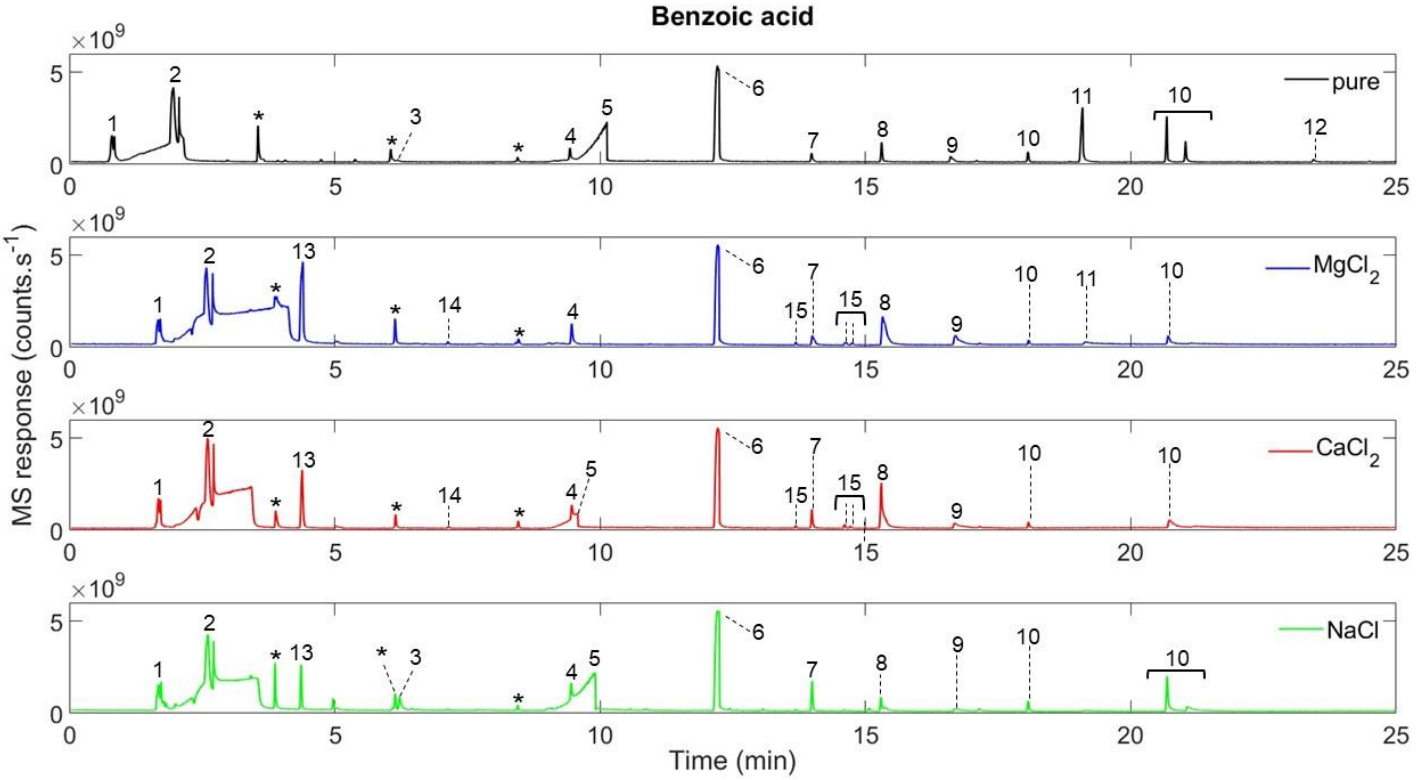

Figure 3: Chromatograms obtained after the SAM-like pyrolysis (35 °C·min^{-1} ramp) of 1:100 benzoic acid (black) in silica, in the presence of 3:100 $MgCl_2$ (blue), $CaCl_2$ (red), and NaCl (green). (*) artifacts related to the GC column (stationary phase bleeding), (1) CO_2, (2) benzene, (3) phenol (4) naphthalene, (5) benzoic acid, (6) biphenyl, (7) dibenzofuran, (8) benzophenone, (9) fluorenone, (10) terphenyl isomers, (11) anthracenedione, (12) triphenylene, (13) chlorobenzene, (14) dichlorobenzene, (15) chlorobiphenyl isomers.

As seen in the EGA, benzoic acid does not degrade entirely in SAM-like pyrolysis conditions and can still be detected as one of the major pyrolysis compounds, as shown by its fronting peak typical of the saturation of the stationary phase (Figure 3, top black chromatogram, compound 5). Moreover, benzoic acid molecules decomposes into CO_2 and benzene from the decarboxylation of the acid. Biphenyl is also among the most abundant products detected in the chromatogram and resulting from reactions between benzene rings. The release of these compounds was expected from the EGA data (Figure 2). However, chromatography provids a better compounds' separation

than EGA and allows the detection of additional compounds, like terphenyls and ketones such as anthracenedione, benzophenone, or fluorenone formed through reactions between benzoic acid and its thermal degradation products (*e.g.*, phenyls).

In the presence of magnesium chloride, benzoic acid is not detected in the chromatogram (Figure 3, blue chromatogram). CO_2, benzene, and biphenyl are among the major degradation products observed. Their relative intensity is within the same order of magnitude as in the chromatogram obtained after pyrolysis of benzoic acid without salts. However, the relative abundances of the terphenyl isomers and the number of isomers detected are drastically impacted, as shown by the detection of a unique terphenyl isomer at lower intensity in the presence of salt compared to benzoic acid without salts. Moreover, a major decrease in the relative abundance of anthracenedione is observed. New organic compounds bearing chlorine are formed compared to the experiment performed without salt, such as chlorobenzene, dichlorobenzene, and chlorobiphenyl isomers.

In the presence of calcium chloride, benzoic acid is still detected but in a much lower relative abundance than the analysis without salt (Figure 3, red chromatogram). The same chlorinated species formed with magnesium chloride are observed with $CaCl_2$ such as chlorobenzene, dichlorobenzene, and two chlorobiphenyl isomers.

Finally, in the presence of sodium chloride, the relative abundance of benzoic acid is only slightly lower compared to benzoic acid in silica but relatively higher than with magnesium and calcium chloride (Figure 3, green chromatogram). We also observed a higher relative abundance of terphenyls with NaCl than with the divalent salts $MgCl_2$ and $CaCl_2$. Moreover, chlorobenzene is the only chlorohydrocarbon detected in the presence of NaCl. Anthracenedione, chlorobiphenyls, and dichlorobenzene are not detected.

3.2.1.2 Undecanoic acid

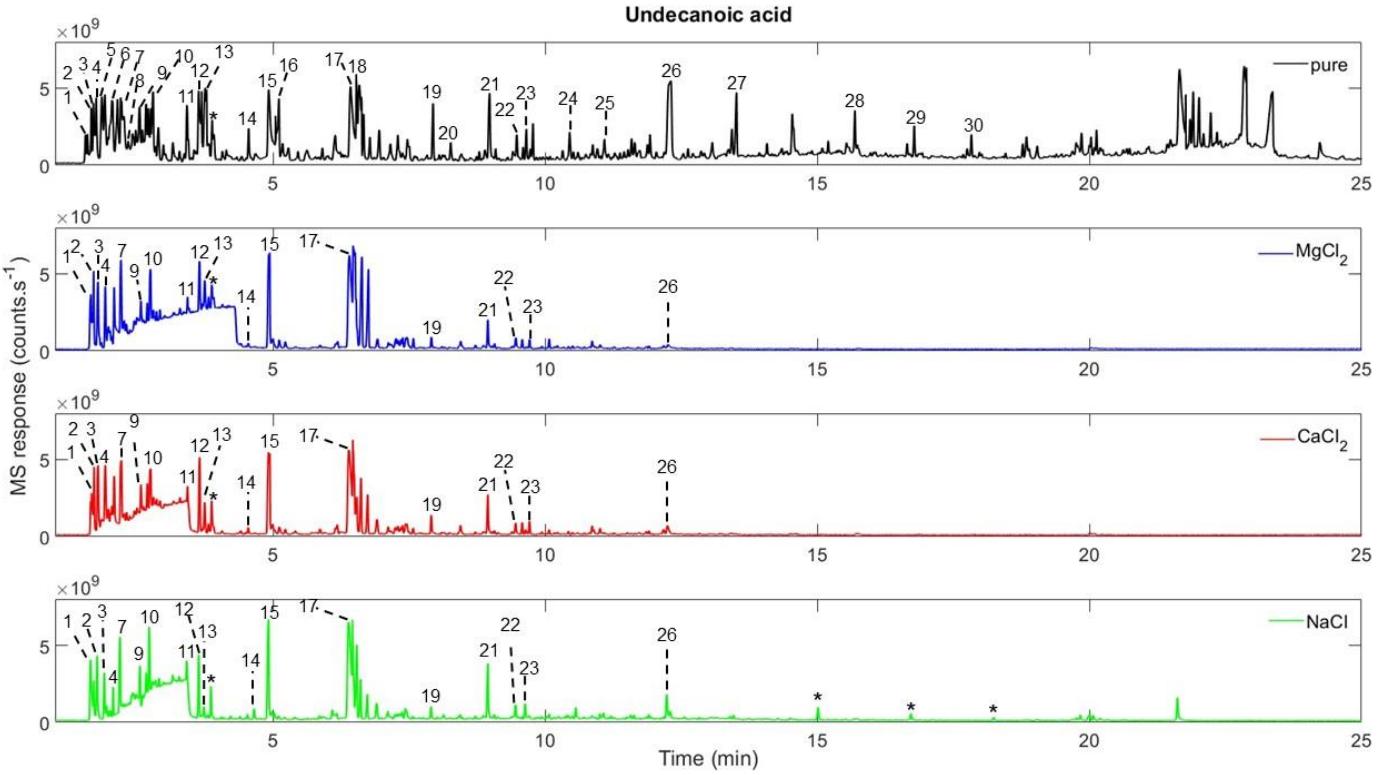

Figure 4: Chromatograms obtained after the SAM-like pyrolysis (35 °C·min^{-1} ramp) of 1:100 undecanoic acid (black) in silica, in the presence of 3:100 $MgCl_2$ (blue), $CaCl_2$ (red), and NaCl (green). All the compounds were diluted in 1 wt% of fused silica. (*) artifacts from the column stationary phase (bleeding), (1) CO_2, (2) propene, (3) butene, (4) pentene, (5) pentane, (6) pentadiene, (7) hexane, (8) hexadiene, (9) benzene, (10) heptane, (11) toluene, (12) octene, (13) octane, (14) ethylbenzene, (15) nonene, (16) nonane, (17) decene, (18) decane, (19) undecene, (20) acetylcyclohexene, (21) Pentylbenzyl, (22) naphthalene, (23) decanal, (24), hexylbenzyl, (25) undecanal, (26) dodecanone, (27) tridecanone, (28) pentadecanone, (29) hexadodecanone, (30) octadecanone. Peaks without a number remained unidentified.

As predicted from the EGA results (Figure 2), undecanoic acid is not detected in the chromatogram. However, many pyrolyzates are formed from the decarboxylation and degradation of undecanoic acid, among which, aliphatic molecules such as alkenes and alkanes up to C_{18}. Aromatic molecules are also detected (*e.g.*, benzene, naphthalene) as well as more complex oxygen-bearing cyclic species up to *m/z* 399 (Figure 4, top

black chromatogram).

In the presence of magnesium chloride, the number and complexity of pyrolysis products drastically decreases (Figure 4, blue chromatogram). The compounds formed are the low-mass alkanes and alkenes related to the thermal degradation of undecanoic acid during pyrolysis. No other products are formed compared to undecanoic acid in silica, including chlorinated compounds. Similar results are obtained in the presence of calcium chloride and sodium chloride (Figure 4, red and green chromatograms). However, a higher molecular compound with NaCl is potentially identified as heneicosanone (C_{21}).

3.2.1.3 Naphthalene

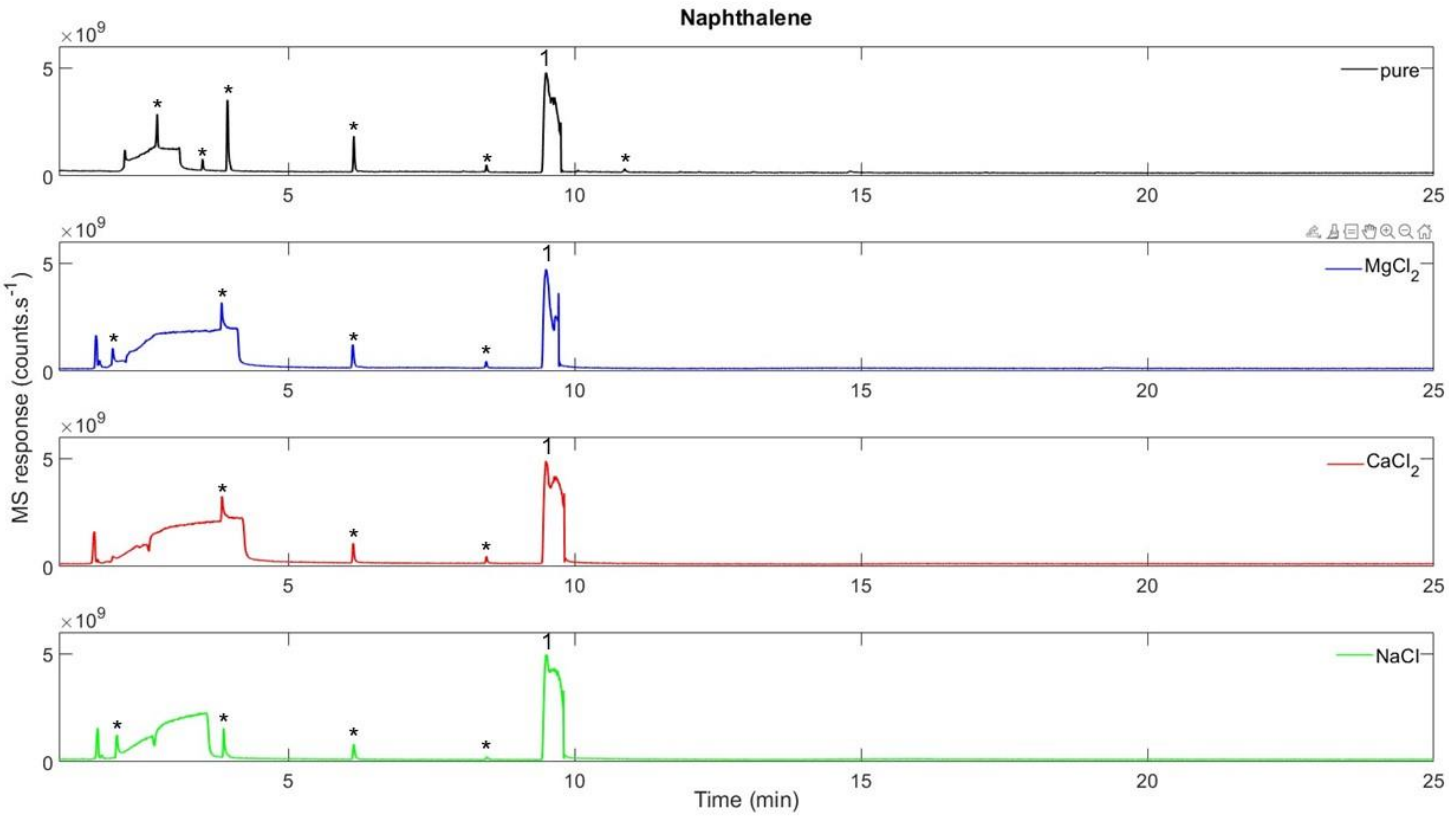

Figure 5: Chromatograms obtained after the SAM-like pyrolysis (35 °C·min^{-1} ramp) of 1:100 naphthalene (black) in silica, in the presence of 3:100 $MgCl_2$ (blue), $CaCl_2$ (red), and NaCl (green). All samples were diluted in 1 wt% of fused silica. (*) artifacts from the stationary phase of the column (bleeding), (1) naphthalene.

As observed in EGA, naphthalene volatilizes at low temperatures (~200 °C) and is the only molecular compound detected (Figure 2). This is confirmed in pyrolysis GC-MS, where naphthalene is the only species observed in the chromatogram (Figure 5, compound 1). The presence of chloride salts does not seem to induce chemical reactions to form new pyrolyzates. Overall, naphthalene did not react with any of the chloride salts when analyzed in SAM-like pyrolysis-GC-MS conditions, as shown by the non-detection of chlorinated molecules.

3.2.1.4 Methylanthracene

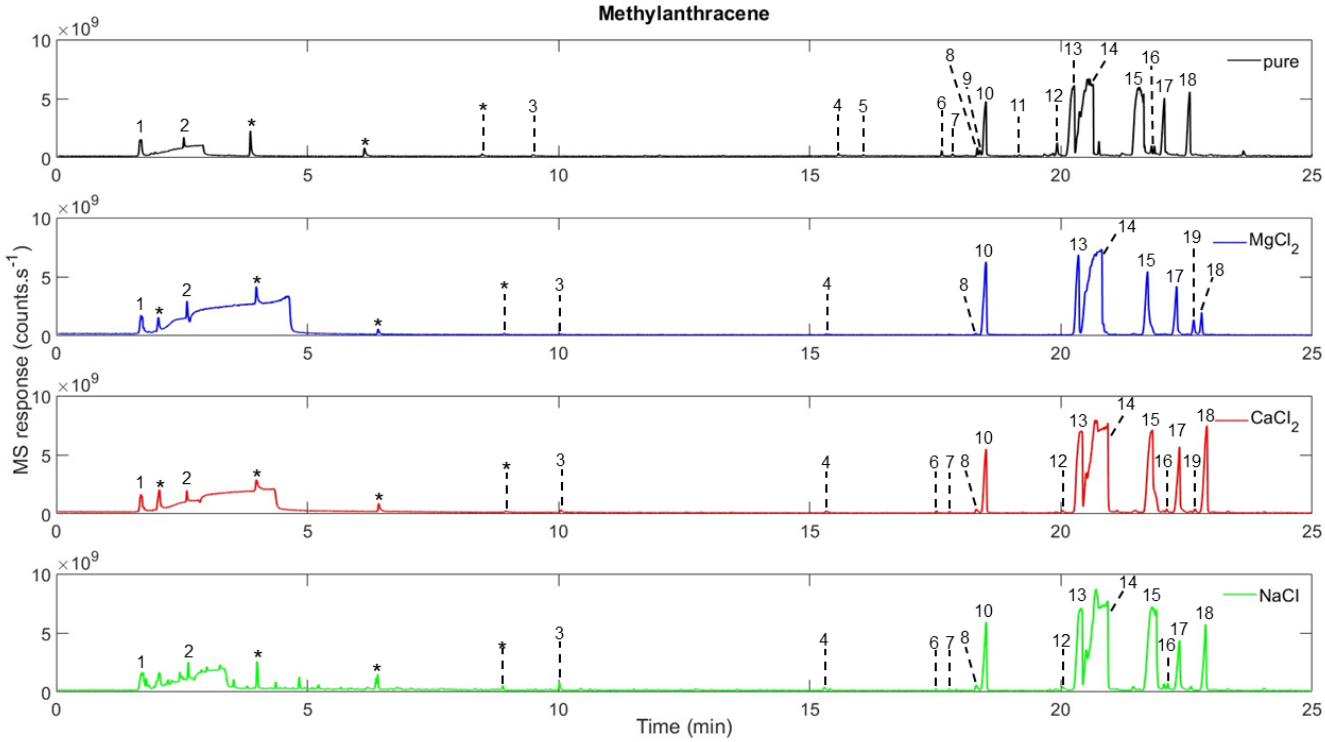

Figure 6: Chromatograms obtained after the SAM-like pyrolysis (35 °C·min^{-1} ramp) of 1:100 methylanthracene (black) in silica, in the presence of 3:100 $MgCl_2$ (blue), $CaCl_2$ (red), and NaCl (green). (*) column bleeding, (1) CO_2, (2) benzene, (3) naphthalene, (4) methylcoumarin, (5) fluorene, (6) anthrone, (7) fluorenone, (8) phenanthrene, (9) phenanthrol, (10) anthracene, (11) xanthone, (12) methylanthracenone, (13) methylanthracene, (14) anthracenedione, (15) dibenzo cycloheptenone, (16) dimethylanthracene, (17) anthracenecarboxaldehyde, (18) methylanthracenecarboxaldehyde, (19) chloromethylanthracene. Peaks without a number remain unidentified.

In SAM-like pyrolysis, methylanthracene is still present as one of the main compounds detected in the chromatogram but it is not the most abundant species. (Figure 6, top black chromatogram, compound 13). The two most abundant compounds observed in GC-MS are the same than the ones observed in EGA: anthracenedione and dibenzocycloheptenone (Figure 6, top black chromatogram, compounds 14 and 15). Moreover, two aldehydes, anthracenecarboxaldehyde, and methylanthracenecarboxaldehyde are also among the major pyrolyzates. The oxygen-bearing groups were likely formed by oxidation of methylanthracene in the presence of water released from the silica. Anthracene is also detected, formed from the demethylation of methylanthracene. Other oxygen-bearing compounds (methyl coumarin, phenanthrol, benzanthrenone) and hydrocarbons (dimethylanthracene, phenanthrene, fluorene, naphthalene) are formed but present in lower intensities compared to the species mentioned above.

The same major compounds than the ones observed in the chromatogram of methylanthracene without salts are still present in the presence of magnesium chloride, however, their relative abundances varied (Figure 6, blue chromatogram). Specifically, dibenzocyloheptenone and methylanthracenecarboxaldehyde decrease in the presence of $MgCl_2$ and the minor pyrolysis products including fluorene, fluorenone, xanthone, methylanthracenone, and dimethylanthracene are no more detected. The pyrolysis of methylanthracene with $MgCl_2$ also leads to the formation of chloromethylanthracene from the direct chlorination of methylanthracene by HCl released during the pyrolysis.

In the presence of calcium chloride, fluorene, phenanthrol, xanthone, and benzanthrenone are not detected. However, the pyrolysis of $CaCl_2$ with methylanthracene leads to the formation of chloromethylanthracene but in lower abundance compared to $MgCl_2$ (Figure 6, red chromatogram, compound 19).

The main thermal degradation products of methylanthracene do not seem to be influenced by NaCl. Only a few minor pyrolyzates (fluorene, phenanthrol, and

xanthone) are absent compared to the sample without salt. Chloromethylanthracene is not detected.

3.2.1.5 Glycine

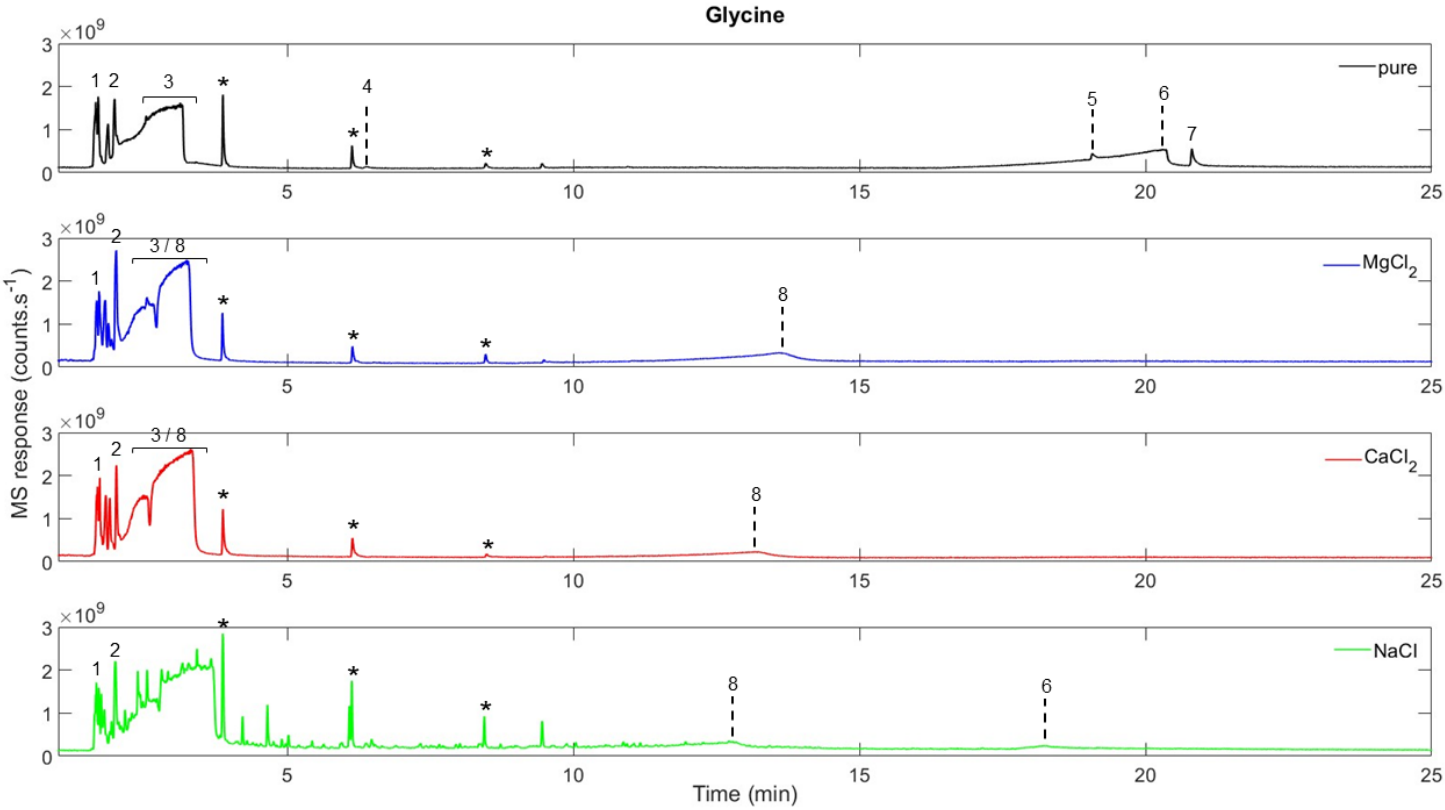

Figure 7: Chromatograms obtained after the SAM-like pyrolysis (35 °C·min^{-1} ramp) of 1:100 glycine (black) in silica, in the presence of 3:100 $MgCl_2$ (blue), $CaCl_2$ (red), and NaCl (green). (*) artefact of the column (stationary phase bleeding), (1) CO_2, (2) acetonitrile, (3) water, (4) phenol, (5) anthracenedione, (6) 2,5-Piperazinedione, (7) bisphenolmethylethylidene, (8) HCl. Peaks without a number remain unidentified.

The SAM-like pyrolysis of glycine leads to the formation of a few products detected with GC-MS. As expected, glycine itself is not detected because of its high polarity and low thermal stability. The main thermal decomposition product of glycine is 2,5-Piperazinedione (Figure 7, top black chromatogram, compound 6), as seen from the EGA data (Figure 2). CO_2 and water from the decarboxylation and dehydration of glycine are observed in high abundance. Acetonitrile is also among the most abundant products formed resulting from glycine degradation and characteristic of its amine

group. Other minor products are observed such as phenol, naphthalene, anthracenedione, and bisphenolmethylethylidene.

In the presence of magnesium chloride, 2,5-piperazinedione is not detected anymore, nor are the minor products from the thermal degradation of glycine (Figure 7, blue chromatogram). However, the main thermal degradation products, CO_2 and acetonitrile are present. No other pyrolyzates are identified. The chromatogram obtained in the presence of calcium chloride is very similar to the chromatogram of magnesium chloride (Figure 7, red chromatogram). In the presence of sodium chloride, 2,5-piperazinedione is detected, however, in a lower amount compared to the sample without salt (Figure 7, green chromatogram, compound 6). CO_2 and acetonitrile are the only other decomposition products identified.

3.2.1.6 Glutamic acid

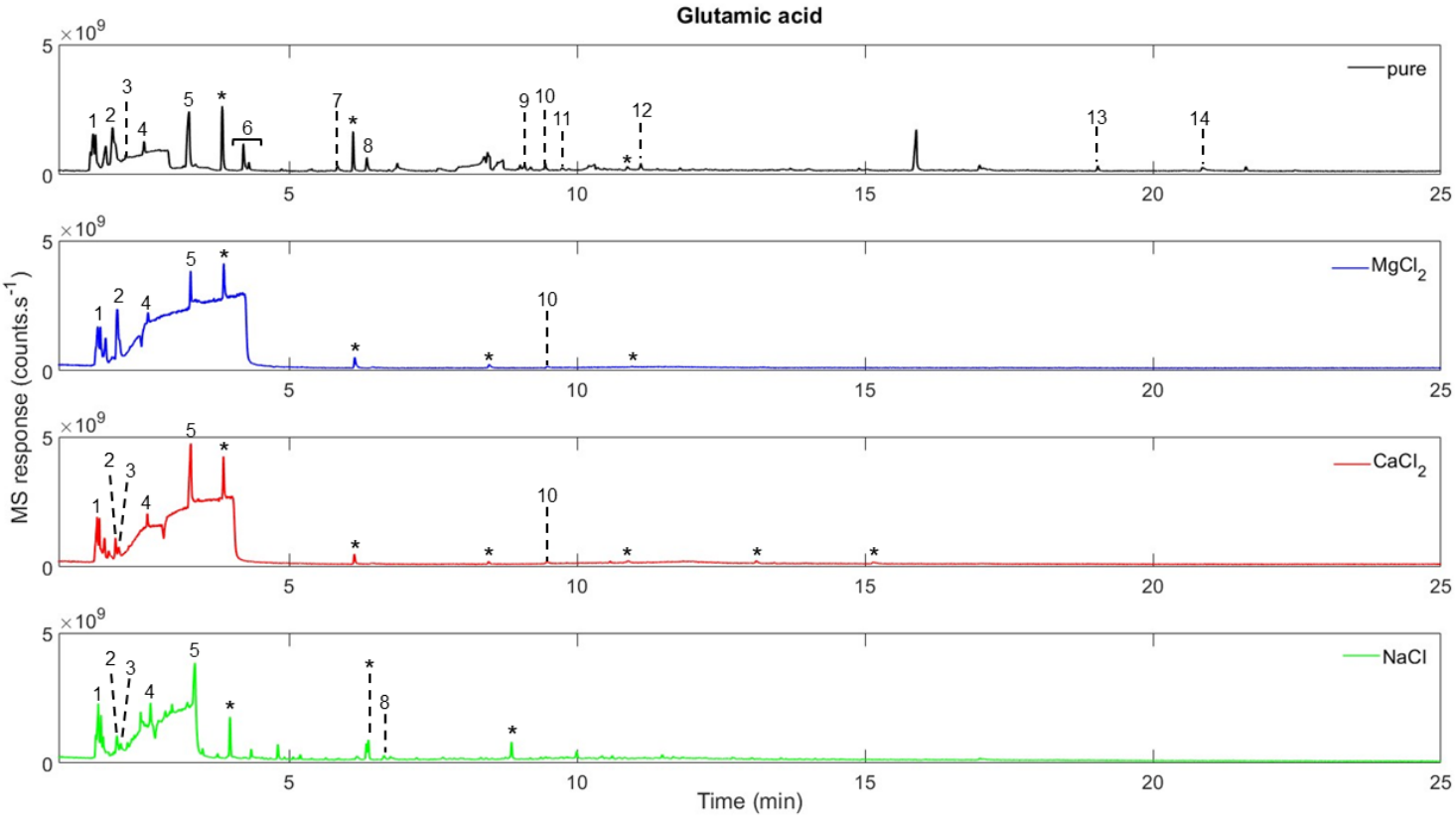

Figure 8: Chromatograms obtained after the SAM-like pyrolysis (35 °C·min^{-1} ramp) of 1:100 glutamic acid (black) in silica, in the presence of 3:100 $MgCl_2$ (blue), $CaCl_2$ (red), and NaCl (green). (*) artefact of the column (stationary phase bleeding), (1) CO_2, (2) acetonitrile, (3) propanenitrile, (4) benzene, (5) pyrrole, (6) methylpyrrole, (7) methylpyridine, (8) benzonitrile, (9) succinimide, (10) naphthalene, (11) glutarimide, (12) indole, (13) anthracenedione, (14) Phenol, 4,4'-(1-methylethylidene)bis. Peaks without a number remain unidentified.

As with glycine, glutamic acid is not thermally stable to be detected with pyrolysis. Instead, we observe the formation of nitrogen- and oxygen-bearing compounds, aromatic hydrocarbons, and PAHs. Pyrrole is one of the most abundant species detected (Figure 8, top black chromatogram, compound 5) and is a characteristic thermal degradation of glutamic acid and was identified in EGA by *m/z* 79 (Figure 2).

In the presence of magnesium chloride, most of the compounds observed in the sample without salt are no longer detected. The only molecules identified are the most

volatile thermal degradation products CO_2, acetonitrile, benzene, and pyrrole (Figure 8, blue chromatogram).

With calcium and sodium chloride, we found similar results as with magnesium chloride (Figure 8, red and green chromatograms), except for propanenitrile, which is not detected in the presence of $MgCl_2$. No chlorinated compounds are observed during pyrolysis of glutamic acid with any of the chloride salts.

3.2.1.7 Phenylalanine

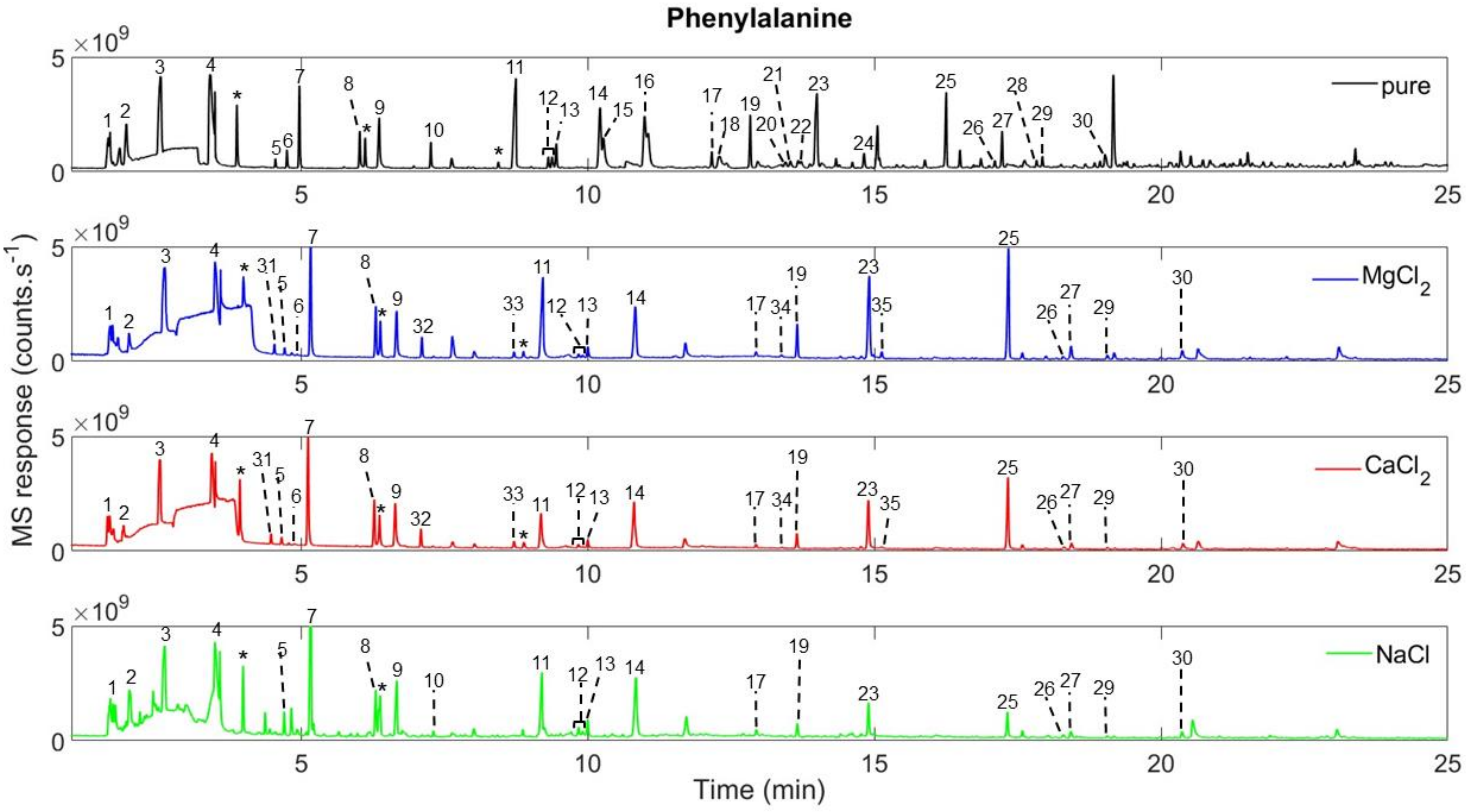

Figure 9: Chromatograms obtained after the SAM-like pyrolysis (35 °C·min^{-1} ramp) of 1:100 phenylalanine (black) in silica, in the presence of 3:100 $MgCl_2$ (blue), $CaCl_2$ (red), and NaCl (green). (*) artefact of the column (stationary phase bleeding), (1) CO_2, (2) acetonitrile, (3) benzene, (4) toluene, (5) ethylbenzene, (6) phenylethyne, (7) styrene, (8) benzaldehyde, (9) benzonitrile, (10) propynylbenzene, (11) benzyl nitrile, (12) phenylporpenenitrile, (13) naphthalene, (14) benzenepropanenitrile, (15) quinoline, (16) indole, (17) biphenyl, (18) methylindole, (19) diphenylmethane, (20) phenylpyridine, (21) biphenylmethyl, (22) naphthalenecarbonitrile, (23) bibenzyle, (24) fluorene, (25) stilbene, (26) phenanthrene, (27) anthracene, (28) anthracene ethenyl, (29) phenylindene, (30) phenylnaphthalene, (31) chlorobenzene, (32) benzyl chloride, (33) chloroethylbenzene, (34) phenylpropenoyl chloride, (35) phenylmethylbenzenemethyl. Peaks without a number remain unidentified.

As seen in EGA (Figure 2), phenylalanine is not detected, but several other thermal products are identified in the chromatogram. They include toluene and benzyl nitrile

(Figure 9, compounds 4 and 11). Other N-bearing aromatic compounds, including benzonitrile, benzene propane nitrile, and indole, are observed in the chromatogram of phenylalanine pyrolyzed in the absence of salt. Polyaromatic hydrocarbons are detected in high concentrations, including, diphenylmethane, stilbene, and anthracene. Higher molecular weight compounds (up to *m/z* 290) are also observed. However, they are difficult to strictly identify as some are not present in the National Institute of Standards and Technology (NIST) database.

The higher molecular weight compounds discussed above are not detected in the presence of magnesium chloride (Figure 9, blue chromatogram). However, new molecules such as chlorobenzene, benzyl chloride, chloro-ethylbenzene, and phenylpropenoyl chloride are identified (Figure 9, blue chromatogram, compounds 31, 32, 33, and 34, respectively). These molecules are produced from the interaction between the salt and the thermal degradation products of phenylalanine. Among these chlorinated compounds, benzyl chloride is the most abundant. The pyrolysis of phenylalanine in the presence of calcium chloride (Figure 9, red chromatogram) is similar to the one obtained with magnesium chloride. Finally, in the presence of NaCl, we observe the loss of the least volatile compounds as observed with the other two chloride salts (Figure 9, green chromatogram). No chlorinated compounds are formed on the contrary to magnesium and calcium chloride.

3.2.2. Influence of chloride salts on the Viking and MOMA-like pyrolysis of organic molecules in the presence of Silica

3.2.2.1. Viking-like (Flash 500 °C)

3.2.2.1.1. Benzoic acid

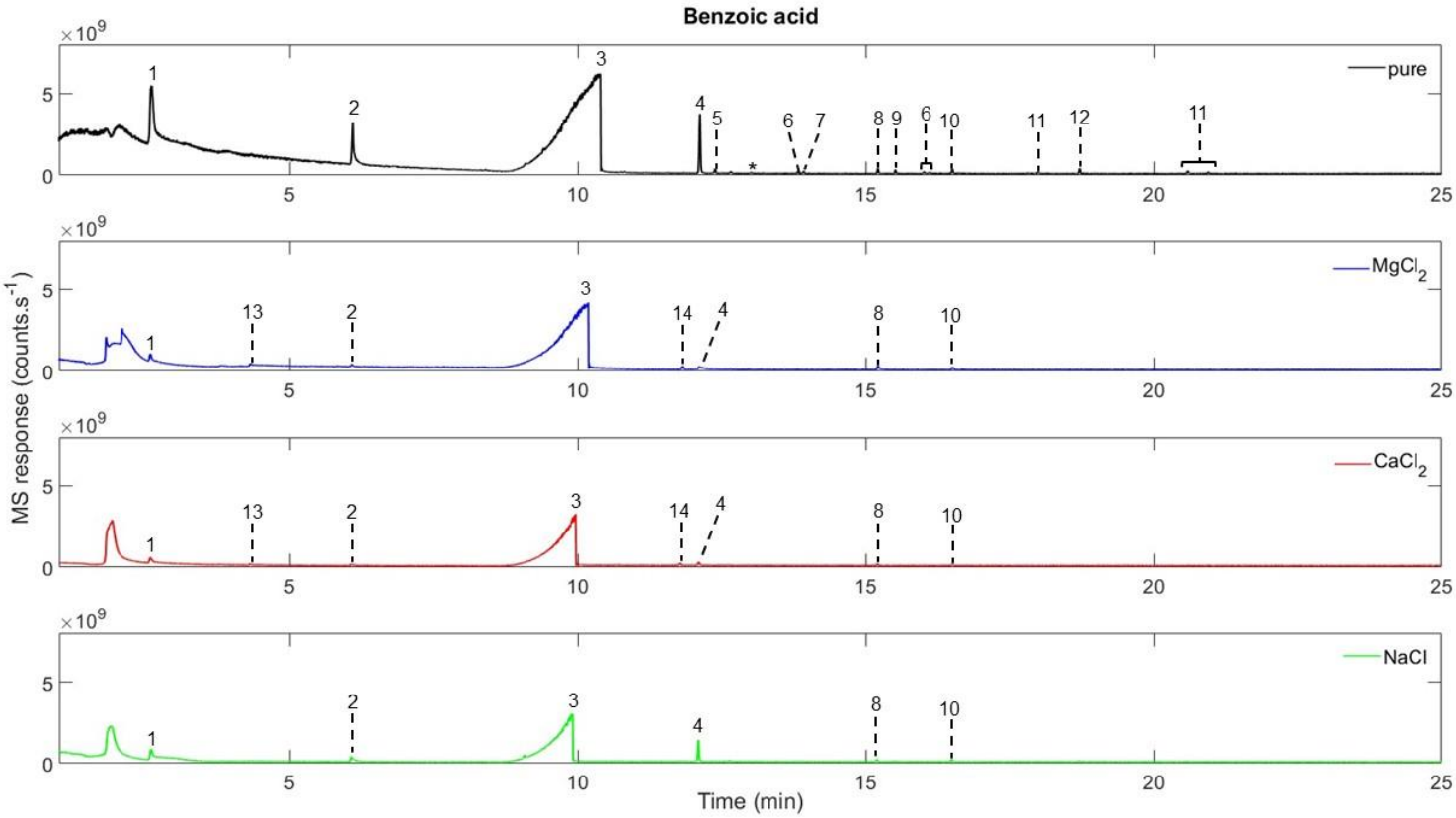

Figure 10: Chromatograms obtained after the flash pyrolysis at 500 °C of 1:100 benzoic acid (black) in silica, in the presence of 3:100 $MgCl_2$ (blue), $CaCl_2$ (red), and NaCl (green). (*) artifact of the column (stationary phase bleeding), (1) benzene, (2) phenol, (3) benzoic acid, (4) biphenyl, (5) diphenyl ether, (6) hydroxybiphenyl isomers, (7) dibenzofuran, (8) benzophenone, (9) benzoic acid, phenyl ester, (10) fluorenone, (11) terphenyl isomers, (12) hydroxyfluorene, (13) chlorobenzene, (14) chlorobenzoic acid. Peaks without a number remain unidentified.

After flash pyrolysis at 500 °C, benzoic acid itself is the most abundant compound detected in the chromatogram (Figure 10, compound 3). Benzene, biphenyl, and phenol are also present in higher abundance comparatively to other species like diphenyl ester, hydroxybiphenyl isomers, dibenzofuran, benzophenone, benzoic acid

phenyl ester, fluorenone, terphenyl, and hydroxyfluorene.

In the presence of $MgCl_2$ and $CaCl_2$, benzoic acid is still the most abundant species observed. However, the number of compounds detected decreases and the relative intensities of benzene, biphenyl, and phenol is lower compared to the chromatogram obtained for the pure acid (Figure 10, blue and red chromatograms, compounds, 1, 2, and 4). Moreover, two new chlorinated organic products are observed: chlorobenzene and chlorobenzoic acid (Figure 10, blue and red chromatograms, compounds 13 and 14).

With sodium chloride (NaCl), the same molecules are detected as with the other two salts except for chlorobenzene and chlorobenzoic acid (Figure 10, green chromatogram).

1.1.1.1.1. Undecanoic acid

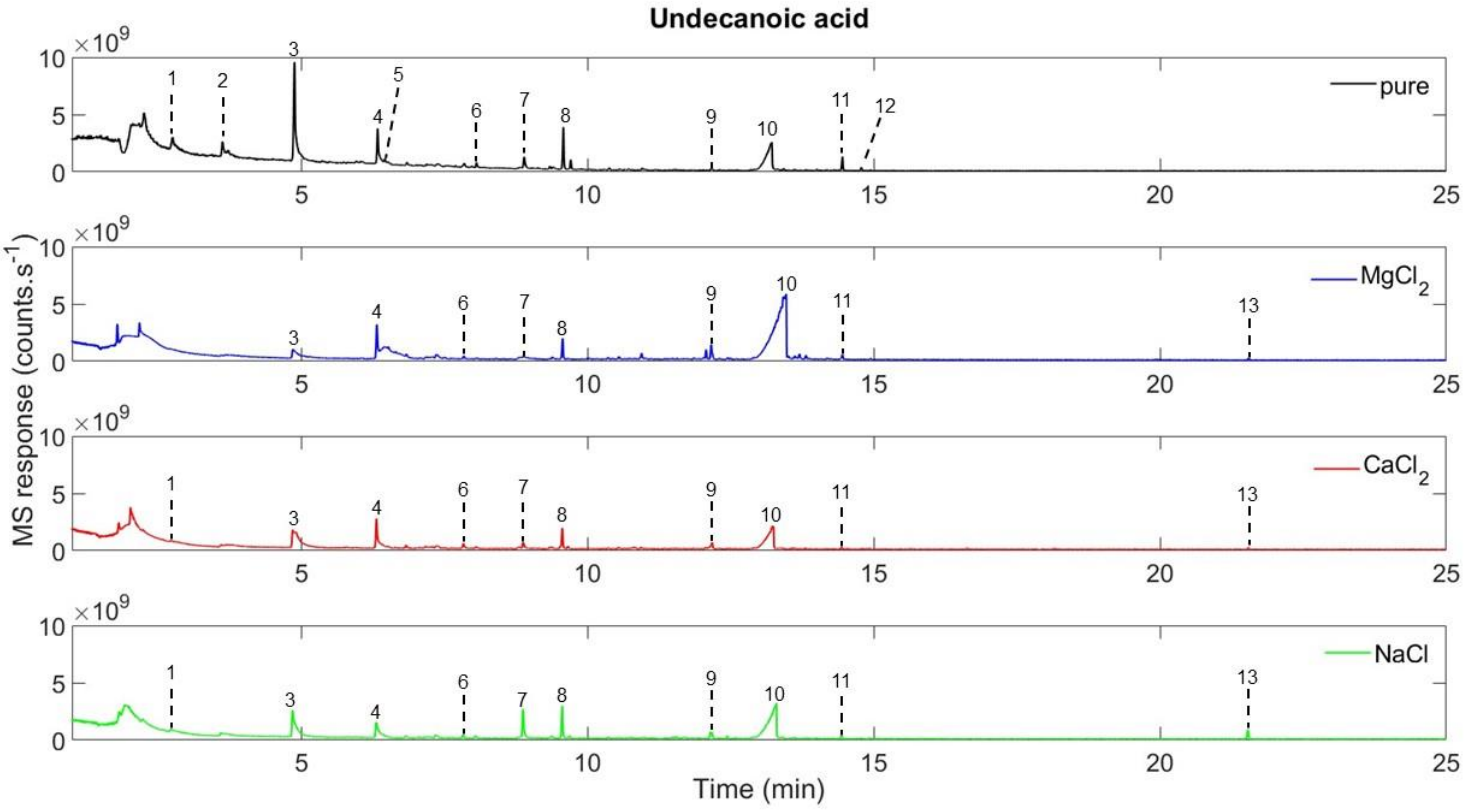

Figure 4 Chromatograms obtained after flash pyrolysis at 500 °C of 1:100 undecanoic acid (black) in silica, in the presence of 3:100 $MgCl_2$ (blue), $CaCl_2$ (red), and NaCl (green). (*) artifact of the column (stationary phase bleeding), (1) heptene, (2) octene, (3) nonene, (4) decene, (5) decane, (6) nonanal, (7) benzene pentyl, (8) decanal, (9) dodecanone, (10) undecanoic acid, (11) furanone, heptyldihydro-, (12) hexyltetrahydro pyranone, (13) heneicosanone. Peaks without a number remain unidentified.

At 500 °C flash-pyrolysis, undecanoic acid (the parent molecule) is detected in relative higher abundance compared to the other species present in the chromatogram (Figure 11, top black chromatogram, compound 10). Other aliphatic and aromatic products are also present such as alkenes, alkanes, and ketones.

In the presence of magnesium chloride, a change in the relative abundance of some species is observed (Figure 11, blue chromatogram). Compounds including octene, decane, and hexyltetrahydro pyranone are not detected anymore. Other molecules

such as nonene drastically decrease in abundance compare to the chromatogram without salt. However, we observe that the relative abundance of the undecanoic acid and dodecanone increased. Finally, heneicosanone, a long chain ketone is detected.

The pyrolysis of undecanoic acid in the presence of calcium and sodium chlorides led to similar chromatograms as the pyrolysis of undecanoic acid in the presence of magnesium chloride.

1.1.1.1.2. Naphthalene

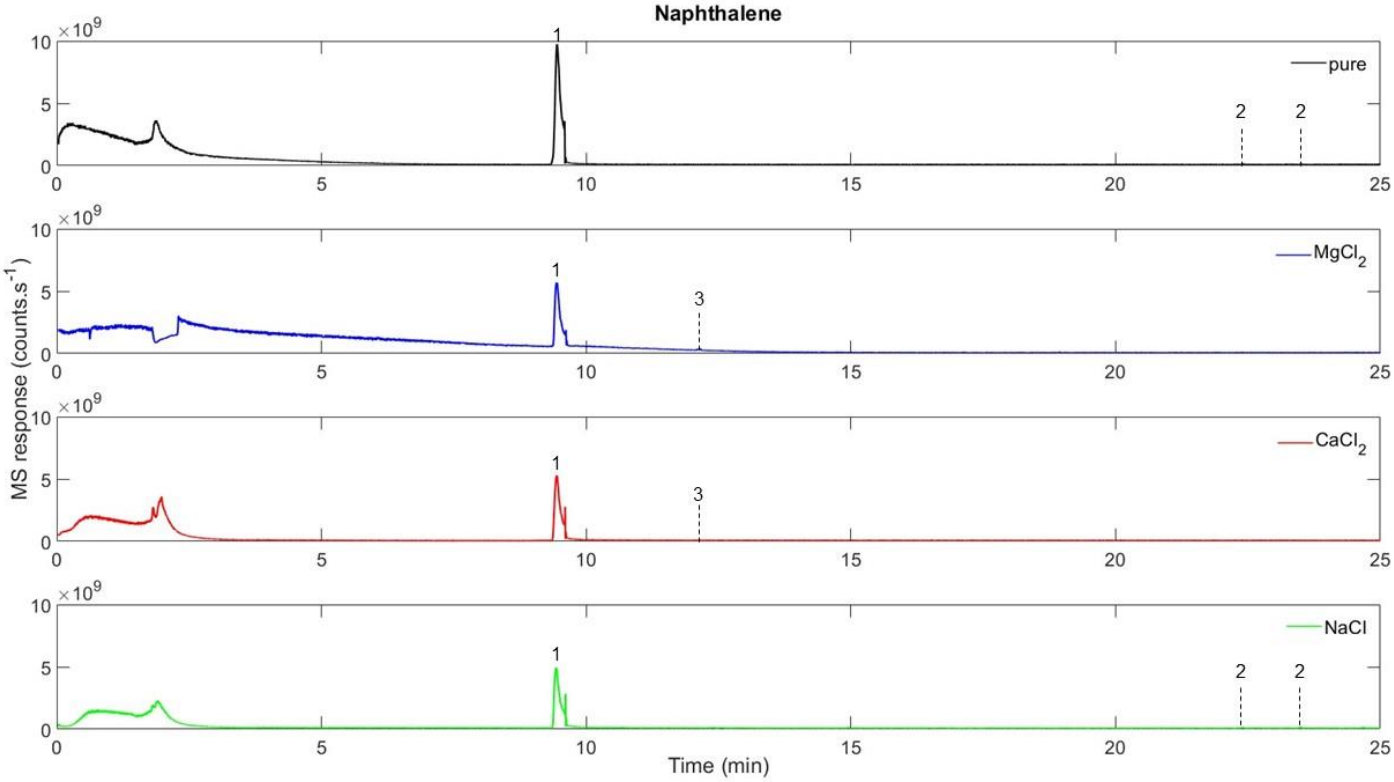

Figure 12: Chromatograms obtained after the flash pyrolysis at 500 °C of 1:100 naphthalene (black) in silica, in the presence of 3:100 $MgCl_2$ (blue), $CaCl_2$ (red), and NaCl (green). (*) artifact of the column (stationary phase bleeding), (1) naphthalene, (2) binapthalene isomers, (3) chlronapthalene.

The naphthalene parent molecule is the major compound observed after flash pyrolysis at 500 °C (Figure 12, compound 1). Minor peaks of binaphthalene isomers are also detected in the chromatogram.

In the presence of $MgCl_2$ and $CaCl_2$, naphthalene is still the most abundant species present but in relatively lower abundance compared to the chromatogram without salt. However, the binaphthalene compounds are not detected anymore and a new molecule, chloronaphthalene, is observed (Figure 12, blue and red chromatograms, compound 3). With NaCl, the two binaphthalene isomers are detected but not chloronaphthalene (Figure 12, green chromatogram).

1.1.1.1.3. Methylanthracene

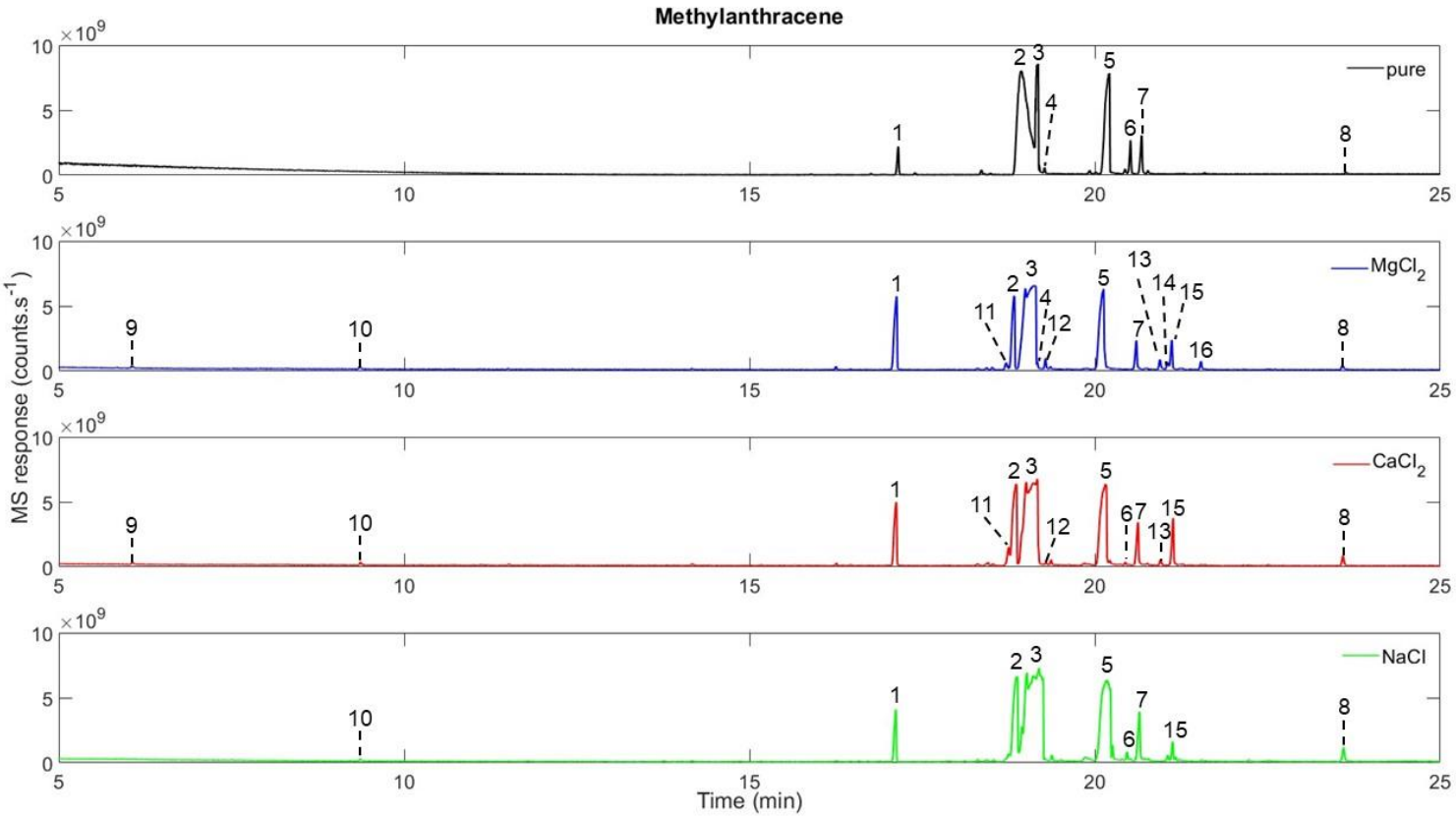

Figure 13: Chromatograms obtained after the flash pyrolysis at 500 °C of 1:100 methylanthracene (black) in silica, in the presence of 3:100 $MgCl_2$ (blue), $CaCl_2$ (red), and NaCl (green). (*) artifact of the column (stationary phase bleeding), (1) anthracene (2) methylanthracene, (3) anthracenedione, (4) ethylanthracene, (5) dibenzocycloheptenone, (6) dimethylanthracene, (7) anthracenecarboxaldehyde, (8) benanthrenone, (9) phenol, (10) naphthalene, (11) anthrone, (12) chloroanthracene, (13) chloromethylanthracene, (14) dichloroanthracene, (15) methylanthracenecarboxaldehyde, (16) chloroanthraldehyde. Peaks without a number remain unidentified.

After the 500 °C flash-pyrolysis, methylanthracene is the most abundant compound observed in the chromatogram, followed by an aromatic ketone: dibenzocycloheptenone (Figure 13, top black chromatogram, compounds 2 and 5). Other O-bearing compounds have been identified such as anthracenedione, anthracenecarboxaldehyde, and bezanthrenone. These oxidized molecules may have been produced from reaction between the water adsorbed on the surface of the silica matrix and the salts during sample preparation which was further liberated during pyrolysis and reacted with the molecules at high temperature. Other species such as anthracene, dimethylanthracene and ethylanthracene are detected which are likely formed through demethylation or methylation processes.

In the presence of magnesium chloride, the mains species as those described in the chromatogram of methylanthracene without salt, are also detected but their relative abundances are different. The parent molecule methylanthracene is less abundant and anthracenedione is now the most abundant compound (Figure 13, blue chromatogram). Moreover, phenol and naphthalene are detected. New species such as anthrone and methylanthracenecarboxaldehyde are formed, whereas dimethylanthracene is absent in the chromatogram obtained in the presence of $MgCl_2$. Moreover, interaction between the HCl released and the molecules during pyrolysis produces several chlorinated compounds such as chloroanthracene, chloromethylanthracene, dichloroanthracene, and chloroanthraldehyde (Figure 13, blue chromatogram, compounds 12, 13, 14 and 16).

In the presence of calcium chloride, some of the chlorinated compounds that are identified with $MgCl_2$ are not detected such as chloromethylanthracene and dichloroantharcene. Only chloroanthracene and chloromethylanthracene are formed (Figure 13, red chromatogram).

The presence of sodium chloride also favors the degradation of methylanthracene with an increased abundance of anthracenedione (Figure 13, green chromatogram, compound 3). However, no new compounds such as anthrone nor chlorinated organic

molecules are detected.

1.1.1.1.4. Glycine

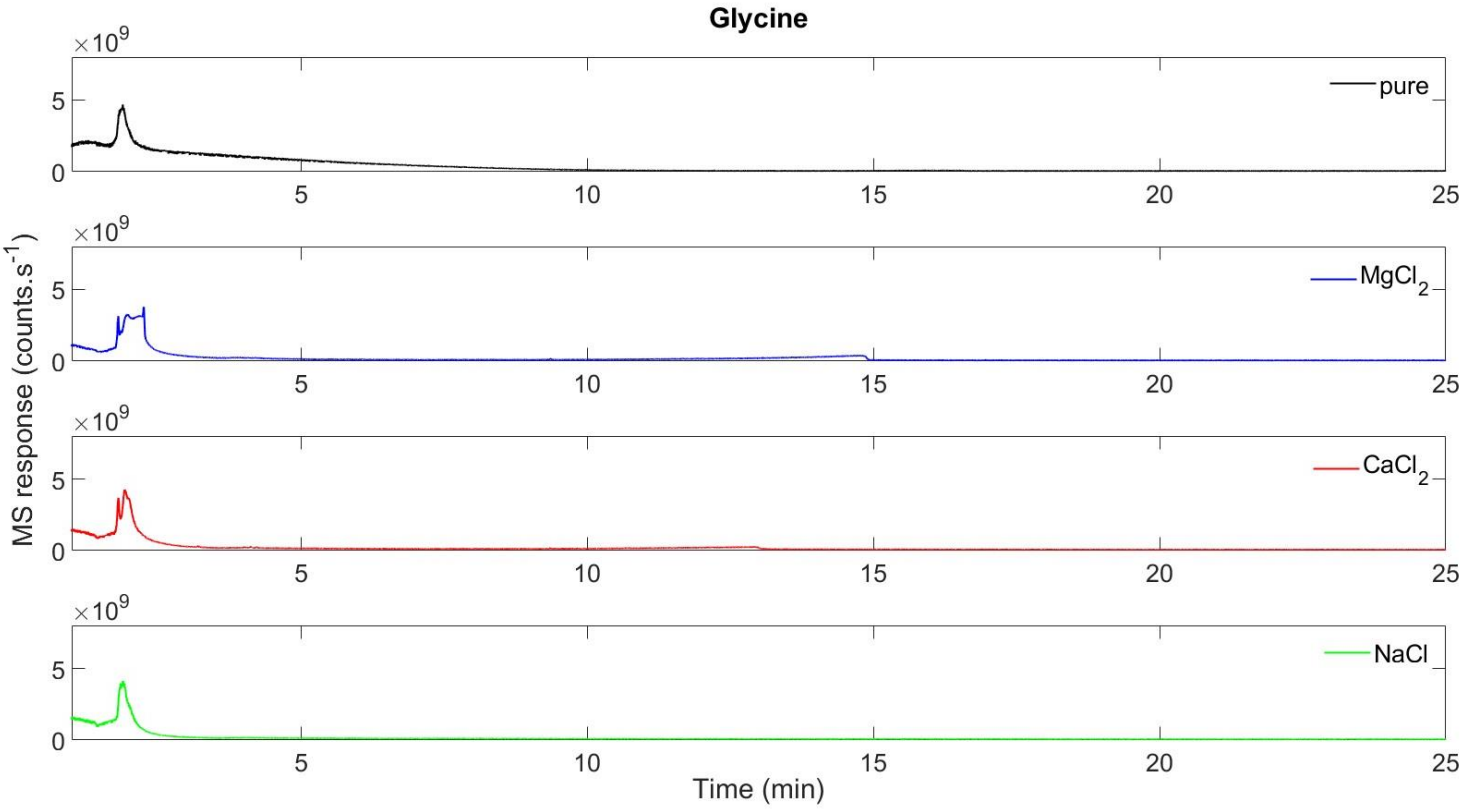

Figure 145: Chromatograms obtained after flash pyrolysis at 500 °C of 1:100 glycine (black) in silica, in the presence of 3:100 $MgCl_2$ (blue), $CaCl_2$ (red), and NaCl (green)

During flash 500 °C pyrolysis analysis of glycine, no compounds are detected any of the samples regardless of the absence or presence of salts (Figure 14). Only water and CO_2 are present in the chromatogram.

1.1.1.1.5. Glutamic acid

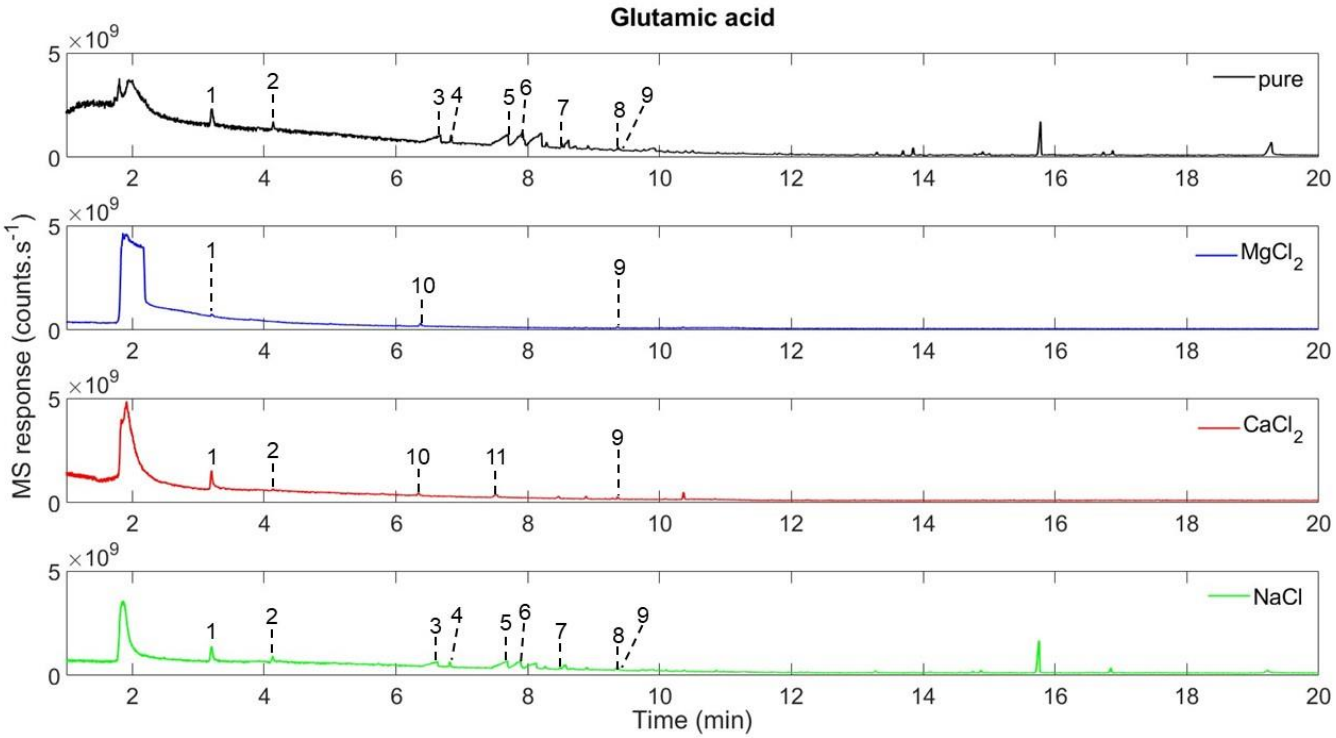

Figure 15: Chromatograms obtained after flash pyrolysis at 500 °C of 1:100 glutamic acid (black) in silica, in the presence of 3:100 $MgCl_2$ (blue), $CaCl_2$ (red), and NaCl (green). (1) pyrrole, (2) methylpyrrole, (3) aminopyrazole, (4) ethylpyridine, (5) pyrrolidinone, (6) aminopyrazine, (7) dimethylbenzamine, (8) glutarimide, (9) naphthalene, (10) pyrroledione, (11) pyrrolidinone. Peaks without a number remain unidentified.

When flash-pyrolyzed at 500 °C, glutamic acid itself is not detected in the chromatograms. However, we observe the formation of N and O-bearing molecules coming from the thermal degradation of glutamic acid (Figure 15).

In the presence of $MgCl_2$ (Figure 15, blue chromatogram), the number of molecules detected in the chromatogram drastically decrease. Only pyrrole and naphthalene are detected. However, a new compound is formed, pyrroledione (Figure 15, blue chromatogram, compound 10).

The chromatogram obtained in the presence of $CaCl_2$ (Figure 15, red chromatogram) is similar to the one obtained in the presence of $MgCl_2$ in which most of the molecules

detected in the sample without salt are now absent. Pyrrole, methylpyrrole, naphthalene, and pyrroledione are detected, as well as pyrrolidinone which is only identified in the sample with calcium chloride.

Finally, with NaCl, the chromatogram obtained is very similar to the chromatogram without salt (Figure 15, black and green chromatograms). The species identified are the same as after pyrolysis of the sample without salt but in lower relative abundances.

1.1.1.1.6. Phenylalanine

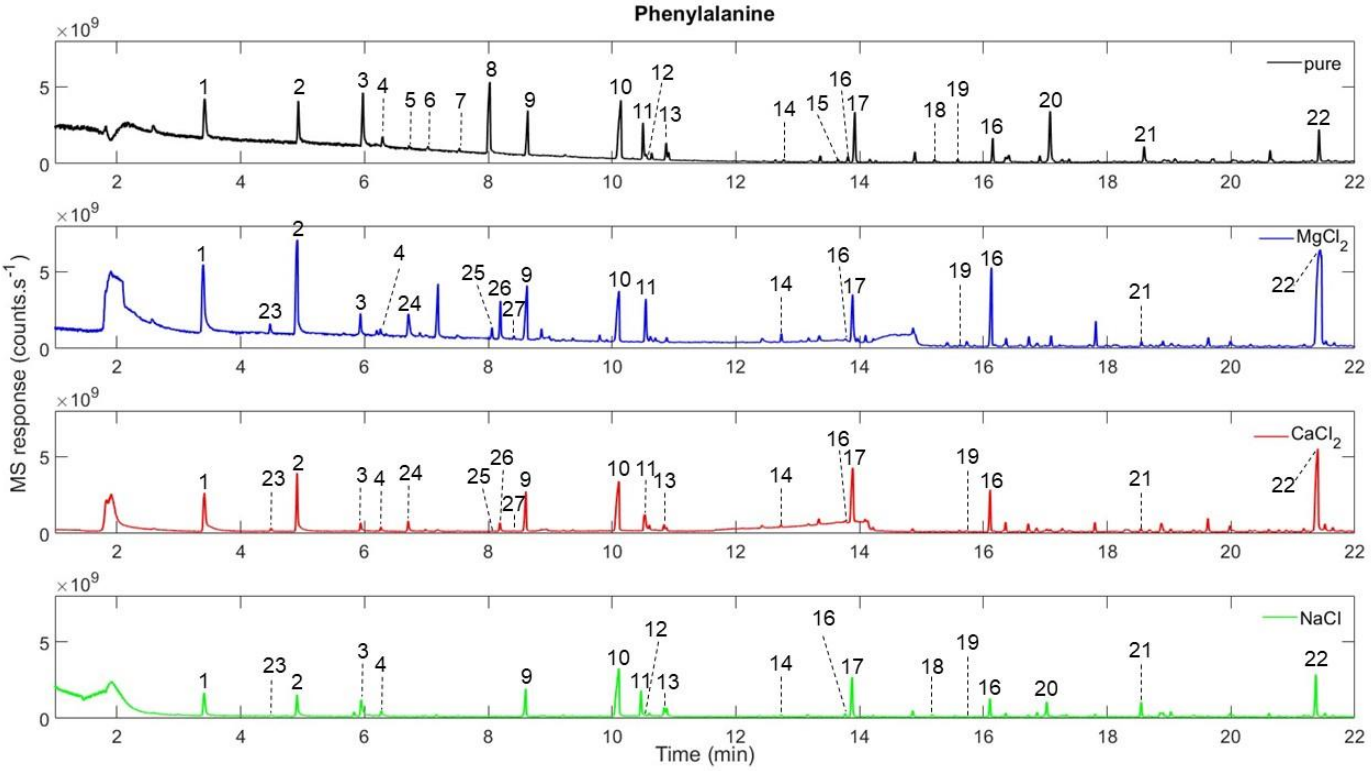

Figure 16: Chromatograms obtained after flash pyrolysis at 500 °C of 1:100 phenylalanine (black) in silica, in the presence of 3:100 $MgCl_2$ (blue), $CaCl_2$ (red), and NaCl (green). (1) toluene, (2) styrene, (3) benzaldehyde, (4) benzonitrile, (5) benzylamine, (6) benzyl alcohol, (7) acetophenone, (8) benzeneethanamine, (9) benzyl nitrile, (10) benzenepropanenitrile, (11) isoquinoline, (12) methylindole, (13) indole, (14) diphenylmethane, (15) acetamide, N-phenethyl-, (16) stilbene (isomers), (17) bibenzyl, (18) benzophenone, (19) diphenylacetylene, (20) benzeneethanamine, N-(phenylmethylene)-, (21) benzeneacetonitrile, α-(phenylmethylene)-, (22) diphenylpyridine, (23) ethylbenzene, (24) chlorobenzyl, (25) hyacinthal, (26) chloroethylbenzene, (27) benzyl methyl ketone, (28) methylquinoline. Peaks without a number remain unidentified.

Phenylalanine itself is not detected in the chromatograms after the 500 °C flash pyrolysis. However, it produces a large number of byproducts. Among the most abundant low molecular weight hydrocarbons that are detected are toluene and styrene, and N-bearing molecules like benzeneethanamine, benzyl nitrile, benzenepropanenitrile or benzeneethanamine-N-(phenylmethylene) (Figure 16).

Most of these molecules have also been identified in the chromatogram of the pyrolysis of phenylalanine with magnesium chloride but with differences in the relative abundances of some species compared to the chromatogram without salts (Figure 16, blue chromatogram). Species such as styrene, stilbene, and diphenylpyridine are present in higher relative abundance whereas other compounds like benzaldehyde, benzeneethanamine, benzeneethanamine-N-(phenylmethylene) or benzeneacetonitrile, α-(phenylmethylene) are less abundant or absent. New species were detected among which chlorinated compounds such as chlorobenzyl and chloroethylbenzene (Figure 16, blue chromatogram, compounds 24 and 26).

In the presence of calcium and sodium chloride, a similar chromatogram as magnesium chloride is obtained (Figure 16, red and green chromatograms), however no chlorinated compounds are detected in the NaCl chromatogram.

1.1.1.2. MOMA-like (Flash 800 °C)

1.1.1.2.1. Benzoic acid

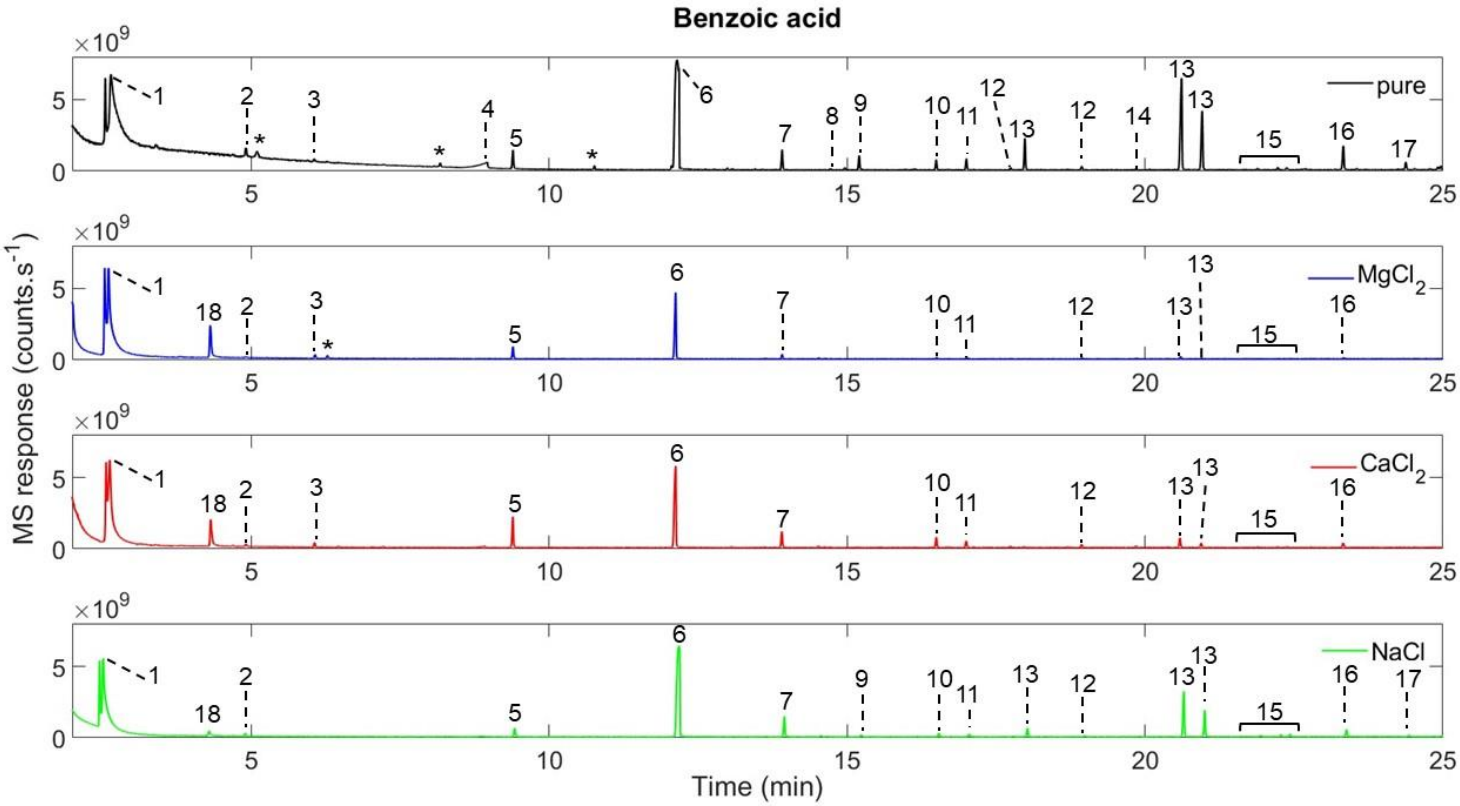

Figure 17: Chromatograms obtained after flash pyrolysis at 800 °C of 1:100 benzoic acid (black) in silica, in the presence of 3:100 $MgCl_2$ (blue), $CaCl_2$ (red), and NaCl (green). (*) artifact of the column (stationary phase bleeding), (1) benzene, (2) styrene, (3) phenol, (4) benzoic acid, (5) naphthalene, (6) biphenyl, (7) dibenzofuran, (8) fluorene, (9) benzophenone, (10) fluorenone, (11) anthracene, (12) phenylnaphthalene (isomers), (13) terphenyl (isomers), (14) pyrene, (15) phenyldibenzofurane (isomers), (16) triphenylene, (17) triphenylbenzene, (18) chlorobenzene.

After flash pyrolysis at 800 °C, the benzoic acid parent molecule is present but biphenyl and benzene are the most abundant compounds detected in the chromatogram (Figure 17, top black chromatogram, compounds 1,4, and 6). Other hydrocarbons and O-bearing compounds are detected such as three terphenyl isomers, triphenylene and dibenzofuran.

In the presence of $MgCl_2$ and $CaCl_2$, benzoic acid is not detected anymore and less

compounds are observed in the chromatogram (Figure 16, blue and red chromatograms). Benzene and biphenyl are still the most abundant species but the relative intensities of other molecules are lower or were even absent from the chromatogram. However, a new species is detected, chlorobenzene, in relatively high abundance compared to the other compounds present (Figure 17, blue and red chromatograms, compound 18).

In the presence of NaCl, byproduct species are detected in higher abundance in comparison with the $MgCl_2$ and $CaCl_2$, and compounds that are not detected with the divalent salts such as phenol, benzophenone, triphenylbenzene are recovered with NaCl (Figure 17, green chromatogram). Chlorobenzene is also detected with NaCl but in lesser intensity than with $MgCl_2$ and $CaCl_2$.

1.1.1.2.2. Undecanoic acid

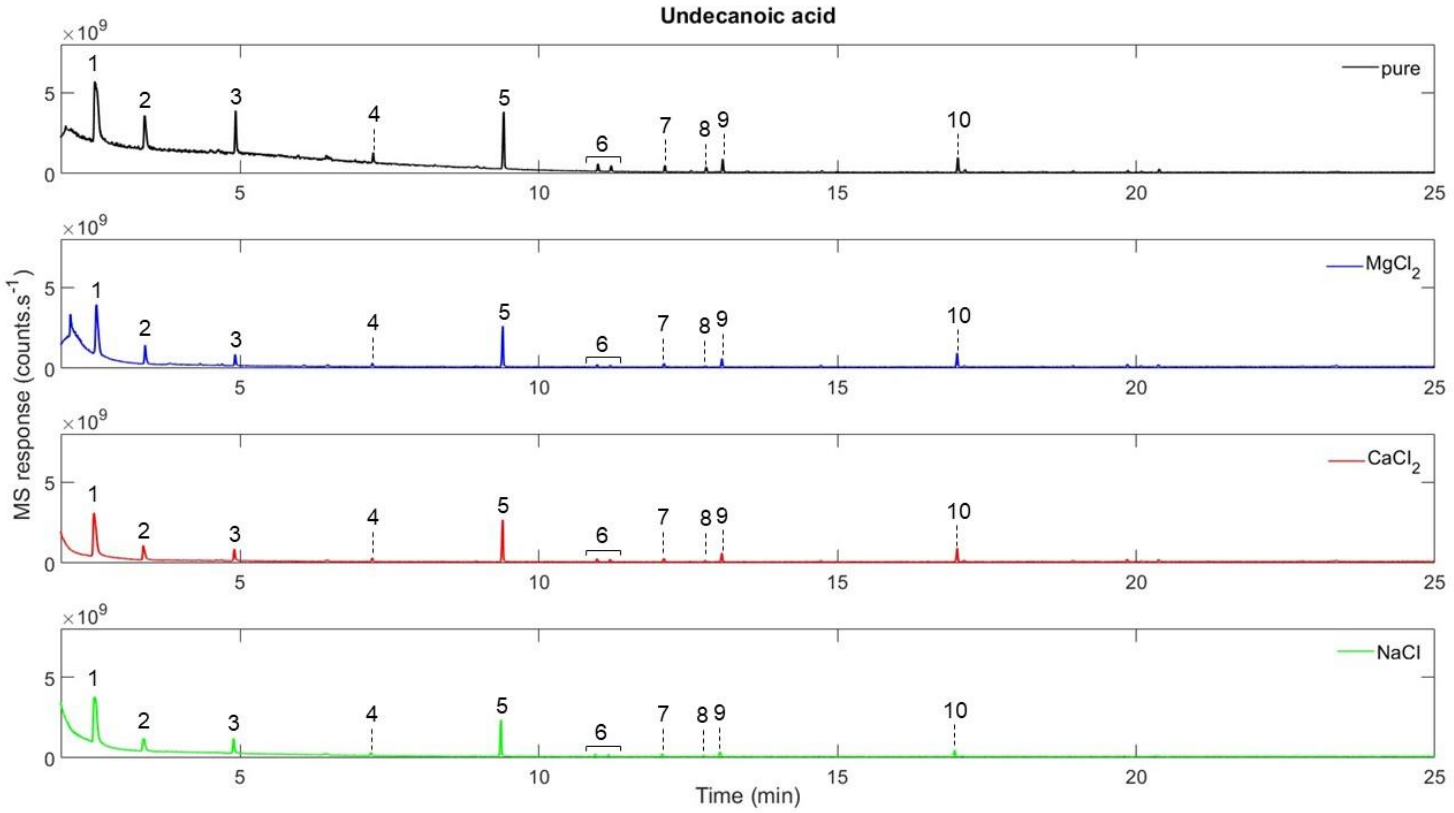

Figure 18: Chromatograms obtained after flash pyrolysis at 800 °C of 1:100 undecanoic acid (black) in silica, in the presence of 3:100 $MgCl_2$ (blue), $CaCl_2$ (red), and NaCl (green). (*) artifact of the column (stationary phase bleeding), (1) benzene, (2) toluene, (3) styrene, (4) indene, (5) naphthalene, (6) methylnaphthalene (isomers), (7) biphenyl, (8) acenaphthene, (9) acenaphthylene, (10) anthracene.

The undecanoic acid molecule is not identified in the chromatograms extracted from the 800 °C flash-pyrolysis. Only aromatic hydrocarbons are detected such as benzene, toluene, styrene, naphthalene and anthracene (Figure 18). The same molecules were obtained in the presence of salts. No chlorinated compounds are detected. The samples with and without chloride salts produced similar products.

1.1.1.2.3. Naphthalene

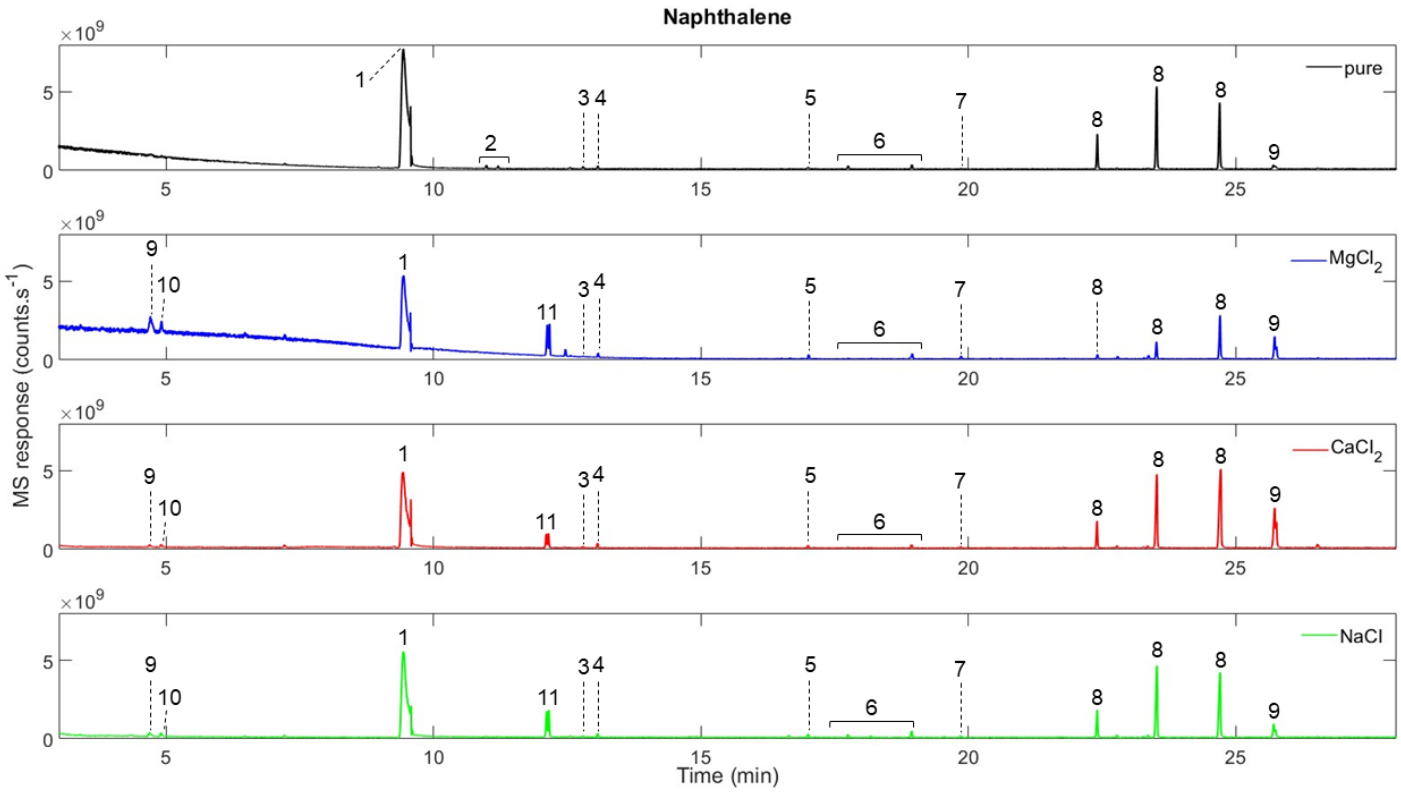

Figure 19: Chromatograms obtained after flash pyrolysis at 800 °C of 1:100 naphthalene (black) in silica, in the presence of 3:100 $MgCl_2$ (blue), $CaCl_2$ (red), and NaCl (green). (*) artifact of the column (stationary phase bleeding), (1) naphthalene, (2) methylnaphthalene, (3) biphenyl, (4) acenaphthylene, (5) anthracene, (6) phenylnaphthalene isomers, (7) binaphthalene, (8) benzofluoranthene isomers, (9) phenylethyne, (10) styrene, (11) chloronaphthalene.

Naphthalene is detected in abundance when flashed pyrolyzed at 800 °C (Figure 19, compound 1). Other compounds are detected, among which three benzofluoranthene isomers in relatively high abundance compared to the other species present in the chromatogram other than naphthalene itself.

In the presence of $MgCl_2$, the majority of the compounds (naphthalene included) decrease in abundance compared to the sample pyrolyzed in the absence of salt. New molecules are detected such as phenylethyne, styrene and chloronaphthalene (Figure 19, blue chromatogram, compounds 9, 10, and 11). In the presence of $CaCl_2$ and NaCl, the pyrolysis of naphthalene led to the production of the same compounds as with

$MgCl_2$.

1.1.1.2.4. Methylanthracene

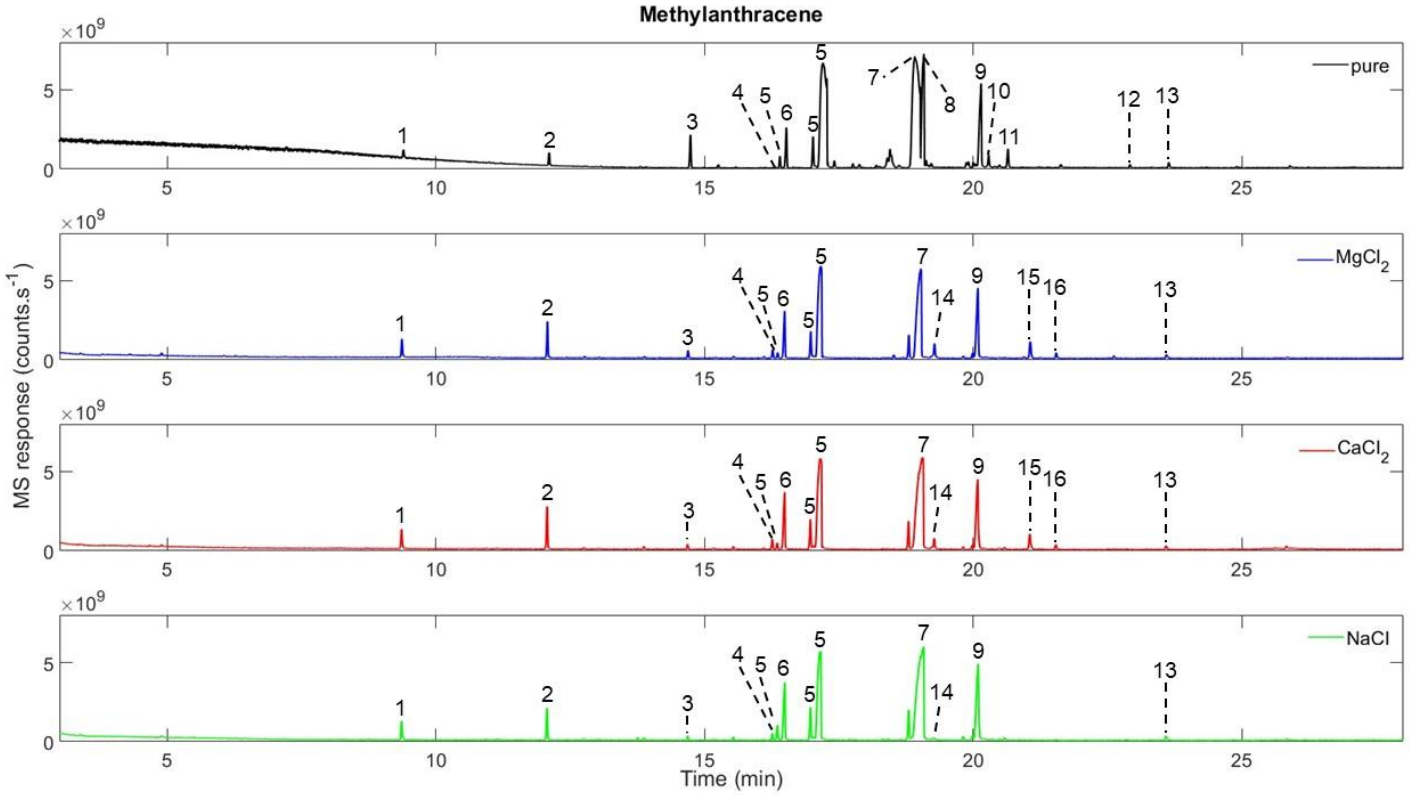

Figure 20: Chromatograms obtained after flash pyrolysis at 800 °C of 1:100 methylanthracene (black) in silica, in the presence of 3:100 $MgCl_2$ (blue), $CaCl_2$ (red), and NaCl (green). (*) artifact of the column (stationary phase bleeding), (1) naphthalene, (2) biphenyl, (3) fluorene, (4) anthrone, (5) anthracene isomers, (6) fluorenone, (7) methylanthracene, (8) anthracenedione, (9) Dibenzocycloheptenone, (10) pyrene, (11) anthracenecarboxaldehyde, (12) phenylanthracene, (13) benzanthracenone, (14) chloroanthracene, (15) dichloroanthracene, (16) chloroanthraldehyde.

Methylanthracene and anthracene are the most abundant compound detected in the chromatogram after flash pyrolysis of methylanthracene in silica at 800 °C (Figure 20, compound 7 and 5, respectively). Other molecules such as anthracenedione, dibenzocycloheptenone, and fluorenone are detected and intensity of their corresponding peaks is high. The formation of O-bearing species, as observed in SAM-like conditions, could be due to the water bearing silica phase producing free radicals

that can oxidize the molecules during high temperature pyrolysis.

In the presence of $MgCl_2$ and $CaCl_2$, several compounds related to the thermal decomposition of methylanthrance are no longer detected such as anthracenedione, pyrene, anthracenecarboxaldehyde and phenylanthracene. Three new compounds bearing chlorine atoms are formed: chloroanthracene, dichloroanthracene and chloroanthraldehyde (Figure 20, blue and red chromatograms, compounds 14, 15, and 16). The chromatogram of methylanthracene pyrolyzed in the presence of NaCl is similar to those with divalent salts except that among the chlorinated molecules produced, only choroanthracene is detected (Figure 20, green chromatogram).

1.1.1.2.5. Glycine

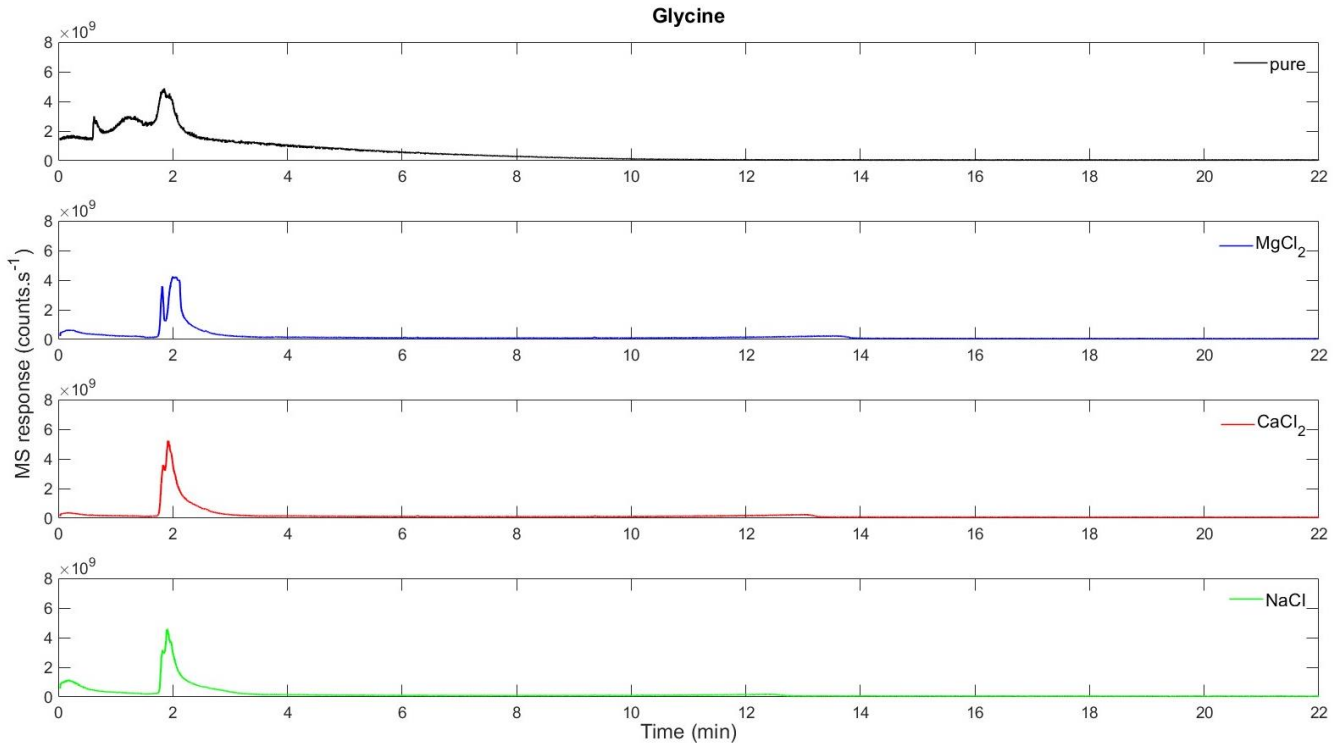

Figure 21: Chromatograms obtained after flash pyrolysis at 800 °C of 1:100 glycine (black) in silica, in the presence of 3:100 $MgCl_2$ (blue), $CaCl_2$ (red), and NaCl (green).

At 800 °C flash-pyrolysis, no organic compounds have been detected in the chromatograms of glycine regardless the presence or absence of salts (Figure 21). Only CO_2 and water at the beginning of the run are observed, with the addition of HCl in the

chromatogram of the three salts.

1.1.1.2.6. Glutamic acid

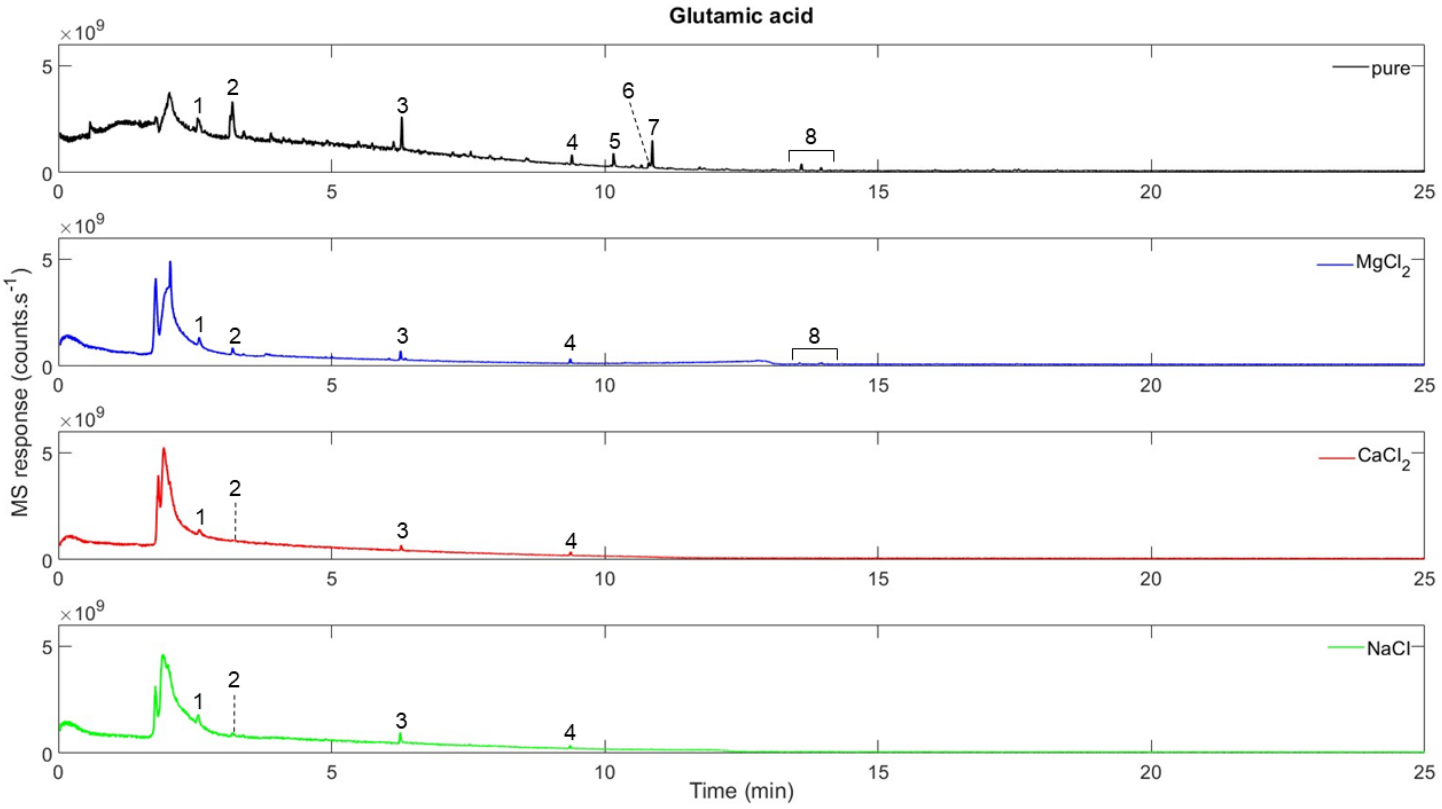

Figure 22: Chromatograms obtained after flash pyrolysis at 800 °C of 1:100 glutamic acid (black) in silica, in the presence of 3:100 $MgCl_2$ (blue), $CaCl_2$ (red), and NaCl (green). (*) artifact of the column (stationary phase bleeding), (1) benzene, (2) pyrrole, (3) benzonitrile, (4) naphthalene, (5) quinoline, (6) pyrrolopyridine, (7) indole, (8) naphthalenecarbonitrile.

Glutamic acid itself is not detected at 800 °C pyrolysis flash as excepted due to its high polarity and low thermal stability. Only a limited number of pyrolyzates are observed in the chromatogram (Figure 22).

In the presence of $MgCl_2$, quinoline, pyrrolopyridine and indole are absent from the chromatogram (Figure 22, blue chromatogram). With $CaCl_2$ and NaCl, naphthalene carbonitrile was no longer detected compared to $MgCl_2$ (Figure 22, red and green chromatograms). No new compound is identified in the presence of chloride salts.

1.1.1.2.7. Phenylalanine

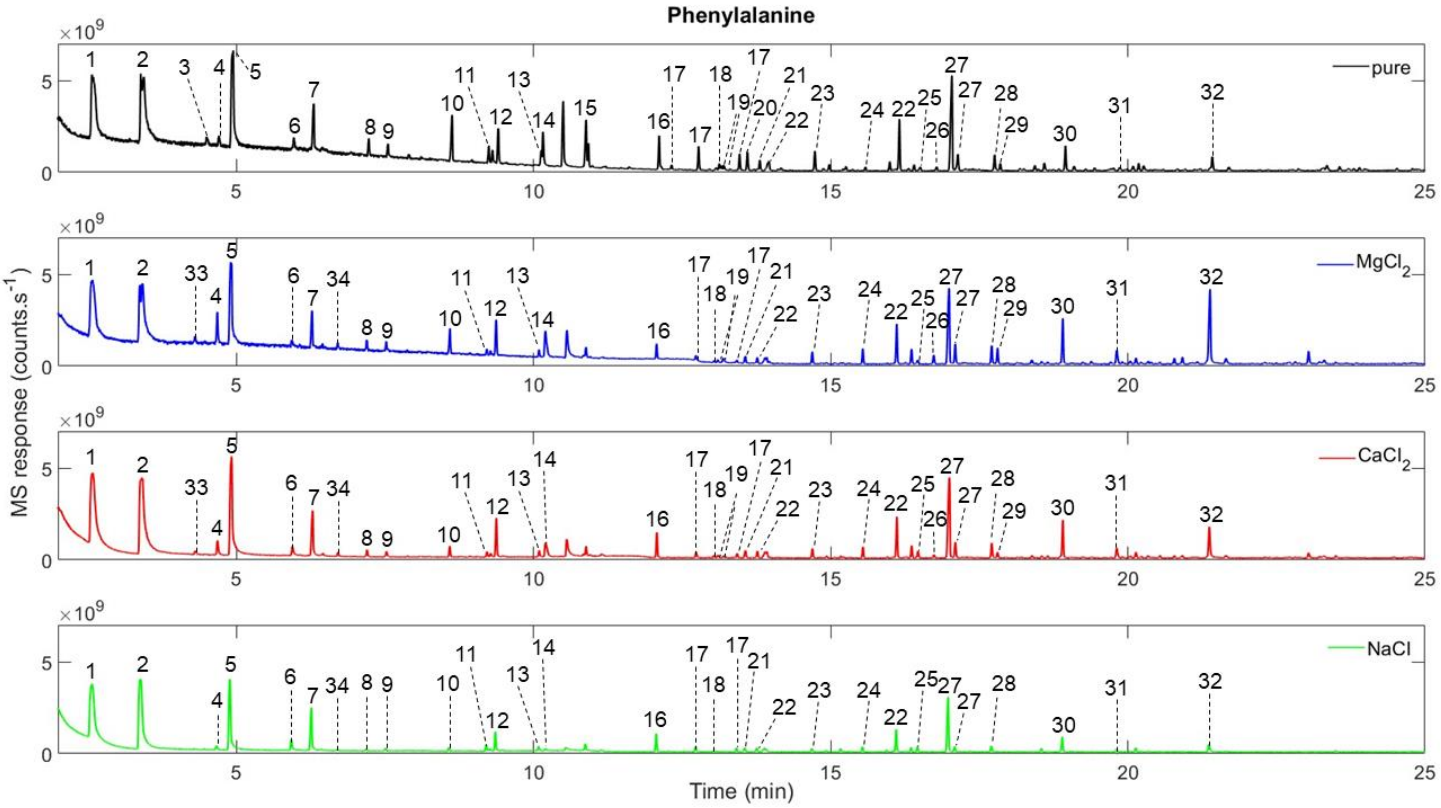

Figure 23: Chromatograms obtained after flash pyrolysis at 800 °C of 1:100 phenylalanine (black) in silica, in the presence of 3:100 $MgCl_2$ (blue), $CaCl_2$ (red), and NaCl (green). (*) artifact of the column (stationary phase bleeding), (1) benzene, (2) toluene, (3) ethylbenzene, (4) phenylethyne, (5) styrene, (6) benzaldehyde, (7) benzonitrile, (8) indene, (9) benzonitrile, methyl, (10) benzyl nitrile, (11) phenyl propenenitrile, (12) naphthalene, (13) quinoline, (14) isoquinoline, (15) indole, (16) biphenyl, (17) biphenylmethyl isomers, (18) acenaphthylene, (19) phenylpyridine isomers, (20) isopopenylnaphthalene, (21) naphthalenecarbonitrile, (22) stilbene isomers, (23) fluorene, (24) diphenylacetylene, (25) fluorenone, (26) methylphenanthrene, (27) phenanthrene isomers, (28) anthracene ethylnyl, (29) phenyl indene, (30) phenyl naphthalene, (31) fluoranthene, (32) diphenylpyridine, (33) chlorobenzene, (34) benzyl chloride.

During flash pyrolysis at 800 °C, phenylalanine degraded in a relatively high number of pyrolyzates including aromatic hydrocarbons, N-bearing compounds, and PAHs (Figure 23).

The presence of chloride salts mostly played a role on the intensity of the chromatographic peaks observed for the phenylalanine pyrolyzed alone but not on the nature of the species detected. However, two new compounds are formed in the presence of salt: chlorobenzene, identified in the chromatogram of $MgCl_2$ and $CaCl_2$ and benzyl chloride identified in the chromatogram of all three salts (Figure 23, blue, red and green chromatograms, compounds, 33 and 34).

2. Discussion

2.1. Influence of the temperature conditions and nature of chloride salts on the detection of organic compounds during pyrolysis

The EGA results showed that the three chloride salts targeted for this study (NaCl, $MgCl_2$, and $CaCl_2$) thermally degarded to produce two inorganic species, H_2O and HCl, which release temperatures where different for each salts, especially HCl. These differences play a role in their interactions with organic molecules. $MgCl_2$ and $CaCl_2$ released HCl in a broad range of temperatures, thus increasing the possibilities of reaction of HCl with the organic species. On the other hand, NaCl only released HCl above 600 °C, decreasing the time and temperature range at which it can interact with the organic molecules. Therefore, the chances of reactions between HCl and the organic compounds are higher for the divalent salts compared to NaCl. In the presence of NaCl, only a few or no chlorinated compounds were produced compared to $MgCl_2$ or $CaCl_2$. However, NaCl still influenced the pyrolysis of most of the organic compounds by reducing the number and/or abundance of their pyrolyzates, as seen with $MgCl_2$ and $CaCl_2$. Overall, GC-MS experiments revealed that in the presence of chloride salts, the number and abundance of organic compounds detected in the chromatograms was significantly reduced. These results suggest that chloride salts have influenced the degradation pathway of the molecules during pyrolysis. Below, we suggest three possible pathways that may have led to the reduction of the number of pyrolyzates when chloride salts were present.

(1) The formation of chlorinated molecules may have been favored in some cases

compared to the formation of other thermal degradation compounds. This hypothesis applies specifically to the aromatic compounds studied. Indeed, the pyrolysis of aromatic molecules (benzoic acid, naphthalene, methylanthracene, and phenylalanine) led to the formation of chlorinated organic. However, linear molecules including undecanoic acid and the amino acids glycine and glutamic acid did not produce chlorinated compounds in the presence of chloride salts. The aromatic ring grants a thermal and chemical stability to the molecules which facilitate the interaction of the HCl released from the salts to form chlorinated compounds. Aliphatic molecules, and more specifically the amino acids decompose at low temperatures which decrease their interaction time with HCl. The differences in the reactivity of the different organic molecules studied can also be explained by the fact that chlorine is being highly selective toward organic compounds, and its reactivity is commonly limited to particular sites. The reactivity of chlorine towards oxygenated functional groups is usually restricted, especially in the case of acid functions which exhibit high stability in the presence of chlorine (Deborde & Von Gunten, 2008). On the other hand, a higher reactivity via substitution or addition mechanisms is usually facilitated with aromatic systems (Deborde & Von Gunten, 2008). The presence of salts in Martian samples where chlorine-reactive organic molecular moieties are present could favor the formation of chlorinated compounds instead of other thermal degradation products, reducing the number of molecules detected in the chromatograms.

(2) The loss of detection of organic molecules in the chromatogram where salts are present may result from the formation of highly polar or refractory molecular compounds. According to this hypothesis, polar species would be retained in the column and would therefore not be detected in the chromatogram. On the other hand, the release of cations (Mg^{2+}/Ca^{2+}/Na^{+}) from the salts may have led to organically ion-bound compounds via ion-exchange reaction mechanisms forming refractory organic species such as organic salts. Organic salts are low volatile molecules due to their high molecular weights and strong intermolecular forces and therefore cannot be detected directly through pyrolysis-GC-MS (Benner et al., 2000; Lewis et al., 2021; Mcintosh et

al., 2022). The loss of detection of organic compounds due to the production of refractory organic material was also suggested in previous studies with Mg perchlorate and K chlorate (Millan et al., in prep). To confirm this hypothesis, measurements with atomic absorption spectroscopy or Inductively Coupled Plasma Mass Spectrometry (ICP-MS) could be performed to quantify the inorganic content in our samples but these were beyond the scope of this study.

(3) chloride salts may have played a role of catalysts during the pyrolysis of organic molecules, favoring the cracking of hydrocarbons chains of the targeted organic molecules into smaller fragments. However, this hypothesis seems less likely compared to the other ones because the sensitivity of the commercial instrument is relatively high and at least some of the fragments should have been detected. It is also possible that these compounds have been completely degraded into CO_2 only, in which case it would be difficult to distinguish it from the background CO_2 present in the instrument and from oxidation of the organics.

Overall, the chlorination processes combined with the formation of low volatile compounds or catalytic breakage could explain the decreased number and relative abundances of pyrolysis products observed in the chromatograms in the presence of chloride salts.

2.2. POTENTIAL SIGNATURES OF CHLORIDE SALTS

Previous studies have investigated the influence of oxychlorine phases, specifically perchlorates and chlorates on the pyrolysis of organic molecules in SAM-like and flash-pyrolysis conditions and their implications for Mars (Millan et al., in prep). Comparing the results obtained by Millan et al. (2020), chloride salts showed dissimilarities that may guide us to the nature of the chlorine family present regarding the organic molecules detected.

Contrary to what was reported for perchlorates, chlorination is not the primary process at play with chloride salts as indicated by the small number of chlorinated species

detected compared to previous studies (Millan et al., 2016). Moreover, *in situ* analysis of the Martian regolith with the SAM experiment identified several key chlorinated molecules (Freissinet et al,. 2015, Szopa et al., 2020). Laboratory experiments in SAM-like conditions with calcium perchlorate showed the major production of chlorinated compounds including chloromethane, dichloromethane, trichloromethane, and tetrachloromethane (Millan et al., 2020). From all these chlorine-bearing species, only chloromethane was detected near the detection limit of the instrument in the present study. The other compounds were not detected when the organic molecules were pyrolyzed in the presence of chloride salts. Moreover, chloride salts did not evolve O_2 and Cl_2 (Clark et al., 2020; Sutter et al., 2017), which provides a valuable distinction from oxychlorine phases such as perchlorates (Clark et al., 2020; Glavin et al., 2013; Millan et al., 2020). This difference could help differentiate between the two chlorine phases (oxychlorine vs. chloride salts) present in a Martian sample. The absence of O_2 release from chloride salts also leads to less oxidation of the initial organic molecules, allowing a detection from lower abundance in the sample.

Furthermore, among the chlorinated compounds detected in our laboratory pyrolysis experiments, some were characteristic of the parent organic compounds pyrolyzed and could help their identification if they were detected in the Martian soil. In SAM-like pyrolysis, chlorobiphenyl isomers were detected only in the chromatogram of benzoic acid with $MgCl_2$ and $CaCl_2$ (Figure 24). Chlorobiphenyl is also a product of interaction between benzoic acid and calcium perchlorate (Millan et al., 2020). This means that if found on Mars, it would not be possible to distinguish which chlorine phase is the precursor of the chlorobiphenyl detected from the GC-MS data alone, but it could indicate that benzoic acid was present in the sample. Methylanthracene produced a single chlorinated compound, chloromethylanthracene, with both divalent salts (Figure 24). Finally, the detection of benzyl chloride, chloroethylbenzene and phenylpropenoyl chloride in addition to chlorobenzene, could infer the presence of phenylalanine and $MgCl_2$ or $CaCl_2$.

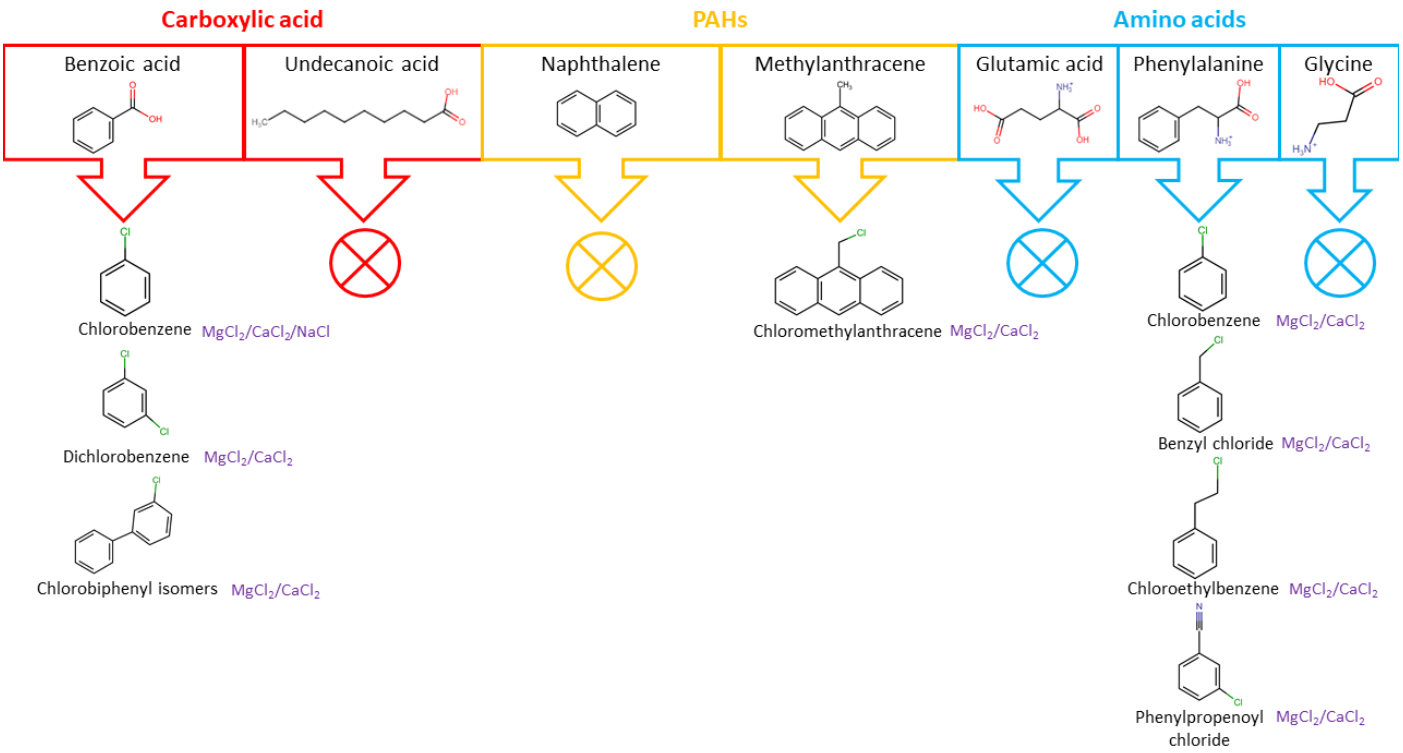

Figure 24: Summary of the chlorinated compounds detected in the chromatogram of each organic molecules of this study after SAM-like pyrolysis.

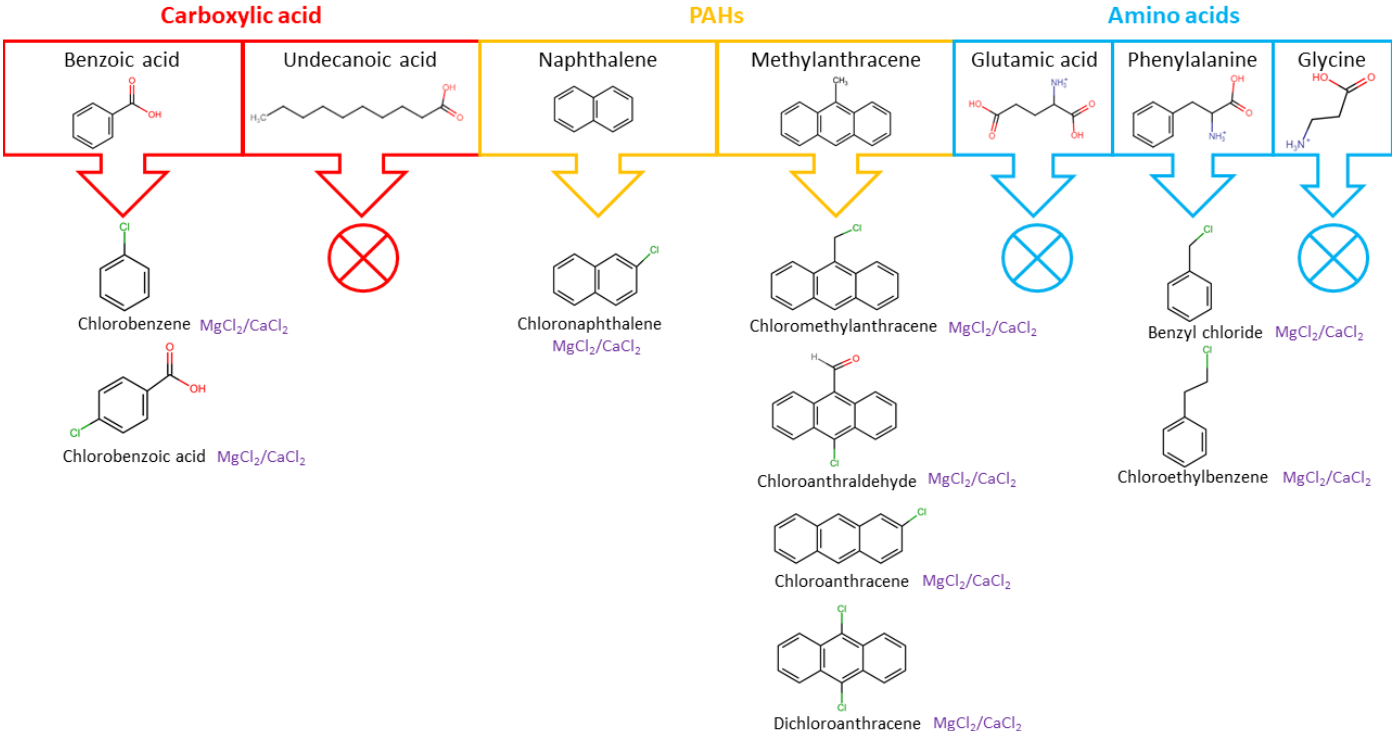

Figure 25: Summary of the chlorinated compounds detected in the chromatogram of each organic molecules of this study after flash 500 °C pyrolysis.

SAM-like pyrolysis did not form the same types of chloroorganics as flash pyrolysis but

the cross-interaction between the organic molecules and chloride salts produced similar organochloride species at both flash temperatures (500 and 800 °C), despite fewer chlorinated compounds detected at flash 800 °C than 500 °C. Perhaps, in Martian samples where the presence of chloride salts is expected, constraining the pyrolysis temperature below 800 °C could allow the formation of more chracateristic chlorinated compounds, therefore enhance the possibility to identify the organic precursors.

Indeed, chlorobenzene is found to be formed with all three salts when interacting with benzoic acid at flash 800 °C (Figure 26) and with the divalent salts at flash 500 °C (Figure 25) due to the higher thermal degradation of NaCl. However, chlorobenzene is also formed through the pyrolysis of phenylalanine in the presence of all three salts at 500 °C, which renders difficult the attribution of a precursor for chlorobenzene if identified on Mars. But, when benzoic acid and phenylalanine interacts with all three chloride salts at flash 800 °C, phenylalanine also produces benzyl chloride, which could help deconvolute the presence of each molecules in the sample. Similarly, at flash 500 °C, benzoic acid produces chlorobenzoic acid in addition to chlorobenzene.

Moreover, chloronaphthalene is detected during the naphthalene pyrolysis as the sole chlorinated compounds for all three salts at flash 800 °C (Figure 26) and with magnesium and calcium chloride at flash 500 °C (Figure 25) as the NaCl did not start to evolve HCl at this temperature. Methylanthracene produces four chlorinated compounds at flash 500 °C with $MgCl_2$ and $CaCl_2$: chloroanthracene, chloromethylanthracene, dichloroanthracene, and chloranthraldehyde (Figure 25). At flash 800 °C methylanthracene produces the same compounds than at 500 °C at the exception of chloromethylantracene (Figure 26).

Overall, these chlorinated organics could help constrain the organic compounds present in the Martian samples if they were present.

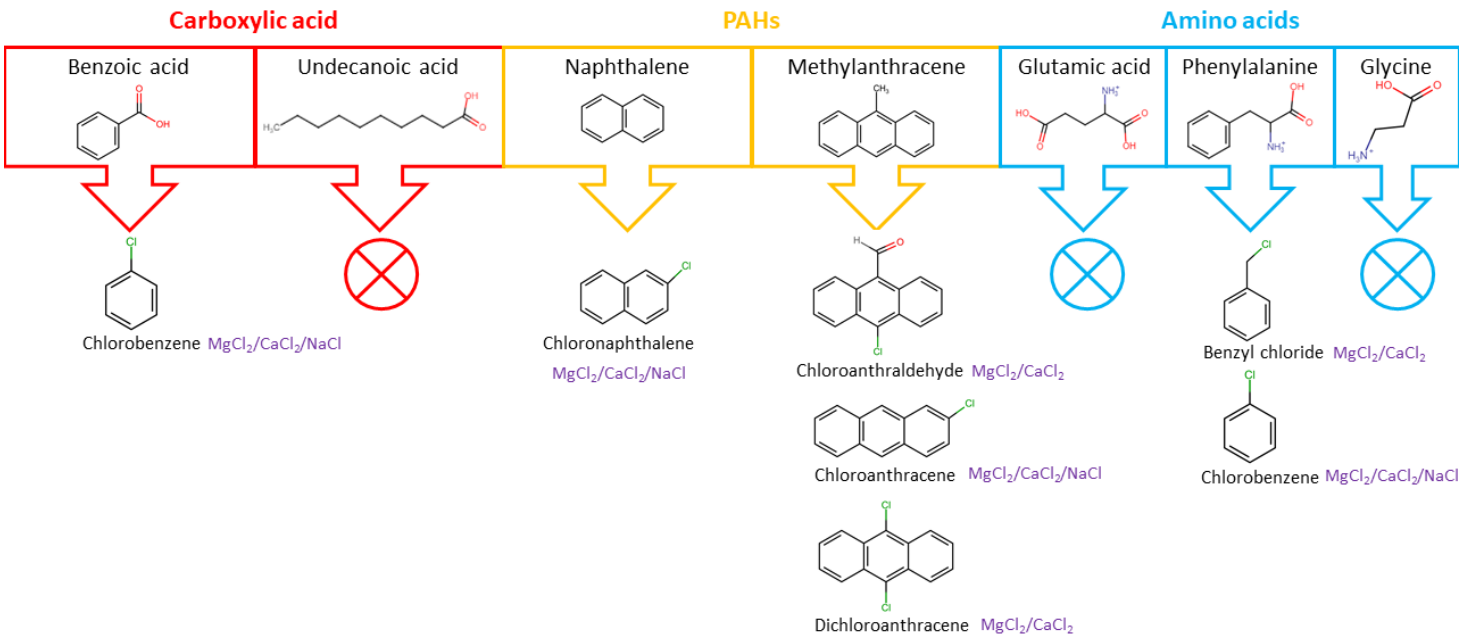

Figure 26: Summary of the chlorinated compounds detected in the chromatogram of each organic molecules of this study after flash 800 °C pyrolysis.

2.3. PRECURSOR OF THE MARTIAN CHLORINATED ORGANIC MOLECULES

Among the chlorinated compounds detected in our study, two were also detected on Mars by the SAM instrument: chlorobenzene and dichlorobenzene (Table 2). Chlorobenzene was detected in the Cumberland (CB) sample on Mars (Freissinet et al., 2020), and benzoic acid was described as its preferred precursor when interacting with magnesium perchlorate. In this study, we show that chlorobenzene can also be formed through the interaction of benzoic acid and phenylalanine with chloride salts. Indeed, chlorobenzene was detected in the chromatogram of benzoic acid with $MgCl_2$, $CaCl_2$, and NaCl, and phenylalanine with $MgCl_2$ and $CaCl_2$ in SAM-like conditions. Moreover, during flash pyrolysis at 500 °C, corresponding to the maximum temperature conditions used by the Viking landers, chlorobenzene was also detected through the interaction of benzoic acid and the divalent salts $MgCl_2$ and $CaCl_2$. Therefore, the chlorobenzene compounds identified by the Viking lander 2 at Utopia Planitia that has been attributed to the interaction of benzoic acid with oxychlorine could also be from the interaction of the acid with chloride salts. Finally, dichlorobenzene was also detected in the CB sample (Szopa et al., 2020) and attributed to chlorinated organic molecules from

the mudstone. Here we show that benzoic acid is also a possible precursor of dichlorobenzene in the presence of $MgCl_2$ or $CaCl_2$ instead of perchlorates.

Table 2: Table summarizing the nature of the chlorinated organics detected on Mars and in laboratory to help identify their potential precursors. B: benzoic acid, Phe: phenylalanine, Naph: naphthalene, and Meth: methylanthracene.

	Chlorinated organics	SAM	Viking	Laboratory
Martian	Chlorobenzene	X	X	B, Phe
	Dichlorobenzene	X		B
	Dichloroethane	X		
	Dichloropropane	X		
	Duchlorobutane	X		
	Trichloromethylpropoane	X		
Terrestrial	Chloromethane	X	X	
	Dichloromethane	X	X	
	Trichloromethane	X		
Detected only in laboratory experiments	Chlorobiphenyl isomers			B
	Chlorobenzoic acid			B
	Benzyl chloride			Phe
	Chloroethylbenzene			Phe
	Phenylpropenoyl chloride			Phe
	Chloronaphthalene			Naph
	Chloromethylanthracene			Meth
	Chloroanthraldehyde			Meth
	Chloroanthracene			Meth
	Dichloroanthracene			Meth

3. CONCLUSION AND PERSPECTIVES

This study showed that chloride salts have a significant impact on the organic molecules targeted during pyrolysis in SAM, MOMA and Viking-like conditions. The nature of the chloride salt and organic molecules present in the samples determines the interactions between the organic and inorganic compounds. The thermal evolution and molecular moieties played a crucial role in the interaction and reactivity of HCl with the organic species. The thermal evolution specific to each salt species as well as the nature of the chlorinated compound formed can be used as clues to identify the

chloride salts and organic molecules present in the Martian samples. Moreover, the differences of products between organic compounds pyrolyzed in the presence of perchlorate and chloride salts highlighted in this study can be used to distinguish the nature of the chlorine phases present in a sample. Furthermore, new potential precursors of chlorohydrocarbons on Mars such as detected by SAM and Viking have been identified from this study (*e.g.* phenylalanine) in addition to benzoic acid described in previous studies.

In addition to the distribution of byproducts and chlorinated products detected, the use of wet chemistry experiments can lead to a more strict identification of precursors. Therefore, wet chemistry and thermochemolysis experiment utilizing the derivatization capability of SAM and MOMA should be performed in order to evaluate if derivatization experiments could be affected by the presence of salts.

Our study only focused on the influence of chloride salts on the targeted organics, and did not consider the complete mineralogy of the samples collected on Mars. Future experiments should include mixtures of oxychlorine and chloride phases, minerals and other relevant lithologies, such as those found at the Mars 2020 and ExoMars landing sites.

REFERENCES

Basile, B. P., Middleditch, B. S., & Oró, J. (1984). Polycyclic aromatic hydrocarbons in the Murchison meteorite. Organic Geochemistry, 5(4), 211-216.

Benner, S. A., Devine, K. G., Matveeva, L. N., & Powell, D. H. (2000). The missing organic molecules on Mars. Proceedings of the National Academy of Sciences, 97(6), 2425-2430. https://doi.org/10.1073/pnas.040539497

Biemann, K., Oro, J., Toulmin, P., Orgel, L. E., Nier, A. O., Anderson, D. M., Simmonds, P. G., Flory, D., Diaz, A. V., Rushneck, D. R., Biller, J. E., & Lafleur, A. L. (1977). The search for organic substances and inorganic volatile compounds in the surface of Mars. Journal of Geophysical Research, 82(28), 4641-4658. https://doi.org/10.1029/js082i028p04641

Blackmond, D. G. (2010). The origin of biological homochirality. Cold Spring Harbor perspectives in biology, 2(5), a002147.

Botta, O., & Bada, J. L. (2002). Surveys in Geophysics, 23(5), 411-467. https://doi.org/10.1023/a:1020139302770

Burton, A. S., Stern, J. C., Elsila, J. E., Glavin, D. P., & Dworkin, J. P. (2012). Understanding prebiotic chemistry through the analysis of extraterrestrial amino acids and nucleobases in meteorites. Chemical Society Reviews, 41(16), 5459-5472.

Clark, B. (1981). The salts of Mars. Icarus, 45(2), 370-378. https://doi.org/10.1016/0019-1035(81)90041-5

Clark, J. V., Sutter, B., McAdam, A. C., Rampe, E. B., Archer, P. D., Ming, D. W., Navarro-Gonzalez, R., Mahaffy, P., & Lapen, T. J. (2020). High-Temperature HCl Evolutions From Mixtures of Perchlorates and Chlorides With Water-Bearing Phases: Implications for the SAM Instrument in Gale Crater, Mars. Journal of Geophysical Research: Planets, 125(2). https://doi.org/10.1029/2019je006173

Cohen, M. D., Flagan, R. C., & Seinfeld, J. H. (1987). Studies of concentrated electrolyte solutions using the electrodynamic balance. 1. Water activities for single-electrolyte solutions. Journal of Physical Chemistry, 91(17), 4563-4574.

Cronin, J., & Pizzarello, S. (1983). Amino acids in meteorites. Advances in space research, 3(9), 5-18.

Deamer, D. W., & Pashley, R. M. (1989). Amphiphilic components of the murchison carbonaceous chondrite: Surface properties and membrane formation. Origins of Life and Evolution of the Biosphere, 19(1), 21-38. https://doi.org/10.1007/bf01808285

Deborde, M., & Von Gunten, U. (2008). Reactions of chlorine with inorganic and organic compounds during water treatment—kinetics and mechanisms: a critical review. Water research, 42(1-2), 13-51.

Fornaro, T., Brucato, J. R., Pace, E., Guidi, M. C., Branciamore, S., & Pucci, A. (2013). Infrared spectral investigations of UV irradiated nucleobases adsorbed on mineral surfaces. Icarus, 226(1), 1068-1085.

Fraissler, G., Jöller, M., Brunner, T., & Obernberger, I. (2009). Influence of dry and humid gaseous atmosphere on the thermal decomposition of calcium chloride and its impact on the remove of heavy metals by chlorination. Chemical Engineering and Processing: Process Intensification, 48(1), 380-388. https://doi.org/10.1016/j.cep.2008.05.003

Freissinet, C., Glavin, D., Buch, A., Szopa, C., Teinturier, S., Archer, P., Williams, A., Williams, R., Millan, M., & Steele, A. (2019). Detection of long-chain hydrocarbons on mars with the Sample Analysis at Mars (SAM) instrument. Ninth International Conference on Mars,

Freissinet, C., Glavin, D. P., Mahaffy, P. R., Miller, K. E., Eigenbrode, J. L., Summons, R. E., Brunner, A. E., Buch, A., Szopa, C., Archer, P. D., Franz, H. B., Atreya, S. K., Brinckerhoff, W. B., Cabane, M., Coll, P., Conrad, P. G., Des Marais, D. J., Dworkin, J. P., Fairén, A. G., François, P., Grotzinger, J. P., Kashyap, S., Ten Kate, I. L., Leshin, L. A., Malespin, C. A., Martin, M. G., Martin-Torres, F. J., McAdam, A. C., Ming, D. W., Navarro-González, R., Pavlov, A. A., Prats, B. D., Squyres, S. W., Steele, A., Stern, J. C., Sumner, D. Y., Sutter, B., & Zorzano, M. P. (2015). Organic molecules in the Sheepbed Mudstone, Gale Crater, Mars. Journal of Geophysical Research: Planets, 120(3), 495-514. https://doi.org/10.1002/2014je004737

Freissinet, C., Knudson, C. A., Graham, H. V., Lewis, J. M., Lasue, J., McAdam, A. C., Teinturier, S., Szopa, C., Dehouck, E., & Morris, R. V. (2020). Benzoic acid as the preferred precursor for the chlorobenzene detected on Mars: insights from the unique Cumberland analog investigation. The Planetary Science Journal, 1(2), 41.

Glavin, D. P., Freissinet, C., Miller, K. E., Eigenbrode, J. L., Brunner, A. E., Buch, A., Sutter, B., Archer, P. D., Atreya, S. K., Brinckerhoff, W. B., Cabane, M., Coll, P., Conrad, P. G., Coscia, D., Dworkin, J. P., Franz, H. B., Grotzinger, J. P., Leshin, L. A., Martin, M. G., McKay, C., Ming, D. W., Navarro-González, R., Pavlov, A., Steele, A., Summons, R. E., Szopa, C., Teinturier, S., & Mahaffy, P. R. (2013). Evidence for perchlorates and the origin of chlorinated hydrocarbons detected by SAM at the Rocknest aeolian deposit in Gale Crater. Journal of Geophysical Research: Planets, 118(10), 1955-1973. https://doi.org/10.1002/jgre.20144

Glotch, T. D., Bandfield, J. L., Tornabene, L. L., Jensen, H. B., & Seelos, F. P. (2010). Distribution and formation of chlorides and phyllosilicates in Terra Sirenum, Mars. Geophysical Research Letters, 37(16), n/a-n/a. https://doi.org/10.1029/2010gl044557

Glotch, T. D., Bandfield, J. L., Wolff, M. J., Arnold, J. A., & Che, C. (2016). Constraints on the composition and particle size of chloride salt-bearing deposits on Mars. Journal of Geophysical Research: Planets, 121(3), 454-471. https://doi.org/10.1002/2015je004921

Goesmann, F., Brinckerhoff, W. B., Raulin, F., Goetz, W., Danell, R. M., Getty, S. A., Siljeström, S., Mißbach, H., Steininger, H., Arevalo, R. D., Buch, A., Freissinet, C., Grubisic, A., Meierhenrich, U. J., Pinnick, V. T., Stalport, F., Szopa, C., Vago, J. L., Lindner, R., Schulte, M. D., Brucato, J. R., Glavin, D. P., Grand, N., Li, X., Van Amerom, F. H. W., & The Moma Science, T. (2017). The Mars Organic Molecule Analyzer (MOMA) Instrument: Characterization of Organic Material in Martian Sediments. Astrobiology, 17(6-7), 655-685. https://doi.org/10.1089/ast.2016.1551

Greenspan, L. (1977). Humidity fixed points of binary saturated aqueous solutions. Journal of research of the National Bureau of Standards. Section A, Physics and chemistry, 81(1), 89.

Guzman, M., McKay, C. P., Quinn, R. C., Szopa, C., Davila, A. F., Navarro-González, R., & Freissinet, C. (2018). Identification of Chlorobenzene in the Viking Gas Chromatograph-Mass Spectrometer Data Sets: Reanalysis of Viking Mission Data Consistent With Aromatic Organic Compounds on Mars. Journal of Geophysical Research: Planets, 123(7), 1674-1683. https://doi.org/10.1029/2018je005544

Handbook, C. C. (2003). A Guide to Properties, Forms, Storage and Handling. Dow Chemical Company.

Hecht, M. H., Kounaves, S. P., Quinn, R., West, S. J., Young, S. M., Ming, D. W., Catling, D., Clark, B., Boynton, W., & Hoffman, J. (2009). Detection of perchlorate and the

soluble chemistry of martian soil at the Phoenix lander site. Science, 325(5936), 64-67.

Huang, Q., Lu, G., Wang, J., & Yu, J. (2011). Thermal decomposition mechanisms of MgCl2·6H2O and MgCl2·H2O. Journal of Analytical and Applied Pyrolysis, 91(1), 159-164. https://doi.org/10.1016/j.jaap.2011.02.005

Karunatillake, S., Keller, J. M., Squyres, S. W., Boynton, W. V., Brückner, J., Janes, D. M., Gasnault, O., & Newsom, H. E. (2007). Chemical compositions at Mars landing sites subject to Mars Odyssey Gamma Ray Spectrometer constraints. Journal of Geophysical Research: Planets, 112(E8). https://doi.org/10.1029/2006je002859

Kipouros, G. J., & Sadoway, D. R. (2001). A thermochemical analysis of the production of anhydrous MgCl2. Journal of Light Metals, 1(2), 111-117.

Lewis, J. M. T., Eigenbrode, J. L., Wong, G. M., McAdam, A. C., Archer, P. D., Sutter, B., Millan, M., Williams, R. H., Guzman, M., Das, A., Rampe, E. B., Achilles, C. N., Franz, H. B., Andrejkovičová, S., Knudson, C. A., & Mahaffy, P. R. (2021). Pyrolysis of Oxalate, Acetate, and Perchlorate Mixtures and the Implications for Organic Salts on Mars. Journal of Geophysical Research: Planets, 126(4). https://doi.org/10.1029/2020je006803

Litvak, M., Mitrofanov, I., Gellert, R., Djachkova, M., Lisov, D., Vasavada, A., & Czarnecki, S. (2023). Depth distribution of Chlorine at Gale crater, Mars, as derived from the DAN and APXS experiments onboard the Curiosity rover. Journal of Geophysical Research: Planets, e2022JE007694.

Mahaffy, P. R., Webster, C. R., Cabane, M., Conrad, P. G., Coll, P., Atreya, S. K., Arvey, R., Barciniak, M., Benna, M., Bleacher, L., Brinckerhoff, W. B., Eigenbrode, J. L., Carignan, D., Cascia, M., Chalmers, R. A., Dworkin, J. P., Errigo, T., Everson, P., Franz, H., Farley, R., Feng, S., Frazier, G., Freissinet, C., Glavin, D. P., Harpold, D. N., Hawk, D., Holmes, V., Johnson, C. S., Jones, A., Jordan, P., Kellogg, J., Lewis, J., Lyness, E., Malespin, C. A., Martin, D. K., Maurer, J., McAdam, A. C., McLennan, D., Nolan, T. J., Noriega, M., Pavlov, A. A., Prats, B., Raaen, E., Sheinman, O., Sheppard, D., Smith, J., Stern, J. C., Tan, F., Trainer, M., Ming, D. W., Morris, R. V., Jones, J., Gundersen, C., Steele, A., Wray, J., Botta, O., Leshin, L. A., Owen, T., Battel, S., Jakosky, B. M., Manning, H., Squyres, S., Navarro-González, R., McKay, C. P., Raulin, F., Sternberg, R., Buch, A., Sorensen, P., Kline-Schoder, R., Coscia, D., Szopa, C., Teinturier, S., Baffes, C., Feldman, J., Flesch, G., Forouhar, S., Garcia, R., Keymeulen, D., Woodward, S., Block, B. P., Arnett, K., Miller, R., Edmonson, C., Gorevan, S., & Mumm, E. (2012). The Sample Analysis at Mars Investigation and Instrument Suite. Space Science Reviews, 170(1-4), 401-478. https://doi.org/10.1007/s11214-012-9879-z

Mcintosh, O., Szopa, C., Freissinet, C., Buch, A., & Boulesteix, D. (2022). Analysis of aromatic organic salts with gas chromatography-mass spectrometry and implications for their detection at Mars surface with in situ experiments.

Millan, M., Szopa, C., Buch, A., Coll, P., Glavin, D. P., Freissinet, C., Navarro-Gonzalez, R., François, P., Coscia, D., Bonnet, J. Y., Teinturier, S., Cabane, M., & Mahaffy, P. R. (2016). In situ analysis of martian regolith with the SAM experiment during the

first mars year of the MSL mission: Identification of organic molecules by gas chromatography from laboratory measurements. Planetary and Space Science, 129, 88-102. https://doi.org/10.1016/j.pss.2016.06.007

Millan, M., Szopa, C., Buch, A., Summons, R. E., Navarro-Gonzalez, R., Mahaffy, P. R., & Johnson, S. S. (2020). Influence of Calcium Perchlorate on Organics Under SAM-Like Pyrolysis Conditions: Constraints on the Nature of Martian Organics. Journal of Geophysical Research: Planets, 125(7). https://doi.org/10.1029/2019je006359

Millan, M., Teinturier, S., Malespin, C., Bonnet, J., Buch, A., Dworkin, J., Eigenbrode, J., Freissinet, C., Glavin, D., & Navarro-González, R. (2022). Organic molecules revealed in Mars's Bagnold Dunes by Curiosity's derivatization experiment. Nature Astronomy, 6(1), 129-140.

Mishra, V. S., Mahajani, V. V., & Joshi, J. B. (1995). Wet air oxidation. Industrial & Engineering Chemistry Research, 34(1), 2-48.

Moldoveanu, S. (2009). Pyrolysis of organic molecules: applications to health and environmental issues. Elsevier.

Moldoveanu, S. (2010). Pyrolysis of carboxylic acids. Techniques and instrumentation in analytical chemistry, 28, 471-526.

Nagy, K., & Tiuca, I.-D. (2017). Importance of Fatty Acids in Physiopathology of Human Body. In. InTech. https://doi.org/10.5772/67407

Naraoka, H., Shimoyama, A., & Harada, K. (1999a). Origins of Life and Evolution of the Biosphere, 29(2), 187-201. https://doi.org/10.1023/a:1006547127028

Naraoka, H., Shimoyama, A., & Harada, K. (1999b). Molecular distribution of monocarboxylic acids in Asuka carbonaceous chondrites from Antarctica. Origins of Life and Evolution of the Biosphere, 29(2), 187-201.

Navarro-González, R., Vargas, E., De La Rosa, J., Raga, A. C., & McKay, C. P. (2010). Reanalysis of the Viking results suggests perchlorate and organics at midlatitudes on Mars. Journal of Geophysical Research, 115(E12). https://doi.org/10.1029/2010je003599

Oró, J., & Holzer, G. (1979). The effects of ultraviolet light on the degradation of organic compounds: a possible explanation for the abscence of organic matter on Mars. Life Sciences and Space Research, 77-86. https://doi.org/10.1016/b978-0-08-023416-8.50013-1

Oró, J., & Holzer, G. (1979). The photolytic degradation and oxidation of organic compounds under simulated Martian conditions. Journal of Molecular Evolution, 14(1-3), 153-160. https://doi.org/10.1007/bf01732374

Osterloo, M., Hamilton, V., Bandfield, J., Glotch, T., Baldridge, A., Christensen, P., Tornabene, L., & Anderson, F. (2008). Chloride-bearing materials in the southern highlands of Mars. Science, 319(5870), 1651-1654.

Pizzarello, S., Cooper, G., & Flynn, G. (2006). The nature and distribution of the organic material in carbonaceous chondrites and interplanetary dust particles. Meteorites and the early solar system II, 1, 625-651.

Rampe, E. B., Blake, D. F., Bristow, T. F., Ming, D. W., Vaniman, D. T., Morris, R. V., Achilles, C. N., Chipera, S. J., Morrison, S. M., Tu, V. M., Yen, A. S., Castle, N., Downs, G. W.,

Downs, R. T., Grotzinger, J. P., Hazen, R. M., Treiman, A. H., Peretyazhko, T. S., Des Marais, D. J., Walroth, R. C., Craig, P. I., Crisp, J. A., Lafuente, B., Morookian, J. M., Sarrazin, P. C., Thorpe, M. T., Bridges, J. C., Edgar, L. A., Fedo, C. M., Freissinet, C., Gellert, R., Mahaffy, P. R., Newsom, H. E., Johnson, J. R., Kah, L. C., Siebach, K. L., Schieber, J., Sun, V. Z., Vasavada, A. R., Wellington, D., & Wiens, R. C. (2020). Mineralogy and geochemistry of sedimentary rocks and eolian sediments in Gale crater, Mars: A review after six Earth years of exploration with Curiosity. Geochemistry, 80(2), 125605. https://doi.org/10.1016/j.chemer.2020.125605

Rushneck, D. R., Diaz, A. V., Howarth, D. W., Rampacek, J., Olson, K. W., Dencker, W. D., Smith, P., McDavid, L., Tomassian, A., Harris, M., Bulota, K., Biemann, K., Lafleur, A. L., Biller, J. E., & Owen, T. (1978). Viking gas chromatograph-mass spectrometer. Rev Sci Instrum, 49(6), 817. https://doi.org/10.1063/1.1135623

Schlten, H.-R., & Leinweber, P. (1993). Pyrolysis-field ionization mass spectrometry of agricultural soils and humic substances: Effect of cropping systems and influence of the mineral matrix. Plant and Soil, 151, 77-90.

Schoors, S., Bruning, U., Missiaen, R., Queiroz, K. C., Borgers, G., Elia, I., Zecchin, A., Cantelmo, A. R., Christen, S., & Goveia, J. (2015). Fatty acid carbon is essential for dNTP synthesis in endothelial cells. Nature, 520(7546), 192-197.

Sephton, M. A. (2002). Organic compounds in carbonaceous meteorites. Natural product reports, 19(3), 292-311.

Skelley, A. M., Scherer, J. R., Aubrey, A. D., Grover, W. H., Ivester, R. H. C., Ehrenfreund, P., Grunthaner, F. J., Bada, J. L., & Mathies, R. A. (2005). Development and evaluation of a microdevice for amino acid biomarker detection and analysis on Mars. Proceedings of the National Academy of Sciences, 102(4), 1041-1046. https://doi.org/10.1073/pnas.0406798102

Sutter, B., McAdam, A. C., Mahaffy, P. R., Ming, D. W., Edgett, K. S., Rampe, E. B., Eigenbrode, J. L., Franz, H. B., Freissinet, C., Grotzinger, J. P., Steele, A., House, C. H., Archer, P. D., Malespin, C. A., Navarro-González, R., Stern, J. C., Bell, J. F., Calef, F. J., Gellert, R., Glavin, D. P., Thompson, L. M., & Yen, A. S. (2017). Evolved gas analyses of sedimentary rocks and eolian sediment in Gale Crater, Mars: Results of the Curiosity rover's sample analysis at Mars instrument from Yellowknife Bay to the Namib Dune. Journal of Geophysical Research: Planets, 122(12), 2574-2609. https://doi.org/10.1002/2016je005225

Szopa, C., Freissinet, C., Glavin, D. P., Millan, M., Buch, A., Franz, H. B., Summons, R. E., Sumner, D. Y., Sutter, B., Eigenbrode, J. L., Williams, R. H., Navarro-González, R., Guzman, M., Malespin, C., Teinturier, S., Mahaffy, P. R., & Cabane, M. (2020). First Detections of Dichlorobenzene Isomers and Trichloromethylpropane from Organic Matter Indigenous to Mars Mudstone in Gale Crater, Mars: Results from the Sample Analysis at Mars Instrument Onboard the Curiosity Rover. Astrobiology, 20(2), 292-306. https://doi.org/10.1089/ast.2018.1908

Thomas, N. H., Ehlmann, B. L., Meslin, P. Y., Rapin, W., Anderson, D. E., Rivera-Hernández, F., Forni, O., Schröder, S., Cousin, A., Mangold, N., Gellert, R., Gasnault, O., & Wiens, R. C. (2019). Mars Science Laboratory Observations of Chloride Salts in

Gale Crater, Mars. Geophysical Research Letters, 46(19), 10754-10763. https://doi.org/10.1029/2019gl082764

Williams, A., Eigenbrode, J., Millan, M., Williams, R., Buch, A., Teinturier, S., Glavin, D., Freissinet, C., Szopa, C., & McIntosh, O. (2021). Organic molecules detected with the first TMAH wet chemistry experiment, Gale crater, Mars. 52nd Lunar and Planetary Science Conference,

Zolotov, M., & Shock, E. (1999). Abiotic synthesis of polycyclic aromatic hydrocarbons on Mars. Journal of Geophysical Research: Planets, 104(E6), 14033-14049. https://doi.org/10.1029/1998je000627

CHAPTER 5: ANALYSIS OF AROMATIC ORGANIC SALTS WITH GAS CHROMATOGRAPHY-MASS SPECTROMETRY: IMPLICATIONS AND COMPARISON WITH *IN SITU* MEASUREMENTS AT MARS' SURFACE

ABSTRACT

Aromatic organic salts such as benzoates or phthalates may be widespread degradation products of organic molecules at the surface of Mars. The low volatility of these organic salts could have compromised their detection through thermal extraction *in situ* analyses such as those performed by the Viking landers. However, over the years, analytical chemistry laboratories on board Martian surface missions, such as the Sample Analysis at Mars (SAM) instrument suite on board the Curiosity rover and the Mars Organic Molecule Analyser (MOMA) instrument of the Rosalind Franklin ExoMars rover have evolved. These instruments have improved in efficiency to detect refractory and polar organic compounds, which could influence the detection of organic salts. To evaluate the capability of detecting aromatic organic salts on Mars with *in situ* instruments, we performed laboratory experiments under Viking, SAM, and MOMA-like Gas Chromatography-Mass Spectrometry (GC-MS) conditions with two carboxylic acid/salt couples: phthalic acid/calcium phthalate and benzoic acid/calcium benzoate. We studied the behavior and signatures of both molecular forms when using pyrolysis and derivatization experiments and the implications of these results in the search for organic molecules on Mars. This study showed that the Viking experiments could not have detected the presence of organic salts in Martian samples because its maximum pyrolysis temperature was too low (500 °C). However, we showed that aromatic organic salts, despite their refractory nature, could be identified indirectly through the detection of thermal and derivatized degradation products, both with SAM and

MOMA. No conclusive proof of the presence of aromatic organic salt species have been found in the SAM *in situ* data, but given the right instrumental set-up they could be detected if present. The conclusions of this work raise essential questions on the detectability of refractory molecules, the analytical efficiency of flight instruments, and the interpretation of *in situ* data.

1. INTRODUCTION

The detection and identification of organic molecules on Mars are of primary importance to establish the existence of a possible ancient prebiotic chemistry or even past or present biological activity and is, therefore, a central goal for Mars exploration missions. A small diversity of organic molecules has been identified such as hydrocarbons, chloroorganics and sulfur-bearing compounds. (Eigenbrode et al., 2018; Freissinet et al., 2015; M Millan et al., 2022; Szopa et al., 2020) despite the harsh environmental conditions present at the surface. Several factors can be involved in this low detection: (a) high doses of ionizing electromagnetic and particle radiation penetrating the thin Martian atmosphere, leading to the destruction or transformation of surface organic compounds, (b) presence of strong oxidants on the soil, (c) technical biases of current flight-instruments such as high temperature pyrolysis or thermochemolysis which could lead to the thermal degradation of organic molecules and (d) insufficient instrument sensitivity. The harsh oxidative and radiative conditions of the Martian environment influence the fate of organic molecules present on its surface. Organic compounds, either endogenous to Mars or from exogenous sources such as meteorites, likely undergo oxidative processes due to the oxidants present in the Martian soil (*e.g.,* oxychlorines such as perchlorates, or hydrogen peroxide (H_2O_2)) (Glavin et al., 2013; Lasne et al., 2016). On Mars, these oxidation processes are also likely accelerated by the presence of iron mineral catalysts (Hassler et al., 2013). Moreover, the surface of Mars is exposed to ultraviolet radiation with wavelengths above 190 nm, which is efficiently absorbed by organic molecules producing photochemical reactions in very short timescales and it is sufficiently energetic to cleave water condensed on

mineral surfaces producing free radicals and molecules (H^+, OH^+, H_2O_2) that can oxidize organic molecules (Fornaro, Steele, et al., 2018). The formation of these radical species may transform organic macromolecules into carboxylic acids through Fenton chemistry (Benner et al., 2000; Oró, 1979) or *via* the irradiation of semiconductor surfaces (possibly clay minerals) (Fox et al., 2019). In this study, we focused on two aromatic carboxylic acids: phthalic acid and benzoic acid. These molecules are thought to be abundant on the Martian surface as they are in stable intermediate oxidation states and can be formed from the oxidation of Polycyclic Aromatic Hydrocarbons (PAHs) or alkylbenzene compounds (Benner et al., 2000; Oró & Holzer, 1979). Moreover, benzoic acid has been detected with the Sample Analysis at Mars (SAM) instrumental suite on board the Curiosity rover (M Millan et al., 2022; Williams et al., 2021), and is considered to be a potential precursor for the chlorinated aromatic organic molecules detected on Mars (Freissinet et al., 2020). Because benzene carboxylates are metastable, they would not be entirely oxidized into volatile molecules such as CO_2 or O_2, but instead, ionized by solar radiation to form organic salts (Benner et al., 2000; Kminek & Bada, 2006; Lasne et al., 2016; Pavlov et al., 2022). Benner et al. (2000) suggested that the low volatility of these salts could have compromised their *in situ* detection through thermal extraction analyses as performed by the Viking landers (Hakkinen et al., 2014). These assumptions are still relevant today as SAM and the Mars Organic Molecule Analyzer (MOMA) instrument of the Rosalind Franklin ExoMars rover, also perform pyrolysis experiments to analyze the molecular composition of the Martian surface. However, whereas the Viking experiments were set to perform flash pyrolysis to a maximum temperature of 500 °C, SAM and MOMA can reach temperatures above 800 °C, therefore widening the window of detectability for low volatility compounds or their thermal decomposition products. Moreover, SAM and MOMA have the capability to perform derivatization experiments which increases the volatility of refractory materials without thermal degradation of the parent molecule. A recent laboratory study by Lewis et al. (2021) examined the CO_2 and CO evolutions produced by the thermal decomposition of small aliphatic organic salts, which were then compared to data from SAM Evolved Gas

Analysis (EGA) experiments. Numerous fits between laboratory and SAM data were observed, indicating that organic salts are compelling candidates for many SAM CO_2 and CO peaks but EGA data alone cannot conclusively identify organic salts.

To complement the Lewis *et al.* (2021) study and to investigate aromatic organic salts molecules through their direct or indirect detection on Mars, we performed laboratory tests using SAM and MOMA-like Gas Chromatography-Mass Spectrometry (GC-MS) analyses of two acid/salt couples: phthalic acid/calcium phthalate and benzoic acid/calcium benzoate.

The widespread availability of calcium on Mars makes it an element of high interest to form organic salt complexes. The calculated representative *in situ* mass fraction of calcium at different landing sites was evaluated between ~4.0 and 4.6 % (Karunatillake et al., 2007). Geochemical analysis, from the ChemCam instrument onboard the Curiosity rover at Gale Crater, reported enhanced calcium associated to sulfur detection interpreted as Ca-sulfates (Nachon et al., 2017) disseminated in the bedrock at 30-50 wt% (Rapin et al., 2019). In Oxia Planum, the planned landing site of the Rosalind Franklin rover, calcium pyroxene signatures were detected from orbit with the Compact Reconnaissance Imaging Spectrometer for Mars (CRISM) aboard the Mars Reconnaissance Orbiter (MRO) (Seelos et al., 2014). Additionally, a Ca/K ratio > 5 wt.% was detected by the Viking X-ray fluorescence spectrometer (Toulmin III et al., 1976) as well as the elemental analysis of the Viking landing sites reporting a significant concentration of several elements like calcium in the Martian regolith (Clark et al., 1976). Finally, the possible presence of calcium chloride brines was also reported by Brass (1980) and Ca-perchlorates were detected at Gale Crater with SAM (Glavin et al., 2013; Ming et al., 2014).

We analyzed two aromatic organic compounds and their salts (phthalic acid/calcium phthalate and benzoic acid/calcium benzoate) using pyrolysis, thermochemistry and wet chemistry experiments, mimicking Viking, SAM and MOMA. If organic salts can be confirmed to be present on Mars, it would help better understand the transformation

of organic matter under the harsh conditions of the Martian surface. Moreover, organic salts can originate from metabolic processes that can be preserved in the geological record (Jehlička & Edwards, 2008), making them primary targets for *in situ* molecular analyses.

2. MATERIALS AND METHODS

2.1 STUDIED ANALYTES

This study was focused on two aromatic carboxylic acid species: phthalic acid and benzoic acid. The corresponding organic salts were selected to be linked with calcium as the carboxylic acids could have reacted with the calcium present at the Martian surface.

Moreover, both calcium phthalate and calcium benzoate were available commercially and allowed consistency with the cation involved in the reaction pathway for both carboxylic acids.

All products were commercially sourced. The benzoic acid C_6H_5COOH (≥ 99.5 %) and 1,2-benzenedioic acid (phthalic acid) (C_6H_4-1,2-$(CO_2H)_2$) (≥ 99.5 %) were purchased from Merck. The calcium benzoate trihydrate ($C_{14}H_{10}CaO_4$. $3H_2O$) was purchased from Unites States Pharmacopeia (USP) and calcium phthalate hydrate ($C_8H_4CaO_4.H_2O$) (98%) from Combi-Blocks.

2.2 SAMPLE PREPARATION

Organic molecules and salts would most likely be present as trace components (~ 100 ppbw) in Martian soil composed of amorphous and crystalline inorganic phases (Rampe et al., 2020). In order to simulate such conditions in our experiments, the carboxylic acid and organic salts standards were dispersed in a chemically inert matrix of fused synthetic silica quartz (Schlten & Leinweber, 1993)(~44 µm grain size powder, supplied by Sigma-Aldrich). The fused silica was conditioned at 1000 °C for 24 h in an

oven to remove any potential organic contamination. Each of the organic compounds studied were diluted in the silica in their solid form at 1:100 mixing ratios for the acid and 2.3:100 and 1.2:100 for calcium benzoate and calcium phthalate, respectively, in order to obtain the same molar abundance with the acids and their respective salts. The solid samples were ground to a powder and mixed in an organically-clean porcelain mortar and pestle which had been baked at 500 °C for two hours prior to sample preparation. To ensure a better homogenization of the powders, the samples were further mixed in a CryoMill Ball Mill (Retsch) (25 Hz for 10 minutes).

2.3 Instrumentation

The pyrolysis instrumental procedures were performed using a Frontier Laboratories 3030D multi-shot pyrolyzer (FrontierLab) mounted on the split/spitless injector of a gas chromatograph Trace Ultra coupled to an ISQ^{TM} quadrupole mass spectrometer (both from ThermoScientific). The pyrolysis oven was in the carrier gas (Helium, purity > 99,999 %, Air Liquide) flow pathway (1.0 mL·min^{-1}), allowing all the gaseous species produced in the chamber to be instantaneously transferred to the injector. For the derivatization experiments, the derivatization reaction was performed offline and the subsequent injection was made directly through the gas chromatograph injector with a microvolume liquid syringe.

2.4 Evolved Gas Analysis (EGA)

Prior to EGA analyses, the samples were deposited in a Frontier Lab stainless steel Eco-Cups pre-cleaned with ethanol (purity > 95 %, Merck) and heated red with a burner (about 1400 °C). 5 mg of the organic/silica mixture were then deposited in the cup and weighed with a microscale (Mettler Toledo) that was precise to 0.001 mg. The sample cup was then lowered into the pyrolysis oven.

The EGA experiments were conducted using an inert Ultra ALLOY-DTM metallic tube (2.5 m long; 0.15 mm internal diameter - Frontier Lab), connected on one end to the GC injector and on the other end to the MS with a deactivated fused silica transfer line (0.4 m long; 0.25 mm internal diameter). The short length of the tube minmized the

duration of transfer of the gases from the injector to the mass spectrometer (~10 s), with a constant helium flow of 1 mL·min^{-1}. The tube was maintained at an isothermal temperature of 250 °C throughout the run to limit any condensation. The GC injector was set in a split mode with a 1:20 split ratio. The ion source and transfer line temperatures of the MS were both set at 300 °C, and ions produced by electron impacts (energy of 70 eV) were scanned between masse to charge ratios (*m/z*) of 10 to 400.

Among the Mars instruments relevant to this study, only SAM can perform EGA. For this reason, the samples were heated from 80 °C to 800 °C with a temperature ramp of 35 °C·min^{-1} to mimic SAM EGA temperature conditions. The time scale given by the chromatographic analysis was converted into temperature scale for EGA by simply using the heating rate of the pyrolysis and the known time of transfer between the pyrolyzer and the MS.

Blank runs were performed between each sample analysis in order to ensure the absence of contamination from the previous experiment. When contamination was detected, the pyrolyzer-GC-MS chain was cleaned by heating the whole sample pathway at the maximum temperature. Each analysis was repeated twice to ensure repeatability.

2.5 Pyrolysis-GC-MS

The sample preparation procedure was identical to the one described above for the EGA experiments.

Three sets pyrolysis conditions were tested: Viking-like, MOMA-like, and SAM-like.

To simulate SAM experiments, the samples were slowly heated in the pyrolyzer furnace from 80 °C to 800 °C with a 35 °C·min^{-1} ramp. The volatiles evolved from the sample throughout the entire duration of the ramp, *i.e.*, in about 22 min. To mimic the Injection Trap (IT) present ahead of three out of six SAM GC columns and utilized to preconcentrate the analytes and to increase the separation power of the chromatograph (Mahaffy et al., 2012), the gases were condensed at the GC column inlet during the whole pyrolysis phase using a cryogenic trap. The cryotrap used a liquid

nitrogen cooling system (T~ -180 °C) supplied by FrontierLab, which was directly coupled to the pyrolyzer control system. Once the pyrolysis was completed, the cryotrap was stopped. The condensates were quickly vaporized to flow through the chromatographic column for their separation with the GC and detection with the MS.

For the MOMA-like experiments, the fast temperature ramp (200 °C·min^{-1}) (Goesmann et al., 2017) which will be performed by the flight instrument present a non-linear heating profile, difficult to accurately simulate with our laboratory setup. Therefore, we performed experiments using flash pyrolysis where the samples were directly heated to the maximal temperature (800 °C) attainable by the MOMA instrument for a few minutes. In the flash heating mode, the chromatographic analysis started as soon as the sample was introduced into the pyrolizer; the gases were produced and transferred to the GC instantaneously.

Finally, the Viking-like experiments consisted in flash heating the samples (within seconds) to 500 °C, held for thirty seconds at this temperature.

For the chromatographic analyses, we used a Zebron 5MS Plus column with a 5% Phenyl-Arylene, 95% Dimethylpolysiloxane stationary phase (30 m long; 0.25 mm internal diameter, 0.25 µm stationary phase thickness) (Phenomenex®) equipped with a 5-meter long integrated guard line to protect the analytical column from contamination and fast degradation. The injector temperature was set to 250 °C in split mode with a 1:20 ratio. The column temperature program started at an initial temperature of 40 °C followed by a 10 °C·min^{-1} ramp up to a final temperature of 300 °C held for 10 minutes. The MS settings were identical to the ones described for the EGA experiments and two replicas of each samples were done.

2.6 Derivatization-GC-MS

2.6.1 Wet chemistry experiments

In this study, wet chemistry derivatization experiments were performed using N-Methyl-N-(tert-butyldimethylsilyl)trifluoroacetamide (MTBSTFA) (98 %, Merck) (used

on SAM (Mahaffy et al., 2012)) and MOMA (Goesmann et al., 2017)) and N,N-Dimethylformamide dimethyl acetal (DMF-DMA) (99.0 %, Merck) (to be used on MOMA for chiral separation (Goesmann et al., 2017)). 5 mg of the organic/silica mixture were placed in a conic 2 mL glass vial. 35 µL of derivatization reagent were added to the mixture in the vial in order to obtain a supernatant that we could draw from with a syringe for further GC-MS injection. The solution used for DMF-DMA derivatization was heated to 145 °C for 3 minutes, suitable for *in situ* analysis in space (Freissinet et al., 2010). The MTBSTFA derivatization reagent was mixed with N,N-Dimethylformamide (DMF) (Merck) in a 4:1 solution (Mahaffy et al., 2012), as employed in the SAM instrumental suite onboard the Curiosity rover. The organic/silica/MTBSTFA/DMF mixture was then heated to 75 °C for 15 minutes. After heating, the supernatant was collected in an Eppendorf tube, and 1 µL of Naphthalene d_8 (99,99% Merck) diluted in DMF (99.0 %, Merck) at 5.10^{-3} M was added and used as an internal standard for all the derivatization experiments to compare their respective performances. The solution was centrifuged for 30 seconds to prevent silica particles from getting stuck in the syringe during the injection. 1 µL of the supernatant was then injected in the instrument. On the SAM and MOMA flight models, the derivatization reagent is contained in dedicated cups or capsules where the sample is dropped. The capsules containing the sample and the reagent are then heated and the volatile products are analyzed through GC-MS (Goesmann et al., 2017; Mahaffy et al., 2012).

2.6.2 Thermochemistry

Thermochemistry experiments were performed using Tetramethylammonium hydroxide (TMAH) diluted at 25% into methanol (Merck) (used on both the SAM and MOMA instruments). 2.5 mg of acid or salts (5.00 mg total) were deposited in the pyrolysis cup. 4 µL of TMAH solution with 1 µL of internal standard (Naphthalene d_8) were then added to the solid mixture. The cup containing the sample was introduced in the pyrolysis oven and heated at 600 °C for 30 seconds under helium flow.

GC-MS analyses for wet chemistry and thermochemolysis experiments were performed

under the same conditions as those used for pyrolysis-GC-MS analyses described above.

2.7 SAM-FLIGHT EXPERIMENTS SIMULATED IN THE LABORATORY

Analyses on SAM spare columns were conducted in the laboratory to evaluate the detectability of the products obtained from the pyrolysis and derivatization experiments of benzoate and phthalate salts if present on the Martian surface. The SAM spare columns kept at the Laboratoire Atmosphères,Observations Spatiales (LATMOS) in France are part of the same set that were integrated into the SAM flight model and allowed to simulate the SAM-like conditions in the laboratory. Among the six columns present on the SAM instrument suite (Mahaffy et al., 2012), two were used in this study: the MXT-5 spare column referred to as GC2 (30 m long; 0.25 mm internal diameter, 0.25 µm stationary phase thickness) (Restek) and the SAM MXT-CLP spare column referred to as GC5 (30 m long; 0.25 mm internal diameter, 0.25 µm stationary phase thickness) (Restek). GC2 was used to reproduce SAM's first *in situ* TMAH thermochemolysis experiment at the Mary Anning (MA) drill site in the Glen Torridon region (Williams et al., 2021). The detection of several compounds of interest in the sample motivated these analyses. GC5 was chosen to evaluate the detectability of the products obtained during the analysis of organic salts with this SAM spare column. Several *in situ* GC5 analyses have been performed by SAM and performance evaluations of the column in the laboratory showed a good separation efficiency of the tested species regardless of their mass (Millan et al., 2019).

A 60 cm fused silica tubing (0.75 µm/ 190 µm) (SGE) was added to the column end going to the injector. This extension acts as a flow restrictor to allow the regulation of the pressure and mimic the low pressure of the SAM instrument (Millan et al., 2019). A 20 cm silica transfer tube (0.25 mm internal diameter; 0.25 µm stationary phase thickness) was used in the MS transfer line to prevent electrical arcs forming from the presence of a metallic column near the mass spectrometer ion source.

In the flight chromatogram of the Mary Anning (MA) sample obtained with the GC2 column, two species of interest, diphenylmethane and benzoic acid methyl ester, were detected. In order to confirm their identification and assess the possibility to detect other compounds of interest on this column, the temperature parameters as performed *in situ* during the SAM MA experiments were retrieved from the SAM flight data set. Because this flight analysis was performed as a dual column experiment where the samples were analyzed with the SAM MXT-20 column (referred to as GC1) prior to GC2, we took into consideration the opening and closing of the hydrocarbon trap valves that could have allowed chemical species to go through GC2 even before the start of the analysis. Therefore, the GC-MS analyses started with a column temperature of 45 °C for 7 minutes corresponding to the opening of the hydrocarbon trap valves, followed by a first ramp of 120 °C·min^{-1} to reach 66 °C. Then a second slow rate ramp of 0.3 °C·min^{-1} to 59 °C and finally a third ramp of 10 °C.min^{-1} to reach a final temperature of 232 °C. The analysis was extended at the final temperature for 30 minutes to ensure the detection of that all the targeted compounds. The pressure was adjusted to match the retention time value of a known molecule, bi-silylated water (BSW), a byproduct of MTBSTFA, identified in the SAM GC2 MA chromatogram.

For GC5, the column temperature program used was identical to the nominal GC5 SAM-flight instrument with an initial temperature of 35 °C for 6.3 min, then 10 °C·min^{-1} rate up to a final temperature of 185 °C. The maximum time of analyses for GC5 is 21 minutes (Millan et al., 2019) but we extended the run for 40 minutes at the final temperature to be able to detect all the compounds of interest. The pressure was adjusted on the commercial GC based on the dead time observed on GC5 (Millan et al., 2019).

For all analyses the GC injector was set in a split mode with a 1:20 split ratio. The ion source and transfer line temperatures of the MS were both set at 300 °C, and ions produced by electron impacts (energy of 70 eV) were scanned between masse to charge ratios (*m/z*) of 10 to 585. 1 µL of a solution with the species targeted was then injected in the GC with a syringe.

3. RESULTS

3.1 EGA

3.1.1 Thermal behavior of benzoic acid compared to calcium benzoate

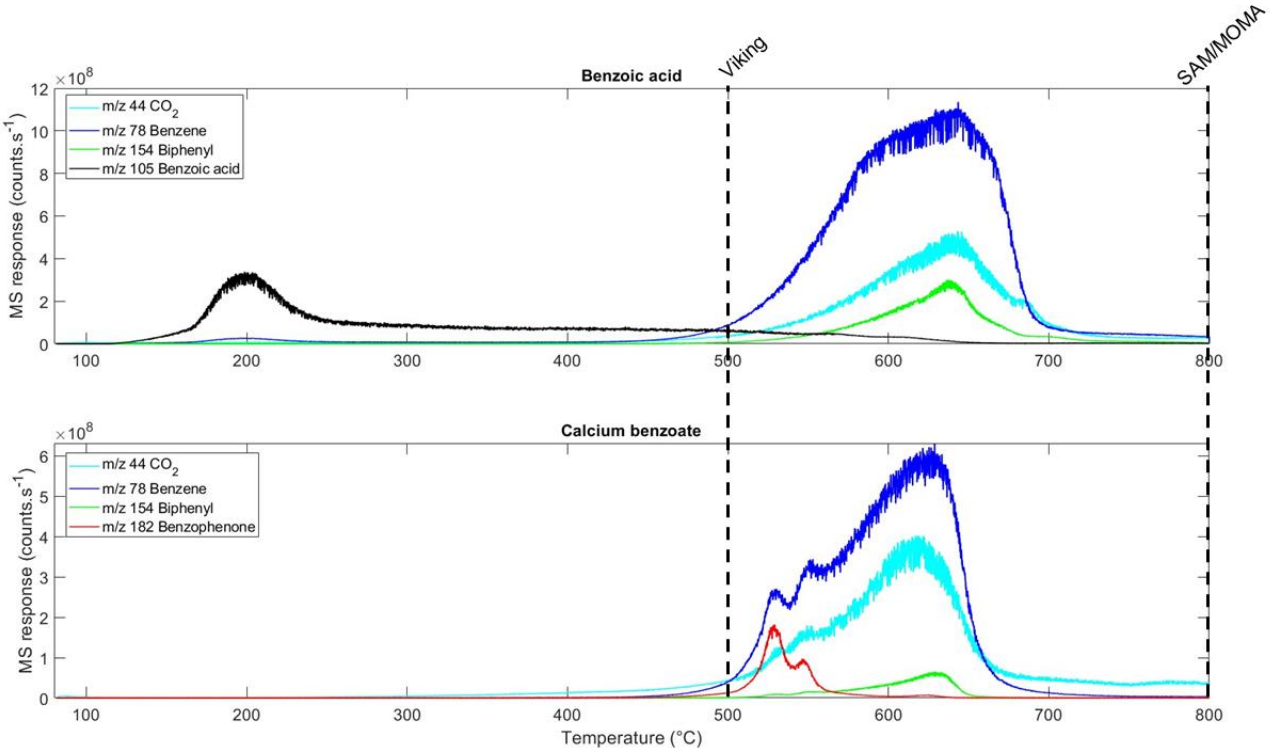

Figure 6 : Evolved gas profile of m/z 44 (CO_2), m/z 78 (Benzene), m/z 154 (Biphenyl), m/z 105 (Benzoic acid), and m/z 182 (Benzophenone) versus temperature obtained in SAM-like EGA conditions (35 °C·min^{-1} ramp) of a 100:1 fused silica-benzoic acid mixture (top), and a 100:2.3 fused silica-calcium benzoate mixture (bottom). The Viking, SAM and MOMA pyrolysis temperature limits are indicated with dashed lines.

Figure 6 represents the evolution of the main ions detected during the EGA of benzoic acid and its associated salt, calcium benzoate. We observed that benzoic acid released gases within two distinct temperature ranges: the first release occurred around 110 °C and reaches a maximum around 200 °C with a tail reaching up to 620 °C. The corresponding organic compound is benzoic acid itself identified from its mass spectrum and characterized by its parent molecular ion (*m/z* 105). The second gas release starts at higher temperatures and ranges from 470 °C to 800 °C, with a

maximum at ~630°C. The signal is more intense than the first peak, indicating that only a small amount of benzoic acid was released at lower temperatures. Three main ions contribute to the second release: *m/z* 44, *m/z* 78 and *m/z* 154 corresponding to CO_2, benzene and biphenyl, respectively, which were identified *via* their mass spectra. CO_2 and benzene are products of the decarboxylation of benzoic acid, and biphenyl results from the interaction of benzene rings. The temperature ranges at which each compound evolve can be found in Table 1.

Table 2: Summary of the ranges and maximum temperatures of released benzoic acid (B), calcium benzoate (CaB), phthalic acid (Ph) and calcium phthalate (CaPh) (observed through their main ion) in EGA. N/A: Not Applicable

m/z	Corresponding molecule	Outagassing temperature range (°C)				Maximum Temperature (°C)			
		B	CaB	Ph	CaPh	B	CaB	Ph	CaPh
44	CO_2	470-800	470-800	300-800	300-800	630	520 and 680	470	690
78	Benzene	470-800	470-800	N/A	470-630	630	630	N/A	550
154	Biphenyl	500-720	500-650	N/A	N/A	630	630	N/A	N/A
105	Benzoic acid	110-620	N/A	N/A	N/A	200	N/A	N/A	N/A
148	Phthalic acid	N/A	N/A	180-280	N/A	N/A	N/A	230	N/A
182	Benzophenone	N/A	470-590	N/A	470-600	N/A	530 and 550	N/A	560

For calcium benzoate, no low-temperature benzoic acid release was observed, indicating that no hydrogenation of the benzoate anion occurred during the heating of the sample. However, as for benzoic acid, we observe that gases are released from the sample mainly within the temperature range 470 °C to 800 °C. Most of the chemical species contributing to this signal are the same as those identified for benzoic acid, *i.e.* CO_2, benzene and biphenyl. However, the EGA of calcium benzoate reveals the presence of an additional species detected in the range 470 °C and 590 °C, with a characteristic ion *m/z* 182 corresponding to benzophenone. This result is in agreement with a study published by Dabestani et al. (2005). The presence of two maxima in the corresponding peak can be explained by the presence of two benzoic acid molecules complexed with Ca^{2+} which ensures electronegativity. The first molecule is transformed into benzophenone followed by the second molecule at slightly higher temperature.

3.1.2 Thermal behavior of phthalic acid compared to calcium phthalate

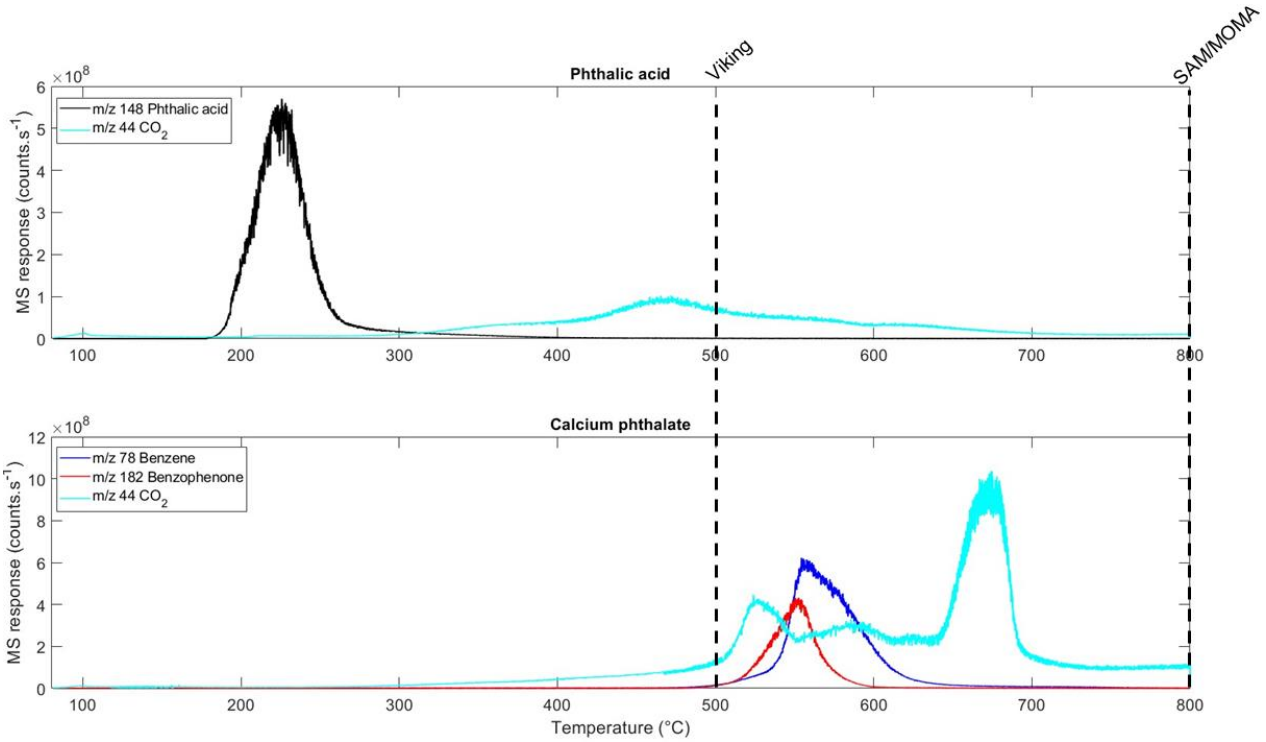

Figure 7: Evolved gas profile for m/z 44 (CO_2), m/z 78 (Benzene), m/z 148 (Phthalic acid), and m/z 182 (Benzophenone) versus temperature obtained in SAM-like EGA conditions (35 °C.min^{-1} ramp) of a 100:1 fused silica-phthalic acid mixture (top), and a 100:1.2 fused silica-calcium phthalate mixture (bottom). The Viking, SAM and MOMA pyrolysis temperature limits are indicated with dashed lines.

Figure 7 represents the evolution of the main ions of phthalic acid and its corresponding salt, calcium phthalate in EGA. We observed that phthalic acid produced a single major peak corresponding to the molecular ion at *m/z* 148 in the relatively low temperature range 180 °C to 280 °C, with a maximum around 230 °C (table 1). No other major species were detected. Release of CO_2 (*m/z* 44) from 300 to 800 °C with a maximum around 470 °C was also observed with a lower intensity (~6 times lower than the phthalic acid peak's maxima). This CO_2 release could come from the decarboxylation of the acid leading to the formation of species such as benzoic acid or benzene. The masses of these two molecules were found in the EGA of phthalic acid, but at level of abundance close to the limit of detection (10^6).

The calcium phthalate did not produce phthalic acid. However, we observed species evolving at high temperatures. Three main ion contributors were identified. As observed in the EGA of calcium benzoate, we identified a peak evolving from 470 °C to 600 °C with a maximum at 560 °C corresponding to benzophenone (*m/z* 182). Benzophenone co-evolved with the release of benzene (*m/z* 78) between 470 °C to 630 °C with a maximum at 560 °C. A major CO_2 release is observed between 300 °C and 800 °C with two maxima: the first peak around 520 °C and a higher intensity peak around 680°C. The release of benzene and CO_2 are related to the decarboxylation of the salt.

The evolution of CO_2 (*m/z* 44) is different for the phthalic acid and calcium phthalate. In the EGA of phthalic acid, the CO_2 peak is widely spread throughout the thermal range at low intensities, whereas, for calcium phthalate, CO_2 has a higher degassing intensity and higher temperatures. The absence of organic compounds during the CO_2 evolution in the EGA of phthalic acid and around 670 °C for calcium phthalate could either mean that the organic molecules formed are below the detection level of our instruments or that there is a complete degradation of the compound resulting only in carbon dioxide in that temperature range.

3.2 Pyrolysis GC-MS

1.1.1 Pyrolysis in slow heating mode (35 °C·min-1) (SAM-like)

3.2.1.1 Benzoic acid versus calcium benzoate

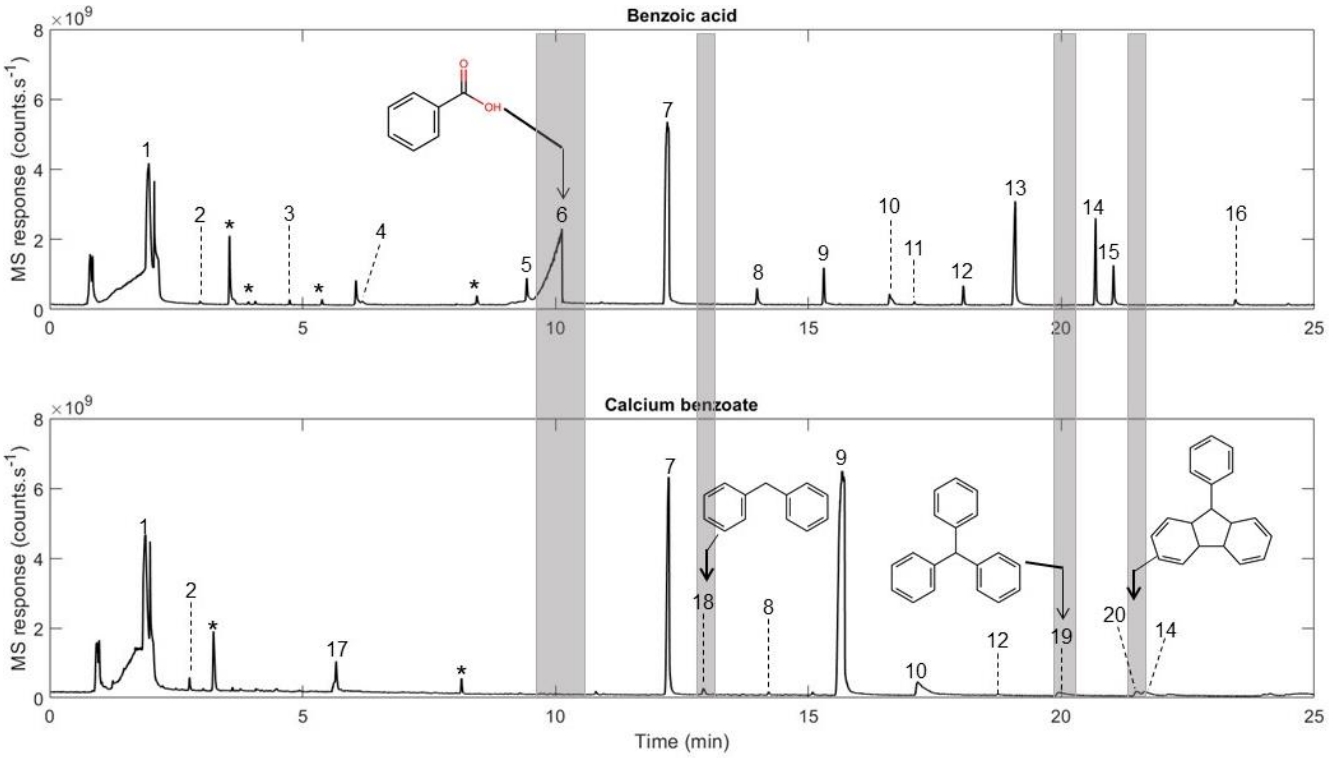

Figure 8: Chromatograms obtained from the pyrolysis (35 °C·min^{-1} ramp, up to 800 °C) of benzoic acid (top) and calcium benzoate (bottom) at 1 wt % in fused silica, in SAM-like pyrolytic conditions (35 °C·min^{-1}). The grey shading corresponds to molecules unique to pyrolysis of the acid or unique to that of the salt. (*)artifact of the column (stationary phase bleeding), (1) benzene, (2) toluene, (3) styrene, (4) phenol, (5) naphthalene, (6) benzoic acid, (7) biphenyl, (8) dibenzofuran, (9) benzophenone, (10) fluorenone, (11) Fluorene, methylene-, (12), (14), and (15) terphenyl isomers, (13) anthracenedione, (16) benzanthracene, (17) trimethylbenzene, (18) diphenylmethane, (19) triphenylmethane, (20) 9H-Fluorene, phenyl-.

Figure 8 shows that pyrolysis of benzoic acid under SAM-like conditions produced a variety of aromatic compounds. The major organic molecules observed in EGA, *i.e.* benzene, benzoic acid and biphenyl, are also detected in GC-MS as the most abundant compounds. The peak shape for the benzoic acid is typical of column overloading

resulting from a poor solubility of the molecule in the stationary phase and/or a quantitative saturation.

Fewer compounds were produced from the pyrolysis of calcium benzoate compared to benzoic acid. This is likely an indication of a higher thermal stability of the salt compared to benzoic acid (from the EGA data). We retrieved the major species detected in EGA, i.e. benzene, biphenyl and benzophenone. As expected, the parent molecule, benzoic acid, identified among the most abundant compounds in the chromatogram of the acid, was not detected in the pyrolysis of calcium benzoate. Instead, calcium benzoate evolved another major compound, benzophenone, as predicted by the EGA results, which was found in much lower concentration in the chromatogram of the acid (area of the benzophenone peak/area of the biphenyl peak = 2.1 for the salt compared to 0.8 for the acid). The salt also produced additional molecules that were not detected in the chromatogram of benzoic acid such as diphenylmethane, triphenylmethane and phenyl fluorene.

3.2.1.2 Phthalic acid versus calcium phthalate

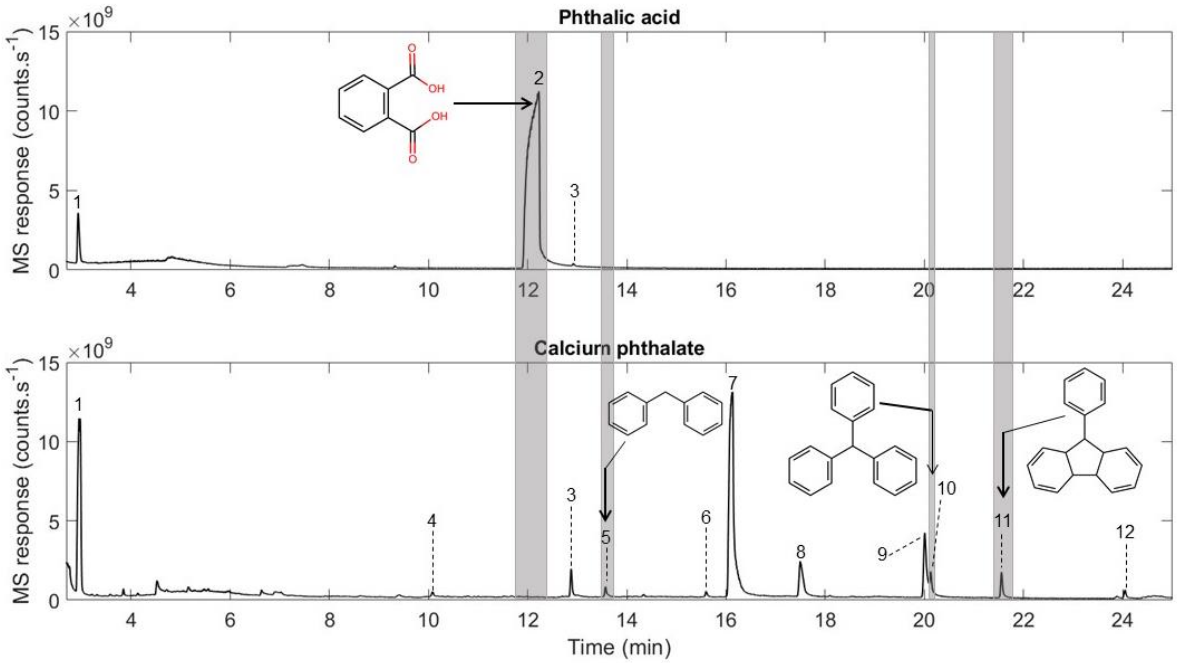

Figure 9 : Chromatograms obtained from the pyrolysis (35 °C·min^{-1} ramp, up to 800 °C) of phthalic acid (top) and calcium phthalate (bottom) at 1 wt % in fused silica in SAM-like pyrolytic conditions. The grey shading corresponds to molecules characteristic of the pyrolysis of the acid or the salt. (1) benzene, (2) phthalic acid, (3) biphenyl, (4) naphthalene, (5) diphenylmethane, (6) fluorene, (7) benzophenone, (8) fluorenone, (9) anthracenedione, (10) triphenylmethane, (11) fluorene, phenyl-, (12) anthracene, phenyl-.

Figure 9 showed that phthalic acid did not evolve many byproducts in ramp pyrolysis conditions and the major product detected was phthalic acid itself. This is consistent with the EGA results (figure 2). On the other hand, phthalic acid was not detected when calcium phthalate was pyrolyzed in SAM-like heating conditions, as expected from the EGA results. However, several byproducts were generated during the ramp pyrolysis of calcium phthalate with benzene and benzophenone as the two major products as well as other compounds such as fluorenone, anthracenedione or phenylflurorenone. The EGA results suggest that calcium phthalate is stable under low temperature conditions, and that the byproducts detected in GC-MS were formed through cleavage when high

temperature (> 500 °C) was reached. As in the pyrolysis of calcium benzoate, diphenylmethane, triphenylmethane and phenyl fluorene were identified as characteristic products of the degradation of calcium phthalate.

3.2.2 Pyrolysis in flash 500°C heating mode (Viking-like)

3.2.2.1 Benzoic acid versus calcium benzoate

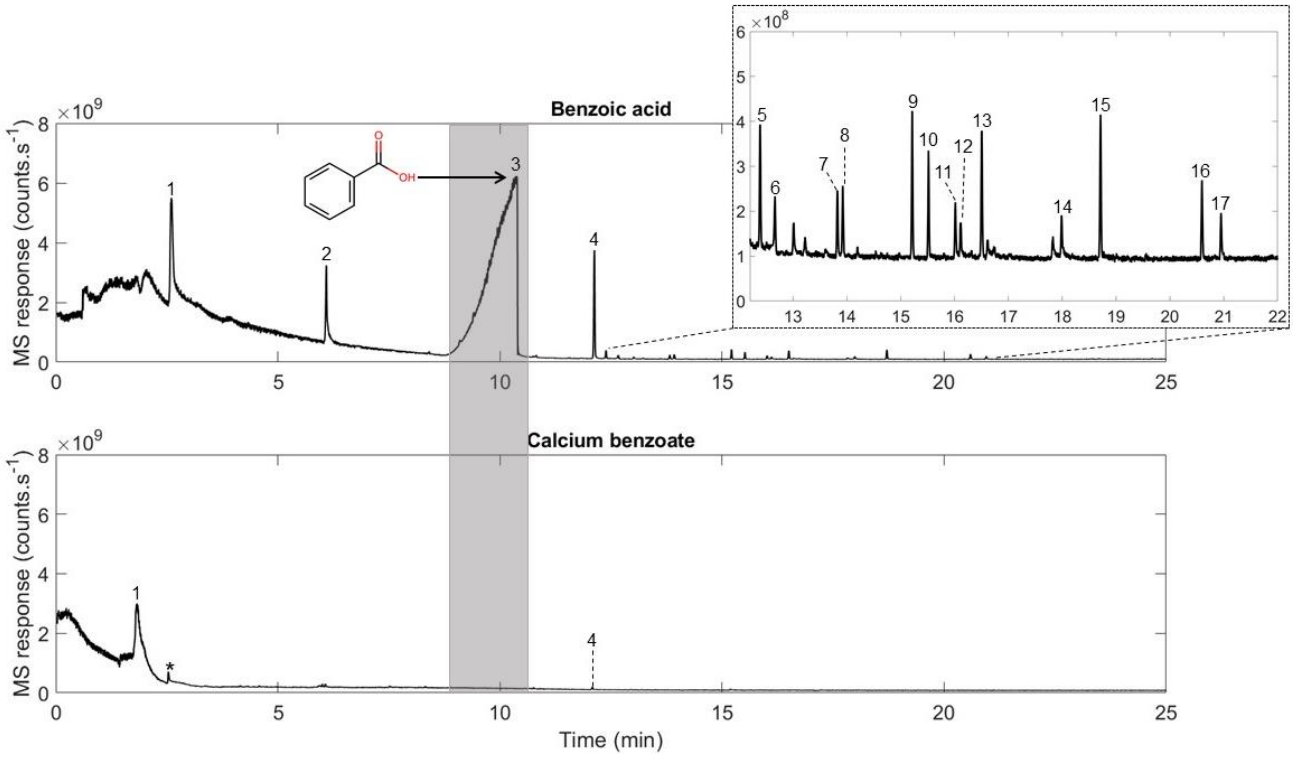

Figure 10: Chromatograms obtained from the flash pyrolysis (500 °C) of benzoic acid (top) and calcium benzoate (bottom) at 1 wt % in fused silica. The grey shading corresponds to the molecules characteristic of the pyrolysis of the acid or the salt. (*) artifact of the column (stationary phase bleeding), (1) benzene, (2) phenol, (3) benzoic acid, (4), biphenyl, (5) diphenyl ether, (6) phenylpropenal, (7), (11), and (12) hydroxybiphenyl (isomers), (8) dibenzofuran, (9) benzophenone, (10) benzoic acid, phenyl ester, (13) 9H-Fluoren-9-one, (14), (16), and (17) terphenyl (isomers), (15) 4-Hydroxy-9-fluoreneone.

Figure 10 shows the stark difference between the compounds detected with benzoic acid and calcium benzoate during flash pyrolysis at 500 °C. In the chromatogram of the

acid, the parent molecule, benzoic acid, is detected as a major compound as predicted by the EGA results. Other molecules were detected in high abundance such as benzene, biphenyl and phenol.

Benzoic acid was not detected when calcium benzoate is flash pyrolyzed to 500 °C. Overall, calcium benzoate did not evolve many gaseous products in flash 500 °C conditions. The major compound observed is benzene in agreement with EGA, showing that this is the major compound among those observed to be released above 470 °C. The absence of byproducts is related to the evolution temperature of calcium benzoate species, which as shown by the EGA, evolved at temperatures above 500 °C.

3.2.2.2 Phthalic acid versus calcium phthalate

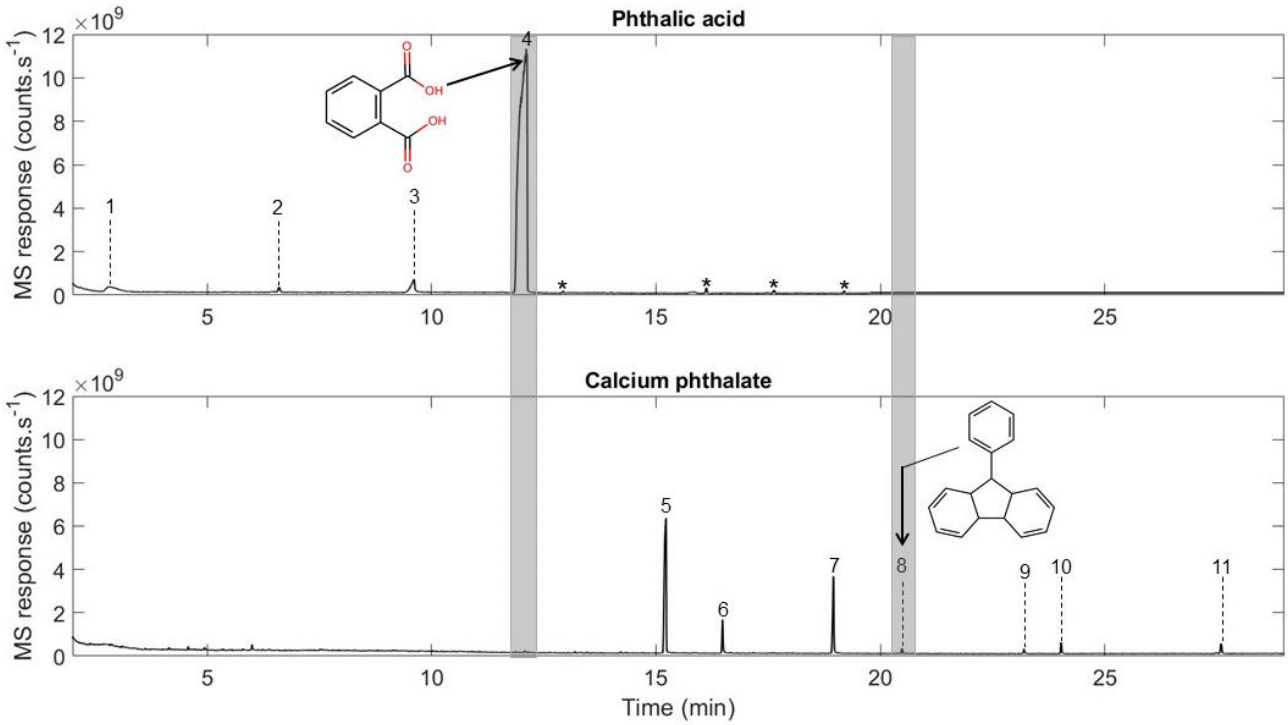

(top) and calcium phthalate (bottom) at 1 wt % in fused silica. The grey shading corresponds to molecules characteristic of the pyrolysis of the acid or the salt. (*) artifact of the column (stationary phase bleeding), (1) benzene, (2) phenol, (3) benzoic acid, (4) phthalic acid, (5) benzophenone, (6) fluorenone, (7) anthracenedione, (8) fluorene, phenyl, (9) and (10) unidentified compound, (11) anthracene, diphenyl-.

Phthalic acid, was not detected when calcium phthalate was pyrolyzed in fast heating

mode to 500 °C whereas it was the major compound observed during the pyrolysis of the acid as expected from EGA results. The flash pyrolysis of calcium phthalate to 500 °C generated benzophenone as the major product followed by fluorenone and anthracenedione. The Total Ion Current (TIC) chromatogram of calcium phthalate represented in Figure 18 did not allow the detection of benzene. However, its presence was confirmed through selected-ion monitoring (SIM) mode by selecting the base peak (*m/z* 78). Moreover, diphenylmethane and triphenylmethane were not observed in the chromatogram of the salt, though we detected phenyl fluorene as a pyrolysis byproduct of aromatic carboxylic salts pyrolysis as mentioned above.

3.2.3 Pyrolysis in flash 800 °C heating mode (MOMA-like)

3.2.3.1 Benzoic acid versus calcium benzoate

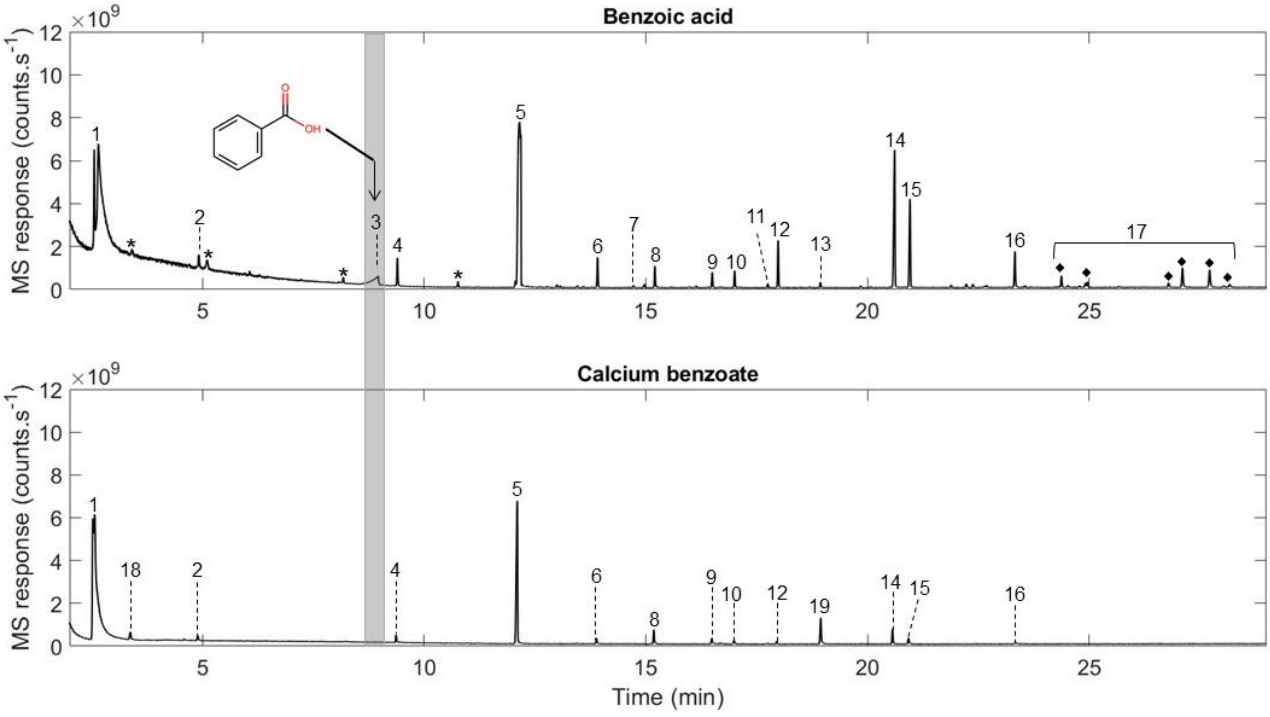

Figure 12: Chromatograms obtained from the flash pyrolysis (at 800 °C) of benzoic acid and calcium benzoate diluted at 1 wt % in fused silica. The grey shading corresponds to the molecule characteristic of the pyrolysis of the acid or the salt. (*) artifact of the column (stationary phase bleeding), (1) benzene, (2) styrene, (3) benzoic acid, (4) naphthalene, (5) biphenyl, (6) dibenzofuran, (7) fluorene, (8) benzophenone, (9) fluorenone, (10) anthracene, (11) 1H-Indene, 1-(phenylmethylene)-, (12), (14), and (15) terphenyl isomers, (13) phenylnaphthalene, (16) benzanthracene, (17) quaterphenyl isomers (peaks indicated by the black diamonds), (18) toluene, (19) anthracenedione.

Figure 12 shows that benzoic acid was more degraded at high flash pyrolysis temperature (800 °C), and therefore was a not the major compound detected contrary to what was observed in the two previous pyrolysis conditions for the acid. Moreover, the major compounds in the chromatograms of benzoic acid flash-pyrolyzed to 800 °C were biphenyl and benzene as seen in EGA. For calcium benzoate the parent molecule was not detected in the chromatogram of calcium benzoate but produced benzene

and biphenyl as major compounds as described in the EGA experiments. The low intensity of the benzophenone peak in the chromatogram can be explained by side-reactions happening at high temperature during flash pyrolysis. Moreover, similar byproducts are formed between the acid and the salts but with intensity differences. Benzoic acid produced a much higher yield of terphenyl isomers, as well as more intense peaks of naphthalene, dibenzofuran, fluorenone, anthracene or Benzanthracene. Moreover, we identified the formation of several quaterphenyl isomers during the pyrolysis of the benzoic acid which were absent with the calcium benzoate. Calcium benzoate did not produce the characteristic byproducts diphenylmethane, triphenylmethane and phenyl fluorene at flash 800 °C.

3.2.3.2 Phthalic acid versus calcium phthalate

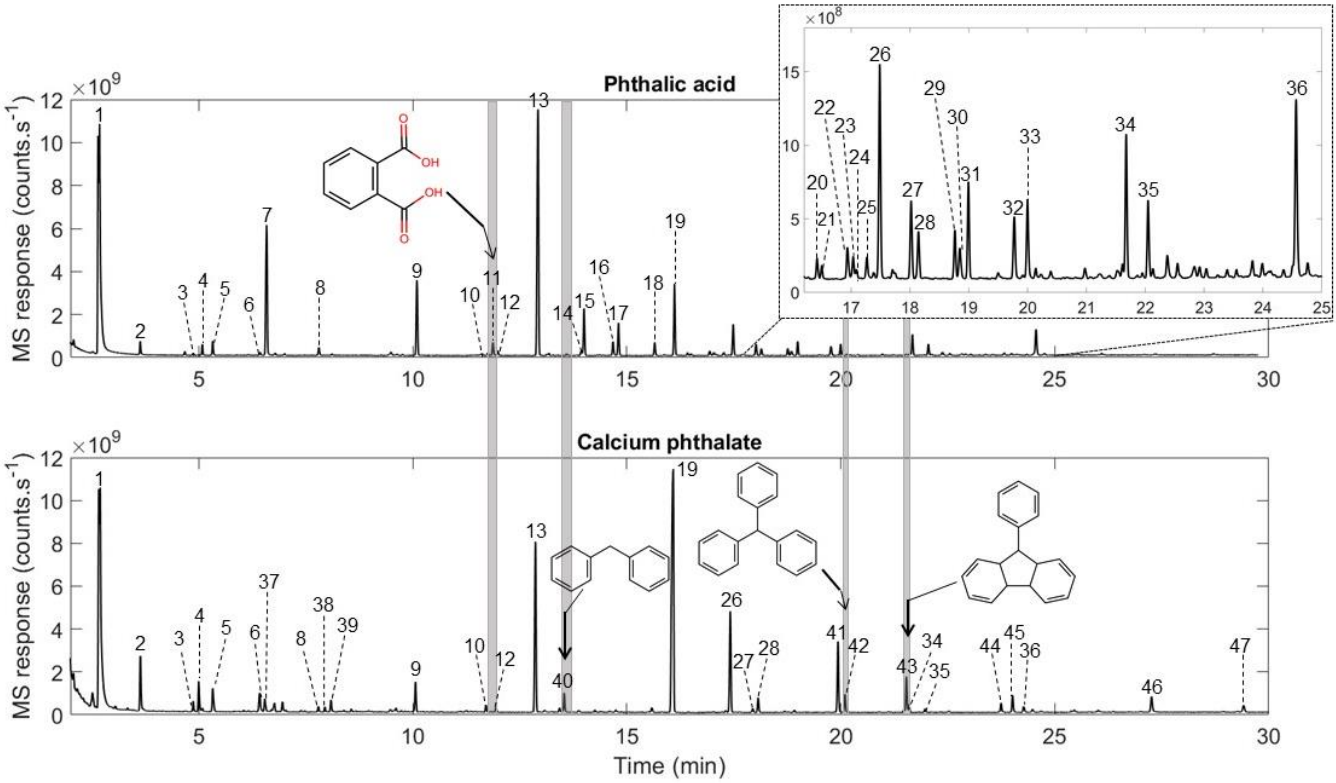

Figure 13: Chromatograms obtained from the flash pyrolysis (at 800 °C) of phthalic acid (top) and calcium phthalate (bottom) diluted at 1 wt% in fused silica. The grey shading corresponds to molecules characteristic of the pyrolysis of the acid or the salt. (*) artifact of the column (stationary phase bleeding), (1) benzene, (2) toluene, (3) ethylbenzene, (4) phenylethyne, (5), styrene, (6) benzaldehyde, (7) phenol, (8) benzene, propynyl, (9) naphthalene, (10) and (12) methylnaphthalene (isomers), (11) phthalic acid, (13) biphenyl, (14) acenaphthylene, (15) biphenylene, (16), (22), and (23) hydroxybiphenyl (isomers), (17) dibenzofuran, (18) fluorene, (19) benzophenone, (20) benzoic acid, phenyl ester, (21) diphenylacetylene, (24) stilbene, (25) Methanone, (2-hydroxyphenyl)phenyl-, (26) fluorenone, (27) anthracene, (28) phenanthrene, (29) anthracene, ethynyl-, (30) xanthone, (31), (34), and (35) terphenyl (isomers), (32) 4-hydroxy-9-fluorenone, (33) phenylnaphthalene, (36) benzanthracene, (37) xylene, (38) trimethylbenzene, (39) Benzene, ethyl-dimethyl-, (40) diphenylmethane, (41) anthracenedione, (42) triphenylmethane, (43) fluorene, phenyl-, (44) phenylanthracene, (45) Methanone, [1,1'-biphenyl]-4-ylphenyl-, (46) benzo fluoranthene, (47) anthracene, diphenyl-.

As previously shown with the benzoate couple, the parent molecule in the phthalic acid chromatogram is present but at much lower intensity compared to the previous conditions used which is likely due to the velocity (flash) and the high temperature of pyrolysis applied here. A high number of molecules were detected including benzene and biphenyl resulting from the decarboxylation of benzoic acid and the recombination of benzene rings. Phenol was also detected in both chromatograms of phthalic acid obtained after flash pyrolysis at 500 °C and 800 °C, but it was not detected in ramp pyrolysis. This further confirms that the type of pyrolysis (flash or ramp) applied can contribute to different reactional pathways of the molecules.

After the flash pyrolysis (800 °C) of calcium phthalate, phthalic acid was not detected but numerous byproducts were produced. Among them, benzene, biphenyl and benzophenone were detected. Finally, as observed in the chromatogram of both organic salts in SAM-like conditions (35 °C·min^{-1}), diphenylmethane, triphenylmethane and phenyl fluorene were detected as characteristic products of pyrolysis of the salt as they were not present in the chromatogram of phthalic acid.

3.3 WET CHEMISTRY DERIVATIZATIONS

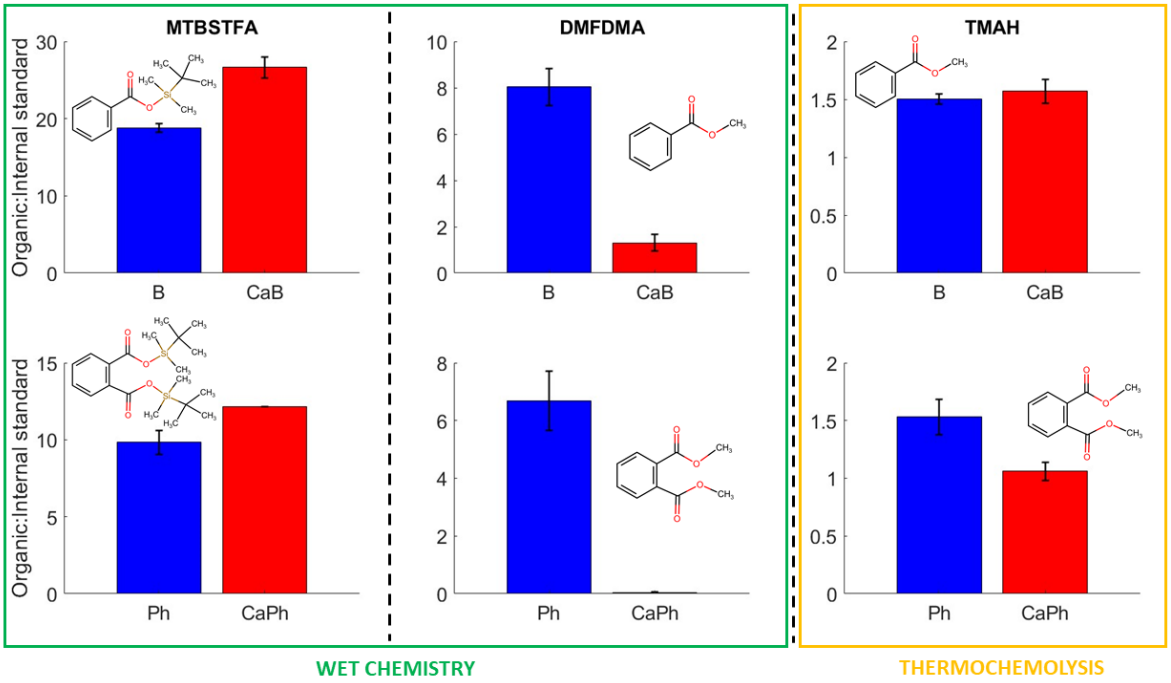

Figure 14: Comparison of the derivatization and thermochemolysis efficiencies of MTBSTFA (left), DMF-DMA (middle) and TMAH (right) reagents as measured by the abundance of derivatized compound obtained with the salt and the acid form of benzoic acid and phthalic acid derivatized, relative to the naphthalene d_8 internal standard. Both acid/salt couple samples were equimolar. Benzoic acid (B), calcium benzoate (CaB), phthalic acid (Ph), calcium phthalate (CaPh). Wet chemistry and thermochemolysis yield are not to be compared as the protocols and instrument used are different.

A comparison of the derivatized species and their yield for all three derivatization reagents was performed to assess the behavior of organic salts versus carboxylic acids in wet chemistry experiments. We observed that both the acid and the salt can be derivatized with MTBSTFA, DMF-DMA and TMAH and that they both were generating the same derivatized molecules under a given derivatization reagent. The derivatization with DMF-DMA and TMAH formed benzoic acid methyl ester with the benzoic acid and calcium benzoate, and dimethyl phthalate with phthalic acid and calcium phthalate. With MTBSTFA, benzoic acid and calcium benzoate both derived benzoic acid tert-butyldimethylsilyl ester, and phthalic acid and calcium phthalate both derived phthalic

acid, bis tert-butyldim ethylsilyl ester. We did not detect other derivatized molecules than the one mentioned, and the usual byproducts of the derivatization reagents.

The derivatization products of the organic salts were detected with the three derivatization reagents. With MTBSTFA, both calcium benzoate and calcium phthalate produced a higher abundance of derivatized byproducts than their acid counterpart. With DMF-DMA, the derivatization products of the organic salts were detected with both derivatization reagents but in significantly lower abundance than that of the acids. Finally, with TMAH, benzoic acid and calcium phthalate had the same derivatization yield, whereas phthalic acid derivatized better than calcium phthalate.

The abundance of the derivatized molecules is substantially higher for both the acid and the salt with MTBSTFA compared to DMF-DMA. However, we were not able to compare the derivatization efficiency of TMAH with MTBSTFA and DMF-DMA as the protocols used for thermochemistry and wet chemistry were different.

3.4 SAM VERSUS LABORATORY EXPERIMENTS

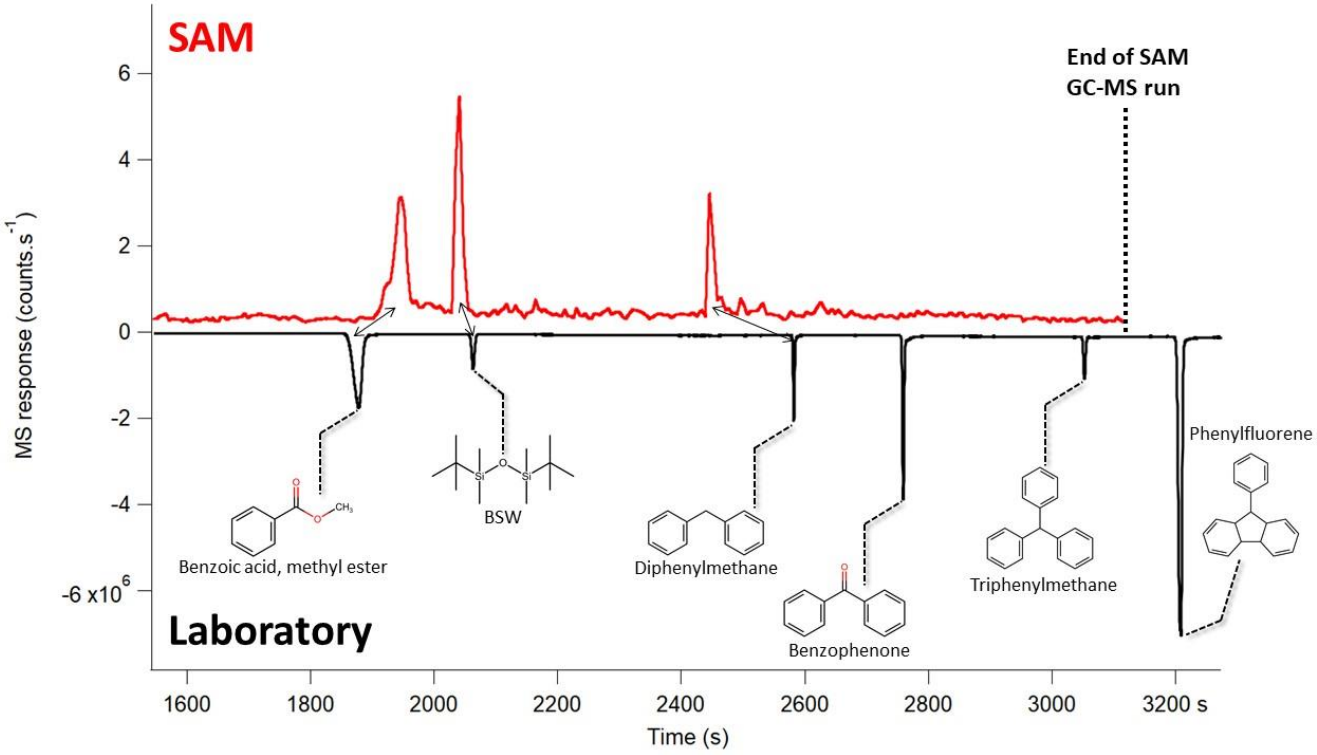

*Figure 15: GC-MS analyses of selected pyrolysis and derivatization products of organic salts in a laboratory GC-2 column (bottom) compared to the same species detected in a SAM chromatogram (top). The reconstructed SAM chromatogram is from the analysis of the Mary Anning sample where the mass to charge ratios (m/z) were adjusted as followed: m/z 105*60 + m/z 147 + m/z 167*600. The temperature program starts at T1=45 °C for 7 minutes, followed by a first ramp of 120 °C·min^{-1} to T2=66 °C, then a second ramp od 0.3 °C·min^{-1} to T3=59 °C and finally a third ramp of 10 °C·min^{-1} to reach a final temperature of 280 °C for 30 minutes. The inlet column pressure was set to 130 kPa to match the retention time of the bi-silylated water (BSW) observed at 34.54 minutes on SAM.*

Two species relevant to this study were identified in the Mary Anning (MA) sample by SAM: benzoic acid methyl ester, a possible thermochemolysis product of benzoate salts with TMAH and diphenylmethane in SAM and one of the characteristic product of pyrolysis of benzoates and phthalates as observed in this study. The mass to charge ratio (*m/z*) of benzoic acid methyl ester and diphenylmethane, *m/z* 105 and *m/z* 167, respectively were retrieved from the SAM chromatogram (Figure 15, top red

chromatogram). The laboratory chromatogram (Figure 15, bottom black chromatogram) shows that both species are within the same retention time range as in the SAM chromatogram, providing a robust identification. Benzophenone and triphenylmethane were not identified in the Mary Anning sample but could be detected with GC2 if they were present above their limit of detection. Finally, phenyl fluorene would elute beyond the end of the SAM run and would not have been detectable in Mary Anning, even if present.

However, it is important to note that while the temperature programs and pressure of the SAM GC2 column were simulated in the laboratory, slight differences remain as the flight and laboratory setups are not strictly identical. The shifts observed between the peaks of the molecule in the SAM and laboratory analyses could be explained by several factors: (1) the temperature profile variations in the flight model is that the columns' temperature control is less precise due to the heating technique employed (Millan et al., 2019; Millan et al., 2016). (2) The lack of adsorption injection trap (IT) prior to the GC2 column on the SAM instrument. However, its absence upstream the GC2 column indicates that all the compounds released during pyrolysis have different retention times, thus making it difficult to match with laboratory measurements despite pressure calibration. (3) Finally, the SAM flight and spare column might have aged differently which could also play a role in the release of organic molecules.

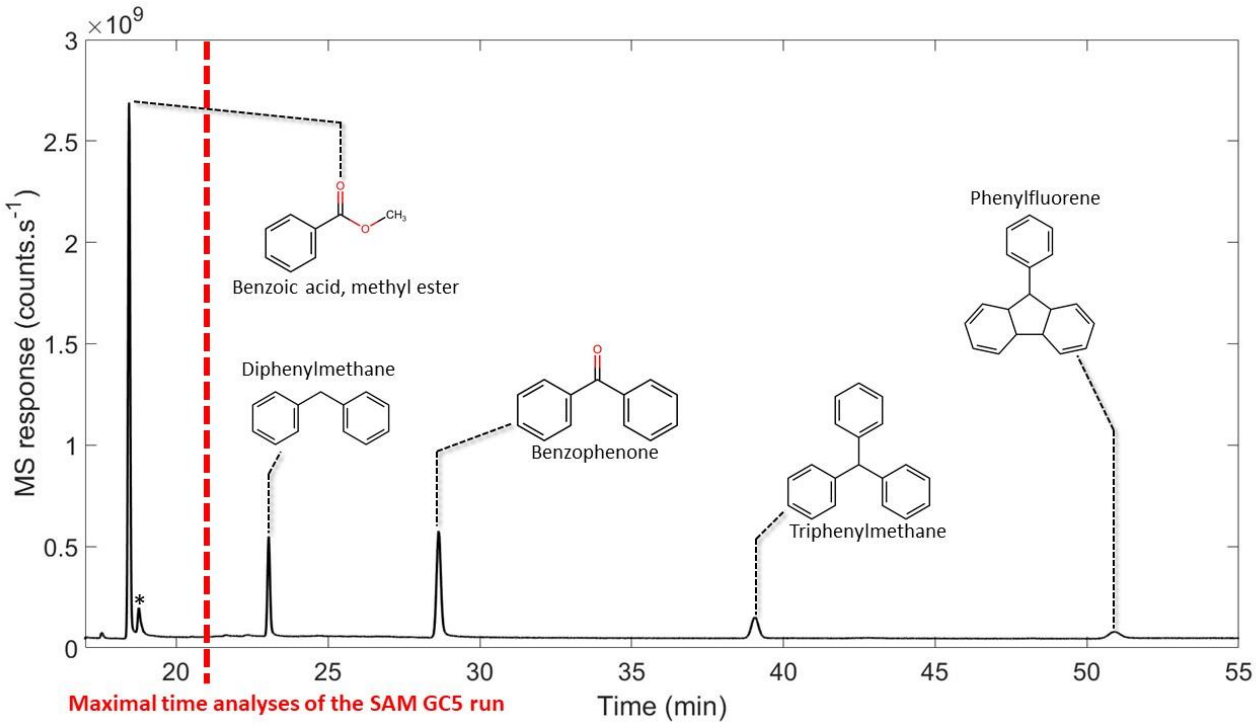

Figure 16: Laboratory GC-MS analyses of the characteristic pyrolysis and derivatization products of organic salts in SAM GC5 conditions. The maximal time of analyses of the SAM GC5 run in situ is 21 minutes. (*) artifact of the column (stationary phase bleeding).

In Figure 16, the retention times of products of interests from the thermal degradation and derivatization of organic salts are shown, within the conditions of a typical GC-5 analysis. The maximum duration of a typical SAM GC5 *in situ* analysis is of 21 minutes. In this chromatogram, only benzoic acid methyl ester elutes within 21 minutes. The other species analyzed (diphenylmethane, benzophenone, triphenylmethane and phenyl fluorene), would elute after the end of the SAM GC-MS analysis, and thus would not be detected even if present in a Martian sample.

4. DISCUSSION

Our laboratory investigations have demonstrated the utility of combining EGA and GC-MS analyses, as well as thermal extraction (pyrolysis) and wet chemistry (derivatization) techniques for the identification of aromatic organic salts on Mars. The results suggest that benzoic acid and phthalic acid, if present in the soil of Mars, could be readily identified through the detection of the acid itself, with EGA and pyrolysis-GC-MS

techniques. However, their salt counterpart, calcium benzoate and calcium phthalate, cannot be detected because of their refractory nature. Indeed, calcium benzoate and calcium phthalate possess strong ion-dipole intermolecular forces as well as higher molecular weight of the salt (benzoic acid MW = 122 $g \cdot mol^{-1}$/Calcium benzoate MW = 282 $g \cdot mol^{-1}$ and phthalic acid MW = 166 $g \cdot mol^{-1}$/calcium phthalate MW = 204 $g \cdot mol^{-1}$), both contributing factors for the decreased volatility of the organic salt.

The outgassing of the thermal decomposition products of the organic salts only occurred at temperatures higher than 470 °C. Thus, only instruments with a sufficient heating capability (> 500 °C) would be able to detect the degradation products of the salts if present in a sample. Therefore, the Viking pyrolysis system would be insufficient and could explains the lack of detection of such organic compounds as discussed by Benner at al. (2000). At high temperature both organic salts released benzophenone in high abundance with both EGA and GC-MS modes. Benzophenone could be used as a qualitative clue to the presence of organic salts. However, the gases produced by the thermal decomposition of calcium phthalate were similar to those produced from calcium benzoate. Thus, identifying the specific parent salt in a sample could be difficult except that calcium benzoate also produced biphenyl which is not observed with calcium phthalate. The presence of biphenyl combined to benzophenone in EGA could thus be a qualitative way to discriminate between these two aromatic organic salts.

In GC-MS, the presence of calcium benzoate and calcium phthalate could only be inferred through the identification of several byproduct characteristic of the degradation of the salts during pyrolysis. For both carboxylic acid couples studied, the acid and the salt did not follow the same degradation pathway resulting in differences in the species detected. Several byproducts characteristic of the thermal degradation of both organic salts have been identified in GC-MS: benzophenone, diphenylmethane, triphenylmethane, and phenyl fluorene. Except for benzophenone which was also identified in EGA, the other compounds are seen in GC-MS only, due to the separation power of the GC and a greater limit of detection, which allows a better identification of

the compounds. This confirms the complementary nature of the EGA and GC-MS techniques, the former giving precious information on the decomposition temperatures and pathways of the original compounds, and the latter to strictly identify compounds with a higher sensitivity. Dabestani et al. (2005) described the reaction pathway of calcium benzoate and suggested that the initial decarboxylation of the benzoate salt leads to the formation of phenyl anion as the key intermediate. The reaction of the phenyl anion with alkali benzoate generates benzophenone as a major product which further reacts to form other compounds such as diphenylmethane, triphenylmethane or phenyl fluorene. A similar behavior between calcium phthalate and benzoate suggests that the pyrolysis of both salts proceeded *via* a similar anionic reaction pathway. Thus, if the parent organic ion of calcium phthalate is not detected, characteristic products of thermal evolution are clearly identified and they could be used as tracers of calcium benzoate and calcium phthalate on Mars despite not being able to discriminate between the mono- and di-acid, with pyrolysis-GC-MS alone.

Diphenylmethane was detected as a Tenax byproduct with and without perchlorate in a study by Buch et al. in 2019. This same study showed that benzophenone was also formed as a Tenax byproduct in the presence of perchlorate. Because the degassing temperature of both organic salts is consistent with the degassing temperature of calcium perchlorate (Millan et al., 2020) and magnesium perchlorate (Clark et al., 2020) into HCl, O_2 and Cl_2, oxychlorine reacting with Tenax could be the source of diphenylmethane or benzophenone if detected *in situ* with SAM. So far, none of these molecules have been detected in the samples analyzed by SAM except for diphenylmethane which was identified at the Mary Anning drill site in the Glen Torridon region (Williams et al., 2021). However, we have demonstrated that all these molecules could have been detected if they were present in the Martian soil with the GC2 SAM column, except phenyl fluorene which would elute after the end of the SAM analysis time (Fig. 10). The absence of benzophenone in the Mary Anning chromatogram is a definitive clue that organic salts are not present in the MA sample. In order to detect phenyl fluorene the temperature ramp could be increased, which would shorten the

elution time of the compounds making the detection of phenyl fluorene more likely in future runs where the presence of aromatic organic salts was to be suspected. With the SAM GC5 column, however, the detection of aromatic salt byproducts is unlikely as they should all elute after the maximum time of analysis for this column in SAM temperatures conditions (21 minutes). A longer analysis would be required in order to identify some of the species in case a clue of the presence of organic salts was detected with EGA and/or derivatization. This shows the importance to have multiple columns on flight instruments and the predictive results such as EGA, which can help predict the detection of refractory compounds. This work should be applied to MOMA columns as well.

The slow pyrolysis ramp (35 °C·min^{-1}) used on the SAM instrument seems to be more appropriate to detect the indirect clues of the presence of organic salts through characteristic compounds, compared to the flash pyrolysis used on the MOMA instrumental set-up. Indeed, the results showed that in SAM-like pyrolysis conditions with a slow rate ramp of 35 °C·min^{-1}, diphenylmethane, triphenylmethane and phenyl fluorene were released. Results gathered from the flash 800 °C pyrolysis experiments showed that both carboxylic acids and their salt counterpart produced similar byproducts which can render their discrimination difficult especially due to the low intensity of the parent molecule in the chromatograms of the acids. Calcium phthalate produced the three characteristic byproducts diphenylmethane, triphenylmethane and phenyl fluorene that, could serve as indirect clue for the identification of phthalate if present above the detection limit of the flight instruments. However, these compounds were not observed in the chromatogram of calcium benzoate making its identification difficult. The kinetic of formation of benzoate products might be slower than for phthalates, which could explain the lack of detection of the characteristic products of calcium benzoate at flash 800 °C. Therefore, MOMA pyrolysis experiments would benefit from step pyrolysis temperatures instead of a direct flash 800 °C pyrolysis to help distinguish features specific to the degradation of both the salts and their acid form. Moreover, if the presence of organic salts was suspected in a Martian sample, a

slower temperature ramp (< 200 °C·min^{-1}) (Goesmann et al., 2017) or a longer duration of the pyrolysis experiment could help the detection of diphenylmethane, triphenylmethane and phenyl fluorene released from the pyrolysis of benzoate salts.

Finally, when derivatized with DMF-DMA, MTBSTFA or TMAH, both the acid and the organic salt produced the same derivatized product. With MTBSTFA, the organic salts derivatized better than their acid. Calcium could serve as a catalyst during the derivatization reaction. Whereas with DMF-DMA, a higher derivatization yield was observed for the acid than for the salt. Moreover, with TMAH, the benzoic acid and salt had a similar derivatization yield, whereas, phthalic acid derivatized better than its salt counterpart. Therefore, when derivatized with DMF-DMA or TMAH, calcium does not serve as a catalytic group but instead lowers the availability of the labile group during the derivatization process. The derivatization reagents can readily react with the labile hydrogen of the carboxylic group of the acid, whereas the salts are in their anionic form, decreasing the reactivity of the reagent toward the salt. The presence of the calcium cation also increased the steric hindrance of the molecules and therefore decreased the access of the derivatization reagent to the reactive group.

Moreover, when comparing the yield between the wet chemistry experiments, we obtained a higher relative abundance of derivatized molecules for both the acid and the salt with MTBSTFA compared to DMF-DMA. This could be explained by a difference in the mass spectrometer's response for DMF-DMA and MTBSTFA derivatized compounds. Molecule derivatized with MTBSTFA could be better ionized in the mass spectrometer source than compounds derivatized with DMF-DMA because the tert-butyldimethylsilyl group added by MTBSTFA has a higher ionization cross section compared to the methyl group added by DMF-DMA. Moreover, the derivatization response is higher for compounds derivatized with MTBSTFA than molecules derivatized with DMF-DMA. Combined, this could explain the highest detection of MTBSTFA derivatized compounds compared to those with DMF-DMA. These results showed that MTBSTFA would be better suited for the derivatization of these salts if

present in the Martian soil since these molecules may not be detectable using DMF-DMA. Furthermore, Williams et al. (2021), reported the potential detection of benzoic acid methyl ester in the first TMAH sample of the SAM instrument suite and Millan et al. (2022) detected benzoic acid tert-butyldimethylsilyl in the Ogunquit Beach (OG) sample collected in the sand of Bagnold Dunes by the Curiosity rover. Therefore, if present in the Martian soil, aromatic organic salts could be derivatized through wet chemistry or thermochemistry experiments present on SAM and MOMA, showing the complementarity of this technique with pyrolysis.

5. CONCLUSIONS AND PERSPECTIVES

These results showed that sample pyrolysis, can provide a signature of parent carboxylic acid molecules but not aromatic organic salts where only byproducts were produced. If present at the Martian surface, aromatic organic salts, such as benzoate and phthalate, could be detected indirectly through high temperature (> 500 °C) thermal extraction analysis such as EGA or pyrolysis-GC-MS or wet chemistry experiments, showing that the missing organic molecules described by Benner *et al.* (2000) could be identified with instrumental set-ups such as SAM or MOMA. This shows the importance of using the different capabilities of these instrument suites in tandem to understand more deeply the data obtained from a sample and increase the possibility to detect refractory molecules. However, the low intensity of the compounds identified in the organic salt pyrolysis chromatogram could fall below the detection limit of the instruments. This observation also agrees with Benner et al.'s conclusion regarding the probable low capability of the Viking GC-MS instruments to detect certain organics such as salts of benzenecarboxylic acids.

Overall, the conclusions of this work raise essential questions on the detectability of refractory molecules and on the interpretation of *in situ* data. To expand this work, experimental study on the high-fidelity Engineering Test Unit (ETU) and/or testbeds of MOMA and SAM instrument suites could help further understand the signature and behavior of aromatic organic salts under relevant Mars operational conditions.

Furthermore, this study focused only on calcium organic salts, other cations, likely to be present on Mars like iron or magnesium, should be tested in order to compare their influence on the thermal degradation and derivatization of the molecules.

REFERENCES

Abbey, W., Anderson, R., Beegle, L., Hurowitz, J., Williford, K., Peters, G., Morookian, J. M., Collins, C., Feldman, J., & Kinnett, R. (2019). A look back: The drilling campaign of the Curiosity rover during the Mars Science Laboratory's Prime Mission. *Icarus*, *319*, 1-13.

Appelbaum, J., Landis, G. A., & Sherman, I. (1993). Solar radiation on Mars—Update 1991. *Solar Energy*, *50*(1), 35-51. https://doi.org/10.1016/0038-092x(93)90006-a

Arvidson, R. E. (2016). Aqueous history of Mars as inferred from landed mission measurements of rocks, soils, and water ice. *Journal of Geophysical Research: Planets*, *121*(9), 1602-1626. https://doi.org/10.1002/2016je005079

Balaram, J., Aung, M., & Golombek, M. P. (2021). The Ingenuity Helicopter on the Perseverance Rover. *Space Science Reviews*, *217*(4). https://doi.org/10.1007/s11214-021-00815-w

Barbieri, R., & Stivaletta, N. (2011). Continental evaporites and the search for evidence of life on Mars. *Geological Journal*, *46*(6), 513-524. https://doi.org/10.1002/gj.1326

Barone, V. (2005). Anharmonic vibrational properties by a fully automated second-order perturbative approach. *The Journal of chemical physics*, *122*(1), 014108.

Barone, V., Biczysko, M., & Bloino, J. (2014). Fully anharmonic IR and Raman spectra of medium-size molecular systems: accuracy and interpretation. *Physical Chemistry Chemical Physics*, *16*(5), 1759-1787.

Basile, B. P., Middleditch, B. S., & Oró, J. (1984). Polycyclic aromatic hydrocarbons in the Murchison meteorite. *Organic Geochemistry*, *5*(4), 211-216.

Bell, J. F., Maki, J. N., Mehall, G. L., Ravine, M. A., Caplinger, M. A., Bailey, Z. J., Brylow, S., Schaffner, J. A., Kinch, K. M., Madsen, M. B., Winhold, A., Hayes, A. G., Corlies, P., Tate, C., Barrington, M., Cisneros, E., Jensen, E., Paris, K., Crawford, K., Rojas, C., Mehall, L., Joseph, J., Proton, J. B., Cluff, N., Deen, R. G., Betts, B., Cloutis, E., Coates, A. J., Colaprete, A., Edgett, K. S., Ehlmann, B. L., Fagents, S., Grotzinger, J. P., Hardgrove, C., Herkenhoff, K. E., Horgan, B., Jaumann, R., Johnson, J. R., Lemmon, M., Paar, G., Caballo-Perucha, M., Gupta, S., Traxler, C., Preusker, F., Rice, M. S., Robinson, M. S., Schmitz, N., Sullivan, R., & Wolff, M. J. (2021). The Mars 2020 Perseverance Rover Mast Camera Zoom (Mastcam-Z) Multispectral, Stereoscopic Imaging Investigation. *Space Science Reviews*, *217*(1). https://doi.org/10.1007/s11214-020-00755-x

Benner, S. A., Devine, K. G., Matveeva, L. N., & Powell, D. H. (2000). The missing organic molecules on Mars. *Proceedings of the National Academy of Sciences*, *97*(6), 2425-2430. https://doi.org/10.1073/pnas.040539497

Benner, S. A., Ricardo, A., & Carrigan, M. A. (2004). Is there a common chemical model for life in the universe? *Current opinion in chemical biology*, *8*(6), 672-689.

Bibring, J.-P., Hamm, V., Pilorget, C., & Vago, J. L. (2017). The micrOmega investigation onboard ExoMars. *Astrobiology*, *17*(6-7), 621-626.

Bibring, J.-P., Langevin, Y., Mustard, J. F., Poulet, F., Arvidson, R., Gendrin, A., Gondet, B., Mangold, N., Pinet, P., & Forget, F. (2006). Global mineralogical and aqueous Mars history derived from OMEGA/Mars Express data. *Science*, *312*(5772), 400-404.

Biczysko, M., Bloino, J., & Puzzarini, C. (2018). Computational challenges in Astrochemistry. *Wiley Interdisciplinary Reviews: Computational Molecular Science*, *8*(3), e1349.

Biemann, K., Oro, J., Toulmin, P., Orgel, L. E., Nier, A. O., Anderson, D. M., Simmonds, P. G., Flory, D., Diaz, A. V., Rushneck, D. R., Biller, J. E., & Lafleur, A. L. (1977). The search for organic substances and inorganic volatile compounds in the surface of Mars. *Journal of Geophysical Research*, *82*(28), 4641-4658. https://doi.org/10.1029/js082i028p04641

Biemann, K. O., J., Toulmin, P., Orgel, L. E., Nier, A. O., Anderson, D. M., ... & Biller, J. A. (1976). Search for Organic and Volatile Inorganic Compounds in Two Surface Samples from the Chryse Planitia Region of Mars. *Science*, *194*(4260), 72-76.

Bish, D. L., Blake, D., Vaniman, D., Chipera, S., Morris, R., Ming, D., Treiman, A., Sarrazin, P., Morrison, S., & Downs, R. (2013). X-ray diffraction results from Mars Science Laboratory: Mineralogy of Rocknest at Gale crater. *Science*, *341*(6153), 1238932.

Blackmond, D. G. (2010). The origin of biological homochirality. *Cold Spring Harbor perspectives in biology*, *2*(5), a002147.

Bloino, J. (2015). A VPT2 route to near-infrared spectroscopy: the role of mechanical and electrical anharmonicity. *The Journal of Physical Chemistry A*, *119*(21), 5269-5287.

Bloino, J., Baiardi, A., & Biczysko, M. (2016). Aiming at an accurate prediction of vibrational and electronic spectra for medium-to-large molecules: an overview. *International Journal of Quantum Chemistry*, *116*(21), 1543-1574.

Bloino, J., Biczysko, M., & Barone, V. (2015). Anharmonic effects on vibrational spectra intensities: infrared, Raman, vibrational circular dichroism, and Raman optical activity. *The Journal of Physical Chemistry A*, *119*(49), 11862-11874.

Bonner, W. A. (1995). Chirality and life. *Origins of Life and Evolution of the Biosphere*, *25*(1-3), 175-190. https://doi.org/10.1007/bf01581581

Botta, O., & Bada, J. L. (2002). *Surveys in Geophysics*, *23*(5), 411-467. https://doi.org/10.1023/a:1020139302770

Boulesteix, D., Buch, A., Samson, J., Millan, M., Jomaa, J., Coscia, D., Moulay, V., McIntosh, O., Freissinet, C., & Stern, J. (2023). Influence of pH and salts on DMF-DMA derivatization for future Space Applications. *Analytica Chimica Acta*, 341270.

Brass, G. W. (1980). Stability of brines on Mars. *Icarus*, *42*(1), 20-28.

Breezee, J., Cady, N., & Staley, J. (2004). Subfreezing growth of the sea ice bacterium "Psychromonas ingrahamii". *Microbial Ecology*, *47*, 300-304.

Brubach, J.-B., Mermet, A., Filabozzi, A., Gerschel, A., & Roy, P. (2005). Signatures of the hydrogen bonding in the infrared bands of water. *The Journal of chemical physics*, *122*(18), 184509.

Buch, A., Belmahdi, I., Szopa, C., Freissinet, C., Glavin, D. P., Millan, M., Summons, R., Coscia, D., Teinturier, S., Bonnet, J. Y., He, Y., Cabane, M., Navarro-Gonzalez, R., Malespin, C. A., Stern, J., Eigenbrode, J., Mahaffy, P. R., & Johnson, S. S. (2019). Role of the Tenax® Adsorbent in the Interpretation of the EGA and GC-MS Analyses Performed With the Sample Analysis at Mars in Gale Crater. *Journal of Geophysical Research: Planets*, *124*(11), 2819-2851. https://doi.org/10.1029/2019je005973

Burton, A. S., Stern, J. C., Elsila, J. E., Glavin, D. P., & Dworkin, J. P. (2012). Understanding prebiotic chemistry through the analysis of extraterrestrial amino acids and nucleobases in meteorites. *Chemical Society Reviews*, *41*(16), 5459-5472.

Cao, X., & Fischer, G. (2000). The infrared spectra and molecular structure of zwitterionic L-β-phenylalanine. *Journal of Molecular Structure*, *519*(1-3), 153-163.

Carter, J., Quantin, C., Thollot, P., Loizeau, D., Ody, A., & Lozach, L. (2016). Oxia planum: A clay-laden landing site proposed for the ExoMars rover mission: Aqueous mineralogy and alteration scenarios. Lunar and planetary science conference,

Chang, S.-T. (1982). *Photodegradation and photoprotection of wood surfaces*. US Forest Products Laboratory.

Chapman, D. (1965). Infrared spectroscopy of lipids. *Journal of the American Oil Chemists' Society*, *42*(5), 353-371.

Chevrier, V. F., Hanley, J., & Altheide, T. S. (2009). Stability of perchlorate hydrates and their liquid solutions at the Phoenix landing site, Mars. *Geophysical Research Letters*, *36*(10).

Clark, B. (1981). The salts of Mars. *Icarus*, *45*(2), 370-378. https://doi.org/10.1016/0019-1035(81)90041-5

Clark, B. C., Baird, A., Rose Jr, H. J., Toulmin III, P., Keil, K., Castro, A. J., Kelliher, W. C., Rowe, C. D., & Evans, P. H. (1976). Inorganic Analyses of Martian Surface Samples at the Viking Landing Sites. *Science*, *194*(4271), 1283-1288.

Clark, J. V., Sutter, B., McAdam, A. C., Rampe, E. B., Archer, P. D., Ming, D. W., Navarro-Gonzalez, R., Mahaffy, P., & Lapen, T. J. (2020). High-Temperature HCl Evolutions From Mixtures of Perchlorates and Chlorides With Water-Bearing Phases: Implications for the SAM Instrument in Gale Crater, Mars. *Journal of Geophysical Research: Planets*, *125*(2). https://doi.org/10.1029/2019je006173

Cloos, P., Calicis, B., Fripiat, J., & Makay, K. (1966). Adsorption of amino-acids and peptides by montmorillonite. I. Chemical and X-ray diffraction studies. Proceedings of the International Clay Conference, Jerusalem, Israel,

Cockell, C. S., Bush, T., Bryce, C., Direito, S., Fox-Powell, M., Harrison, J. P., Lammer, H., Landenmark, H., Martin-Torres, J., & Nicholson, N. (2016). Habitability: a review. *Astrobiology*, *16*(1), 89-117.

Cohen, M. D., Flagan, R. C., & Seinfeld, J. H. (1987). Studies of concentrated electrolyte solutions using the electrodynamic balance. 1. Water activities for single-electrolyte solutions. *Journal of Physical Chemistry*, *91*(17), 4563-4574.

Cronin, J., & Pizzarello, S. (1983). Amino acids in meteorites. *Advances in space research*, *3*(9), 5-18.

Cull, S., Arvidson, R. E., Mellon, M. T., Skemer, P., Shaw, A., & Morris, R. V. (2010). Compositions of subsurface ices at the Mars Phoenix landing site. *Geophysical Research Letters*, *37*(24), n/a-n/a. https://doi.org/10.1029/2010gl045372

Dabestani, R., Britt, P. F., & Buchanan, A. C. (2005). Pyrolysis of Aromatic Carboxylic Acid Salts: Does Decarboxylation Play a Role in Cross-Linking Reactions? *Energy & Fuels*, *19*(2), 365-373. https://doi.org/10.1021/ef0400722

Dartnell, L. R., Desorgher, L., Ward, J. M., & Coates, A. J. (2007). Martian sub-surface ionising radiation: biosignatures and geology. *Biogeosciences*, *4*(4), 545-558. https://doi.org/10.5194/bg-4-545-2007

de Araújo, D. T., Ciuffi, K. J., Nassar, E. J., Vicente, M. A., Trujillano, R., Rives, V., Bernal, E. P., & de Faria, E. H. (2021). Grafting of L-proline and L-phenylalanine amino acids on kaolinite through synthesis catalyzed by boric acid. *Applied Surface Science Advances*, *4*, 100081.

Deamer, D. W., & Pashley, R. M. (1989). Amphiphilic components of the murchison carbonaceous chondrite: Surface properties and membrane formation. *Origins of Life and Evolution of the Biosphere*, *19*(1), 21-38. https://doi.org/10.1007/bf01808285

Deborde, M., & Von Gunten, U. (2008). Reactions of chlorine with inorganic and organic compounds during water treatment—kinetics and mechanisms: a critical review. *Water research*, *42*(1-2), 13-51.

dos Santos, R., Patel, M., Cuadros, J., & Martins, Z. (2016). Influence of mineralogy on the preservation of amino acids under simulated Mars conditions. *Icarus*, *277*, 342-353.

Dundas, C. M., Bramson, A. M., Ojha, L., Wray, J. J., Mellon, M. T., Byrne, S., McEwen, A. S., Putzig, N. E., Viola, D., & Sutton, S. (2018). Exposed subsurface ice sheets in the Martian mid-latitudes. *Science*, *359*(6372), 199-201.

E. Dehouck, O. F., C. Quantin-Nataf, P. Beck,, N. Mangold, C. R., E. Clavé, O. Beyssac, J. R. Johnson, L. Mandon, F. Poulet, S. Le Mouélic, G. Caravaca, H. Kalucha,, E. Gibbons, G. D., P. Gasda, P.-Y. Meslin, S. Schroeder, A. Udry, R. B. Anderson, S. Clegg, A. Cousin, T. S., Gabriel, J. L., T. Fouchet, P. Pilleri, C. Pilorget, J. Hurowitz, J. Núñez, A. Williams, P. Russell, J. I. Simon, S., & Maurice, R. C. W. (2023). *Overview of the bedrock geochemistry and mineralogy observed by SuperCam during Perseverance's delta front campaign* 54th Lunar and Planetary Science Conference 2023,

Ehlmann, B. L., Mustard, J. F., Fassett, C. I., Schon, S. C., Head III, J. W., Des Marais, D. J., Grant, J. A., & Murchie, S. L. (2008). Clay minerals in delta deposits and organic preservation potential on Mars. *Nature Geoscience*, *1*(6), 355-358.

Ehrlich, S., Moellmann, J., Reckien, W., Bredow, T., & Grimme, S. (2011). System-dependent dispersion coefficients for the DFT-D3 treatment of adsorption processes on ionic surfaces. *ChemPhysChem*, *12*(17), 3414-3420.

Eigenbrode, J. L., Summons, R. E., Steele, A., Freissinet, C., Millan, M., Navarro-González, R., Sutter, B., McAdam, A. C., Franz, H. B., Glavin, D. P., Archer, P. D., Mahaffy, P. R., Conrad, P. G., Hurowitz, J. A., Grotzinger, J. P., Gupta, S., Ming, D. W., Sumner, D. Y., Szopa, C., Malespin, C., Buch, A., & Coll, P. (2018). Organic matter preserved in 3-billion-year-old mudstones at Gale crater, Mars. *Science*, *360*(6393), 1096-1101. https://doi.org/10.1126/science.aas9185

Ertem, G., Ertem, M., McKay, C., & Hazen, R. (2017). Shielding biomolecules from effects of radiation by Mars analogue minerals and soils. *International Journal of Astrobiology*, *16*(3), 280-285.

Farias, A. P. S., Tadayozzi, Y. S., Carneiro, C. E., & Zaia, D. A. (2014). Salinity and pH affect Na+-montmorillonite dissolution and amino acid adsorption: a prebiotic chemistry study. *International Journal of Astrobiology*, *13*(3), 259-270.

Farley, K. A., Williford, K. H., Stack, K. M., Bhartia, R., Chen, A., Manuel, Hand, K., Goreva, Y., Herd, C. D. K., Hueso, R., Liu, Y., Maki, J. N., Martinez, G., Moeller, R. C., Nelessen, A., Newman, C. E., Nunes, D., Ponce, A., Spanovich, N., Willis, P. A., Beegle, L. W., Bell, J. F., Brown, A. J., Hamran, S.-E., Hurowitz, J. A., Maurice, S., Paige, D. A., Rodriguez-Manfredi, J. A., Schulte, M., & Wiens, R. C. (2020). Mars 2020 Mission Overview. *Space Science Reviews*, *216*(8). https://doi.org/10.1007/s11214-020-00762-y

Farmer, J. D., & Des Marais, D. J. (1999). Exploring for a record of ancient Martian life. *Journal of Geophysical Research: Planets*, *104*(E11), 26977-26995. https://doi.org/10.1029/1998je000540

Filopoulou, A., Vlachou, S., & Boyatzis, S. C. (2021). Fatty Acids and Their Metal Salts: A Review of Their Infrared Spectra in Light of Their Presence in Cultural Heritage. *Molecules*, *26*(19), 6005.

Fornaro, T., Biczysko, M., Bloino, J., & Barone, V. (2016). Reliable vibrational wavenumbers for C [double bond, length as m-dash] O and N–H stretchings of isolated and hydrogen-bonded nucleic acid bases. *Physical Chemistry Chemical Physics*, *18*(12), 8479-8490.

Fornaro, T., Biczysko, M., Monti, S., & Barone, V. (2014). Dispersion corrected DFT approaches for anharmonic vibrational frequency calculations: nucleobases and their dimers. *Physical Chemistry Chemical Physics*, *16*(21), 10112-10128.

Fornaro, T., Boosman, A., Brucato, J. R., Ten Kate, I. L., Siljeström, S., Poggiali, G., Steele, A., & Hazen, R. M. (2018). UV irradiation of biomarkers adsorbed on minerals under Martian-like conditions: Hints for life detection on Mars. *Icarus*, *313*, 38-60. https://doi.org/10.1016/j.icarus.2018.05.001

Fornaro, T., Brucato, J. R., Feuillie, C., Sverjensky, D. A., Hazen, R. M., Brunetto, R., d'Amore, M., & Barone, V. (2018). Binding of nucleic acid components to the serpentinite-hosted hydrothermal mineral brucite. *Astrobiology*, *18*(8), 989-1007.

Fornaro, T., Brucato, J. R., Pace, E., Guidi, M. C., Branciamore, S., & Pucci, A. (2013). Infrared spectral investigations of UV irradiated nucleobases adsorbed on mineral surfaces. *Icarus*, *226*(1), 1068-1085.

Fornaro, T., Brucato, J. R., Poggiali, G., Corazzi, M. A., Biczysko, M., Jaber, M., Foustoukos, D. I., Hazen, R. M., & Steele, A. (2020). UV irradiation and near infrared characterization of laboratory Mars soil analog samples. *Frontiers in Astronomy and Space Sciences*, *7*, 539289.

Fornaro, T., Burini, D., Biczysko, M., & Barone, V. (2015). Hydrogen-bonding effects on infrared spectra from anharmonic computations: uracil–water complexes and uracil dimers. *The Journal of Physical Chemistry A*, *119*(18), 4224-4236.

Fornaro, T., Steele, A., & Brucato, J. (2018). Catalytic/Protective Properties of Martian Minerals and Implications for Possible Origin of Life on Mars. *Life*, *8*(4), 56. https://doi.org/10.3390/life8040056

Fouchet, T., Reess, J.-M., Montmessin, F., Hassen-Khodja, R., Nguyen-Tuong, N., Humeau, O., Jacquinod, S., Lapauw, L., Parisot, J., & Bonafous, M. (2022). The SuperCam infrared spectrometer for the perseverance rover of the Mars2020 mission. *Icarus*, *373*, 114773.

Fox, A. C., Eigenbrode, J. L., & Freeman, K. H. (2019). Radiolysis of Macromolecular Organic Material in Mars-Relevant Mineral Matrices. *Journal of Geophysical Research: Planets*, *124*(12), 3257-3266. https://doi.org/10.1029/2019je006072

Fox, J. L. (1993). On the escape of oxygen and hydrogen from Mars. *Geophysical Research Letters*, *20*(17), 1747-1750. https://doi.org/10.1029/93gl01118

Fraissler, G., Jöller, M., Brunner, T., & Obernberger, I. (2009). Influence of dry and humid gaseous atmosphere on the thermal decomposition of calcium chloride and its impact on the remove of heavy metals by chlorination. *Chemical Engineering and Processing: Process Intensification*, *48*(1), 380-388. https://doi.org/10.1016/j.cep.2008.05.003

Freissinet, C., Buch, A., Sternberg, R., Szopa, C., Geffroy-Rodier, C., Jelinek, C., & Stambouli, M. (2010). Search for evidence of life in space: Analysis of enantiomeric organic molecules by N,N-dimethylformamide dimethylacetal derivative dependant Gas Chromatography–Mass Spectrometry. *Journal of Chromatography A*, *1217*(5), 731-740. https://doi.org/10.1016/j.chroma.2009.11.009

Freissinet, C., Glavin, D., Buch, A., Szopa, C., Teinturier, S., Archer, P., Williams, A., Williams, R., Millan, M., & Steele, A. (2019). Detection of long-chain hydrocarbons on mars with

the Sample Analysis at Mars (SAM) instrument. Ninth International Conference on Mars,

Freissinet, C., Glavin, D. P., Mahaffy, P. R., Miller, K. E., Eigenbrode, J. L., Summons, R. E., Brunner, A. E., Buch, A., Szopa, C., Archer, P. D., Franz, H. B., Atreya, S. K., Brinckerhoff, W. B., Cabane, M., Coll, P., Conrad, P. G., Des Marais, D. J., Dworkin, J. P., Fairén, A. G., François, P., Grotzinger, J. P., Kashyap, S., Ten Kate, I. L., Leshin, L. A., Malespin, C. A., Martin, M. G., Martin-Torres, F. J., McAdam, A. C., Ming, D. W., Navarro-González, R., Pavlov, A. A., Prats, B. D., Squyres, S. W., Steele, A., Stern, J. C., Sumner, D. Y., Sutter, B., & Zorzano, M. P. (2015). Organic molecules in the Sheepbed Mudstone, Gale Crater, Mars. *Journal of Geophysical Research: Planets*, *120*(3), 495-514. https://doi.org/10.1002/2014je004737

Freissinet, C., Knudson, C. A., Graham, H. V., Lewis, J. M., Lasue, J., McAdam, A. C., Teinturier, S., Szopa, C., Dehouck, E., & Morris, R. V. (2020). Benzoic acid as the preferred precursor for the chlorobenzene detected on Mars: insights from the unique Cumberland analog investigation. *The Planetary Science Journal*, *1*(2), 41.

Frisch, M., Trucks, G., Schlegel, H., Suzerain, G., Robb, M., Cheeseman Jr, J., Montgomery, J., Vreven, T., Kudin, K., & Burant, J. (2016). Gaussian 09 (now Gaussian 16). *Gaussian Inc., Wallingford (CT)*.

Glavin, D. P., Freissinet, C., Miller, K. E., Eigenbrode, J. L., Brunner, A. E., Buch, A., Sutter, B., Archer, P. D., Atreya, S. K., Brinckerhoff, W. B., Cabane, M., Coll, P., Conrad, P. G., Coscia, D., Dworkin, J. P., Franz, H. B., Grotzinger, J. P., Leshin, L. A., Martin, M. G., McKay, C., Ming, D. W., Navarro-González, R., Pavlov, A., Steele, A., Summons, R. E., Szopa, C., Teinturier, S., & Mahaffy, P. R. (2013). Evidence for perchlorates and the origin of chlorinated hydrocarbons detected by SAM at the Rocknest aeolian deposit in Gale Crater. *Journal of Geophysical Research: Planets*, *118*(10), 1955-1973. https://doi.org/10.1002/jgre.20144

Glotch, T. D., Bandfield, J. L., Tornabene, L. L., Jensen, H. B., & Seelos, F. P. (2010). Distribution and formation of chlorides and phyllosilicates in Terra Sirenum, Mars. *Geophysical Research Letters*, *37*(16), n/a-n/a. https://doi.org/10.1029/2010gl044557

Glotch, T. D., Bandfield, J. L., Wolff, M. J., Arnold, J. A., & Che, C. (2016). Constraints on the composition and particle size of chloride salt-bearing deposits on Mars. *Journal of Geophysical Research: Planets*, *121*(3), 454-471. https://doi.org/10.1002/2015je004921

Goesmann, F., Brinckerhoff, W. B., Raulin, F., Goetz, W., Danell, R. M., Getty, S. A., Siljeström, S., Mißbach, H., Steininger, H., Arevalo, R. D., Buch, A., Freissinet, C., Grubisic, A., Meierhenrich, U. J., Pinnick, V. T., Stalport, F., Szopa, C., Vago, J. L., Lindner, R., Schulte, M. D., Brucato, J. R., Glavin, D. P., Grand, N., Li, X., Van Amerom, F. H. W., & The Moma Science, T. (2017). The Mars Organic Molecule Analyzer (MOMA) Instrument: Characterization of Organic Material in Martian Sediments. *Astrobiology*, *17*(6-7), 655-685. https://doi.org/10.1089/ast.2016.1551

Golombek, M., Grant, J., Kipp, D., Vasavada, A., Kirk, R., Fergason, R., Bellutta, P., Calef, F., Larsen, K., Katayama, Y., Huertas, A., Beyer, R., Chen, A., Parker, T., Pollard, B., Lee, S., Sun, Y., Hoover, R., Sladek, H., Grotzinger, J., Welch, R., E, Michalski, J., & Watkins, M. (2012). Selection of the Mars Science Laboratory Landing Site. *Space Science Reviews*, *170*(1-4), 641-737. https://doi.org/10.1007/s11214-012-9916-y

Golombek, M. P., Phillips, R. J., Watters, T., & Schultz, R. (2010). Mars tectonics. *Planetary tectonics*, *11*, 183-232.

Goudge, T. A., Mustard, J. F., Head, J. W., Fassett, C. I., & Wiseman, S. M. (2015). Assessing the mineralogy of the watershed and fan deposits of the Jezero crater paleolake system, Mars. *Journal of Geophysical Research: Planets*, *120*(4), 775-808.

Grabska, J., Ishigaki, M., Bec, K. B., Wójcik, M. J., & Ozaki, Y. (2017). Correlations between structure and near-infrared spectra of saturated and unsaturated carboxylic acids. Insight from anharmonic density functional theory calculations. *The Journal of Physical Chemistry A*, *121*(18), 3437-3451.

Greenspan, L. (1977). Humidity fixed points of binary saturated aqueous solutions. *Journal of research of the National Bureau of Standards. Section A, Physics and chemistry*, *81*(1), 89.

Griffith, E. C., & Vaida, V. (2013). Ionization state of L-phenylalanine at the air–water interface. *Journal of the American Chemical Society*, *135*(2), 710-716.

Grimme, S., Antony, J., Ehrlich, S., & Krieg, H. (2010). A consistent and accurate ab initio parametrization of density functional dispersion correction (DFT-D) for the 94 elements H-Pu. *The Journal of chemical physics*, *132*(15), 154104.

Grimme, S., Ehrlich, S., & Goerigk, L. (2011). Effect of the damping function in dispersion corrected density functional theory. *Journal of computational chemistry*, *32*(7), 1456-1465.

Guzman, M., McKay, C. P., Quinn, R. C., Szopa, C., Davila, A. F., Navarro-González, R., & Freissinet, C. (2018). Identification of Chlorobenzene in the Viking Gas Chromatograph-Mass Spectrometer Data Sets: Reanalysis of Viking Mission Data Consistent With Aromatic Organic Compounds on Mars. *Journal of Geophysical Research: Planets*, *123*(7), 1674-1683. https://doi.org/10.1029/2018je005544

Hakkinen, S. A., McNeill, V. F., & Riipinen, I. (2014). Effect of inorganic salts on the volatility of organic acids. *Environ Sci Technol*, *48*(23), 13718-13726. https://doi.org/10.1021/es5033103

Handbook, C. C. (2003). A Guide to Properties, Forms, Storage and Handling. *Dow Chemical Company*.

Hashizume, H. (2012). Role of clay minerals in chemical evolution and the origins of life. *Clay Minerals in Nature—Their characterization, modification and application*.

Hassler, Cary Zeitlin, 1 Robert F. Wimmer- Schweingruber, 2 Bent Ehresmann, 1 Scot Rafkin, L., J., Eigenbrode, 3 David E. Brinza, 4 Gerald Weigle, 5 Stephan Böttcher, 2, Eckart Böhm, 2 Soenke Burmeister, 2 Jingnan Guo, 2 Jan Köhler, 2, Cesar Martin, 2 Guenther Reitz, 6 Francis A. Cucinotta, Myung-Hee, Kim, 8 David Grinspoon, 9 Mark A. Bullock, 1 Arik Posner, Javier, Gómez-Elvira, 11 Ashwin Vasavada, 4 John P. Grotzinger, MSL, & Team†, S. (2013). Mars' Surface Radiation Environment with the Mars Science Laboratory's Curiosity Rover. *Science*. https://doi.org/10.1126/science.1244797

He, Y., Buch, A., Szopa, C., Williams, A. J., Millan, M., Guzman, M., Freissinet, C., Malespin, C., Glavin, D. P., Eigenbrode, J. L., Coscia, D., Teinturier, S., Pin, L., Cabane, M., & Mahaffy, P. R. (2020). The search for organic compounds with TMAH thermochemolysis: From Earth analyses to space exploration experiments. *TrAC Trends in Analytical Chemistry*, *127*, 115896. https://doi.org/10.1016/j.trac.2020.115896

Hecht, M. H., Kounaves, S. P., Quinn, R., West, S. J., Young, S. M., Ming, D. W., Catling, D., Clark, B., Boynton, W., & Hoffman, J. (2009). Detection of perchlorate and the soluble chemistry of martian soil at the Phoenix lander site. *Science*, *325*(5936), 64-67.

Hoffman, J. A., Hecht, M. H., Rapp, D., Hartvigsen, J. J., SooHoo, J. G., Aboobaker, A. M., McClean, J. B., Liu, A. M., Hinterman, E. D., & Nasr, M. (2022). Mars Oxygen ISRU

Experiment (MOXIE)—Preparing for human Mars exploration. *Science Advances*, *8*(35), eabp8636.

Horgan, B. H., Anderson, R. B., Dromart, G., Amador, E. S., & Rice, M. S. (2020). The mineral diversity of Jezero crater: Evidence for possible lacustrine carbonates on Mars. *Icarus*, *339*, 113526.

Huang, Q., Lu, G., Wang, J., & Yu, J. (2011). Thermal decomposition mechanisms of MgCl2·6H2O and MgCl2·H2O. *Journal of Analytical and Applied Pyrolysis*, *91*(1), 159-164. https://doi.org/10.1016/j.jaap.2011.02.005

Hynek, B. M., Beach, M., & Hoke, M. R. (2010). Updated global map of Martian valley networks and implications for climate and hydrologic processes. *Journal of Geophysical Research: Planets*, *115*(E9).

Ivanov, M. A., Slyuta, E. N., Grishakina, E. A., & Dmitrovskii, A. A. (2020). Geomorphological Analysis of ExoMars Candidate Landing Site Oxia Planum. *Solar System Research*, *54*(1), 1-14. https://doi.org/10.1134/s0038094620010050

Jakosky, B. M. (2022). How did Mars lose its atmosphere and water? *Physics Today*, *75*(4), 62-63.

Jakosky, B. M., Slipski, M., Benna, M., Mahaffy, P., Elrod, M., Yelle, R., Stone, S., & Alsaeed, N. (2017). Mars' atmospheric history derived from upper-atmosphere measurements of 38Ar/36Ar. *Science*, *355*(6332), 1408-1410.

Jehlička, J., & Edwards, H. (2008). Raman spectroscopy as a tool for the non-destructive identification of organic minerals in the geological record. *Organic Geochemistry*, *39*(4), 371-386.

Junge, K., Eicken, H., & Deming, J. W. (2004). Bacterial activity at− 2 to− 20 C in Arctic wintertime sea ice. *Applied and Environmental Microbiology*, *70*(1), 550-557.

Karunatillake, S., Keller, J. M., Squyres, S. W., Boynton, W. V., Brückner, J., Janes, D. M., Gasnault, O., & Newsom, H. E. (2007). Chemical compositions at Mars landing sites subject to Mars Odyssey Gamma Ray Spectrometer constraints. *Journal of Geophysical Research: Planets*, *112*(E8). https://doi.org/10.1029/2006je002859

Kate, I. L., Garry, J. R. C., Peeters, Z., Quinn, R., Foing, B., & Ehrenfreund, P. (2005). Amino acid photostability on the Martian surface. *Meteoritics & Planetary Science*, *40*(8), 1185-1193. https://doi.org/10.1111/j.1945-5100.2005.tb00183.x

Kipouros, G. J., & Sadoway, D. R. (2001). A thermochemical analysis of the production of anhydrous MgCl2. *Journal of Light Metals*, *1*(2), 111-117.

Klein, H. P. (1979). The Viking mission and the search for life on Mars. *Reviews of Geophysics*, *17*(7), 1655. https://doi.org/10.1029/rg017i007p01655

Kminek, G., & Bada, J. L. (2006). The effect of ionizing radiation on the preservation of amino acids on Mars. *Earth and Planetary Science Letters*, *245*(1-2), 1-5.

Knapp, D. R. (1979). *Handbook of analytical derivatization reactions*. John Wiley & Sons.

Knoevenagel, K., & Himmelreich, R. (1976). Degradation of compounds containing carbon atoms by photooxidation in the presence of water. *Archives of environmental contamination and toxicology*, *4*, 324-333.

Lagaly, G., Ogawa, M., & Dékány, I. (2013). Clay mineral–organic interactions. In *Developments in clay science* (Vol. 5, pp. 435-505). Elsevier.

Lammer, H., Chassefière, E., Karatekin, Ö., Morschhauser, A., Niles, P. B., Mousis, O., Odert, P., Möstl, U. V., Breuer, D., Dehant, V., Grott, M., Gröller, H., Hauber, E., & Pham, L. B. S. (2013). Outgassing History and Escape of the Martian Atmosphere and Water

Inventory. *Space Science Reviews*, *174*(1-4), 113-154. https://doi.org/10.1007/s11214-012-9943-8

Lasne, J., Noblet, A., Szopa, C., Navarro-Gonzalez, R., Cabane, M., Poch, O., Stalport, F., Francois, P., Atreya, S. K., & Coll, P. (2016). Oxidants at the Surface of Mars: A Review in Light of Recent Exploration Results. *Astrobiology*, *16*(12), 977-996. https://doi.org/10.1089/ast.2016.1502

Lewis, J. M. T., Eigenbrode, J. L., Wong, G. M., McAdam, A. C., Archer, P. D., Sutter, B., Millan, M., Williams, R. H., Guzman, M., Das, A., Rampe, E. B., Achilles, C. N., Franz, H. B., Andrejkovičová, S., Knudson, C. A., & Mahaffy, P. R. (2021). Pyrolysis of Oxalate, Acetate, and Perchlorate Mixtures and the Implications for Organic Salts on Mars. *Journal of Geophysical Research: Planets*, *126*(4). https://doi.org/10.1029/2020je006803

Litvak, M., Mitrofanov, I., Gellert, R., Djachkova, M., Lisov, D., Vasavada, A., & Czarnecki, S. (2023). Depth distribution of Chlorine at Gale crater, Mars, as derived from the DAN and APXS experiments onboard the Curiosity rover. *Journal of Geophysical Research: Planets*, e2022JE007694.

Mackenzie, S. M., Birch, S. P. D., Hörst, S., Sotin, C., Barth, E., Lora, J. M., Trainer, M. G., Corlies, P., Malaska, M. J., Sciamma-O'Brien, E., Thelen, A. E., Turtle, E., Radebaugh, J., Hanley, J., Solomonidou, A., Newman, C., Regoli, L., Rodriguez, S., Seignovert, B., Hayes, A. G., Journaux, B., Steckloff, J., Nna-Mvondo, D., Cornet, T., Palmer, M. Y., Lopes, R. M. C., Vinatier, S., Lorenz, R., Nixon, C., Czaplinski, E., Barnes, J. W., Sittler, E., & Coates, A. (2021). Titan: Earth-like on the Outside, Ocean World on the Inside. *The Planetary Science Journal*, *2*(3), 112. https://doi.org/10.3847/psj/abf7c9

Mahaffy, P. R., Webster, C. R., Cabane, M., Conrad, P. G., Coll, P., Atreya, S. K., Arvey, R., Barciniak, M., Benna, M., Bleacher, L., Brinckerhoff, W. B., Eigenbrode, J. L., Carignan, D., Cascia, M., Chalmers, R. A., Dworkin, J. P., Errigo, T., Everson, P., Franz, H., Farley, R., Feng, S., Frazier, G., Freissinet, C., Glavin, D. P., Harpold, D. N., Hawk, D., Holmes, V., Johnson, C. S., Jones, A., Jordan, P., Kellogg, J., Lewis, J., Lyness, E., Malespin, C. A., Martin, D. K., Maurer, J., McAdam, A. C., McLennan, D., Nolan, T. J., Noriega, M., Pavlov, A. A., Prats, B., Raaen, E., Sheinman, O., Sheppard, D., Smith, J., Stern, J. C., Tan, F., Trainer, M., Ming, D. W., Morris, R. V., Jones, J., Gundersen, C., Steele, A., Wray, J., Botta, O., Leshin, L. A., Owen, T., Battel, S., Jakosky, B. M., Manning, H., Squyres, S., Navarro-González, R., McKay, C. P., Raulin, F., Sternberg, R., Buch, A., Sorensen, P., Kline-Schoder, R., Coscia, D., Szopa, C., Teinturier, S., Baffes, C., Feldman, J., Flesch, G., Forouhar, S., Garcia, R., Keymeulen, D., Woodward, S., Block, B. P., Arnett, K., Miller, R., Edmonson, C., Gorevan, S., & Mumm, E. (2012). The Sample Analysis at Mars Investigation and Instrument Suite. *Space Science Reviews*, *170*(1-4), 401-478. https://doi.org/10.1007/s11214-012-9879-z

Mandon, L., Parkes Bowen, A., Quantin-Nataf, C., Bridges, J. C., Carter, J., Pan, L., Beck, P., Dehouck, E., Volat, M., Thomas, N., Cremonese, G., Tornabene, L. L., & Thollot, P. (2021). Morphological and Spectral Diversity of the Clay-Bearing Unit at the ExoMars Landing Site Oxia Planum. *Astrobiology*, *21*(4), 464-480. https://doi.org/10.1089/ast.2020.2292

Mastrogiuseppe, M., Poggiali, V., Hayes, A., Lunine, J., Seu, R., Mitri, G., & Lorenz, R. (2019). Deep and methane-rich lakes on Titan. *Nature Astronomy*, *3*(6), 535-542.

Masursky, H., & Crabill, N. (1976a). Search for the Viking 2 landing site. *Science*, *194*(4260), 62-68.

Masursky, H., & Crabill, N. (1976b). The Viking landing sites: Selection and certification. *Science*, *193*(4255), 809-812.

Mcintosh, O., Szopa, C., Freissinet, C., Buch, A., & Boulesteix, D. (2022). *Analysis of aromatic organic salts with gas chromatography-mass spectrometry and implications for their detection at Mars surface with in situ experiments*.

McKay, C. P. (2009). Planetary ecosynthesis on Mars: restoration ecology and environmental ethics. *Exploring the origin, extent, and future of life: Philosophical, ethical, and theological perspectives*, 245-260.

Meslin, P.-Y., Forni, O., Beck, P., Cousin, A., Beyssac, O., Lopez-Reyes, G., Benzerara, K., Ollila, A., Mandon, L., & Wiens, R. (2022). Evidence for perchlorate and sulfate salts in jezero crater, mars, from supercam observations. Lunar and Planetary Science Conference,

Millan, M., Szopa, C., Buch, A., Cabane, M., Teinturier, S., Mahaffy, P., & Johnson, S. (2019). Performance of the SAM gas chromatographic columns under simulated flight operating conditions for the analysis of chlorohydrocarbons on Mars. *Journal of Chromatography A*, *1598*, 183-195.

Millan, M., Szopa, C., Buch, A., Coll, P., Glavin, D. P., Freissinet, C., Navarro-Gonzalez, R., François, P., Coscia, D., Bonnet, J. Y., Teinturier, S., Cabane, M., & Mahaffy, P. R. (2016). In situ analysis of martian regolith with the SAM experiment during the first mars year of the MSL mission: Identification of organic molecules by gas chromatography from laboratory measurements. *Planetary and Space Science*, *129*, 88-102. https://doi.org/10.1016/j.pss.2016.06.007

Millan, M., Szopa, C., Buch, A., Summons, R. E., Navarro-Gonzalez, R., Mahaffy, P. R., & Johnson, S. S. (2020). Influence of Calcium Perchlorate on Organics Under SAM-Like Pyrolysis Conditions: Constraints on the Nature of Martian Organics. *Journal of Geophysical Research: Planets*, *125*(7). https://doi.org/10.1029/2019je006359

Millan, M., Teinturier, S., Malespin, C., Bonnet, J., Buch, A., Dworkin, J., Eigenbrode, J., Freissinet, C., Glavin, D., & Navarro-González, R. (2022). Organic molecules revealed in Mars's Bagnold Dunes by Curiosity's derivatization experiment. *Nature Astronomy*, *6*(1), 129-140.

Millan, M., Williams, A. J., McAdam, A. C., Eigenbrode, J. L., Steele, A., Freissinet, C., Glavin, D. P., Szopa, C., Buch, A., Summons, R. E., Lewis, J. M. T., Wong, G. M., House, C. H., Sutter, B., McIntosh, O., Bryk, A. B., Franz, H. B., Pozarycki, C., Stern, J. C., Navarro-Gonzalez, R., Archer, D. P., Fox, V., Bennett, K., Teinturier, S., Malespin, C., Johnson, S. S., & Mahaffy, P. R. (2022). Sedimentary Organics in Glen Torridon, Gale Crater, Mars: Results From the SAM Instrument Suite and Supporting Laboratory Analyses. *Journal of Geophysical Research: Planets*, *127*(11). https://doi.org/10.1029/2021je007107

Ming, D. W., Archer Jr, P., Glavin, D., Eigenbrode, J., Franz, H., Sutter, B., Brunner, A., Stern, J., Freissinet, C., & McAdam, A. (2014). Volatile and organic compositions of sedimentary rocks in Yellowknife Bay, Gale Crater, Mars. *Science*, *343*(6169), 1245267.

Mishra, V. S., Mahajani, V. V., & Joshi, J. B. (1995). Wet air oxidation. *Industrial & Engineering Chemistry Research*, *34*(1), 2-48.

Moeller, R. C., Jandura, L., Rosette, K., Robinson, M., Samuels, J., Silverman, M., Brown, K., Duffy, E., Yazzie, A., Jens, E., Brockie, I., White, L., Goreva, Y., Zorn, T., Okon, A., Lin, J., Frost, M., Collins, C., Williams, J. B., Steltzner, A., Chen, F., & Biesiadecki, J. (2021). The Sampling and Caching Subsystem (SCS) for the Scientific Exploration of Jezero Crater by the Mars 2020 Perseverance Rover. *Space Science Reviews*, *217*(1). https://doi.org/10.1007/s11214-020-00783-7

Moldoveanu, S. (2009). *Pyrolysis of organic molecules: applications to health and environmental issues*. Elsevier.

Moldoveanu, S. (2010). Pyrolysis of carboxylic acids. *Techniques and instrumentation in analytical chemistry*, *28*, 471-526.

Moulay, V., Freissinet, C., Rizk-Bigourd, M., Buch, A., Ancelin, M., Couturier, E., Breton, C., Trainer, M. G., & Szopa, C. (2023). Selection and Analytical Performances of the Dragonfly Mass Spectrometer Gas Chromatographic Columns to Support the Search for Organic Molecules of Astrobiological Interest on Titan. *Astrobiology*, *23*(2), 213-229.

Mustard, J. F., Murchie, S. L., Pelkey, S., Ehlmann, B., Milliken, R., Grant, J. A., Bibring, J.-P., Poulet, F., Bishop, J., & Dobrea, E. N. (2008). Hydrated silicate minerals on Mars observed by the Mars Reconnaissance Orbiter CRISM instrument. *Nature*, *454*(7202), 305-309.

Mykytczuk, N., Foote, S. J., Omelon, C. R., Southam, G., Greer, C. W., & Whyte, L. G. (2013). Bacterial growth at− 15 C; molecular insights from the permafrost bacterium Planococcus halocryophilus Or1. *The ISME journal*, *7*(6), 1211-1226.

Nachon, M., Mangold, N., Forni, O., Kah, L., Cousin, A., Wiens, R., Anderson, R., Blaney, D., Blank, J., & Calef, F. (2017). Chemistry of diagenetic features analyzed by ChemCam at Pahrump Hills, Gale crater, Mars. *Icarus*, *281*, 121-136.

Nagy, K., & Tiuca, I.-D. (2017). Importance of Fatty Acids in Physiopathology of Human Body. In. InTech. https://doi.org/10.5772/67407

Naraoka, H., Shimoyama, A., & Harada, K. (1999a). *Origins of Life and Evolution of the Biosphere*, *29*(2), 187-201. https://doi.org/10.1023/a:1006547127028

Naraoka, H., Shimoyama, A., & Harada, K. (1999b). Molecular distribution of monocarboxylic acids in Asuka carbonaceous chondrites from Antarctica. *Origins of Life and Evolution of the Biosphere*, *29*(2), 187-201.

Navarro-González, R., Navarro, K. F., Rosa, J. D. L., Iñiguez, E., Molina, P., Miranda, L. D., Morales, P., Cienfuegos, E., Coll, P., Raulin, F., Amils, R., & McKay, C. P. (2006). The limitations on organic detection in Mars-like soils by thermal volatilization–gas chromatography–MS and their implications for the Viking results. *Proceedings of the National Academy of Sciences*, *103*(44), 16089-16094. https://doi.org/10.1073/pnas.0604210103

Navarro-González, R., Vargas, E., De La Rosa, J., Raga, A. C., & McKay, C. P. (2010). Reanalysis of the Viking results suggests perchlorate and organics at midlatitudes on Mars. *Journal of Geophysical Research*, *115*(E12). https://doi.org/10.1029/2010je003599

Norén, K., Loring, J. S., & Persson, P. (2008). Adsorption of alpha amino acids at the water/goethite interface. *Journal of colloid and interface science*, *319*(2), 416-428.

Ojha, L., McEwen, A., Dundas, C., Byrne, S., Mattson, S., Wray, J., Masse, M., & Schaefer, E. (2014). HiRISE observations of recurring slope lineae (RSL) during southern summer on Mars. *Icarus*, *231*, 365-376.

Ojha, L., Wilhelm, M. B., Murchie, S. L., McEwen, A. S., Wray, J. J., Hanley, J., Massé, M., & Chojnacki, M. (2015). Spectral evidence for hydrated salts in recurring slope lineae on Mars. *Nature Geoscience*, *8*(11), 829-832.

Olsztynska, S., Komorowska, M., Vrielynck, L., & Dupuy, N. (2001). Vibrational spectroscopic study of L-phenylalanine: Effect of pH. *Applied Spectroscopy*, *55*(7), 901-907.

Oró, J., & Holzer, G. (1979). The effects of ultraviolet light on the degradation of organic compounds: a possible explanation for the abscence of organic matter on Mars. *Life*

Sciences and Space Research, 77-86. https://doi.org/10.1016/b978-0-08-023416-8.50013-1

Oró, J., & Holzer, G. (1979). The photolytic degradation and oxidation of organic compounds under simulated Martian conditions. *Journal of Molecular Evolution*, *14*(1-3), 153-160. https://doi.org/10.1007/bf01732374

Osterloo, M., Hamilton, V., Bandfield, J., Glotch, T., Baldridge, A., Christensen, P., Tornabene, L., & Anderson, F. (2008). Chloride-bearing materials in the southern highlands of Mars. *Science*, *319*(5870), 1651-1654.

Patel, M., Zarnecki, J., & Catling, D. (2002). Ultraviolet radiation on the surface of Mars and the Beagle 2 UV sensor. *Planetary and Space Science*, *50*(9), 915-927.

Pavlov, A. A., McLain, H. L., Glavin, D. P., Roussel, A., Dwork2in, J. P., Elsila, J. E., & Yocum, K. M. (2022). Rapid Radiolytic Degradation of Amino Acids in the Martian Shallow Subsurface: Implications for the Search for Extinct Life. *Astrobiology*, *22*(9), 1099-1115.

Pedersen, G. B. M., & Head, J. W. (2010). Evidence of widespread degraded Amazonian-aged ice-rich deposits in the transition between Elysium Rise and Utopia Planitia, Mars: Guidelines for the recognition of degraded ice-rich materials. *Planetary and Space Science*, *58*(14-15), 1953-1970.

Perrier, S., Bertaux, J. L., Lefèvre, F., Lebonnois, S., Korablev, O., Fedorova, A., & Montmessin, F. (2006). Global distribution of total ozone on Mars from SPICAM/MEX UV measurements. *Journal of Geophysical Research*, *111*(E9). https://doi.org/10.1029/2006je002681

Pietrogrande, M., & Basaglia, G. (2010). Enantiomeric resolution of biomarkers in space analysis: Chemical derivatization and signal processing for gas chromatography–mass spectrometry analysis of chiral amino acids. *Journal of Chromatography A*, *1217*(7), 1126-1133.

Pietrogrande, M. C. (2012). Gas chromatography in space exploration. In *Gas chromatography* (pp. 865-874). Elsevier.

Pizzarello, S., Cooper, G., & Flynn, G. (2006). The nature and distribution of the organic material in carbonaceous chondrites and interplanetary dust particles. *Meteorites and the early solar system II*, *1*, 625-651.

Poch, O., Jaber, M., Stalport, F., Nowak, S., Georgelin, T., Lambert, J.-F., Szopa, C., & Coll, P. (2015). Effect of nontronite smectite clay on the chemical evolution of several organic molecules under simulated martian surface ultraviolet radiation conditions. *Astrobiology*, *15*(3), 221-237.

Poch, O., Kaci, S., Stalport, F., Szopa, C., & Coll, P. (2014). Laboratory insights into the chemical and kinetic evolution of several organic molecules under simulated Mars surface UV radiation conditions. *Icarus*, *242*, 50-63.

Postberg, F., Khawaja, N., Abel, B., Choblet, G., Glein, C. R., Gudipati, M. S., Henderson, B. L., Hsu, H.-W., Kempf, S., Klenner, F., Moragas-Klostermeyer, G., Magee, B., Nölle, L., Perry, M., Reviol, R., Schmidt, J., Srama, R., Stolz, F., Tobie, G., Trieloff, M., & Waite, J. H. (2018). Macromolecular organic compounds from the depths of Enceladus. *Nature*, *558*(7711), 564-568. https://doi.org/10.1038/s41586-018-0246-4

Poulet, F., Bibring, J.-P., Mustard, J., Gendrin, A., Mangold, N., Langevin, Y., Arvidson, R., Gondet, B., & Gomez, C. (2005). Phyllosilicates on Mars and implications for early Martian climate. *Nature*, *438*(7068), 623-627.

Quantin, C., Carter, J., Thollot, P., Broyer, J., Lozach, L., Davis, J., Grindrod, P., Pajola, M., Baratti, E., & Rossato, S. (2016). Oxia Planum, the landing site for ExoMars 2018. 47th Lunar and Planetary Science Conference Abstracts, Abstract,

Rampe, E. B., Blake, D. F., Bristow, T. F., Ming, D. W., Vaniman, D. T., Morris, R. V., Achilles, C. N., Chipera, S. J., Morrison, S. M., Tu, V. M., Yen, A. S., Castle, N., Downs, G. W., Downs, R. T., Grotzinger, J. P., Hazen, R. M., Treiman, A. H., Peretyazhko, T. S., Des Marais, D. J., Walroth, R. C., Craig, P. I., Crisp, J. A., Lafuente, B., Morookian, J. M., Sarrazin, P. C., Thorpe, M. T., Bridges, J. C., Edgar, L. A., Fedo, C. M., Freissinet, C., Gellert, R., Mahaffy, P. R., Newsom, H. E., Johnson, J. R., Kah, L. C., Siebach, K. L., Schieber, J., Sun, V. Z., Vasavada, A. R., Wellington, D., & Wiens, R. C. (2020). Mineralogy and geochemistry of sedimentary rocks and eolian sediments in Gale crater, Mars: A review after six Earth years of exploration with Curiosity. *Geochemistry*, *80*(2), 125605. https://doi.org/10.1016/j.chemer.2020.125605

Rao, M., Odom, D., & Oro, J. (1980). Clays in prebiological chemistry. *Journal of Molecular Evolution*, *15*(4), 317-331.

Rapin, W., Ehlmann, B. L., Dromart, G., Schieber, J., Thomas, N., Fischer, W. W., Fox, V., Stein, N. T., Nachon, M., & Clark, B. C. (2019). An interval of high salinity in ancient Gale crater lake on Mars. *Nature Geoscience*, *12*(11), 889-895.

Raulin, F., Coll, P., Coscia, D., Gazeau, M., Sternberg, R., Bruston, P., Israel, G., & Gautier, D. (1998). An exobiological view of Titan and the Cassini-Huygens mission. *Advances in space research*, *22*(3), 353-362.

Remick, K. A., & Helmann, J. D. (2023). The elements of life: A biocentric tour of the periodic table. In *Advances in Microbial Physiology* (Vol. 82, pp. 1-127). Elsevier.

Rosenbauer, H., Fuselier, S., Ghielmetti, A., Greenberg, J., Goesmann, F., Ulamec, S., Israel, G., Livi, S., MacDermott, J., & Matsuo, T. (1999). The COSAC experiment on the lander of the ROSETTA mission. *Advances in space research*, *23*(2), 333-340.

Rothschild, L. J., & Mancinelli, R. L. (2001). Life in extreme environments. *Nature*, *409*(6823), 1092-1101.

Rushneck, D. R., Diaz, A. V., Howarth, D. W., Rampacek, J., Olson, K. W., Dencker, W. D., Smith, P., McDavid, L., Tomassian, A., Harris, M., Bulota, K., Biemann, K., Lafleur, A. L., Biller, J. E., & Owen, T. (1978). Viking gas chromatograph-mass spectrometer. *Rev Sci Instrum*, *49*(6), 817. https://doi.org/10.1063/1.1135623

Russell, M. J., Murray, A. E., & Hand, K. P. (2017). The Possible Emergence of Life and Differentiation of a Shallow Biosphere on Irradiated Icy Worlds: The Example of Europa. *Astrobiology*, *17*(12), 1265-1273. https://doi.org/10.1089/ast.2016.1600

Sagan, C. (1973). Ultraviolet selection pressure on the earliest organisms. *Journal of theoretical biology*, *39*(1), 195-200.

Scheller, E. L., Hollis, J. R., Cardarelli, E. L., Steele, A., Beegle, L. W., Bhartia, R., Conrad, P., Uckert, K., Sharma, S., & Ehlmann, B. L. (2022). Aqueous alteration processes in Jezero crater, Mars− implications for organic geochemistry. *Science*, eabo5204.

Schlten, H.-R., & Leinweber, P. (1993). Pyrolysis-field ionization mass spectrometry of agricultural soils and humic substances: Effect of cropping systems and influence of the mineral matrix. *Plant and Soil*, *151*, 77-90.

Schon, S. C., Head, J. W., & Fassett, C. I. (2012). An overfilled lacustrine system and progradational delta in Jezero crater, Mars: Implications for Noachian climate. *Planetary and Space Science*, *67*(1), 28-45.

Schoors, S., Bruning, U., Missiaen, R., Queiroz, K. C., Borgers, G., Elia, I., Zecchin, A., Cantelmo, A. R., Christen, S., & Goveia, J. (2015). Fatty acid carbon is essential for dNTP synthesis in endothelial cells. *Nature*, *520*(7546), 192-197.

Schuerger, A. C., Golden, D., & Ming, D. W. (2012). Biotoxicity of Mars soils: 1. Dry deposition of analog soils on microbial colonies and survival under Martian conditions. *Planetary and Space Science*, *72*(1), 91-101.

Schulze-Makuch, D., & Irwin, L. N. (2006). The prospect of alien life in exotic forms on other worlds. *Naturwissenschaften*, *93*, 155-172.

Seelos, K. D., Seelos, F. P., Viviano-Beck, C. E., Murchie, S. L., Arvidson, R. E., Ehlmann, B. L., & Fraeman, A. A. (2014). Mineralogy of the MSL Curiosity landing site in Gale crater as observed by MRO/CRISM. *Geophysical Research Letters*, *41*(14), 4880-4887. https://doi.org/10.1002/2014gl060310

Sephton, M. A. (2002). Organic compounds in carbonaceous meteorites. *Natural product reports*, *19*(3), 292-311.

Shkrob, I. A., Chemerisov, S. D., & Marin, T. W. (2010). Photocatalytic decomposition of carboxylated molecules on light-exposed martian regolith and its relation to methane production on Mars. *Astrobiology*, *10*(4), 425-436.

Skelley, A. M., Scherer, J. R., Aubrey, A. D., Grover, W. H., Ivester, R. H. C., Ehrenfreund, P., Grunthaner, F. J., Bada, J. L., & Mathies, R. A. (2005). Development and evaluation of a microdevice for amino acid biomarker detection and analysis on Mars. *Proceedings of the National Academy of Sciences*, *102*(4), 1041-1046. https://doi.org/10.1073/pnas.0406798102

Soffen, G. A., & Young, A. T. (1972). The viking missions to mars. *Icarus*, *16*(1), 1-16.

Stalport, F., Glavin, D. P., Eigenbrode, J., Bish, D., Blake, D., Coll, P., Szopa, C., Buch, A., Mcadam, A., & Dworkin, J. (2012). The influence of mineralogy on recovering organic acids from Mars analogue materials using the “one-pot” derivatization experiment on the Sample Analysis at Mars (SAM) instrument suite. *Planetary and Space Science*, *67*(1), 1-13.

Stillman, D. E., Michaels, T. I., & Grimm, R. E. (2017). Characteristics of the numerous and widespread recurring slope lineae (RSL) in Valles Marineris, Mars. *Icarus*, *285*, 195-210.

Stillman, D. E., Michaels, T. I., Grimm, R. E., & Harrison, K. P. (2014). New observations of martian southern mid-latitude recurring slope lineae (RSL) imply formation by freshwater subsurface flows. *Icarus*, *233*, 328-341.

Sutter, B., McAdam, A. C., Mahaffy, P. R., Ming, D. W., Edgett, K. S., Rampe, E. B., Eigenbrode, J. L., Franz, H. B., Freissinet, C., Grotzinger, J. P., Steele, A., House, C. H., Archer, P. D., Malespin, C. A., Navarro-González, R., Stern, J. C., Bell, J. F., Calef, F. J., Gellert, R., Glavin, D. P., Thompson, L. M., & Yen, A. S. (2017). Evolved gas analyses of sedimentary rocks and eolian sediment in Gale Crater, Mars: Results of the Curiosity rover's sample analysis at Mars instrument from Yellowknife Bay to the Namib Dune. *Journal of Geophysical Research: Planets*, *122*(12), 2574-2609. https://doi.org/10.1002/2016je005225

Szopa, C., Freissinet, C., Glavin, D. P., Millan, M., Buch, A., Franz, H. B., Summons, R. E., Sumner, D. Y., Sutter, B., Eigenbrode, J. L., Williams, R. H., Navarro-González, R., Guzman, M., Malespin, C., Teinturier, S., Mahaffy, P. R., & Cabane, M. (2020). First Detections of Dichlorobenzene Isomers and Trichloromethylpropane from Organic Matter Indigenous to Mars Mudstone in Gale Crater, Mars: Results from the Sample Analysis

at Mars Instrument Onboard the Curiosity Rover. *Astrobiology*, *20*(2), 292-306. https://doi.org/10.1089/ast.2018.1908

Szopa, C., Goesmann, F., Rosenbauer, H., & Sternberg, R. (2007). The COSAC experiment of the Rosetta mission: Performance under representative conditions and expected scientific return. *Advances in space research*, *40*(2), 180-186.

Szopa, C., Sternberg, R., Rodier, C., Coscia, D., & Raulin, F. (2001). Development and analytical aspects of gas chromatography for space exploration. *LC GC EUROPE*, *14*(2), 114-121.

Thomas, N. H., Ehlmann, B. L., Meslin, P. Y., Rapin, W., Anderson, D. E., Rivera-Hernández, F., Forni, O., Schröder, S., Cousin, A., Mangold, N., Gellert, R., Gasnault, O., & Wiens, R. C. (2019). Mars Science Laboratory Observations of Chloride Salts in Gale Crater, Mars. *Geophysical Research Letters*, *46*(19), 10754-10763. https://doi.org/10.1029/2019gl082764

Toulmin III, P., Clark, B. C., Baird, A., Keil, K., & Rose Jr, H. J. (1976). Preliminary results from the Viking X-ray fluorescence experiment: The first sample from Chryse Planitia, Mars. *Science*, *194*(4260), 81-84.

Valášková, M., & Martynkova, G. S. (2012). Vermiculite: structural properties and examples of the use. *Clay Minerals in Nature–Their Characterization, Modification and Application*, 209-238.

Waite, J. H., Glein, C. R., Perryman, R. S., Teolis, B. D., Magee, B. A., Miller, G., Grimes, J., Perry, M. E., Miller, K. E., & Bouquet, A. (2017). Cassini finds molecular hydrogen in the Enceladus plume: evidence for hydrothermal processes. *Science*, *356*(6334), 155-159.

Wang, A., Ling, Z., Yan, Y., McEwen, A. S., Mellon, M. T., Smith, M. D., Jolliff, B. L., & Head, J. (2019). Subsurface Cl-bearing salts as potential contributors to recurring slope lineae (RSL) on Mars. *Icarus*, *333*, 464-480.

Wells, L. E., & Deming, J. W. (2006). Significance of bacterivory and viral lysis in bottom waters of Franklin Bay, Canadian Arctic, during winter. *Aquatic microbial ecology*, *43*(3), 209-221.

Williams, A., Eigenbrode, J., Millan, M., Williams, R., Buch, A., Teinturier, S., Glavin, D., Freissinet, C., Szopa, C., & McIntosh, O. (2021). Organic molecules detected with the first TMAH wet chemistry experiment, Gale crater, Mars. 52nd Lunar and Planetary Science Conference,

Wray, J. J. (2013). Gale crater: the Mars Science Laboratory/Curiosity Rover Landing Site. *International Journal of Astrobiology*, *12*(1), 25-38. https://doi.org/10.1017/s1473550412000328

Yariv, S., & Shoval, S. (1982). The effects of thermal treatment on associations between fatty acids and montmorillonite. *Israel Journal of Chemistry*, *22*(3), 259-265.

Yu, W. H., Li, N., Tong, D. S., Zhou, C. H., Lin, C. X. C., & Xu, C. Y. (2013). Adsorption of proteins and nucleic acids on clay minerals and their interactions: A review. *Applied Clay Science*, *80*, 443-452.

Zaia, D. A. (2012). Adsorption of amino acids and nucleic acid bases onto minerals: a few suggestions for prebiotic chemistry experiments. *International Journal of Astrobiology*, *11*(4), 229-234.

Zeitlin, C., Hassler, D., Cucinotta, F., Ehresmann, B., Wimmer-Schweingruber, R., Brinza, D., Kang, S., Weigle, G., Böttcher, S., & Böhm, E. (2013). Measurements of energetic particle radiation in transit to Mars on the Mars Science Laboratory. *Science*, *340*(6136), 1080-1084.

Zhao, Y., Hochlaf, M., & Biczysko, M. (2021). Identification of DNA Bases and Their Cations in Astrochemical Environments: Computational Spectroscopy of Thymine as a Test Case. *Frontiers in Astronomy and Space Sciences*, *8*, 757007.

Zolotov, M., & Shock, E. (1999). Abiotic synthesis of polycyclic aromatic hydrocarbons on Mars. *Journal of Geophysical Research: Planets*, *104*(E6), 14033-14049. https://doi.org/10.1029/1998je000627

CHAPTER 6: CONCLUSIONS AND PERSPECTIVES

The search for organic molecules on the surface and subsurface of Mars represents a major challenge for the characterization of the past and present habitability of the

planet. *In situ* space exploration constitute a major step forward in the comprehension of its surface chemistry. However, laboratory experiments are still necessary to understand the influence of the environment on organic compounds and the biases generated by the analyses of the samples.

This Ph.D. Thesis aimed at understanding the influence of salts on the preservation and detection of organic molecules on Mars.

The central questions for my research were as follows:

1. *What is the effect of UV radiation on organic molecules in the presence of chloride salts and vermiculite?*
2. *What is the influence of chloride salts on organic molecules when analyzed in situ with pyrolysis-GC-MS?*
3. *Could refractory molecules such as aromatic organic salts be detected in situ on Mars?*

The information retrieved by our laboratory analyses will help the decision-making process for the analysis of samples on Mars and the interpretation of *in situ* data.

1. EFFECT OF UV RADIATION ON ORGANIC MOLECULES IN THE PRESENCE OF CHLORIDE SALTS

The first part of my thesis was to characterize the influence of chloride salts and vermiculite on the photocatalysis of organic molecules under UV radiation conditions.

Mars sample analogs were prepared by doping organic-cleaned vermiculite with phenylalanine and undecanoic acid. Sodium chloride (NaCl) and magnesium chloride ($MgCl_2$) were added to some of the analog samples. The degradation of the organic molecules under UV light was then monitored through IR spectroscopy in a nitrogen atmosphere.

This study aimed to **determine the organic preservation potential** of these two

inorganic phases (vermiculite and chloride salts) and, thus, **help choose targets for future *in situ* analysis**.

I showed that the presence of vermiculite catalyzed and inhibited the degradation of undecanoic acid and L-phenylalanine, respectively, under UV light. Therefore, conclusions on the preservation potential of vermiculite on organic molecules cannot be drawn from this study. We should repeat the experiments on a much larger and more diverse number of organic molecules to see if tendencies in the photocatalytic/photoprotective properties of vermiculite can apply to specific groups of organic compounds.

On the other hand, both chloride salts species (NaCl and $MgCl_2$) hindered the degradation of phenylalanine and undecanoic acid when added to the analog samples. These results demonstrated that **chloride salts on Mars could help preserve organic molecules from solar radiation and make good analytical targets for future *in situ* experiments**. Several studies have looked at the influence of different mineral matrices on organic compounds such as carboxylic acid, amino acids, HAPs, or nucleotides, but this work should be extended by adding chloride salts. This would help to **determine if chloride salts could be an overall indicator of preserved organic matter on the Martian surface**.

While this study gives a first perspective on the effect of vermiculite and chloride salts on the protection of organic matter on the Martian surface, the experiments were performed at ambient temperature and under an N_2 atmosphere due to instrumental constraints in the laboratory. This work should be repeated under low pressure, low temperature, and CO_2 atmosphere to be as close to the Martian environmental conditions as possible. These parameters could influence the hydration state of the chloride salts, thus affecting the interaction of the organic compounds with the mineral matrice and their degradation under UV irradiation. Additionally, the CO_2 atmosphere under UV radiation could lead to oxidation processes and, thus, to chemical reactions influencing the degradation and/or transformation of the organic molecules in the

samples.

This study on the influence of radiations on organic molecules in the presence of vermiculite and chloride salts is currently continued by subjecting the samples to ion irradiation (H^+ and He^+) which aims at mimicking secondary particles emitted by the galactic cosmic rays (GCRs) arriving on Mars and which could interact with organic species dispersed in deeper layers of the Martian soil. Indeed, the ExoMars rover, scheduled to land on the planet's surface in 2028, will be able to collect and analyze samples from up to two meters deep in the Martian subsurface. This unique feature of the ExoMars rover was designed to analyze samples where organic matter is believed to be better preserved from radiation than on the surface. Understanding the possible effects of GCRs radiations is crucial to prepare future *in situ* experiments and data analysis.

2. Influence of chloride salts on organic molecules during pyrolysis-GC-MS analyses

The positive effect of chloride salts on preserving organic compounds in the Martian environment led me to investigate their influence on organic molecules under analytical conditions as performed by Martian probes.

Three pyrolysis conditions were tested, each corresponding to the analytical set-up used by an instrumental suite (Viking, SAM, or MOMA). Samples containing organic molecules of astrobiological interest (Carboxylic acids amino acids or PAHs) and chloride salts (NaCl, $MgCl_2$, or $CaCl_2$) were pyrolyzed. The chromatograms obtained in the presence of each salt were compared to a chromatogram of the pyrolyzed organic without salt.

This study aimed to **determine if the presence of chloride salts affected the detection of organic molecules during molecular analyses**.

The results of this study showed that **despite the preservation potential of chloride**

salts from UV radiations, their presence in a sample analyzed through **pyrolysis-GC-MS could affect the thermal degradation of the organic molecules**. Indeed, I showed that chloride salts can influence the number and abundance of pyrolyzates detected in the chromatogram of the organic compounds. This is especially the case in slow ramp pyrolysis as performed by SAM compared to flash pyrolysis at 500 °C and 800 °C. However, I also determined potential signatures of the presence of these salts, as well as characteristic chlorinated organic molecules that could help interpret the *in situ* data and trace back to the original parent organic molecule. Specifically, in flash pyrolysis, lower temperatures (500 °C) lead to a higher number of chlorinated compounds. Therefore, when analyzed *in situ* by pyrolysis-GC-MS experiments, **a fast temperature ramp or flash pyrolysis at temperatures below 800 °C seem to be the best experimental conditions** to analyze samples where chloride salts are believed to be present.

Finally, this study showed that **chloride salts could be the precursors of some of the chlorinated compounds detected on the Martian surface by Viking and Curiosity**, attributed so far exclusively to the interaction of organic molecules with oxychlorines.

This study again stresses the importance of laboratory work for interpreting *in situ* data due to the interactions of inorganic and organic phases during *in situ* experiments. It also emphasizes that systematic laboratory studies on other salts present on Mars are essential as some of the compounds detected on Mars (and so far, mostly attributed to the presence of perchlorates) could have another origin.

The next step of this study, in collaboration with Centrale Supelec, is to study the influence of chloride salts during derivatization experiments. A paper on the influence of these salts on DMFDMA derivatization was published by Boulesteix et al. in 2023, and I have been working on a similar study with MTBSTFA/DMF. Studying the influence of TMAH should also be considered.

Overall, understanding the effect of chloride salts on the analyses of organic matter is

not limited to Mars. Indeed, the presence of chloride-bearing phases has also been identified on other planetary objects of astrobiological interest, which will or might be explored soon by probes containing GC-MS instruments in their payload, such as the Dragonfly mission on Titan with the DraMS instrument or icy moons such as Europa, Enceladus or Ceres.

3. DETECTION OF AROMATIC ORGANIC SALTS

The radiative environment and the interaction of organic molecules with the mineral phases in which they are embedded have been suggested to **lead to the formation of organic salts**. Moreover, the interaction of chloride salts and organic compounds during pyrolysis analysis also raised the hypothesis that these compounds could be formed during *in situ* analyses (Chapter 4). However, organic salts are non-volatile molecules and, therefore, **challenging to detect through typical space analytical chemistry techniques such as GC-MS**.

Thus, I investigated the behavior and signatures of two acid/salt couples (benzoic acid/calcium benzoate and phthalic acid/calcium phthalate) under EGA, pyrolysis, and derivatization GC-MS experiments.

This study aimed to better **understand the behavior of refractory compounds** like organic salts during flight instrument analysis on Mars and, thus, **help interpret *in situ* data**.

This work demonstrated that the acid and their salt counterparts do not follow the same degradation pathway during thermal analysis like EGA or pyrolysis GC-MS, which could enable their differentiation. I showed that **organic salts, despite their refractory character, could be identified indirectly by the detection of thermal degradation products (pyrolysis), and by the formation of derivatized products (derivatization)**, both with SAM and with MOMA. Finally, the temperature and speed (ramp or flash) of pyrolysis as well as the derivatization reagent and column used to analyze a sample where aromatic organic salts could be present can be a determining

factors in detecting these compounds by GC-MS.

Organic salts are metastable molecules that could be ubiquitous on Mars. Therefore, the conclusions of this work raise essential questions on the detectability of refractory molecules, the analytical power of flight instruments, and the interpretation of *in situ* data.

This work is currently applied to other benzoate and phthalate molecules with different ions (magnesium, iron, potassium) to widen our knowledge on the behavior of such compounds under analytical conditions and evaluate the influence of these ions on the thermal degradation/derivatization of organic salts in flight-like analytical conditions.

REFERENCES

Boulesteix, D., Buch, A., Samson, J., Millan, M., Jomaa, J., Coscia, D., ... & Szopa, C. (2023). Influence of pH and salts on DMF-DMA derivatization for future Space Applications. Analytica Chimica Acta, 1266, 341270.

RESUME DE THESE

Introduction : Mars est considérée comme ayant été une planète similaire à la Terre il y a plusieurs milliards d'années, faisant d'elle l'un des environnements les plus prometteurs dans la recherche de traces de vie extraterrestre. Diverses missions spatiales d'exploration ont été développées afin déchiffré ses mystères; de son atmosphère, à sa surface, et son habitabilité. A-t-elle réuni les conditions nécessaires au développement de la vie ? L'un des objectifs scientifiques majeur des missions d'exploration martienne de ces dernières décennies a été de rechercher la présence de molécules organiques dans le sol, grâce au déploiement d'instruments d'analyses chimique [1]. Or plusieurs facteurs rendent la détection de matière organique difficile : (a) les fortes doses de rayonnement électromagnétique et particulaire ionisant impliquées dans la destruction ou la transformation des composés organiques de surface, (b) la matrice minérale oxydante, (c) le traitement de l'échantillon tel que la pyrolyse à haute température ou la thermochimie qui pourrait conduire à la dégradation thermique des molécules organiques et (d) la sensibilité des instruments. Mes travaux de recherche consistent à tester l'influence de ces facteurs sur les performances de nos techniques d'analyses, et d'aider à l'interprétation et la compréhension des données in situ pour mettre en évidence des bioindicateurs et biosignatures organiques.

Méthode : Mes études s'insèrent dans le contexte de deux missions martiennes, la Mars Science Laboratory (MSL) de la NASA et son rover Curiosity, ainsi que la mission ExoMars de l'Agence Spatiale Européenne (ESA) et son rover Rosalind Franklin . Les deux sondes disposent de laboratoires d'analyse chimique embarqués, et notamment d'un chromatographe en phase gazeuse couplé à un spectromètre de masse (GC-MS). Les échantillons de sol martien peuvent être traités en amont par différentes méthodes : extraction thermique des molécules ou réactions chimiques dites de dérivatisation, permettant d'augmenter la volatilité des composés chimiques réfractaires tels que les acides aminés. En laboratoire j'ai reproduis ces différents

procédés sur des échantillons d'intérêts en me basant sur les capacités expérimentales des deux suites instrumentales liées à ces analyses : le Sample Analysis at Mars (SAM) à bord de Curiosity et le Mars Organic Molecules Analyser (MOMA) présent sur Rosalind-Franklin. Ces études permettent d'une part de mieux comprendre la chimie réactionnelle fondamentale lors d'analyses GC-MS sur des échantillons de type martien, mais également de mieux interpréter les données martiennes du rover Curiosity et de préparer la future mission ExoMars 2028.

Résultats :

1. Influence des sels de chlorures sur la détection in situ de molécules organiques

J'ai saisi l'opportunité de la récente découverte sur Mars de sels de chlorure par Curiosity pour [2] déterminer l'influence de ces sels sur la détectabilité de différentes molécules organiques d'intérêt astrobiologique recherchés avec SAM : acides aminés, acides carboxyliques, et hydrocarbures aromatiques polycycliques (HAPs). La présence de matière inorganique, tels que les sels, dans les échantillons analysés peut empêcher la détection des composés organiques et donc fortement biaiser l'interprétation des résultats *in situ* [3]. J'ai tout d'abord évalué le comportement catalytique/protecteur des sels de chlorure sur différentes molécules organiques sous rayonnement UV et étudié le profil cinétique de dégradation de bandes caractéristiques de chacune des molécules par spectrométrie infrarouge. Mes résultats ont montré que la présence de sels de chlorure empêchait la dégradation de nos composés organiques faisant de ces environnements salés d'excellents candidats d'échantillonnage pour analyses *in situ*. La suite de ces travaux a été d'analyser les échantillons par pyrolyse-GC-MS dans les conditions SAM et MOMA. J'ai pu montrer que la dégradation thermique des sels, via le relargage de chlorure d'hydrogène (HCl) dans l'échantillon, influait sur l'intensité, le nombre et le type de produits de pyrolyse détectés dans les chromatogrammes. L'identification de certains composés spécifiques à la dégradation thermique d'une molécule en présence de sel permettraient de remonter à la composition organique

initiale de l'échantillon martien et donc d'améliorer nos connaissances sur l'environnement chimique de la planète. Ces informations sont cruciales dans la recherche d'indices de trace de vie passé ou présente à la surface de Mars, mais également d'autres objets planétaires riches en sels tel que les lunes glacées Encelade et Europe.

2. Détectabilité de sels organiques aromatiques par analyses *in situ*

Dans un deuxième temps, je me suis intéressée aux sels organiques, qui ont pu être formés par des processus oxydatifs et radiatifs à la surface de Mars. Il a été suggéré que la faible volatilité de ces sels aurait pu compromettre leur détection *in situ* par des analyses d'extraction thermique telles que réalisées par les sondes Viking en 1976 [4]. Ces hypothèses sont toujours d'actualité puisque les laboratoires de chimie analytique embarqués à bord des sondes de surface martiennes, comme les suites instrumentales SAM et MOMA, réalisent toujours des expériences de pyrolyse pour analyser la composition moléculaire des sols martiens. Cependant, alors que les expériences Viking étaient réglées pour effectuer une pyrolyse à une température maximale de 500 °C, les instruments SAM et MOMA peuvent atteindre des températures allant jusqu'à 850 °C et ont la capacité d'effectuer des expériences de dérivatisation, augmentant ainsi la possibilité de détecter des composés peu volatils ou leurs produits de décomposition thermique. J'ai alors choisi de comparer les différences de comportement de deux couples acide/sel dans les conditions analytiques Viking, SAM et MOMA afin d'établir leur détectabilité *in situ*. Cette étude a permis de confirmer que Viking n'était pas en capacité de détecter la présence de sels organiques dans les échantillons martiens, de par sa température maximale de pyrolyse trop faible. Cependant, j'ai montré pour la première fois que les sels organiques, malgré leur caractère réfractaire, pouvait être identifiés indirectement par la détection de produits de dégradation thermique (pyrolyse), ainsi que par la formation de produits dérivatisés (dérivatisation), à la fois avec SAM et avec MOMA. Les conclusions de ces travaux soulèvent des questions essentielles sur la détectabilité de molécules réfractaires, sur

le pouvoir analytique des instruments de vols et sur l'interprétation des données *in situ*.

Discussion et perspectives : Mes travaux de thèse sont clé pour l'interprétation des données *in situ* martiennes, et de ce fait à la compréhension globale de l'habitabilité de la planète Mars. De plus, l'ensemble de ces recherches m'ont poussé à m'interroger sur les interactions organiques-minérales et à la possibilité de détecter directement ou indirectement les composés organiques d'intérêt avec les instruments à notre disposition *in situ*.

Références: [1] Freissinet et al., Organic molecules in the Sheepbed Mudstone, Gale Crater, Mars. Journal of Geophysical Research: Planets, 120(3), 495-51. [2] Thomas, et al., Mars Science Laboratory Observations of Chloride Salts in Gale Crater, Mars. Geophysical Research Letters 2019 Vol. 46 Issue 19 Pages 10754-10763. [3] Glavin et al., Evidence for perchlorates and the origin of chlorinated hydrocarbons detected by SAM at the Rocknest aeolian deposit in Gale Crater. Journal of Geophysical Research: Planets 2013 Vol. 118 Issue 10 Pages 1955-1973. [4] Benner et al,.The missing organic molecules on Mars. Proceedings of the National Academy of Sciences 2000 Vol. 97 Issue 6 Pages 2425-2430. [5] Fioroni, Transition metal organometallic/metallorganic chemistry: Its role in prebiotic chemistry and life's origin. Prebiotic Chemistry and the Origin of Life, 2021. 1-41.